

Supplement of Geosci. Model Dev., 10, 4257–4283, 2017
<https://doi.org/10.5194/gmd-10-4257-2017-supplement>
© Author(s) 2017. This work is distributed under
the Creative Commons Attribution 4.0 License.



Supplement of

The method ADAMONT v1.0 for statistical adjustment of climate projections applicable to energy balance land surface models

Deborah Verfaillie et al.

Correspondence to: Samuel Morin (samuel.morin@meteo.fr)

The copyright of individual parts of the supplement might differ from the CC BY 4.0 License.

Chablais

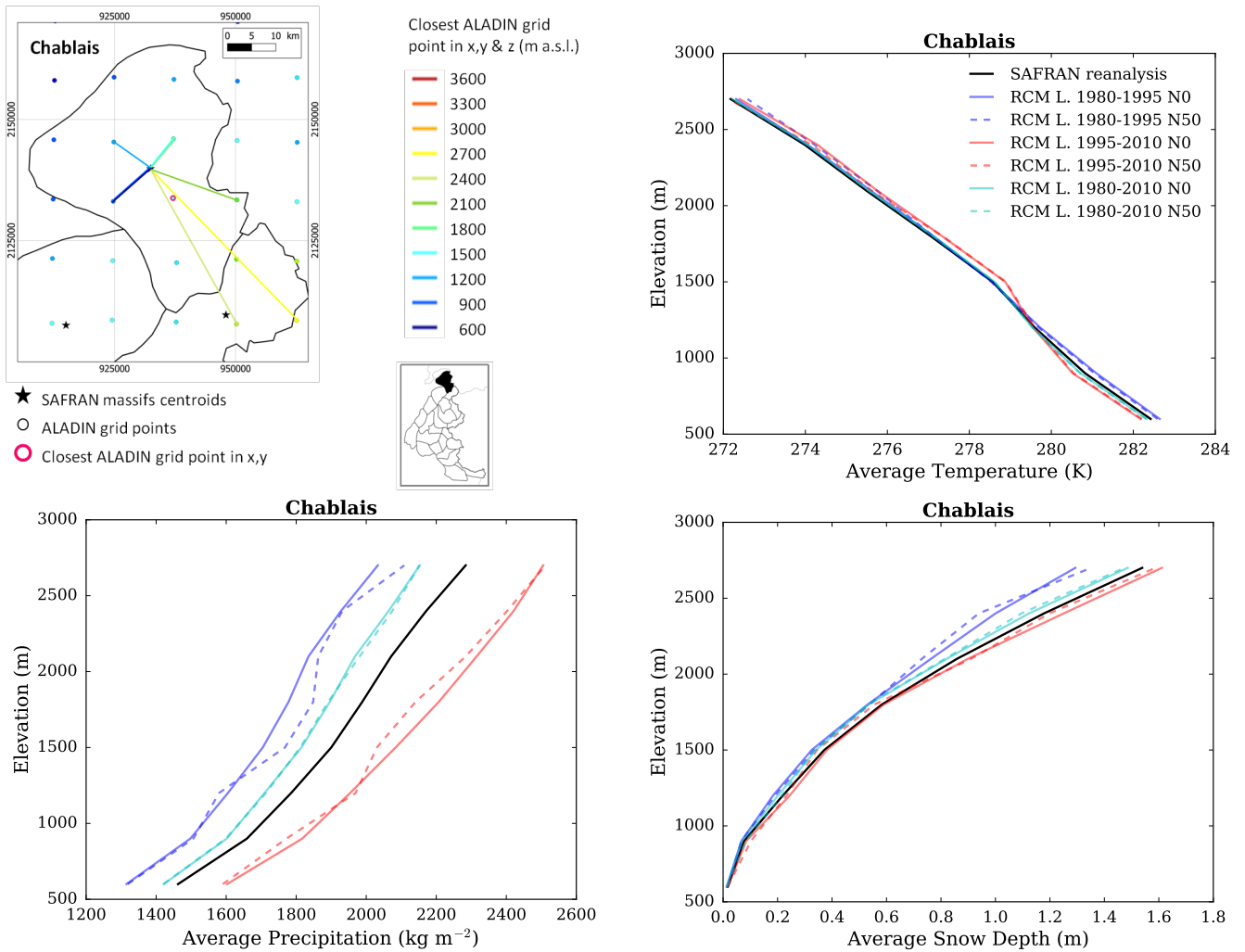


Figure S1: (top left) Location of the Chablais massif, with ALADIN RCM grid points chosen as the closest in x, y ($N = 0$, pink contour) and in x, y and z (using $N \neq 0$). Coloured lines link each SAFRAN massif centre point with the corresponding grid point in ALADIN for the different elevations considered (in m above sea level (a.s.l.)). (top right) Mean temperature, (bottom left) precipitation and (bottom right) snow depth (using Crocus in this case) for each elevation band for the Chablais massif, over the evaluation period in each adjusted RCM simulation (different learning periods and 2 neighbour selection methods) and in SAFRAN (1980-2010).

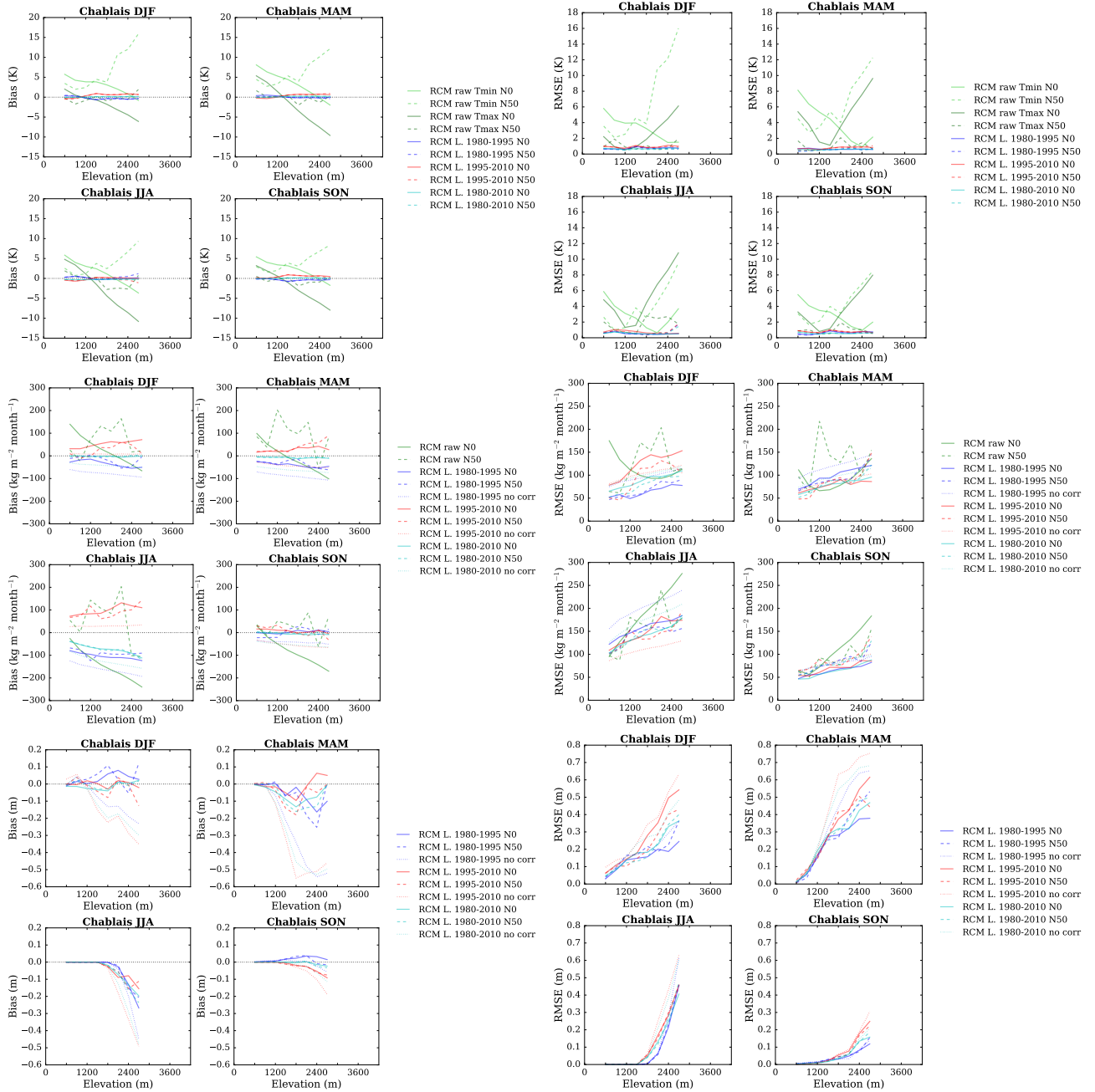


Figure S2: (top) Temperature, (middle) precipitation and (bottom) snow depth (using Crocus in this case) mean bias and root mean square error of each raw and adjusted RCM simulation compared to the SAFRAN reanalysis over the evaluation period for the Chablais massif as a function of elevation. Scores computed for the raw RCM simulations concern minimum and maximum daily temperatures.

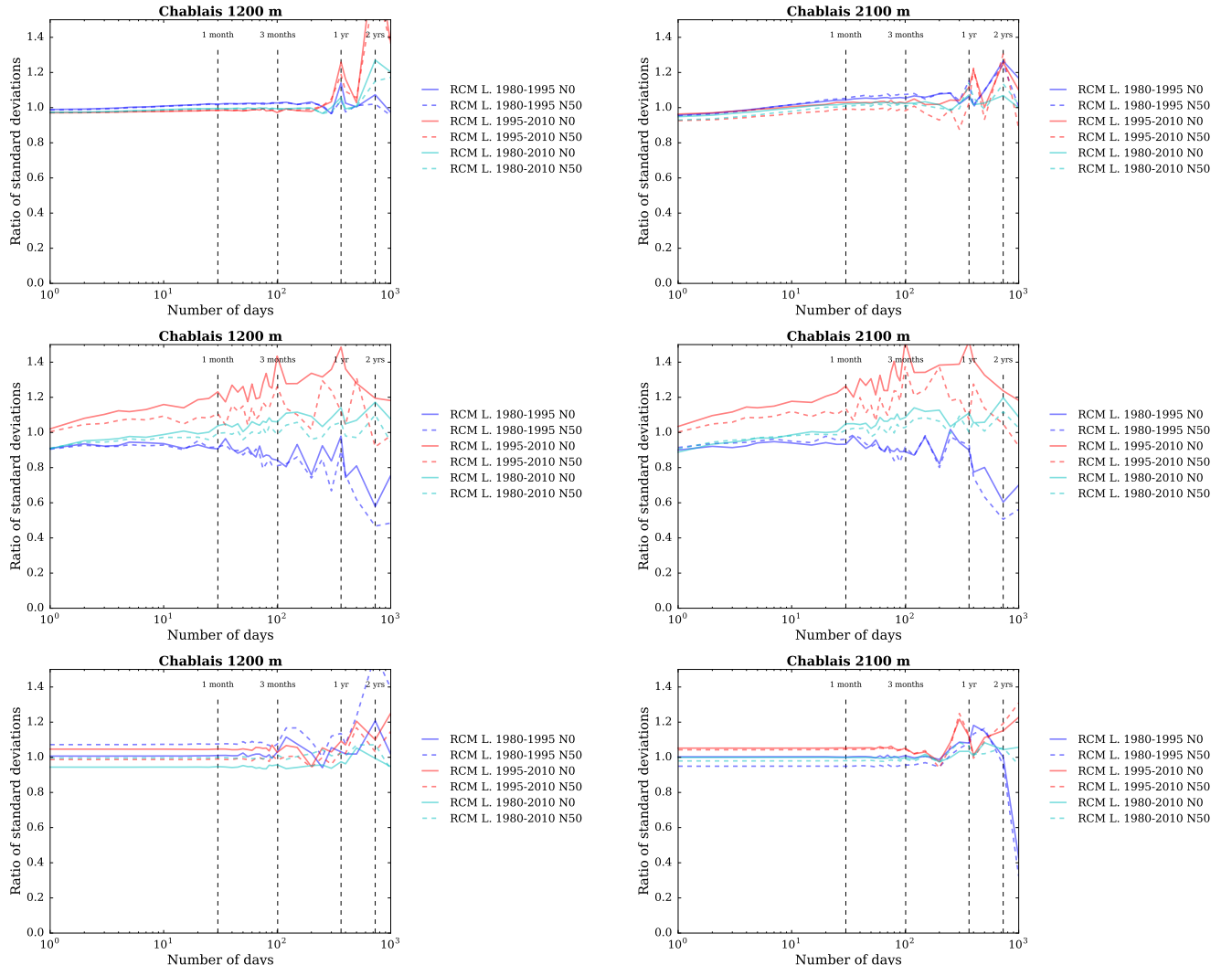


Figure S3: Ratios of standard deviations between the SAFRAN reanalysis and adjusted RCM (top) temperature, (middle) precipitation and (bottom) snow depth (using Crocus in this case) as a function of the integration window over the evaluation period, for the Chablais massif, at (left) 1200 m a.s.l. and (right) 2100 m a.s.l..

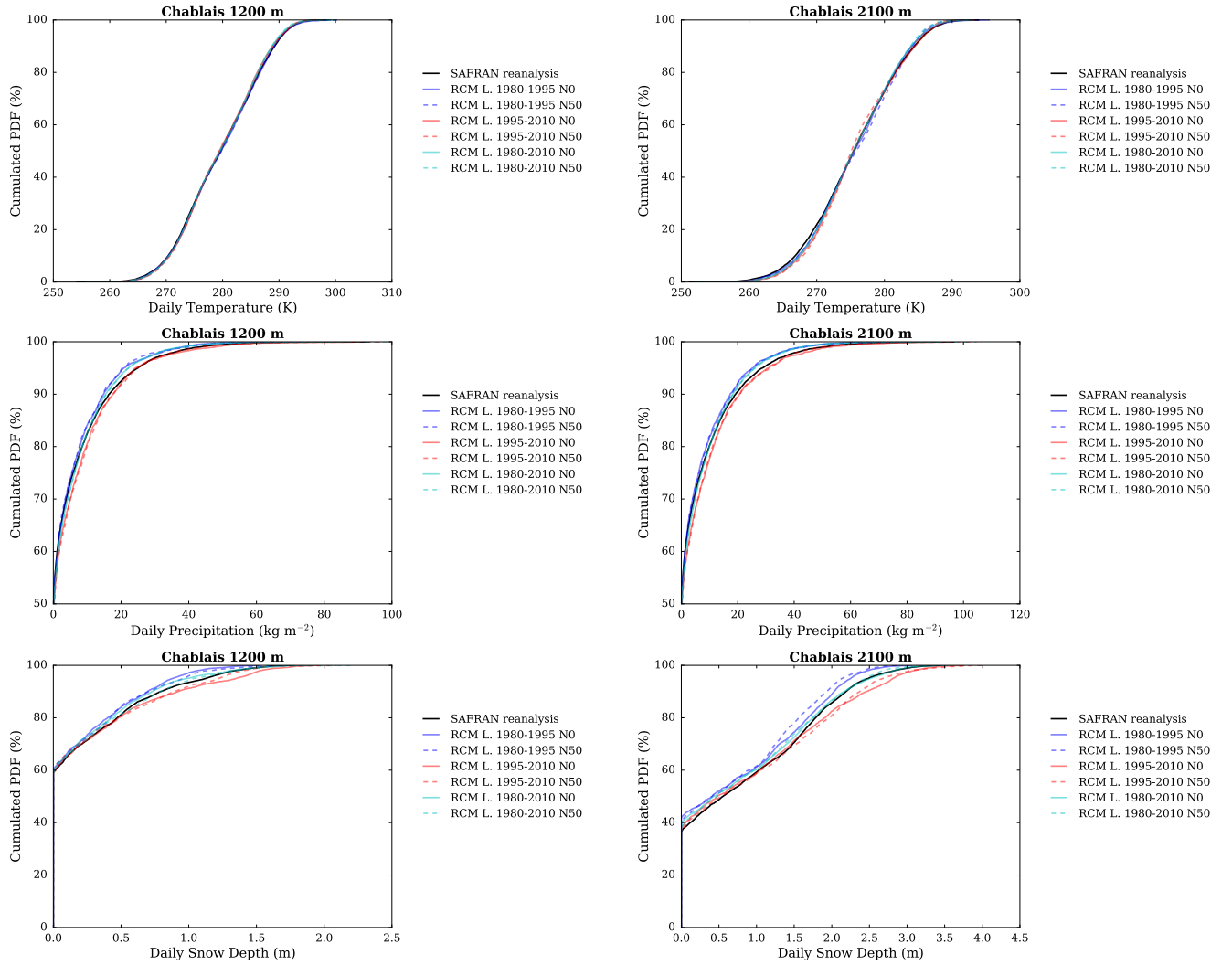


Figure S4: Cumulated probability density functions (PDFs) of daily (top) temperature, (middle) precipitation and (bottom) snow depth (using Crocus in this case) in each adjusted RCM simulation and in the SAFRAN reanalysis (1980-2010) over the evaluation period, for the Chablais massif, at (left) 1200 m a.s.l. and (right) 2100 m a.s.l..

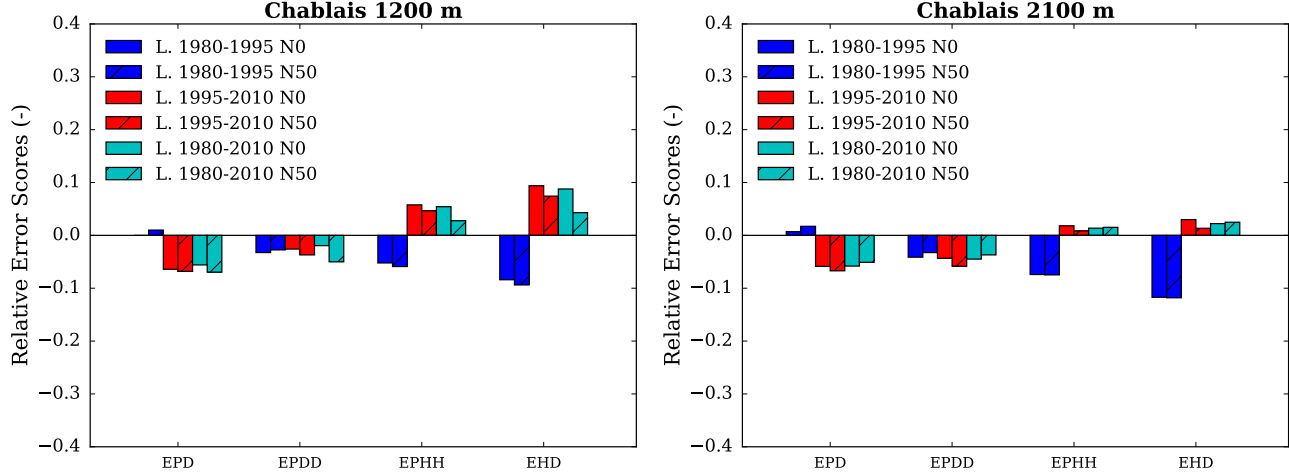


Figure S5: Scores for the duration and persistence of precipitation events in each adjusted RCM simulation compared to the SAFRAN reanalysis over the evaluation period, for the Chablais massif, at (left) 1200 m a.s.l. and (right) 2100 m a.s.l.. EPD = relative error on the probability of a dry day, EPDD = relative error on the probability of a dry day following a dry day, EPHH = relative error on the probability of a wet day following a wet day, EHD = relative error on the mean duration of wet periods.

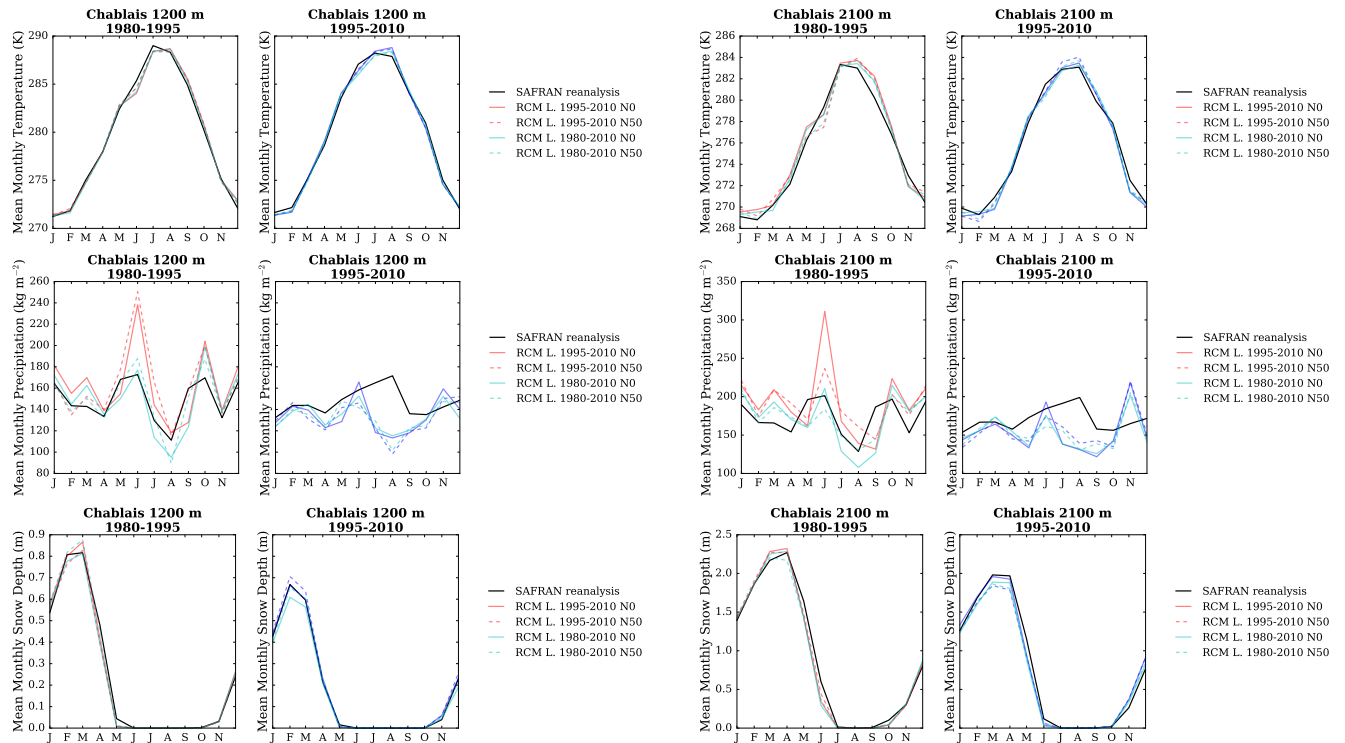


Figure S6: (top) Temperature, (middle) precipitation and (bottom) snow depth (using Crocus in this case) mean annual cycle in each adjusted RCM simulation and in the SAFRAN reanalysis over the period 1980-1995 and 1995-2010, for the Chablais massif, and at (left) 1200 m a.s.l. and (right) 2100 m a.s.l.. Letters on the x-axis correspond to the different months of the calendar (J = January, F = February, etc.).

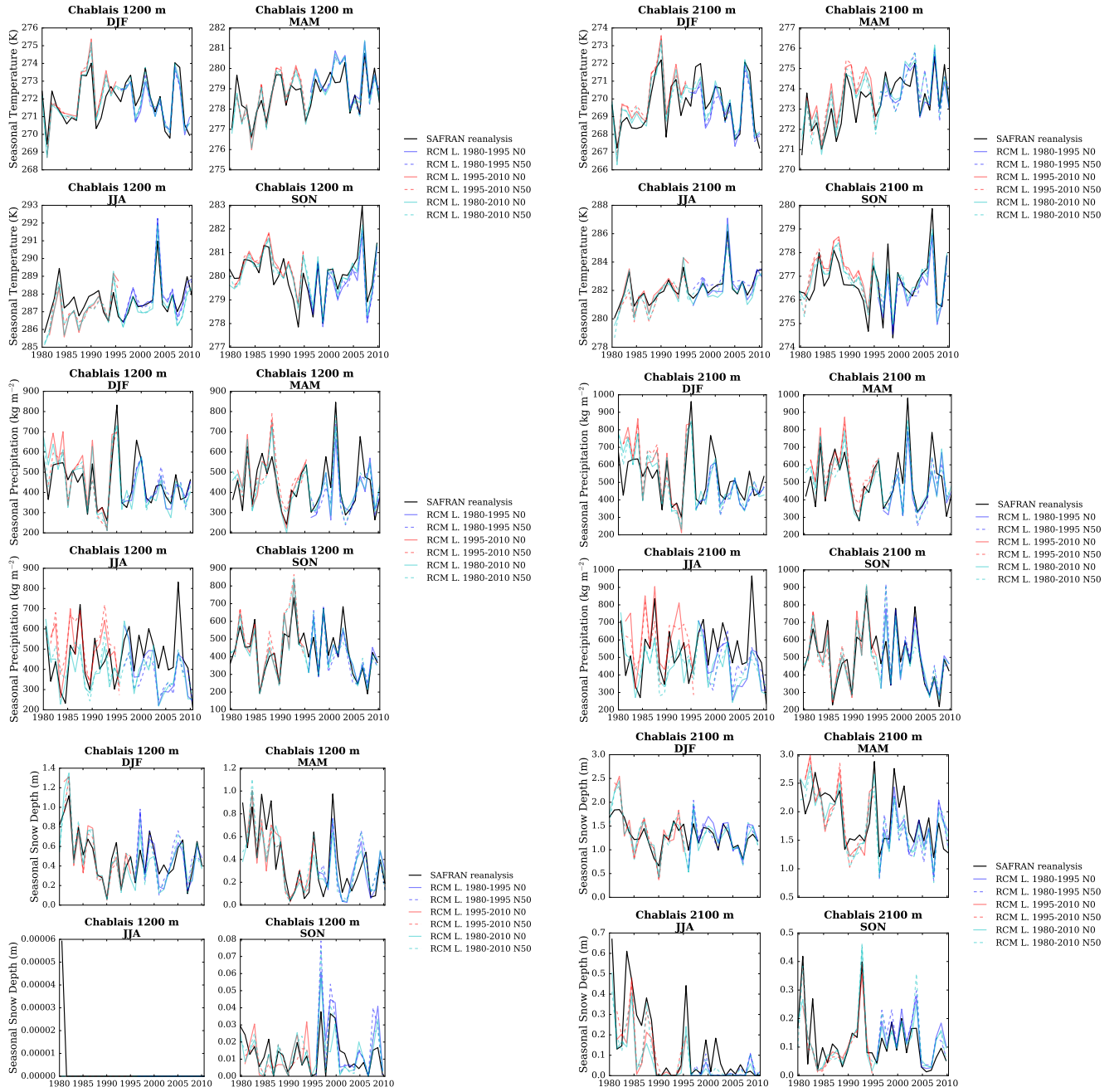


Figure S7: (top) Temperature, (middle) precipitation and (bottom) snow depth (using Crocus in this case) seasonal average time series from 1980 to 2010 in each adjusted RCM simulation and in the SAFRAN reanalysis, for the Chablais massif, and at (left) 1200 m a.s.l. and (right) 2100 m a.s.l..

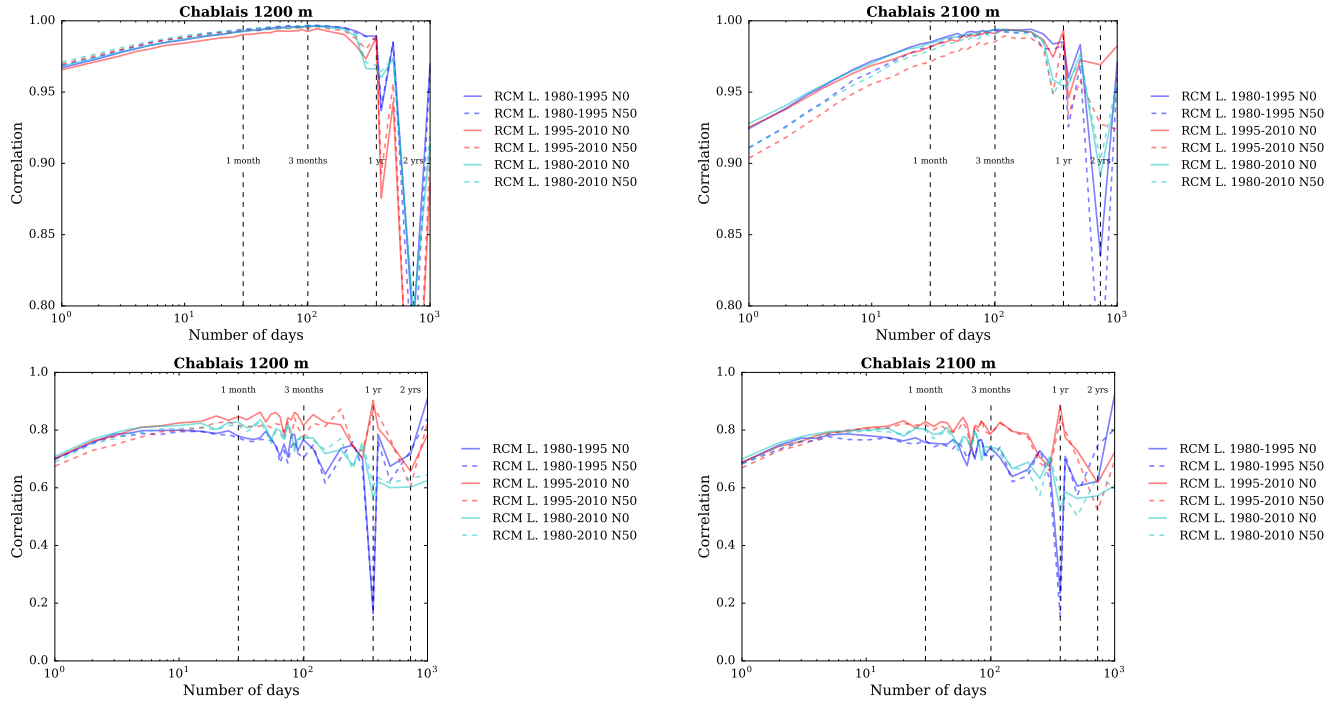


Figure S8: Correlation between the SAFRAN reanalysis and adjusted RCM (top) temperature and (bottom) precipitation as a function of the integration window over the evaluation period, for the Chablais massif, and at (left) 1200 m a.s.l. and (right) 2100 m a.s.l..

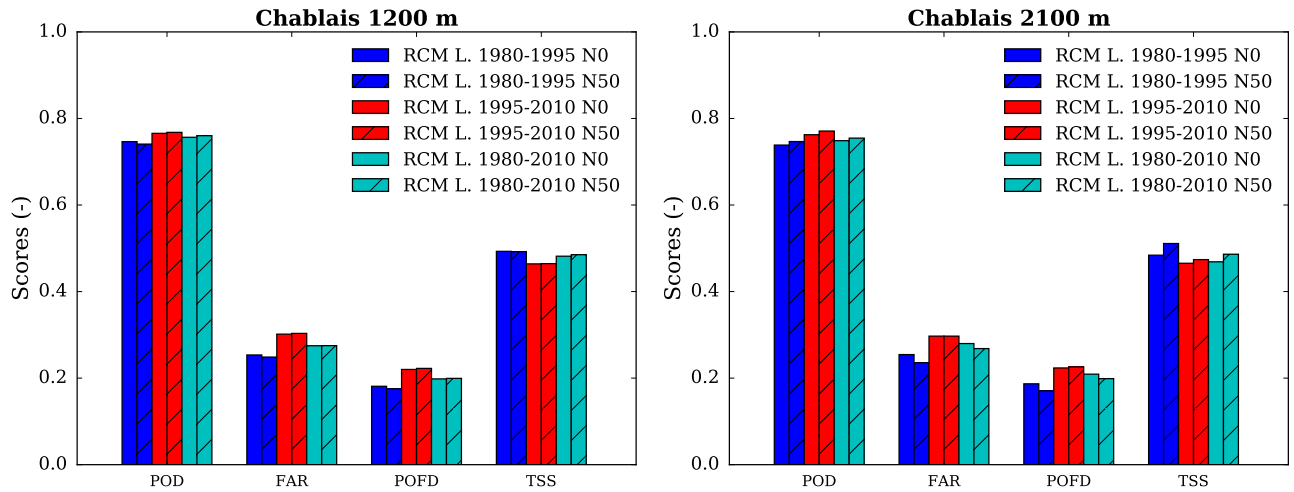


Figure S9: Scores for the detection of precipitation events in each adjusted RCM simulation compared to the SAFRAN reanalysis over the evaluation period, for the Chablais massif, at (left) 1200 m a.s.l. and (right) 2100 m a.s.l.. POD = probability of detection, FAR = false alarm rate, POFD = probability of false detection, TSS = true skill score.

Aravis

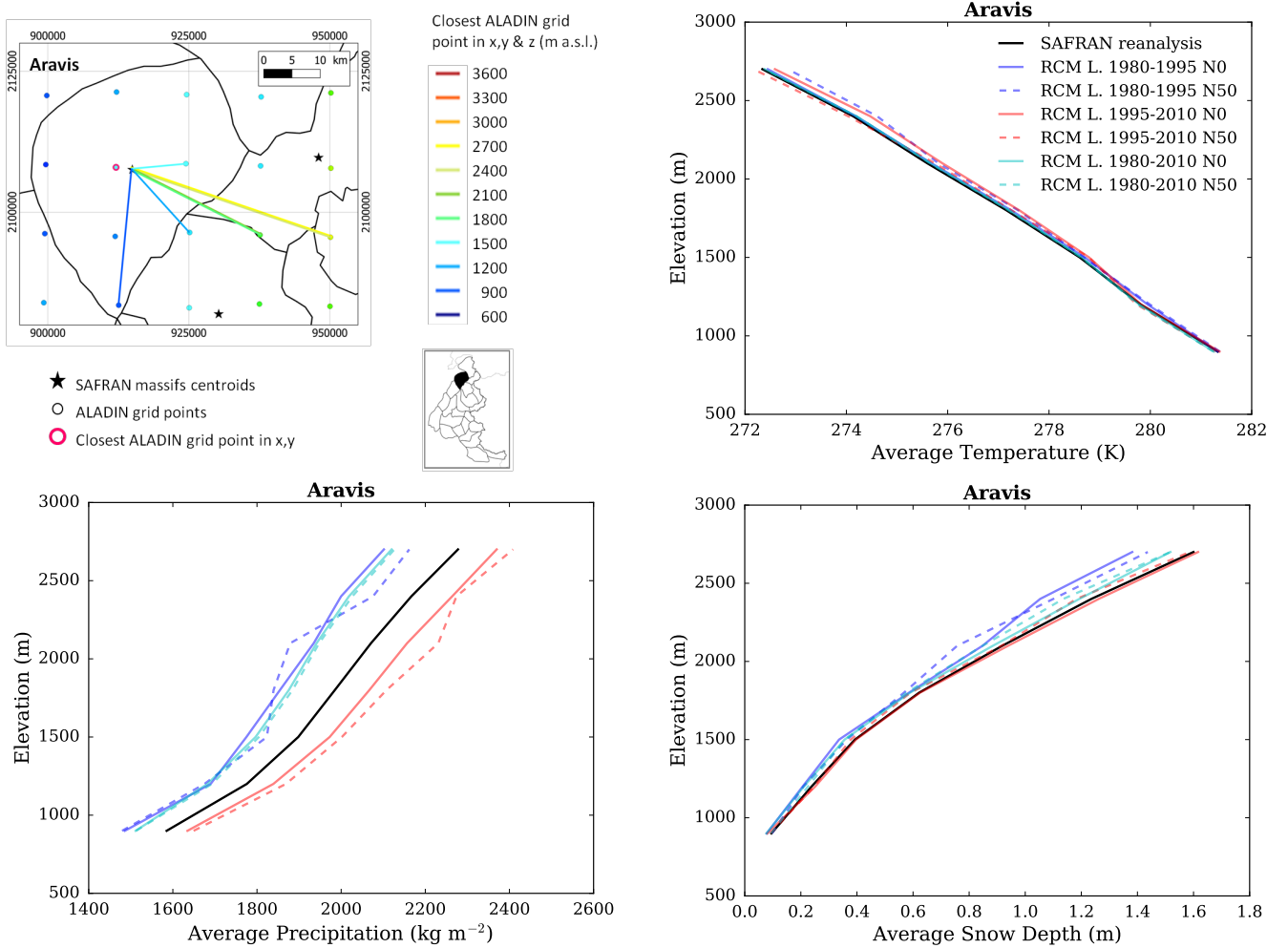


Figure S10: (top left) Location of the Aravis massif, with ALADIN RCM grid points chosen as the closest in x, y ($N = 0$, pink contour) and in x, y and z (using $N \neq 0$). Coloured lines link each SAFRAN massif centre point with the corresponding grid point in ALADIN for the different elevations considered (in m above sea level (a.s.l.)). (top right) Mean temperature, (bottom left) precipitation and (bottom right) snow depth (using Crocus in this case) for each elevation band for the Aravis massif, over the evaluation period in each adjusted RCM simulation (different learning periods and 2 neighbour selection methods) and in SAFRAN (1980-2010).

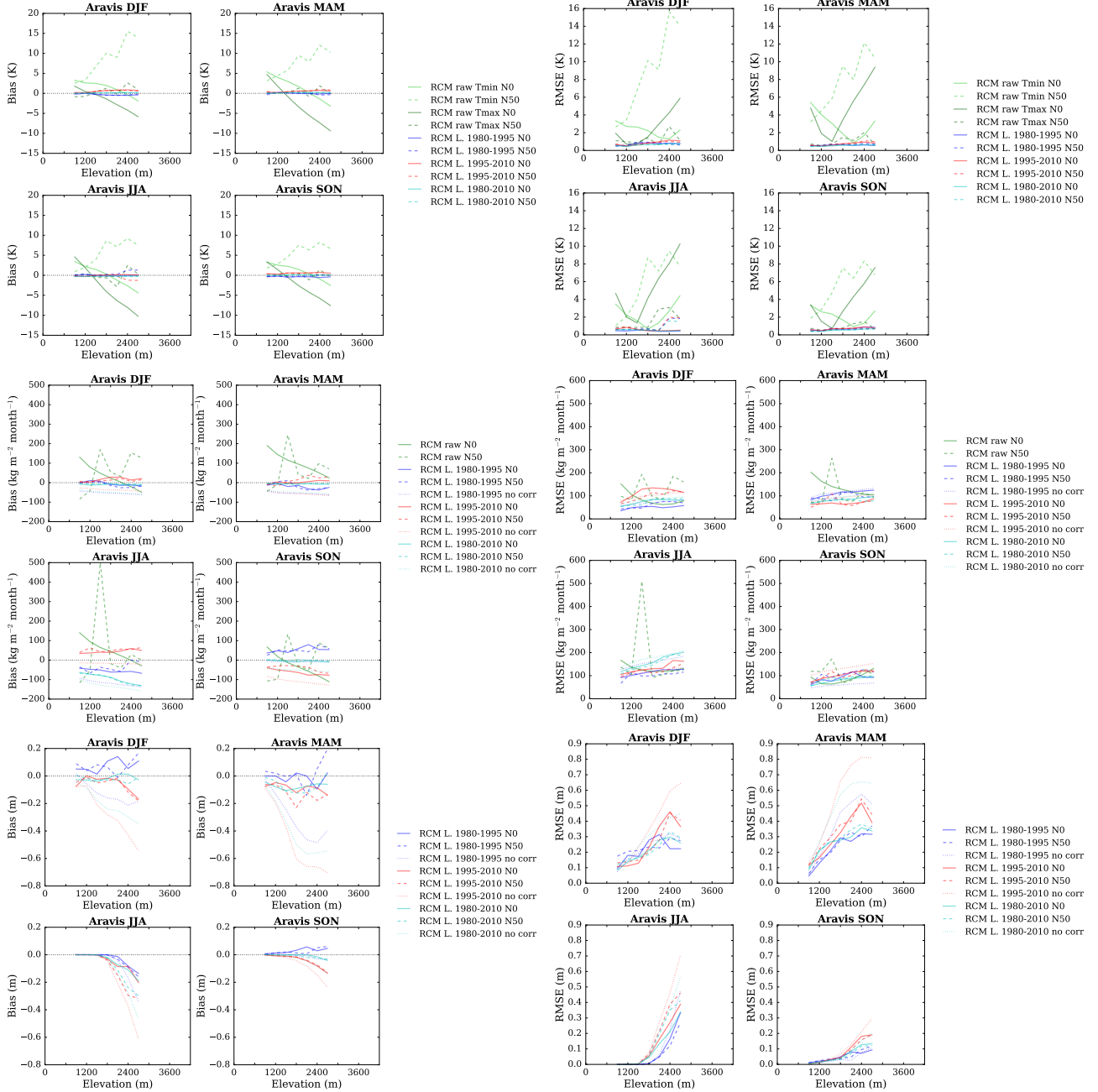


Figure S11: (top) Temperature, (middle) precipitation and (bottom) snow depth (using Crocus in this case) mean bias and root mean square error of each raw and adjusted RCM simulation compared to the SAFRAN reanalysis over the evaluation period for the Aravis massif as a function of elevation. Scores computed for the raw RCM simulations concern minimum and maximum daily temperatures.

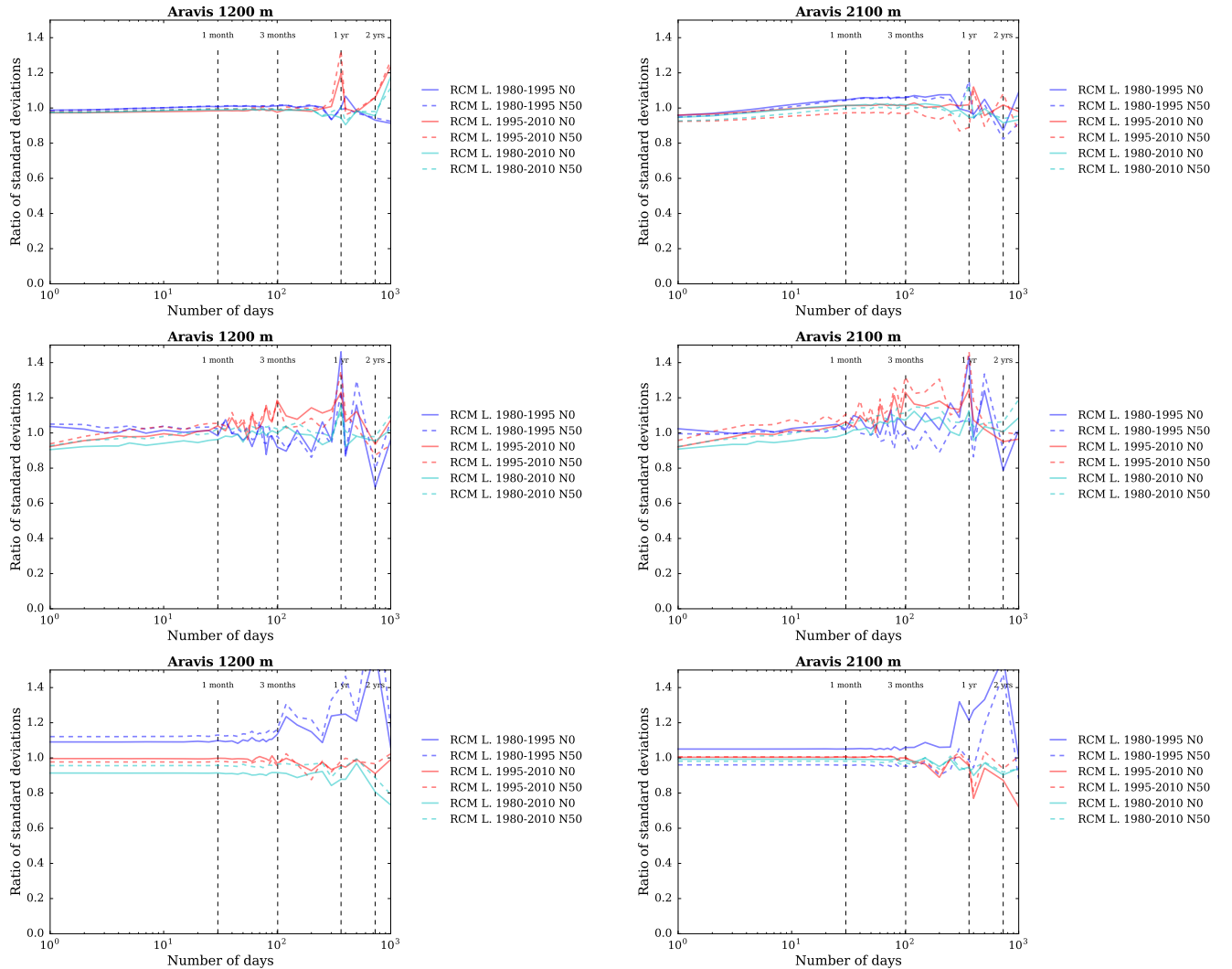


Figure S12: Ratios of standard deviations between the SAFRAN ranalysis and adjusted RCM (top) temperature, (middle) precipitation and (bottom) snow depth (using Crocus in this case) as a function of the integration window over the evaluation period, for the Aravis massif, at (left) 1200 m a.s.l. and (right) 2100 m a.s.l..

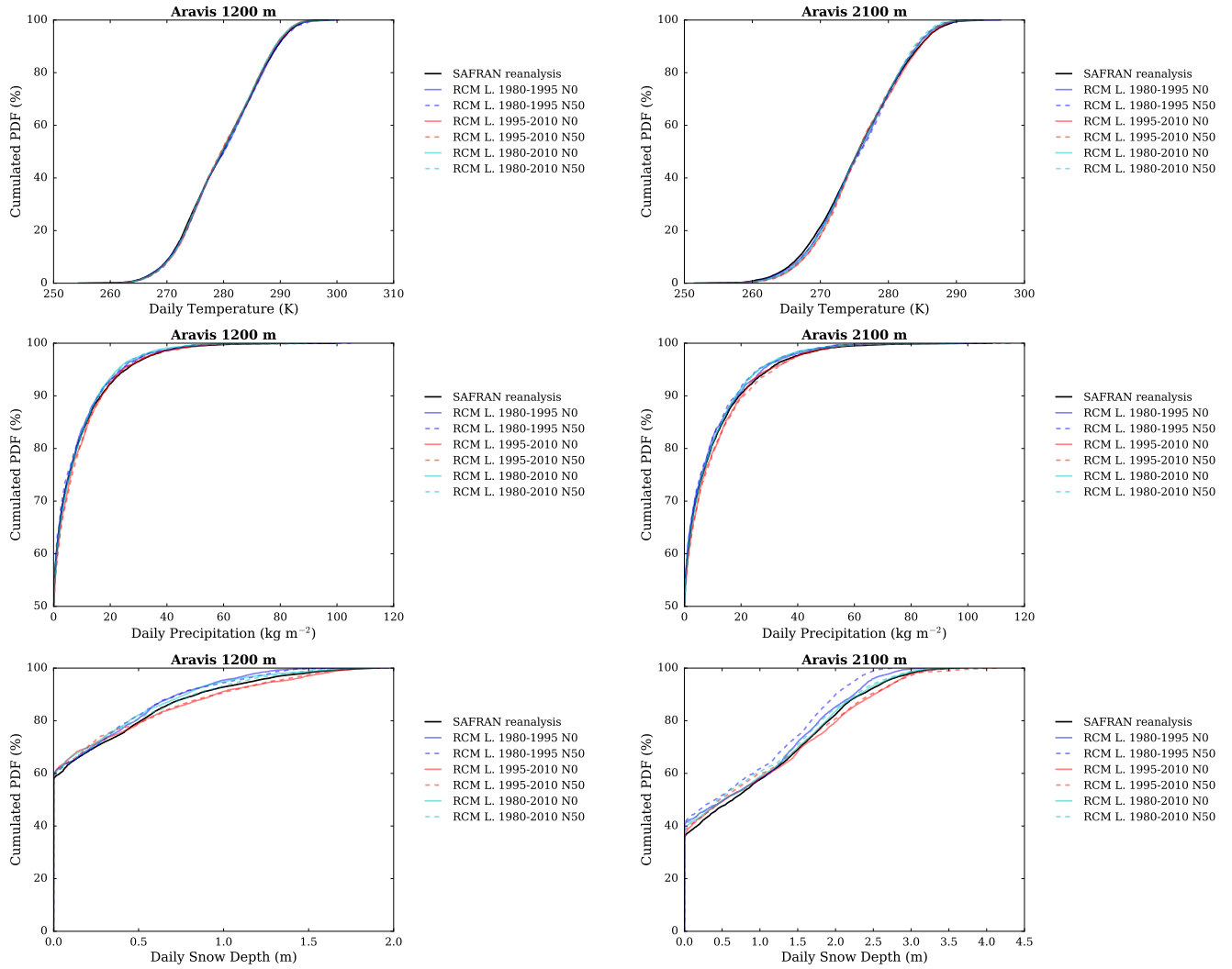


Figure S13: Cumulated probability density functions (PDFs) of daily (top) temperature, (middle) precipitation and (bottom) snow depth (using Crocus in this case) in each adjusted RCM simulation and in the SAFRAN reanalysis (1980-2010) over the evaluation period, for the Aravis massif, at (left) 1200 m a.s.l. and (right) 2100 m a.s.l..

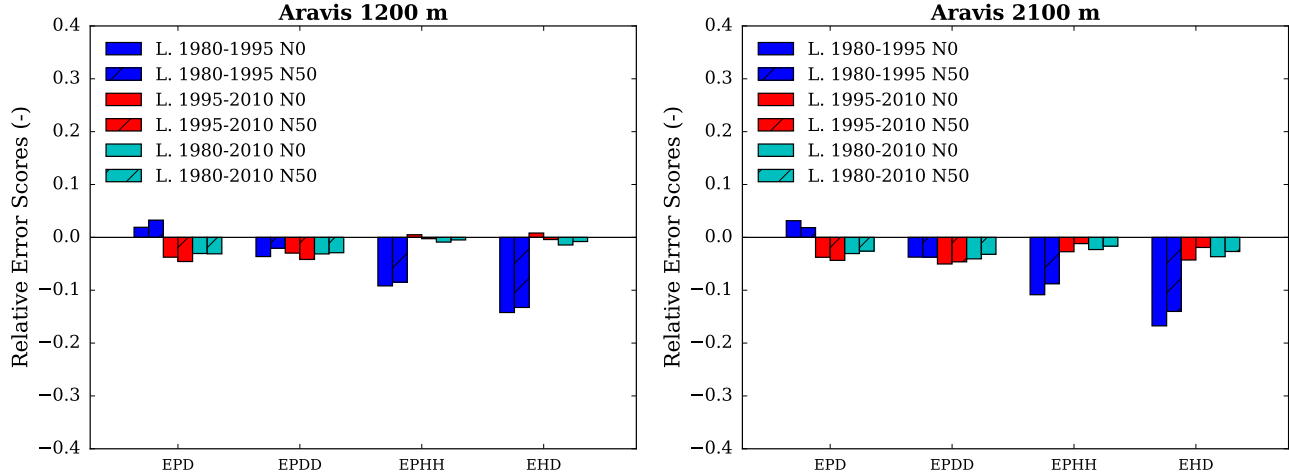


Figure S14: Scores for the duration and persistence of precipitation events in each adjusted RCM simulation compared to the SAFRAN reanalysis over the evaluation period, for the Aravis massif, at (left) 1200 m a.s.l. and (right) 2100 m a.s.l.. EPD = relative error on the probability of a dry day, EPDD = relative error on the probability of a dry day following a dry day, EPHH = relative error on the probability of a wet day following a wet day, EHD = relative error on the mean duration of wet periods.

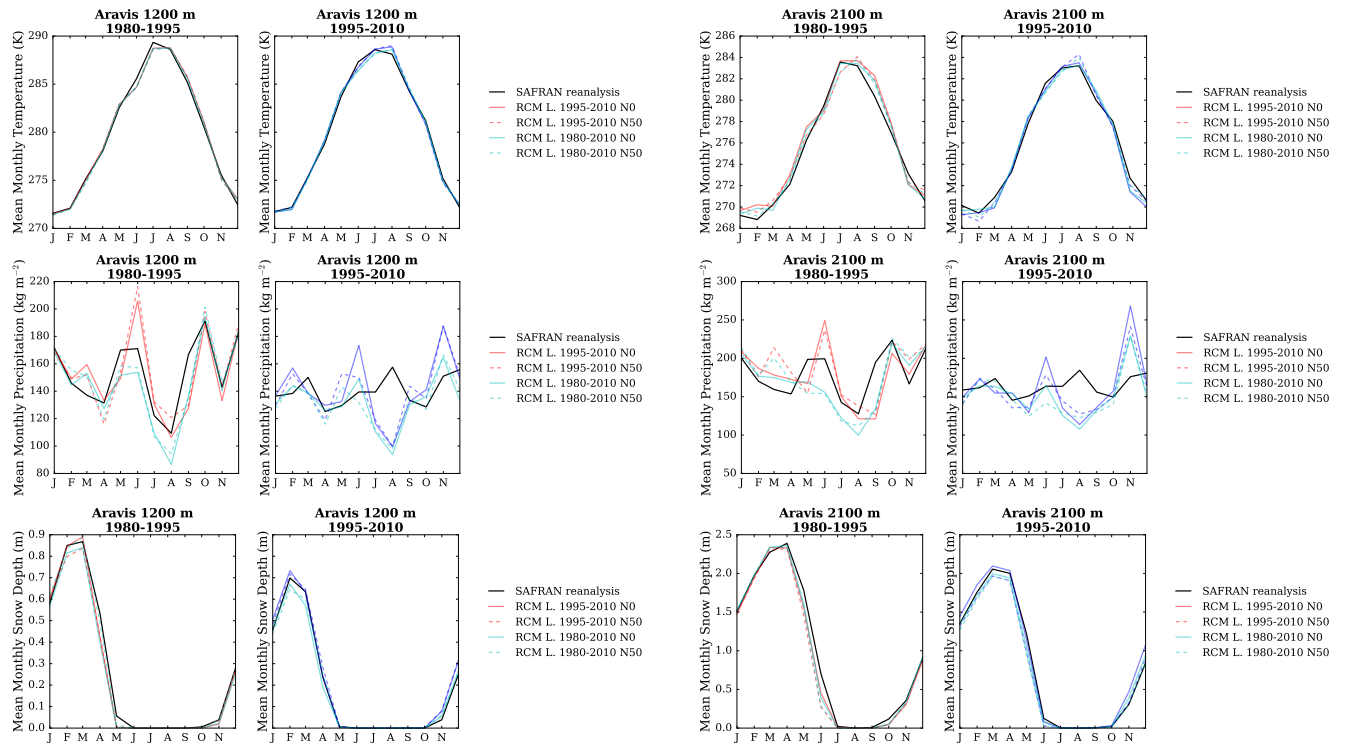


Figure S15: (top) Temperature, (middle) precipitation and (bottom) snow depth (using Crocus in this case) mean annual cycle in each adjusted RCM simulation and in the SAFRAN reanalysis over the period 1980-1995 and 1995-2010, for the Aravis massif, and at (left) 1200 m a.s.l. and (right) 2100 m a.s.l.. Letters on the x-axis correspond to the different months of the calendar (J = January, F = February, etc.).

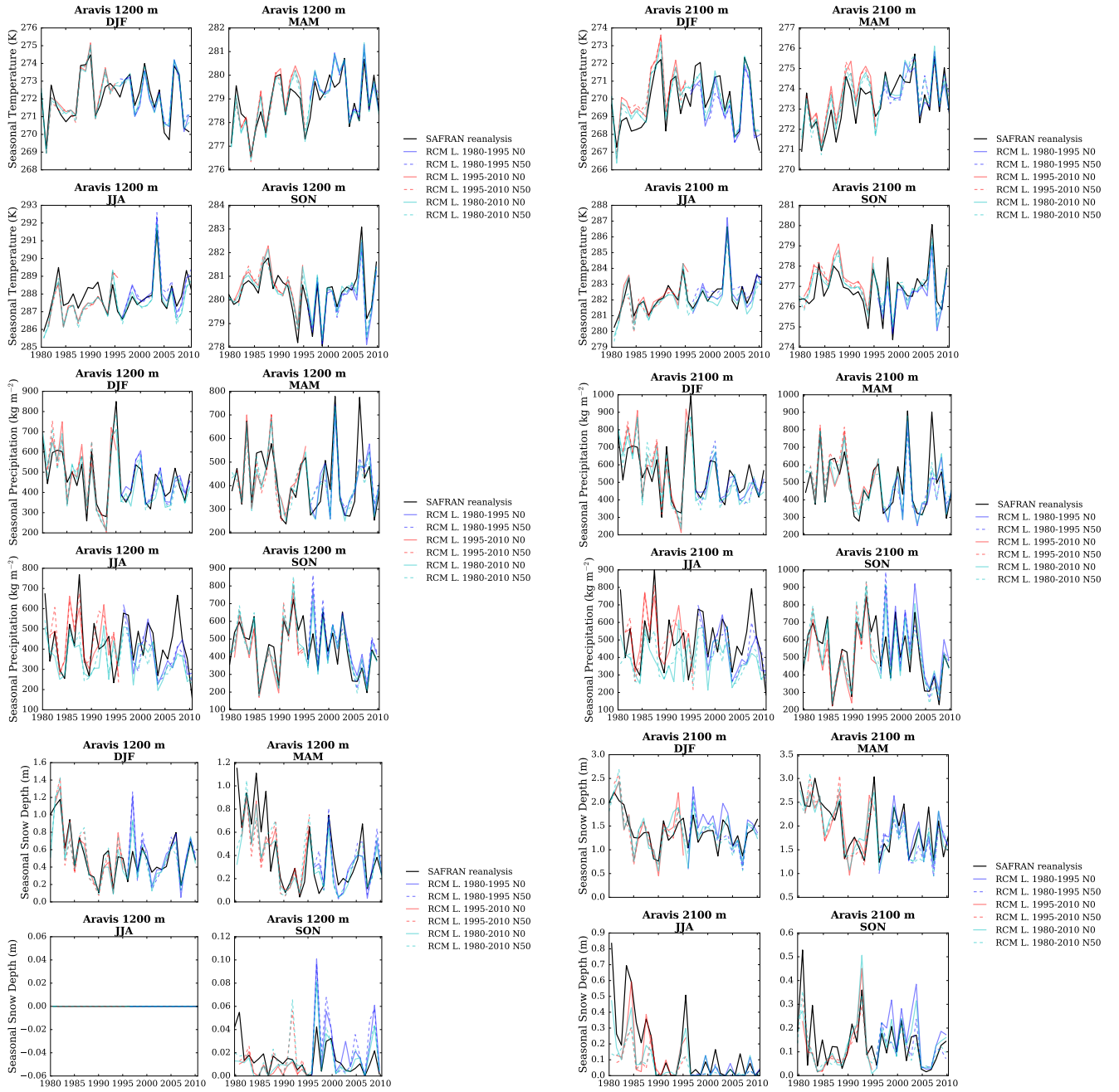


Figure S16: (top) Temperature, (middle) precipitation and (bottom) snow depth (using Crocus in this case) seasonal average time series from 1980 to 2010 in each adjusted RCM simulation and in the SAFRAN reanalysis, for the Aravis massif, and at (left) 1200 m a.s.l. and (right) 2100 m a.s.l..

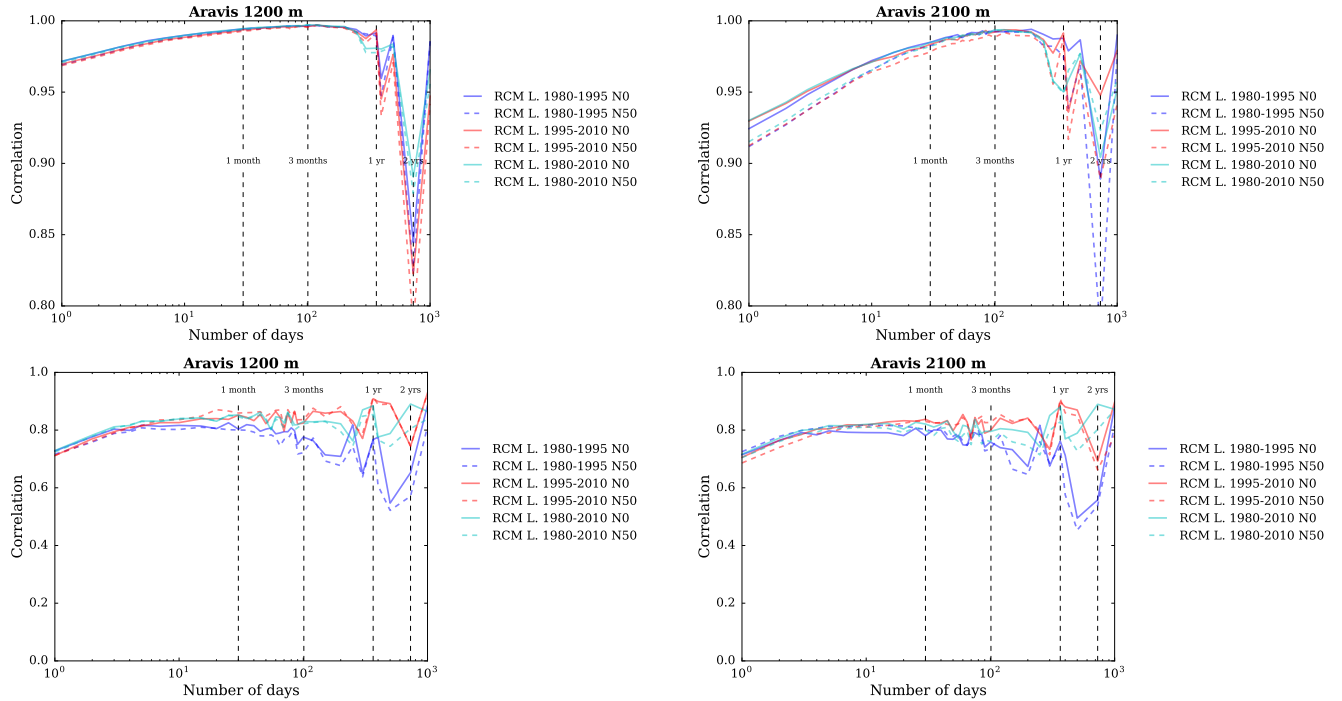


Figure S17: Correlation between the SAFRAN reanalysis and adjusted RCM (top) temperature and (bottom) precipitation as a function of the integration window over the evaluation period, for the Aravis massif, and at (left) 1200 m a.s.l. and (right) 2100 m a.s.l..

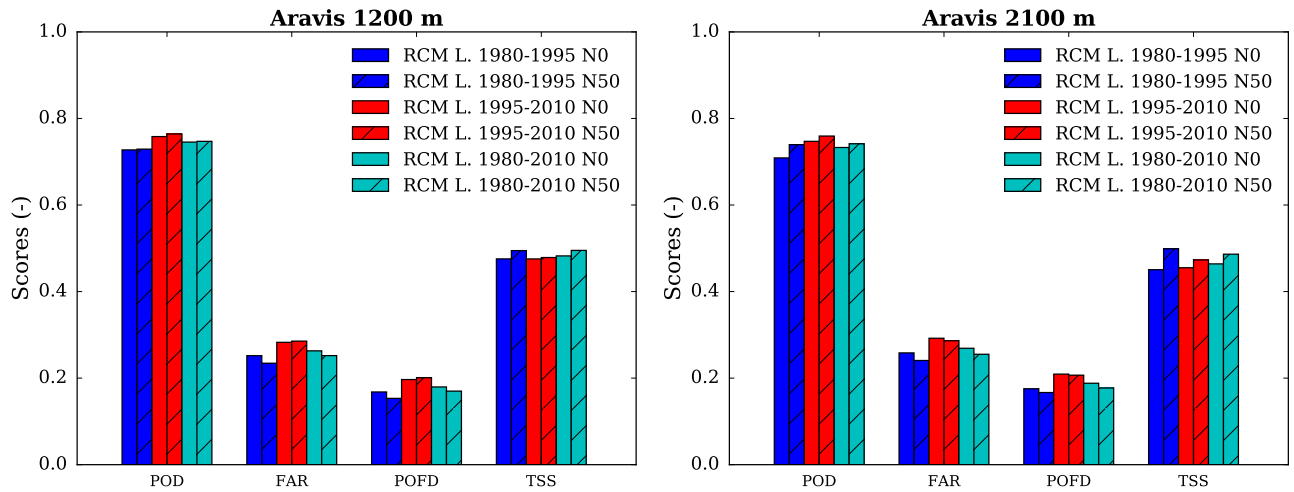


Figure S18: Scores for the detection of precipitation events in each adjusted RCM simulation compared to the SAFRAN reanalysis over the evaluation period, for the Aravis massif, at (left) 1200 m a.s.l. and (right) 2100 m a.s.l.. POD = probability of detection, FAR = false alarm rate, POFD = probability of false detection, TSS = true skill score.

Mont Blanc

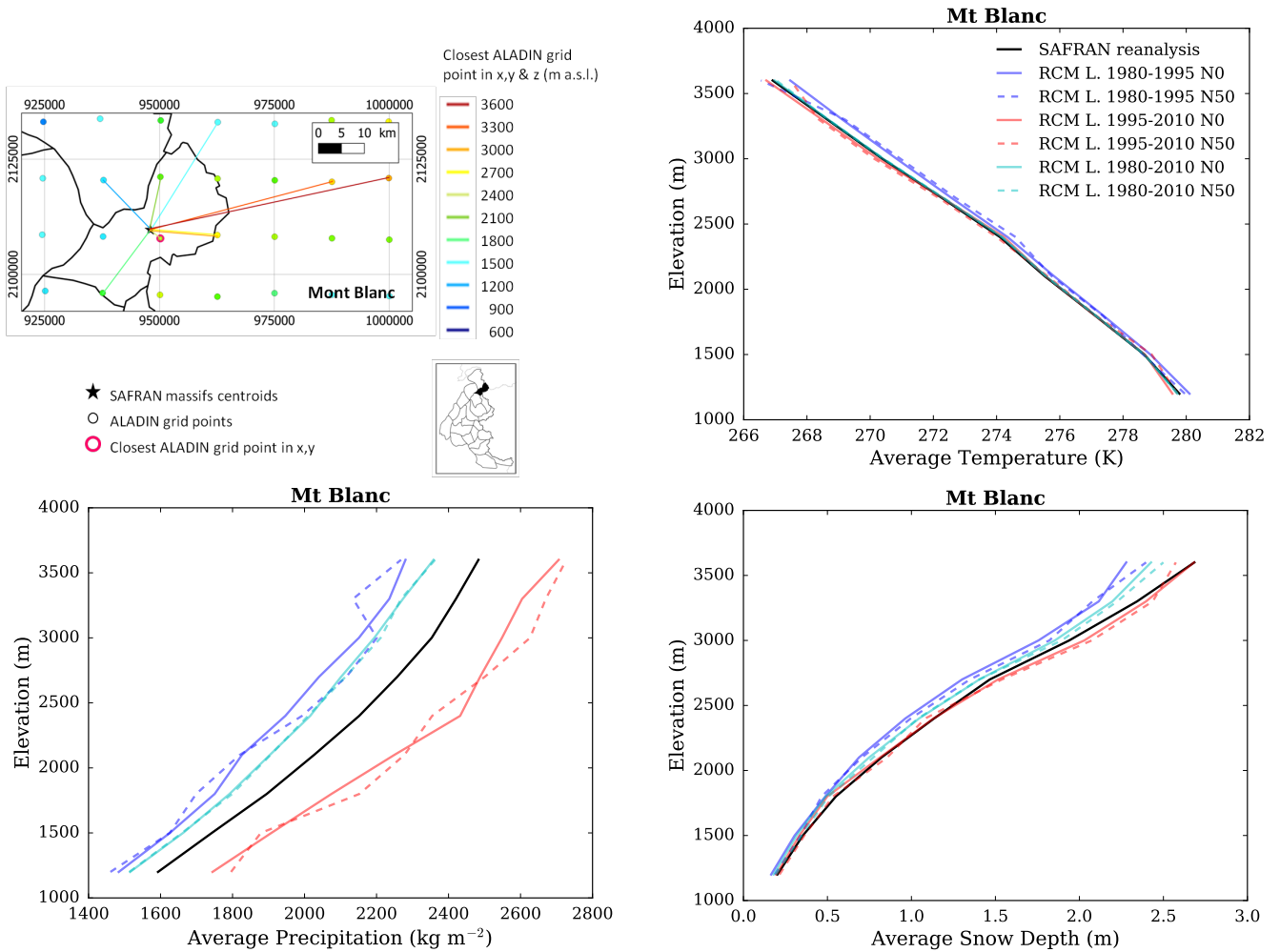


Figure S19: (top left) Location of the Mont Blanc massif, with ALADIN RCM grid points chosen as the closest in x, y ($N = 0$, pink contour) and in x, y and z (using $N \neq 0$). Coloured lines link each SAFRAN massif centre point with the corresponding grid point in ALADIN for the different elevations considered (in m above sea level (a.s.l.)). (top right) Mean temperature, (bottom left) precipitation and (bottom right) snow depth (using Crocus in this case) for each elevation band for the Mont Blanc massif, over the evaluation period in each adjusted RCM simulation (different learning periods and 2 neighbour selection methods) and in SAFRAN (1980-2010).

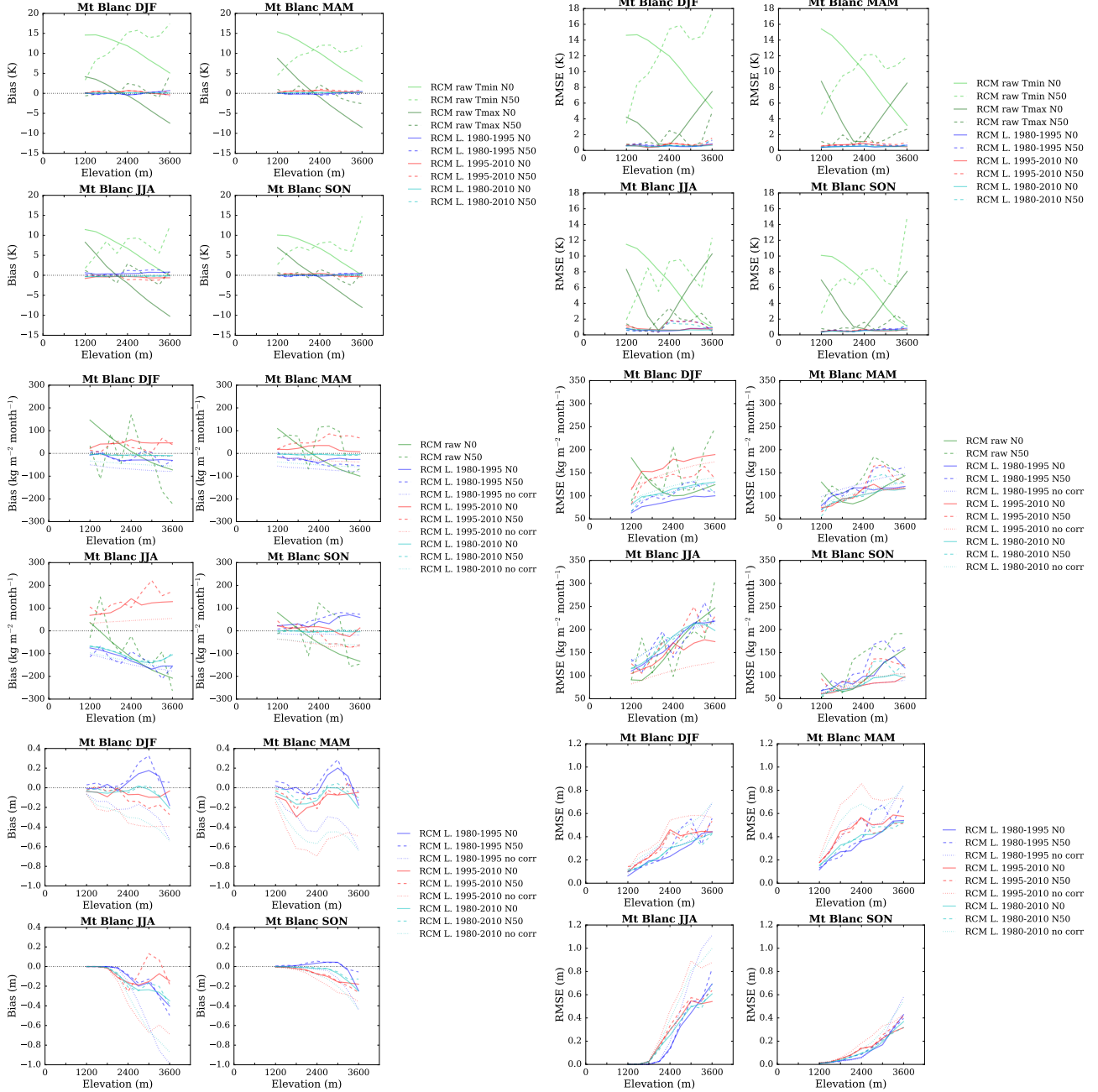


Figure S20: (top) Temperature, (middle) precipitation and (bottom) snow depth (using Crocus in this case) mean bias and root mean square error of each raw and adjusted RCM simulation compared to the SAFRAN reanalysis over the evaluation period for the Mont Blanc massif as a function of elevation. Scores computed for the raw RCM simulations concern minimum and maximum daily temperatures.

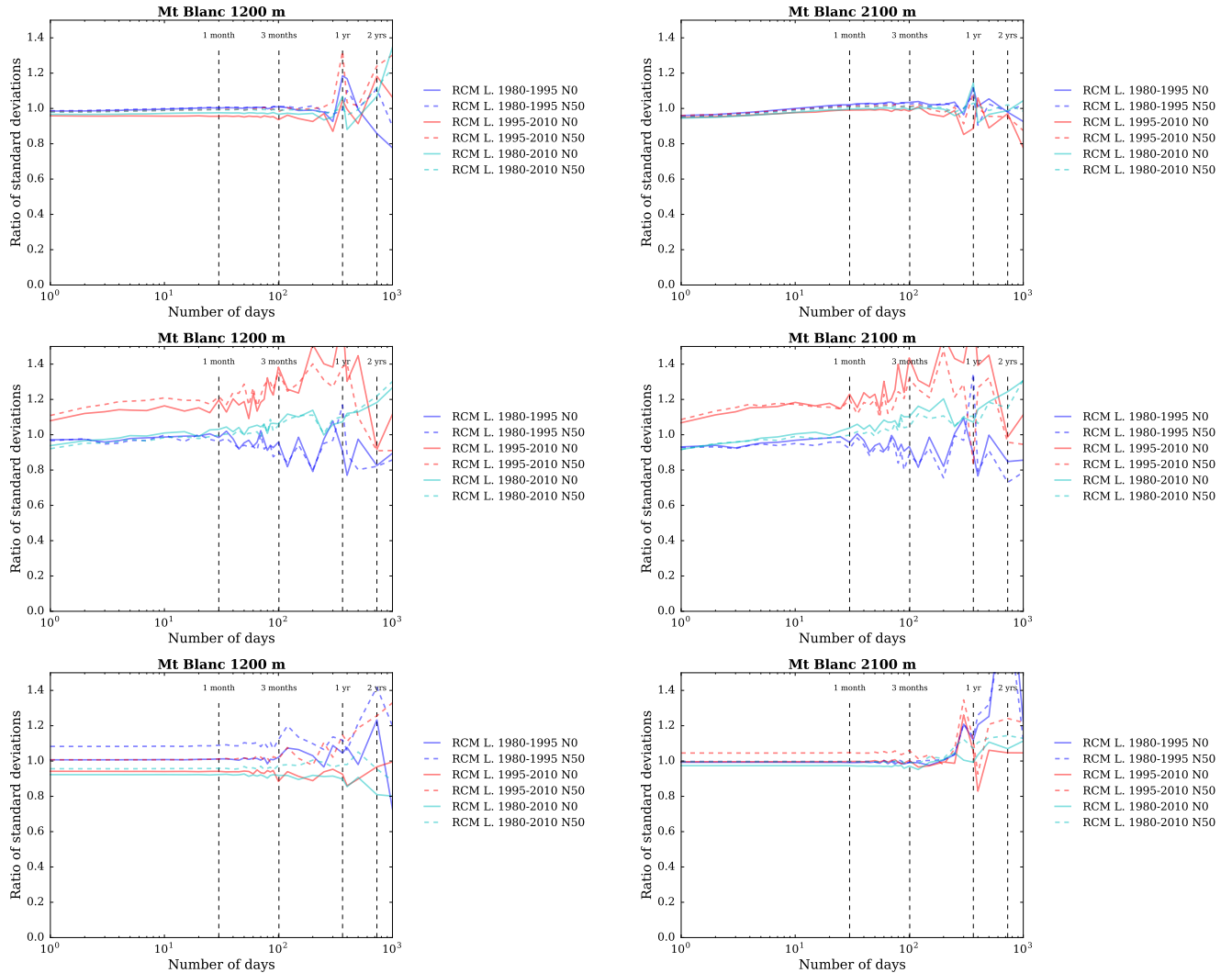


Figure S21: Ratios of standard deviations between the SAFRAN reanalysis and adjusted RCM (top) temperature, (middle) precipitation and (bottom) snow depth (using Crocus in this case) as a function of the integration window over the evaluation period, for the Mont Blanc massif, at (left) 1200 m a.s.l. and (right) 2100 m a.s.l..

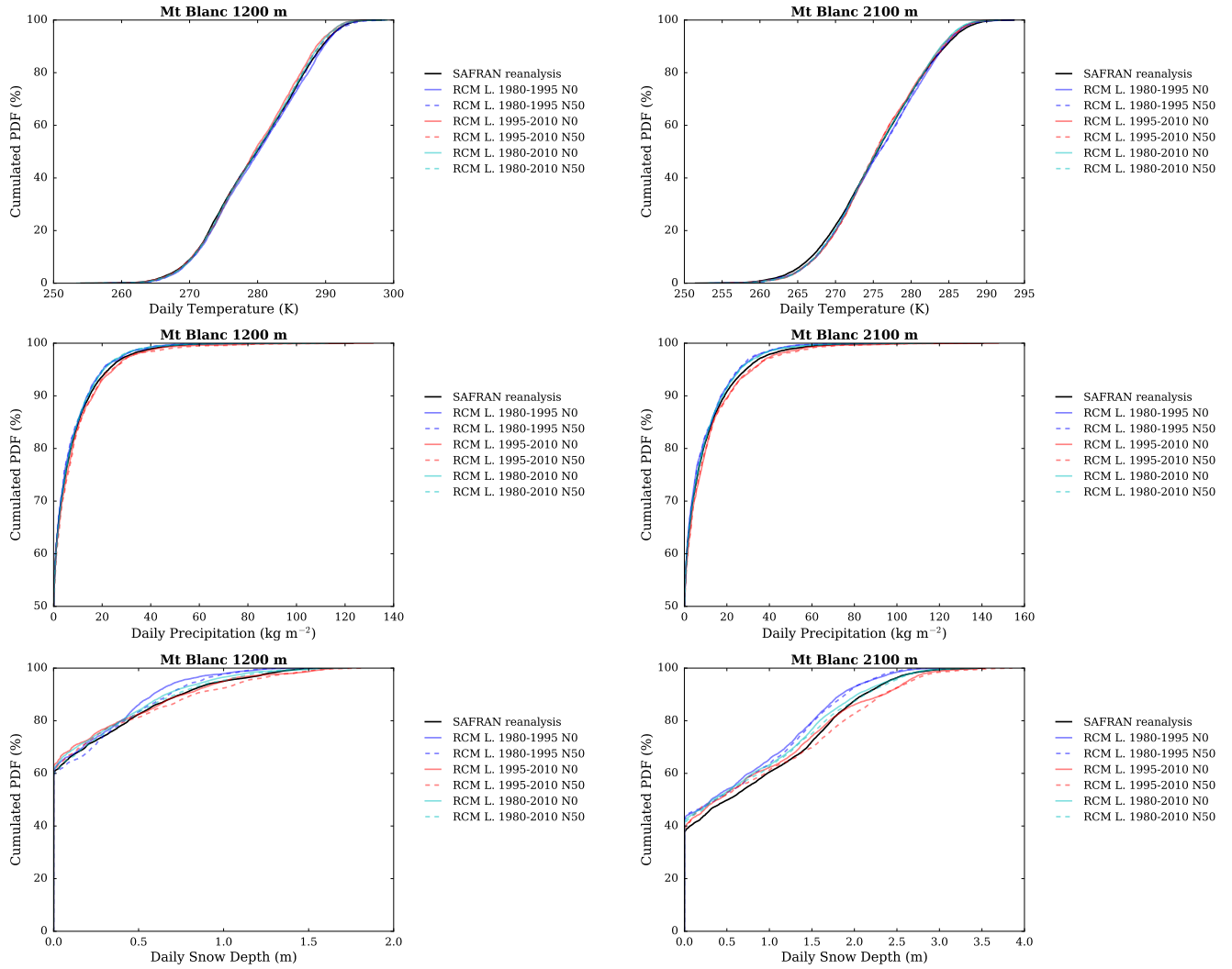


Figure S22: Cumulated probability density functions (PDFs) of daily (top) temperature, (middle) precipitation and (bottom) snow depth (using Crocus in this case) in each adjusted RCM simulation and in the SAFRAN reanalysis (1980-2010) over the evaluation period, for the Mont Blanc massif, at (left) 1200 m a.s.l. and (right) 2100 m a.s.l.

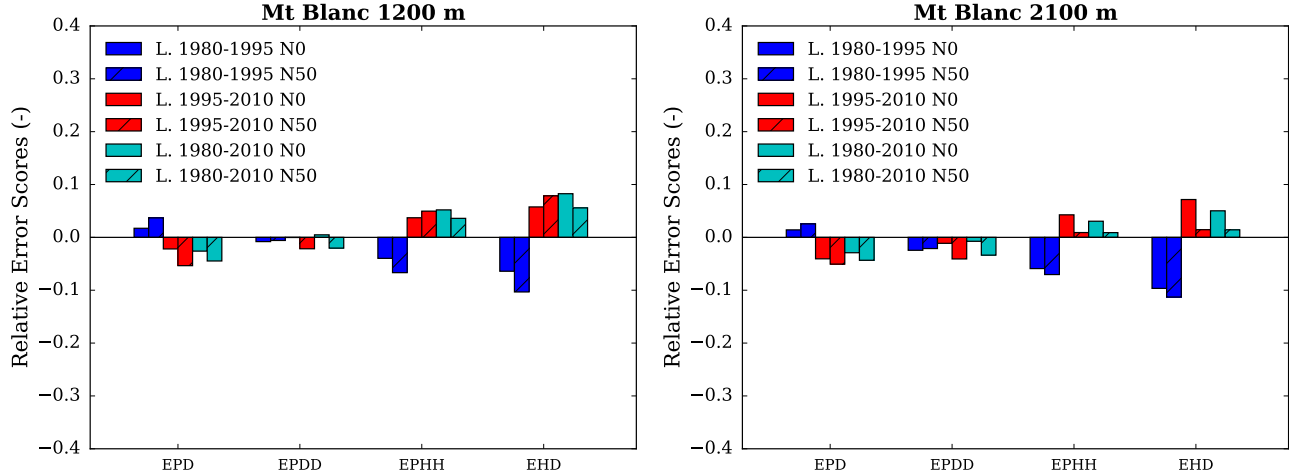


Figure S23: Scores for the duration and persistence of precipitation events in each adjusted RCM simulation compared to the SAFRAN reanalysis over the evaluation period, for the Mont Blanc massif, at (left) 1200 m a.s.l. and (right) 2100 m a.s.l.. EPD = relative error on the probability of a dry day, EPDD = relative error on the probability of a dry day following a dry day, EPHH = relative error on the probability of a wet day following a wet day, EHD = relative error on the mean duration of wet periods.

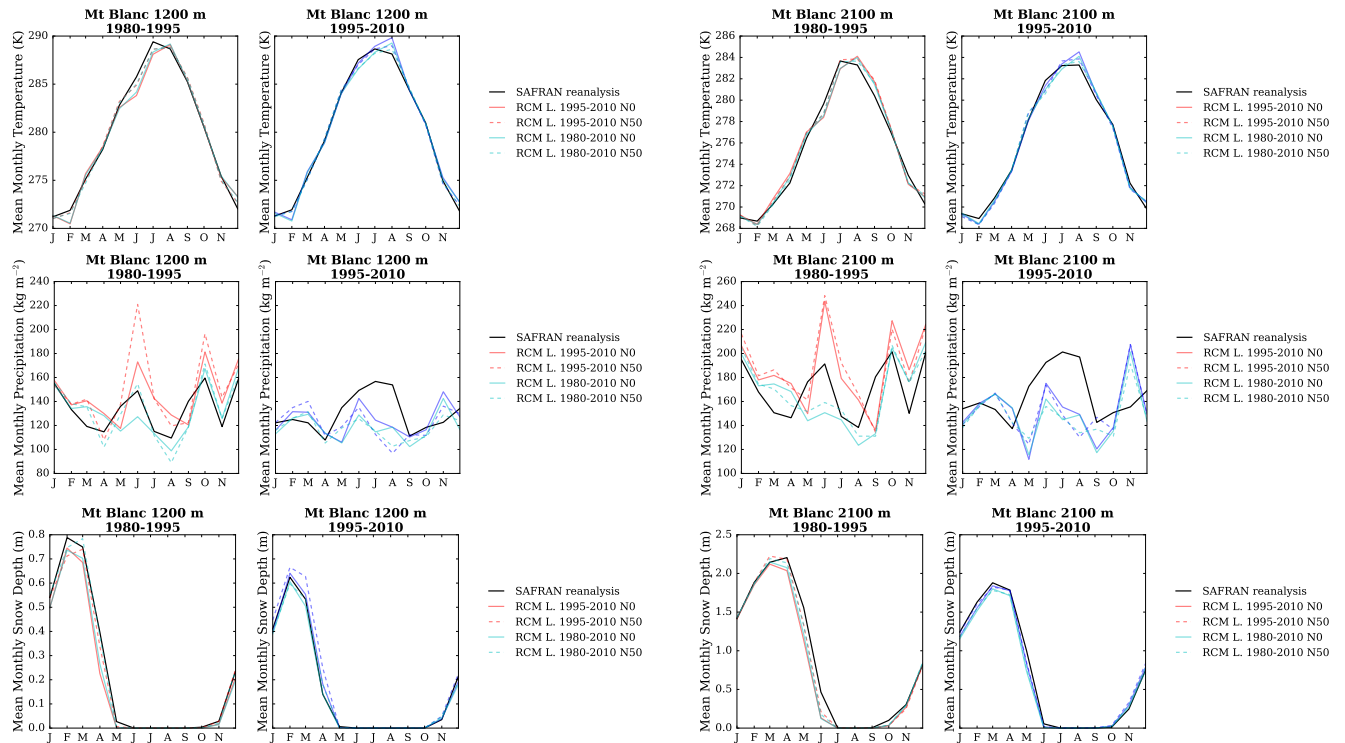


Figure S24: (top) Temperature, (middle) precipitation and (bottom) snow depth (using Crocus in this case) mean annual cycle in each adjusted RCM simulation and in the SAFRAN reanalysis over the period 1980-1995 and 1995-2010, for the Mont Blanc massif, and at (left) 1200 m a.s.l. and (right) 2100 m a.s.l.. Letters on the x-axis correspond to the different months of the calendar (J = January, F = February, etc.).

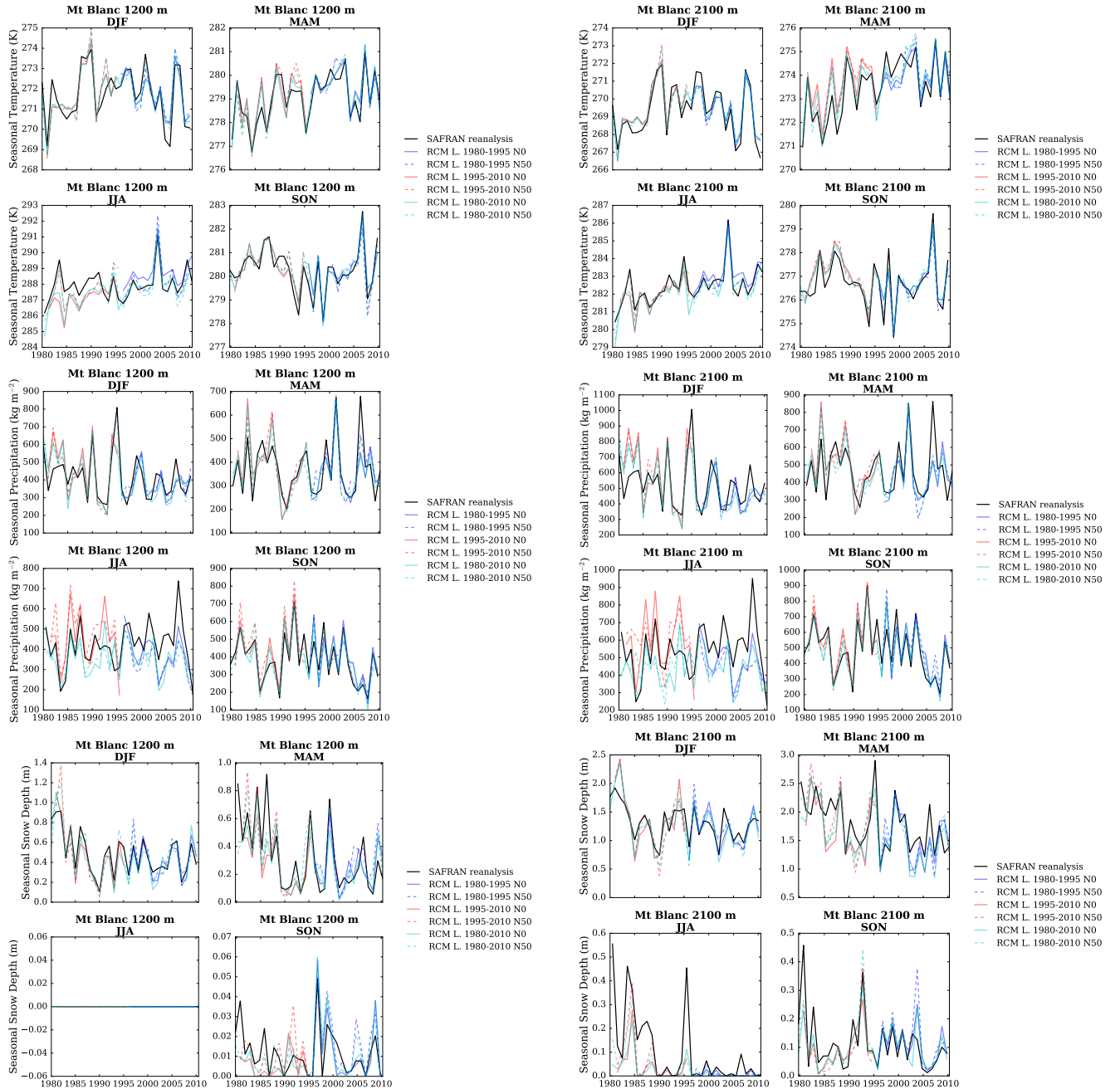


Figure S25: (top) Temperature, (middle) precipitation and (bottom) snow depth (using Crocus in this case) seasonal average time series from 1980 to 2010 in each adjusted RCM simulation and in the SAFRAN reanalysis, for the Mont Blanc massif, and at (left) 1200 m a.s.l. and (right) 2100 m a.s.l..

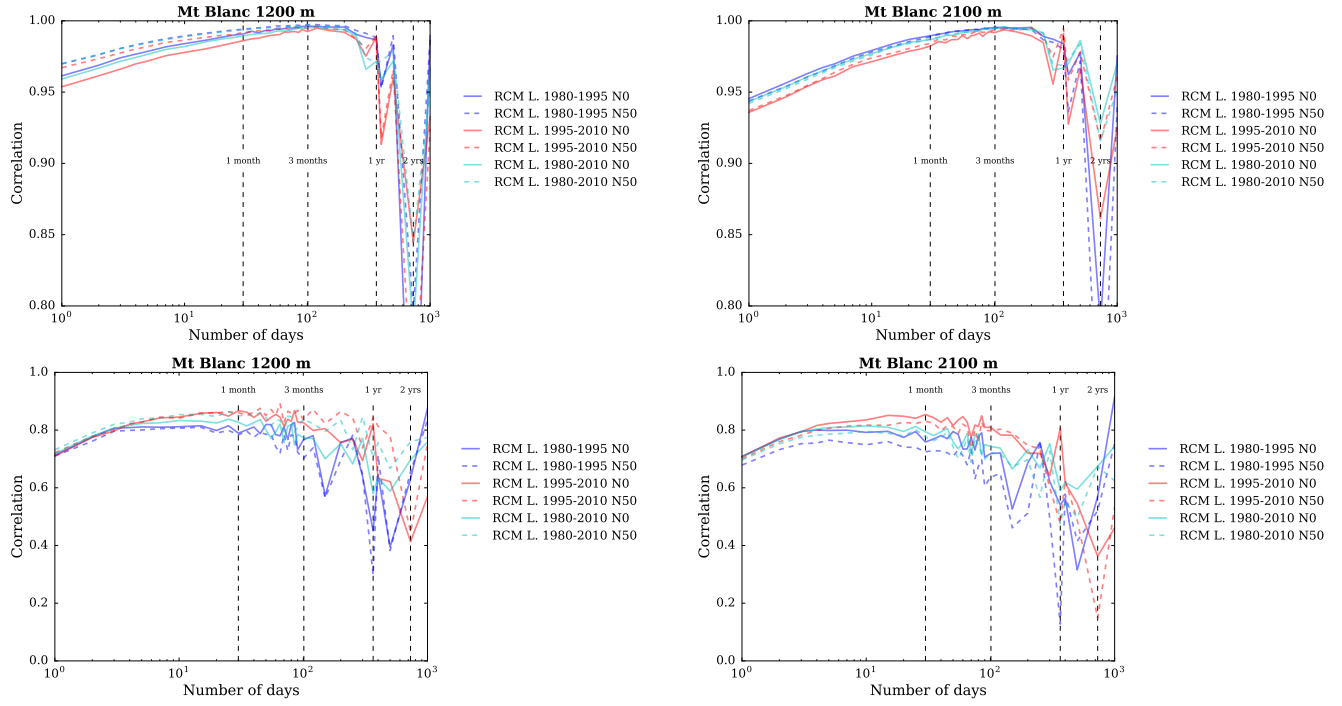


Figure S26: Correlation between the SAFRAN reanalysis and adjusted RCM (top) temperature and (bottom) precipitation as a function of the integration window over the evaluation period, for the Mont Blanc massif, and at (left) 1200 m a.s.l. and (right) 2100 m a.s.l..

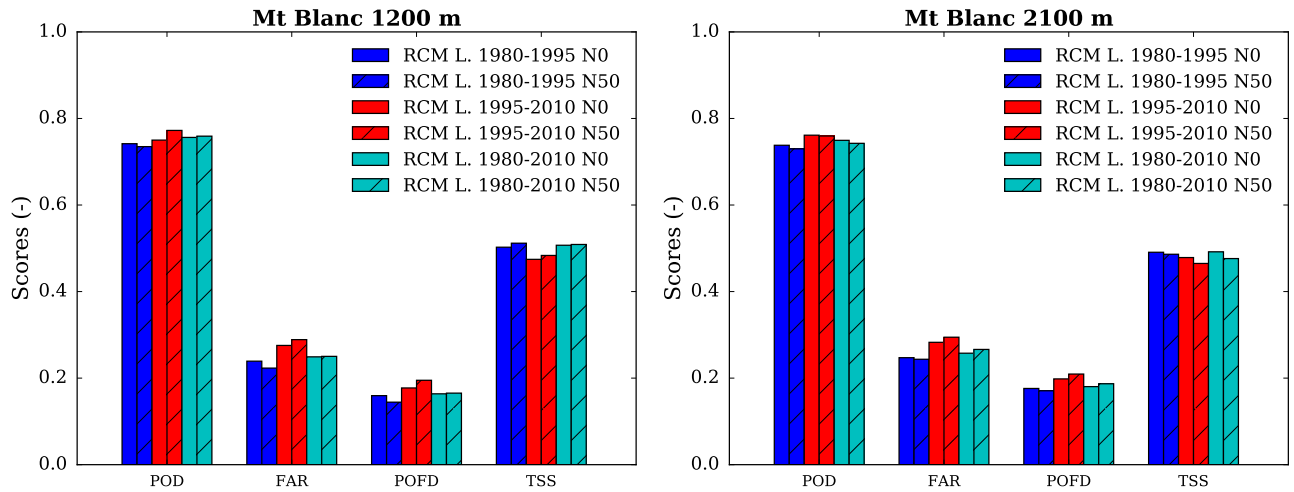


Figure S27: Scores for the detection of precipitation events in each adjusted RCM simulation compared to the SAFRAN reanalysis over the evaluation period, for the Mont Blanc massif, at (left) 1200 m a.s.l. and (right) 2100 m a.s.l.. POD = probability of detection, FAR = false alarm rate, POFD = probability of false detection, TSS = true skill score.

Bauges

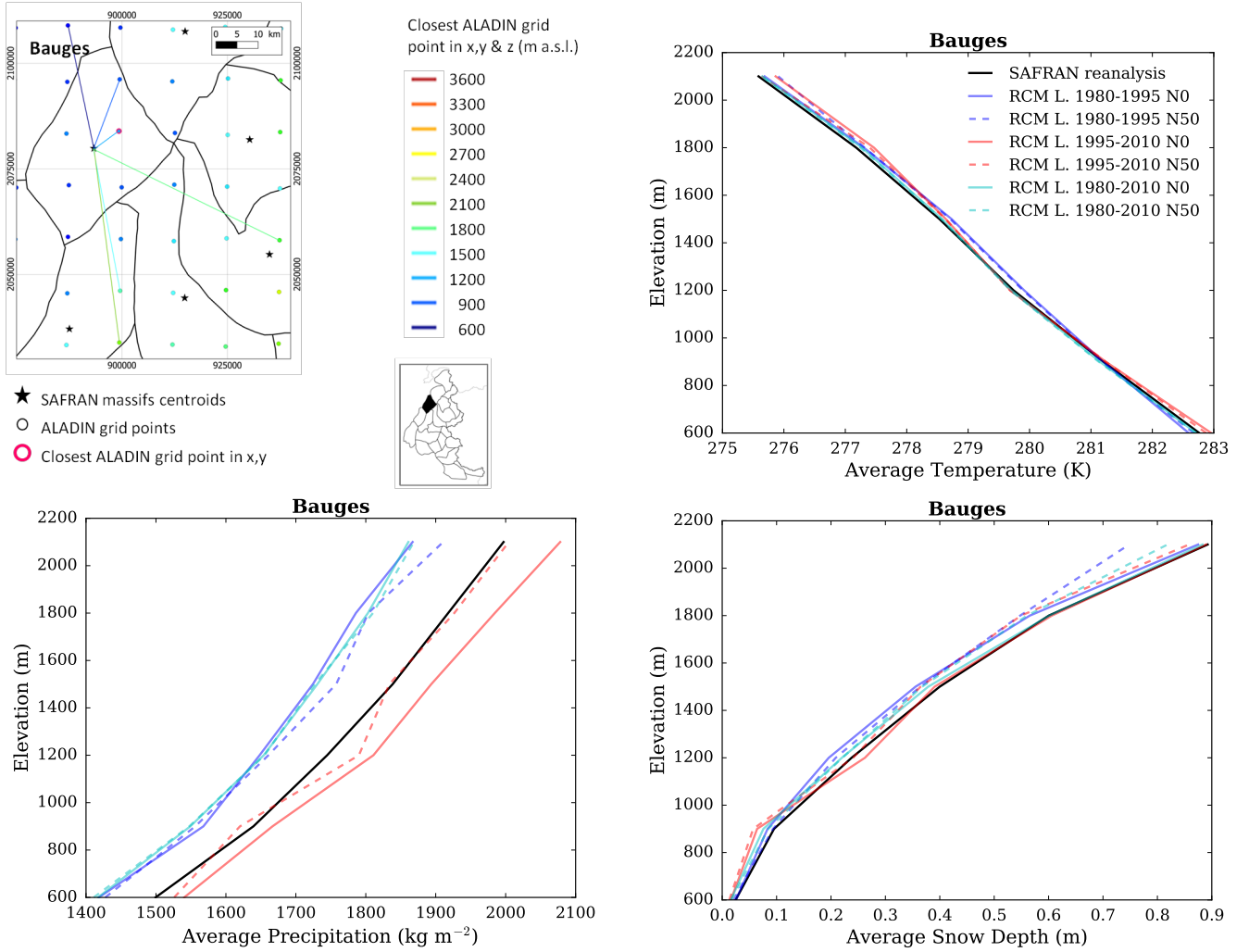


Figure S28: (top left) Location of the Bauges massif, with ALADIN RCM grid points chosen as the closest in x, y ($N = 0$, pink contour) and in x, y and z (using $N \neq 0$). Coloured lines link each SAFRAN massif centre point with the corresponding grid point in ALADIN for the different elevations considered (in m above sea level (a.s.l.)). (top right) Mean temperature, (bottom left) precipitation and (bottom right) snow depth (using Crocus in this case) for each elevation band for the Bauges massif, over the evaluation period in each adjusted RCM simulation (different learning periods and 2 neighbour selection methods) and in SAFRAN (1980-2010).

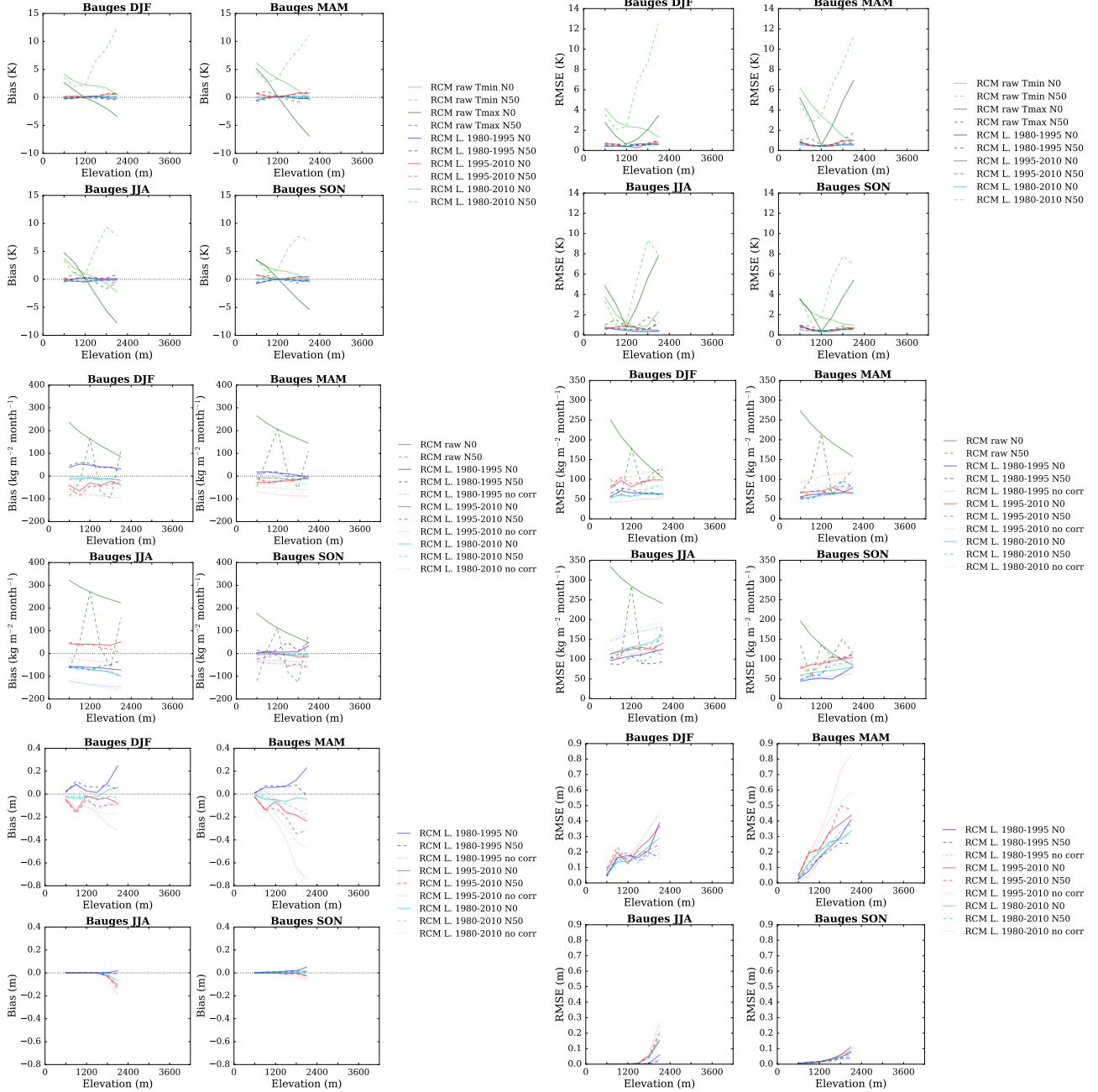


Figure S29: (top) Temperature, (middle) precipitation and (bottom) snow depth (using Crocus in this case) mean bias and root mean square error of each raw and adjusted RCM simulation compared to the SAFRAN reanalysis over the evaluation period for the Bauges massif as a function of elevation. Scores computed for the raw RCM simulations concern minimum and maximum daily temperatures.

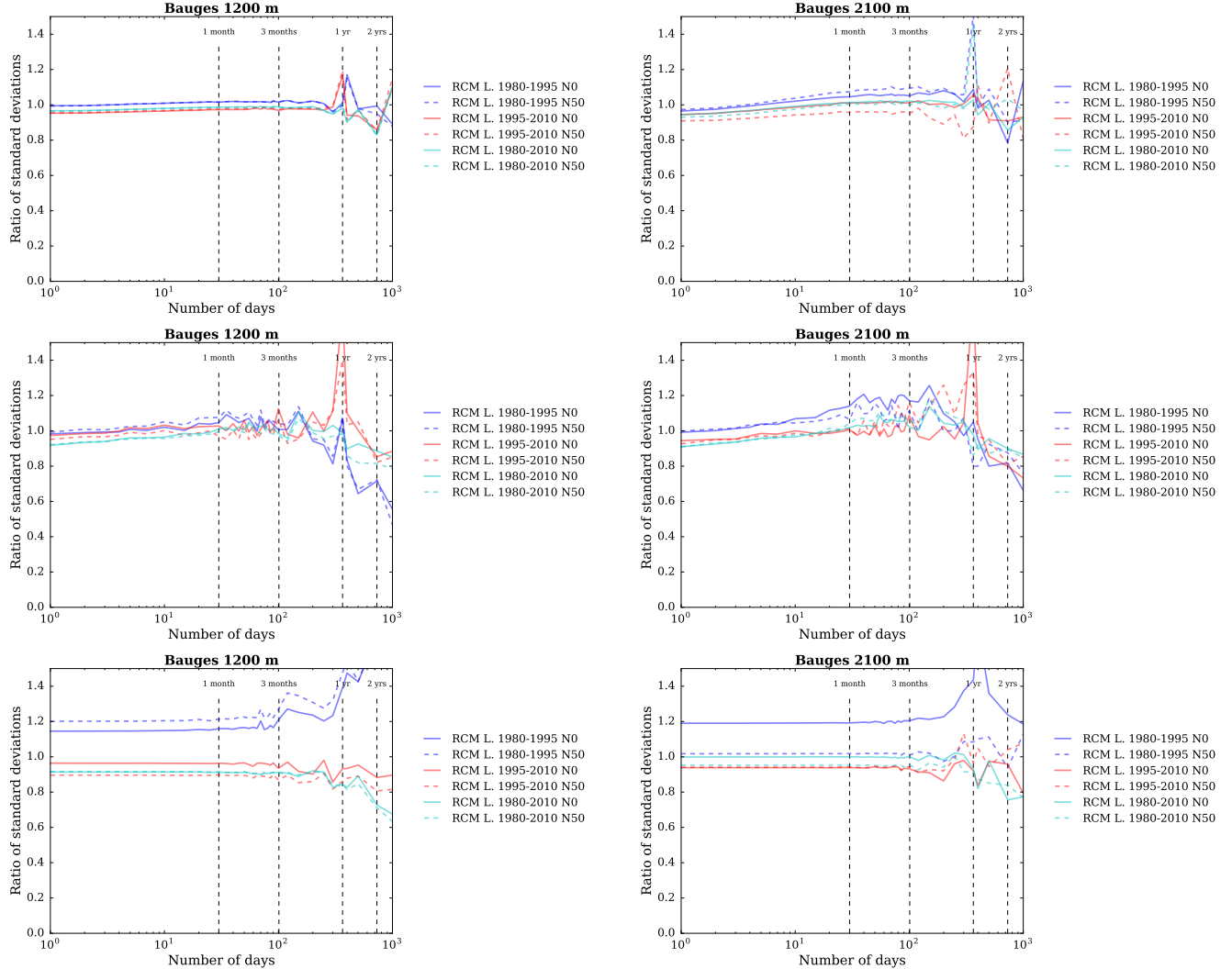


Figure S30: Ratios of standard deviations between the SAFRAN ranalysis and adjusted RCM (top) temperature, (middle) precipitation and (bottom) snow depth (using Crocus in this case) as a function of the integration window over the evaluation period, for the Bauges massif, at (left) 1200 m a.s.l. and (right) 2100 m a.s.l..

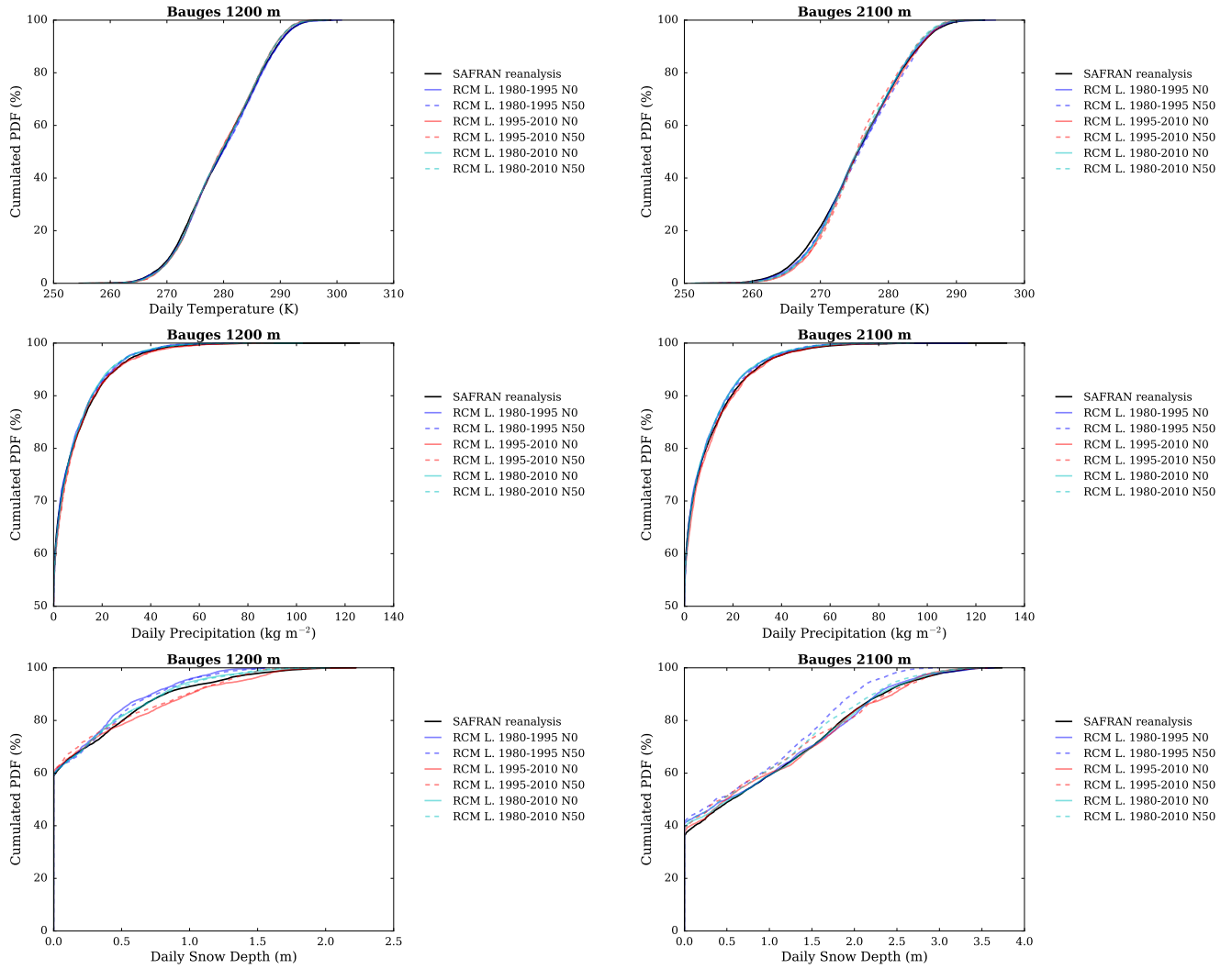


Figure S31: Cumulated probability density functions (PDFs) of daily (top) temperature, (middle) precipitation and (bottom) snow depth (using Crocus in this case) in each adjusted RCM simulation and in the SAFRAN reanalysis (1980-2010) over the evaluation period, for the Bauges massif, at (left) 1200 m a.s.l. and (right) 2100 m a.s.l..

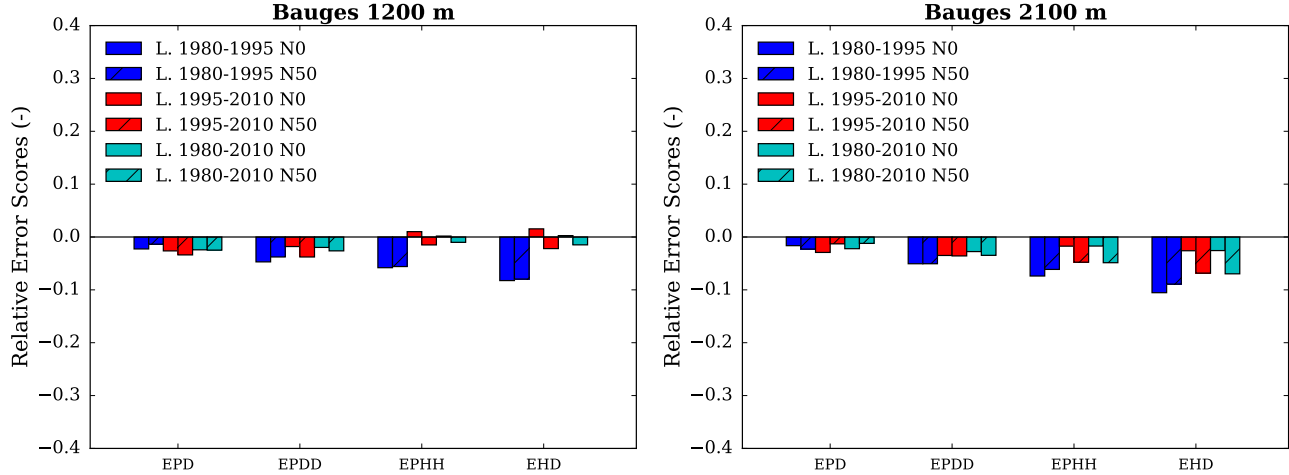


Figure S32: Scores for the duration and persistence of precipitation events in each adjusted RCM simulation compared to the SAFRAN reanalysis over the evaluation period, for the Bauges massif, at (left) 1200 m a.s.l. and (right) 2100 m a.s.l.. EPD = relative error on the probability of a dry day, EPDD = relative error on the probability of a dry day following a dry day, EPHH = relative error on the probability of a wet day following a wet day, EHD = relative error on the mean duration of wet periods.

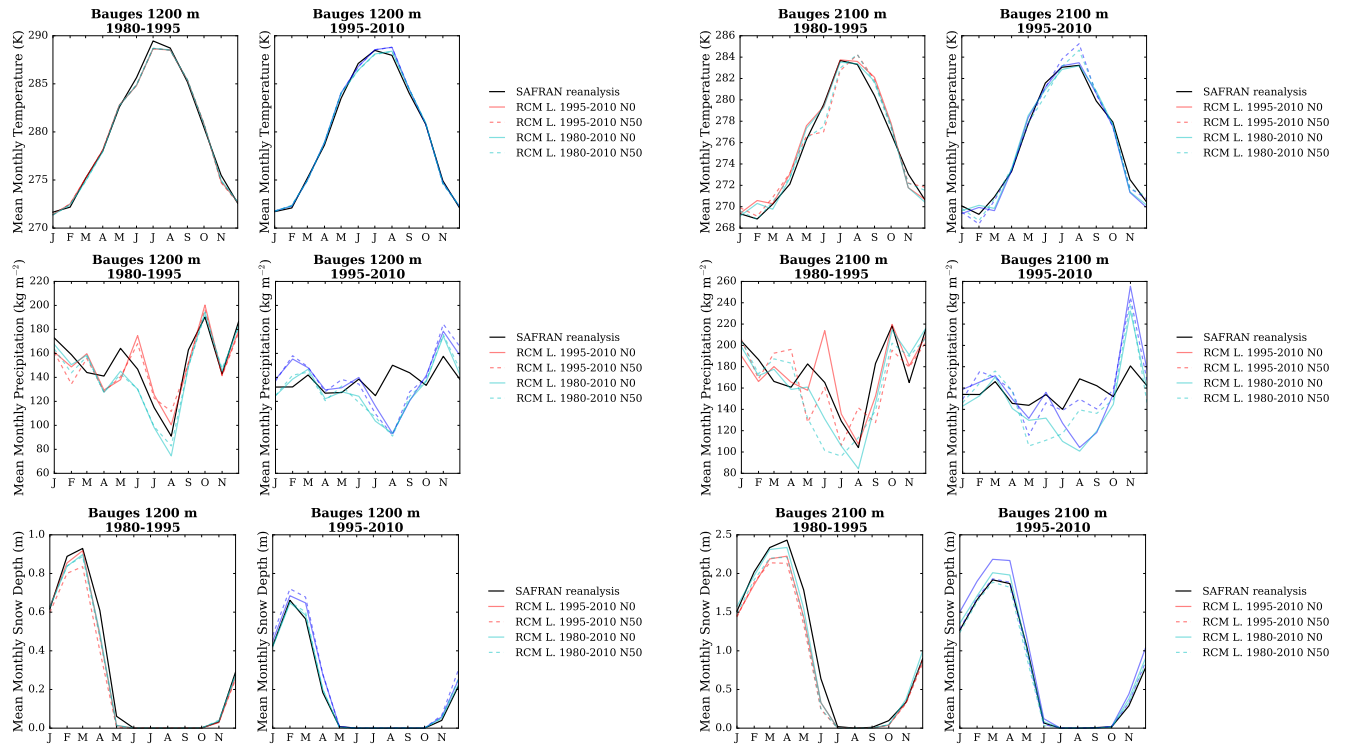


Figure S33: (top) Temperature, (middle) precipitation and (bottom) snow depth (using Crocus in this case) mean annual cycle in each adjusted RCM simulation and in the SAFRAN reanalysis over the period 1980-1995 and 1995-2010, for the Bauges massif, and at (left) 1200 m a.s.l. and (right) 2100 m a.s.l.. Letters on the x-axis correspond to the different months of the calendar (J = January, F = February, etc.).

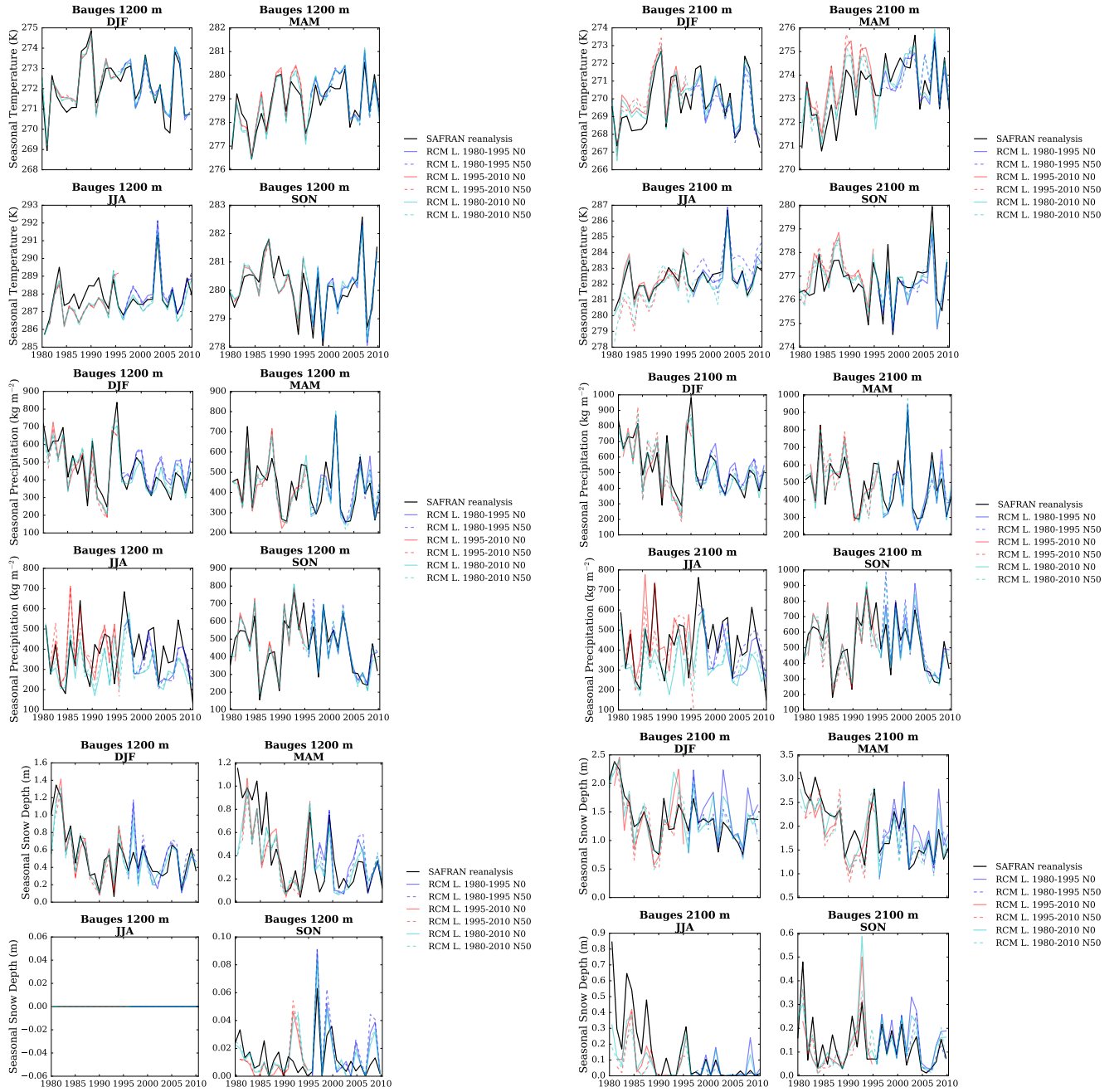


Figure S34: (top) Temperature, (middle) precipitation and (bottom) snow depth (using Crocus in this case) seasonal average time series from 1980 to 2010 in each adjusted RCM simulation and in the SAFRAN reanalysis, for the Bauges massif, and at (left) 1200 m a.s.l. and (right) 2100 m a.s.l..

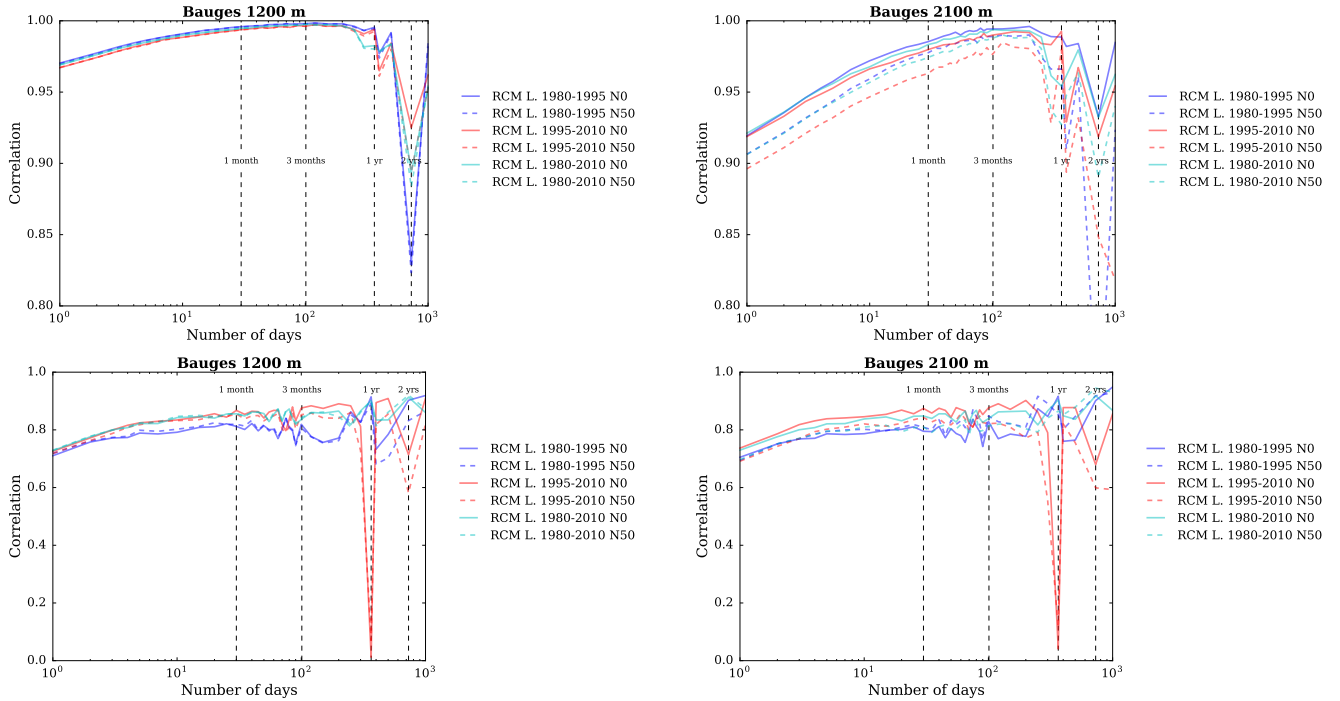


Figure S35: Correlation between the SAFRAN reanalysis and adjusted RCM (top) temperature and (bottom) precipitation as a function of the integration window over the evaluation period, for the Bauges massif, and at (left) 1200 m a.s.l. and (right) 2100 m a.s.l..

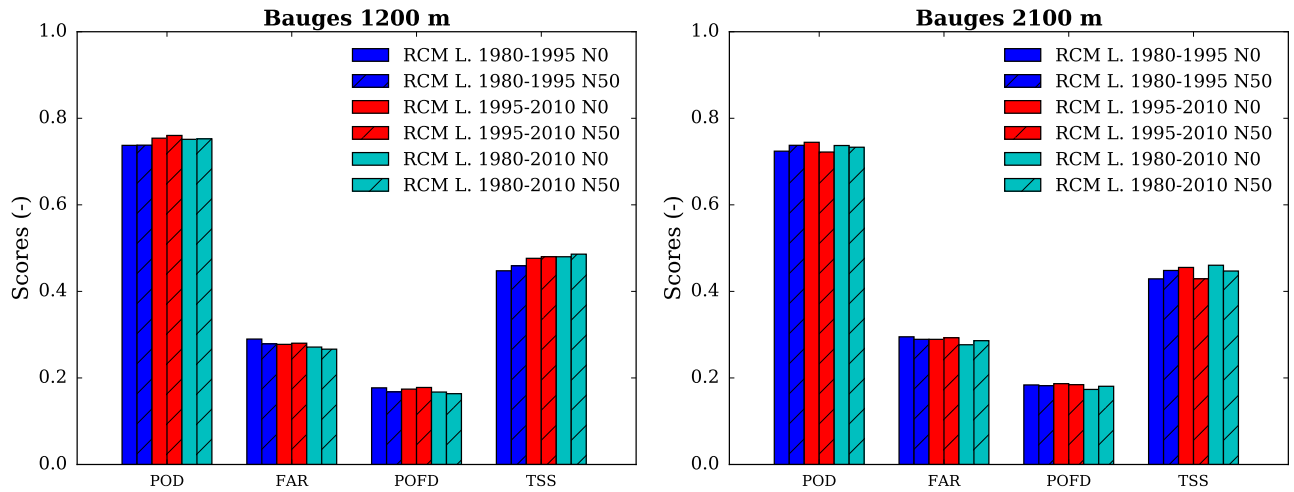


Figure S36: Scores for the detection of precipitation events in each adjusted RCM simulation compared to the SAFRAN reanalysis over the evaluation period, for the Bauges massif, at (left) 1200 m a.s.l. and (right) 2100 m a.s.l.. POD = probability of detection, FAR = false alarm rate, POFD = probability of false detection, TSS = true skill score.

Beaufortin

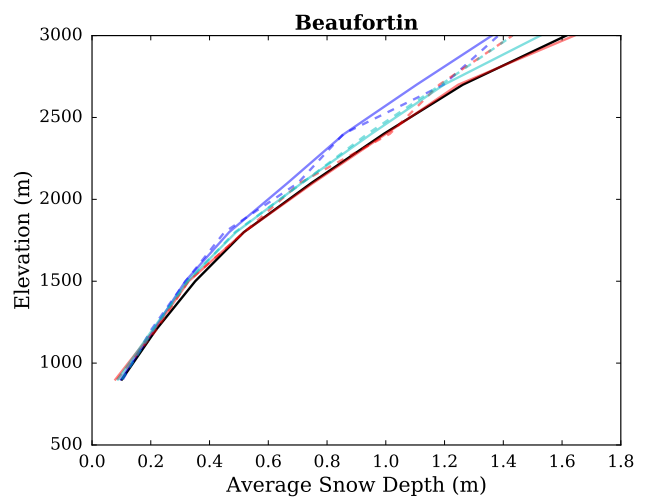
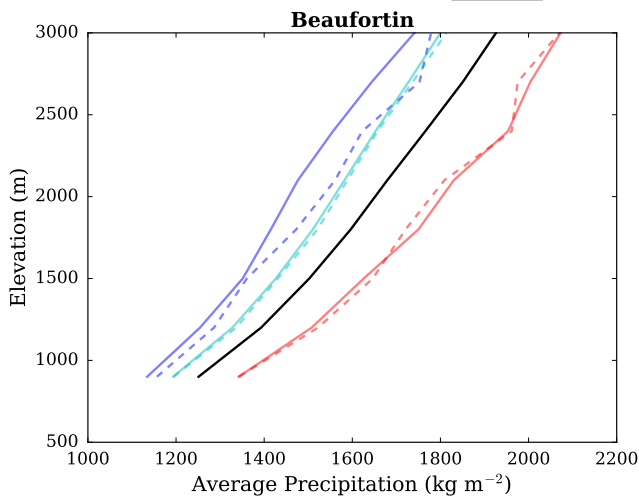
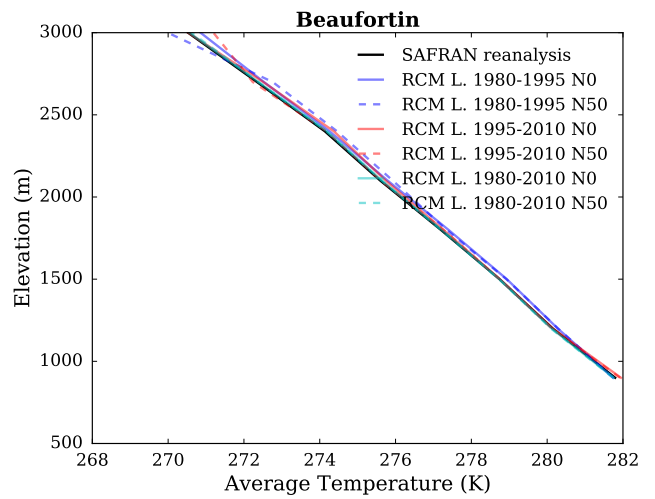
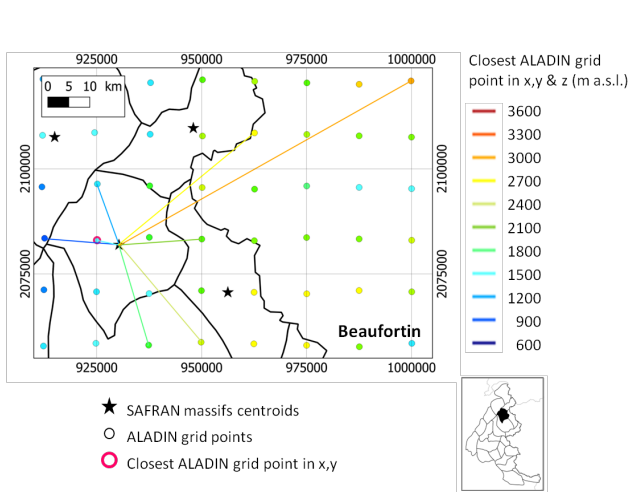


Figure S37: (top left) Location of the Beaufortin massif, with ALADIN RCM grid points chosen as the closest in x, y ($N = 0$, pink contour) and in x, y and z (using $N \neq 0$). Coloured lines link each SAFRAN massif centre point with the corresponding grid point in ALADIN for the different elevations considered (in m above sea level (a.s.l.)). (top right) Mean temperature, (bottom left) precipitation and (bottom right) snow depth (using Crocus in this case) for each elevation band for the Beaufortin massif, over the evaluation period in each adjusted RCM simulation (different learning periods and 2 neighbour selection methods) and in SAFRAN (1980-2010).

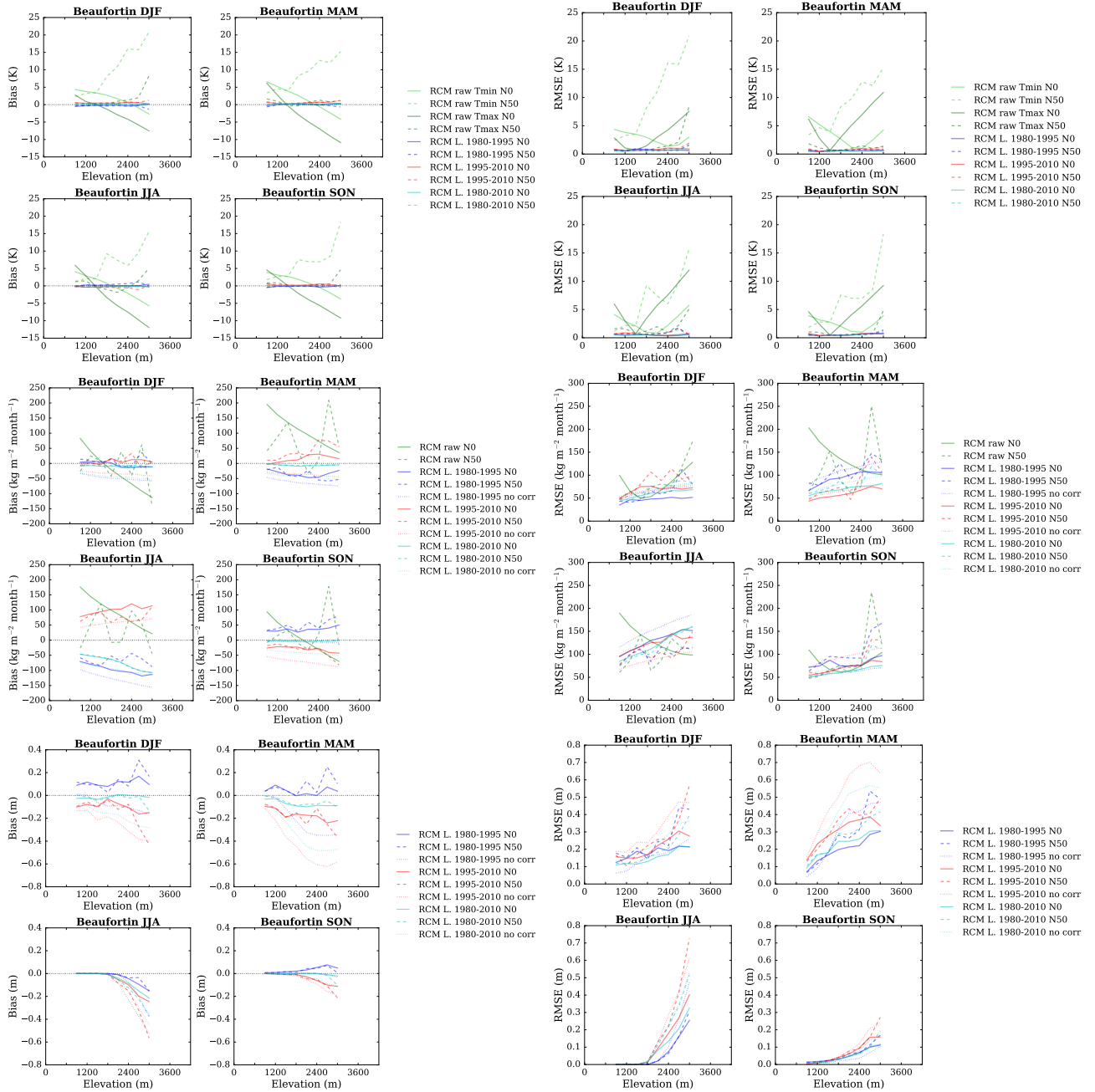


Figure S38: (top) Temperature, (middle) precipitation and (bottom) snow depth (using Crocus in this case) mean bias and root mean square error of each raw and adjusted RCM simulation compared to the SAFRAN reanalysis over the evaluation period for the Beaufortin massif as a function of elevation. Scores computed for the raw RCM simulations concern minimum and maximum daily temperatures.

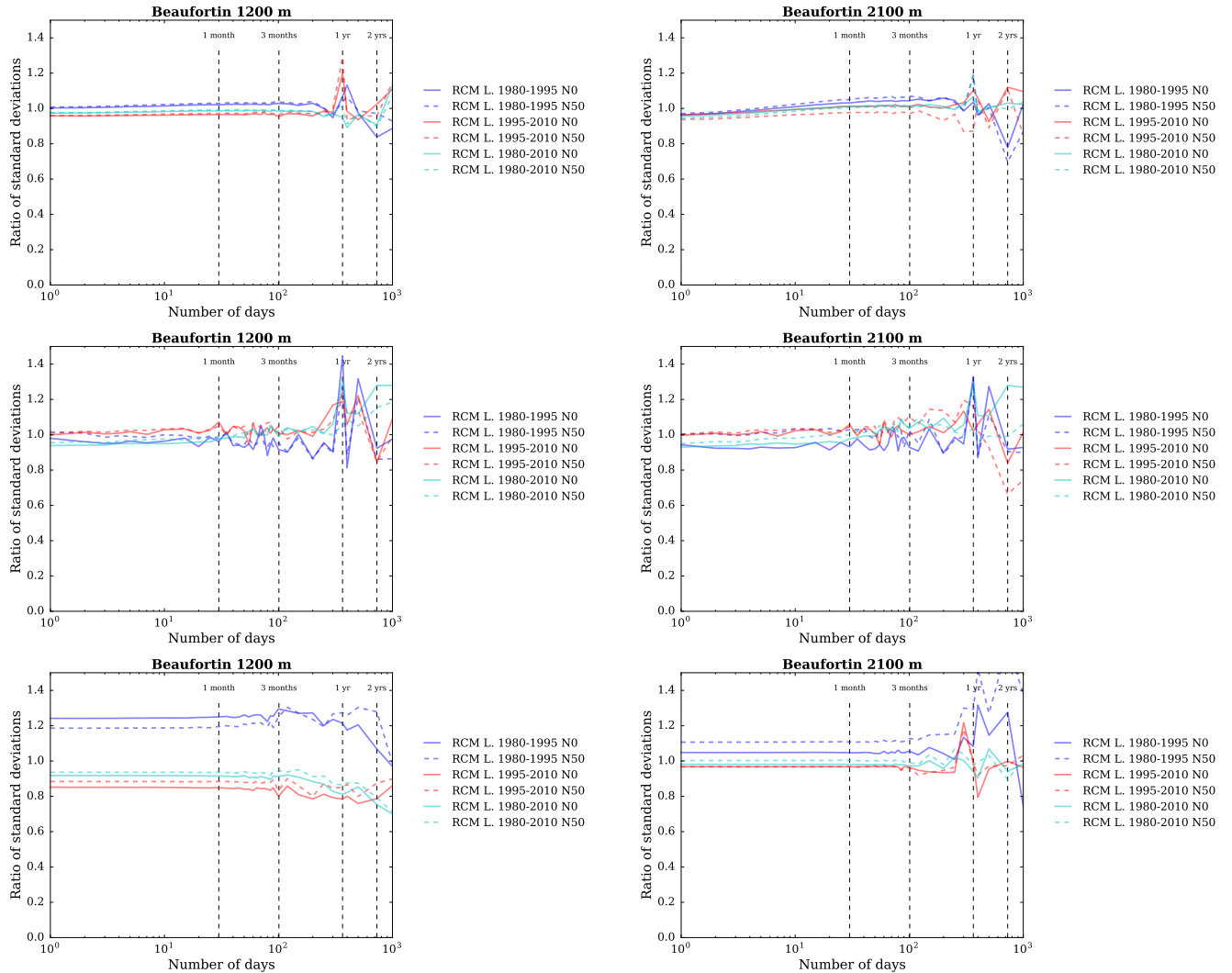


Figure S39: Ratios of standard deviations between the SAFRAN reanalysis and adjusted RCM (top) temperature, (middle) precipitation and (bottom) snow depth (using Crocus in this case) as a function of the integration window over the evaluation period, for the Beaufortin massif, at (left) 1200 m a.s.l. and (right) 2100 m a.s.l..

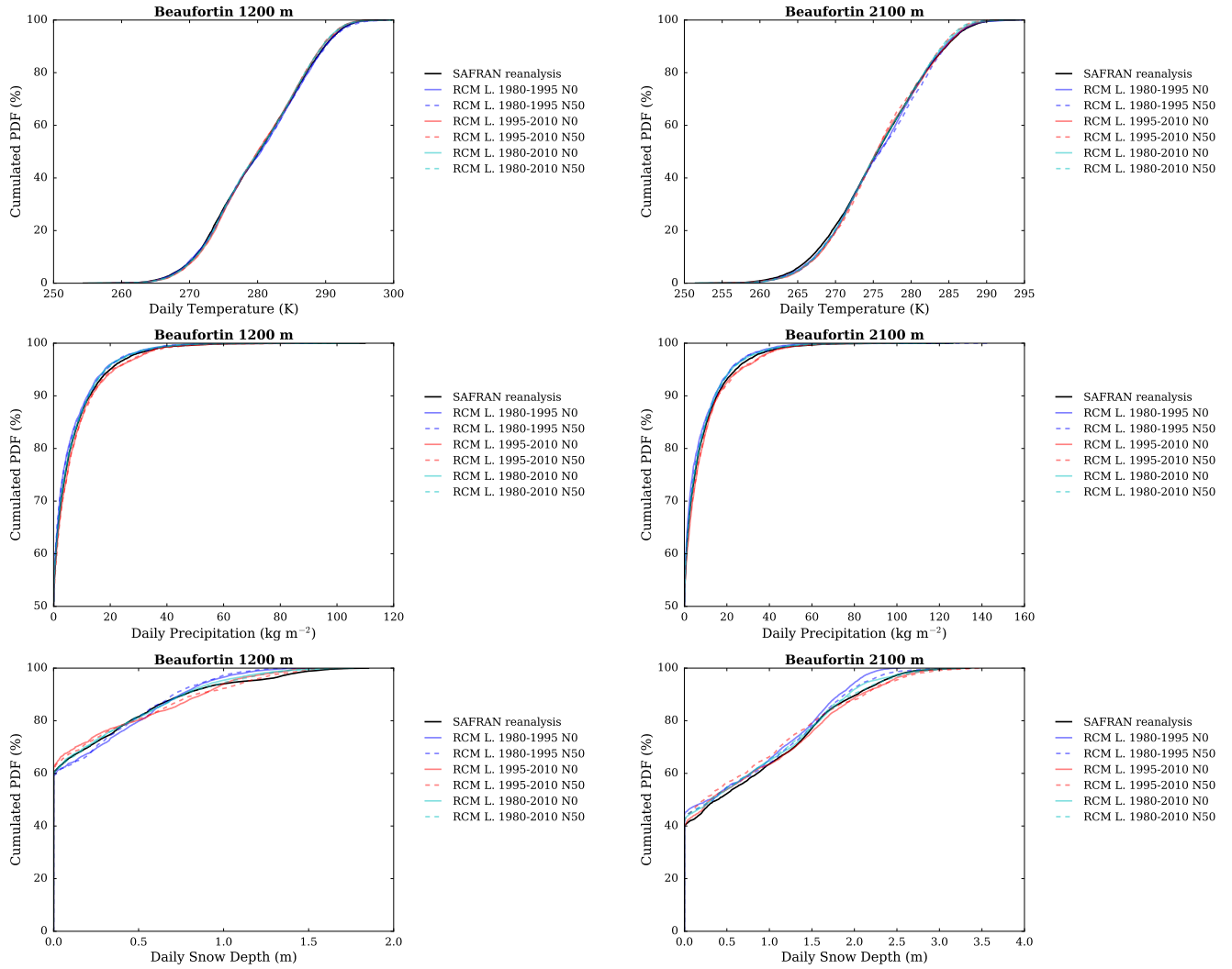


Figure S40: Cumulated probability density functions (PDFs) of daily (top) temperature, (middle) precipitation and (bottom) snow depth (using Crocus in this case) in each adjusted RCM simulation and in the SAFRAN reanalysis (1980-2010) over the evaluation period, for the Beaufortin massif, at (left) 1200 m a.s.l. and (right) 2100 m a.s.l..

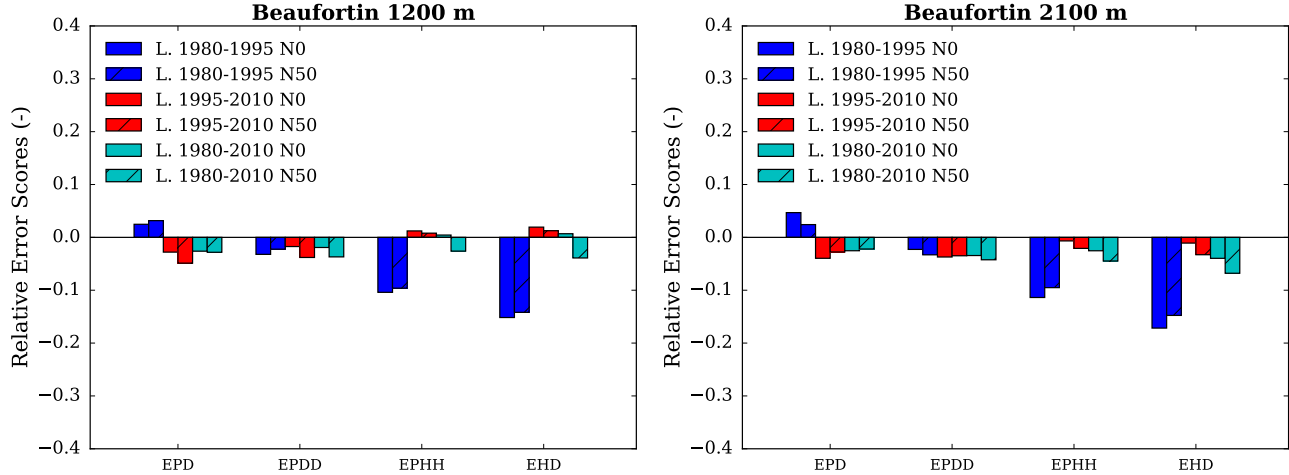


Figure S41: Scores for the duration and persistence of precipitation events in each adjusted RCM simulation compared to the SAFRAN reanalysis over the evaluation period, for the Beaufortin massif, at (left) 1200 m a.s.l. and (right) 2100 m a.s.l.. EPD = relative error on the probability of a dry day, EPDD = relative error on the probability of a dry day following a dry day, EPHH = relative error on the probability of a wet day following a wet day, EHD = relative error on the mean duration of wet periods.

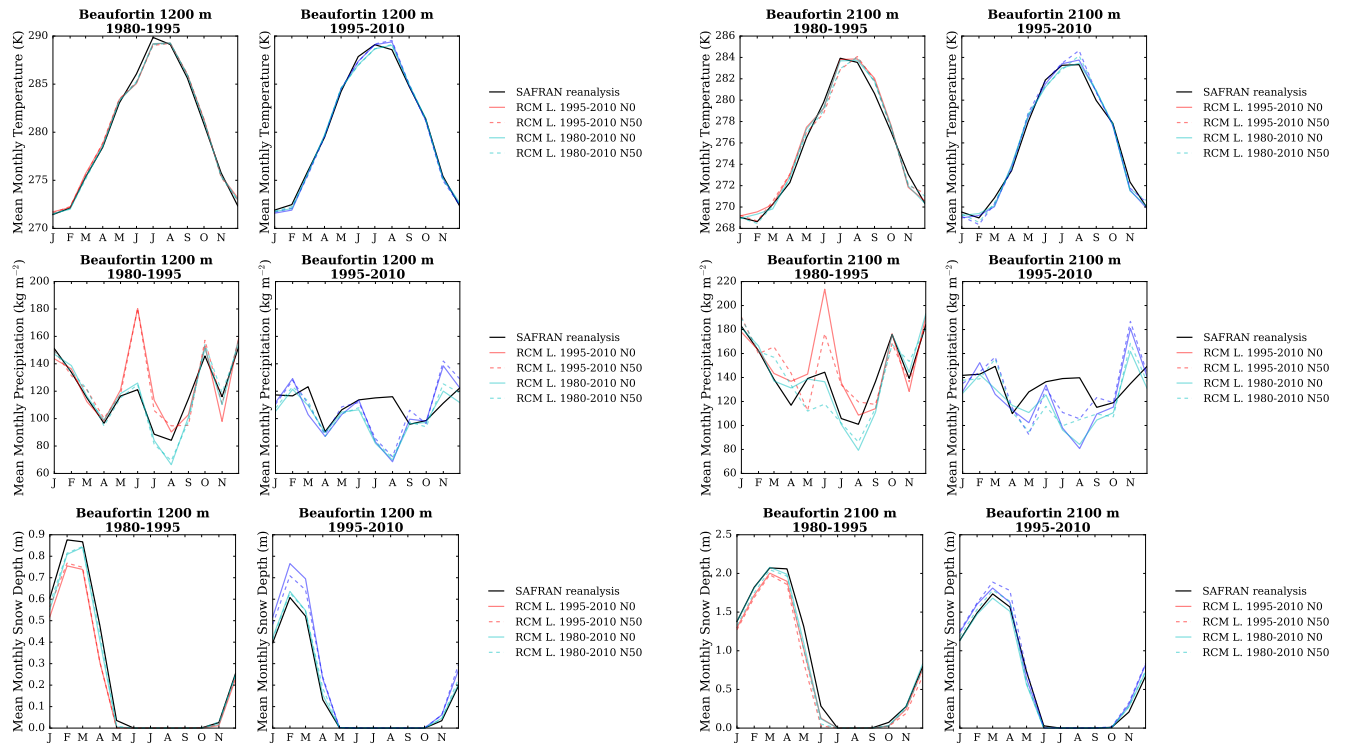


Figure S42: (top) Temperature, (middle) precipitation and (bottom) snow depth (using Crocus in this case) mean annual cycle in each adjusted RCM simulation and in the SAFRAN reanalysis over the period 1980-1995 and 1995-2010, for the Beaufortin massif, and at (left) 1200 m a.s.l. and (right) 2100 m a.s.l.. Letters on the x-axis correspond to the different months of the calendar (J = January, F = February, etc.).

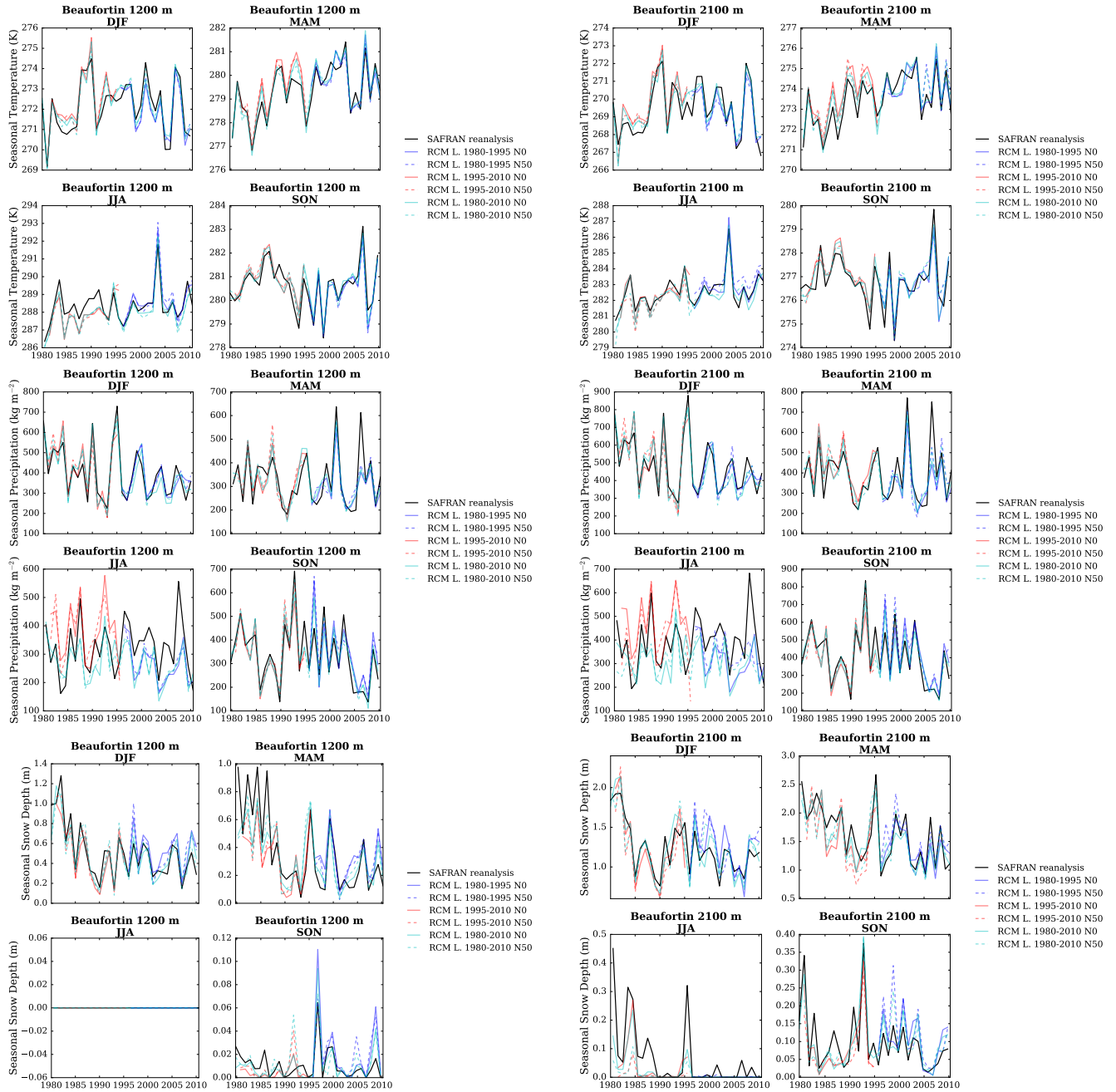


Figure S43: (top) Temperature, (middle) precipitation and (bottom) snow depth (using Crocus in this case) seasonal average time series from 1980 to 2010 in each adjusted RCM simulation and in the SAFRAN reanalysis, for the Beaufortin massif, and at (left) 1200 m a.s.l. and (right) 2100 m a.s.l..

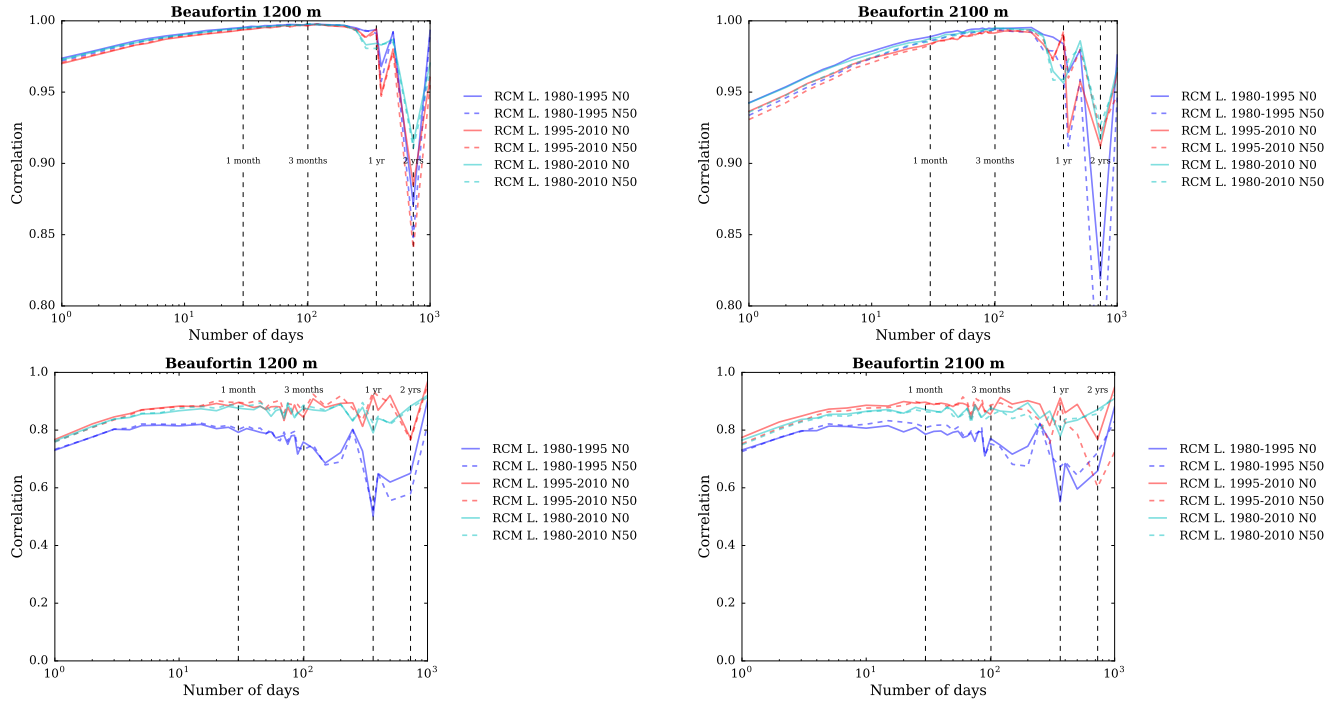


Figure S44: Correlation between the SAFRAN reanalysis and adjusted RCM (top) temperature and (bottom) precipitation as a function of the integration window over the evaluation period, for the Beaufortin massif, and at (left) 1200 m a.s.l. and (right) 2100 m a.s.l..

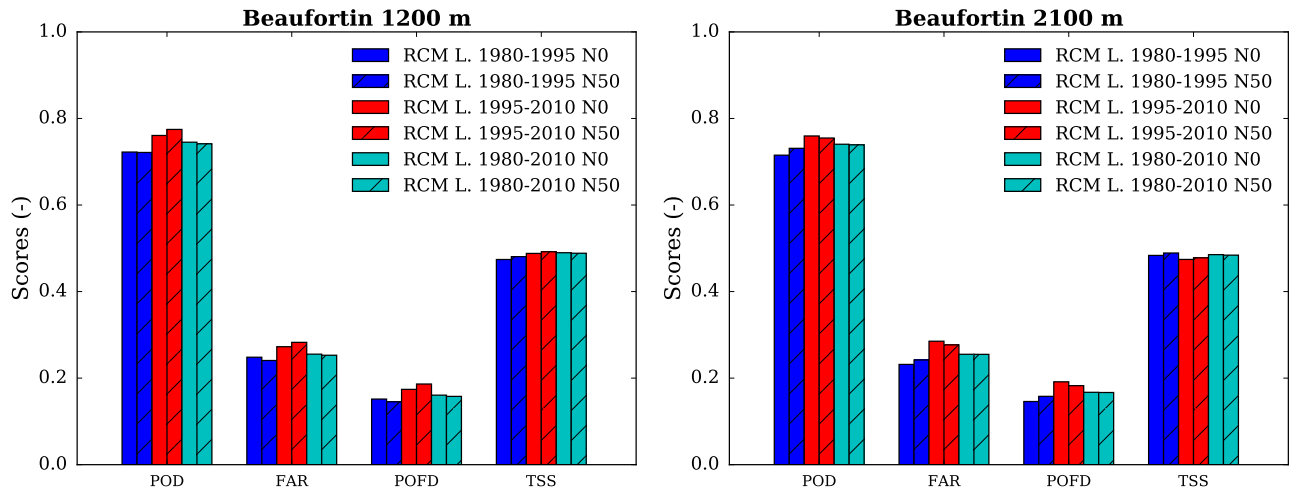


Figure S45: Scores for the detection of precipitation events in each adjusted RCM simulation compared to the SAFRAN reanalysis over the evaluation period, for the Beaufortin massif, at (left) 1200 m a.s.l. and (right) 2100 m a.s.l.. POD = probability of detection, FAR = false alarm rate, POFD = probability of false detection, TSS = true skill score.

Haute Tarentaise

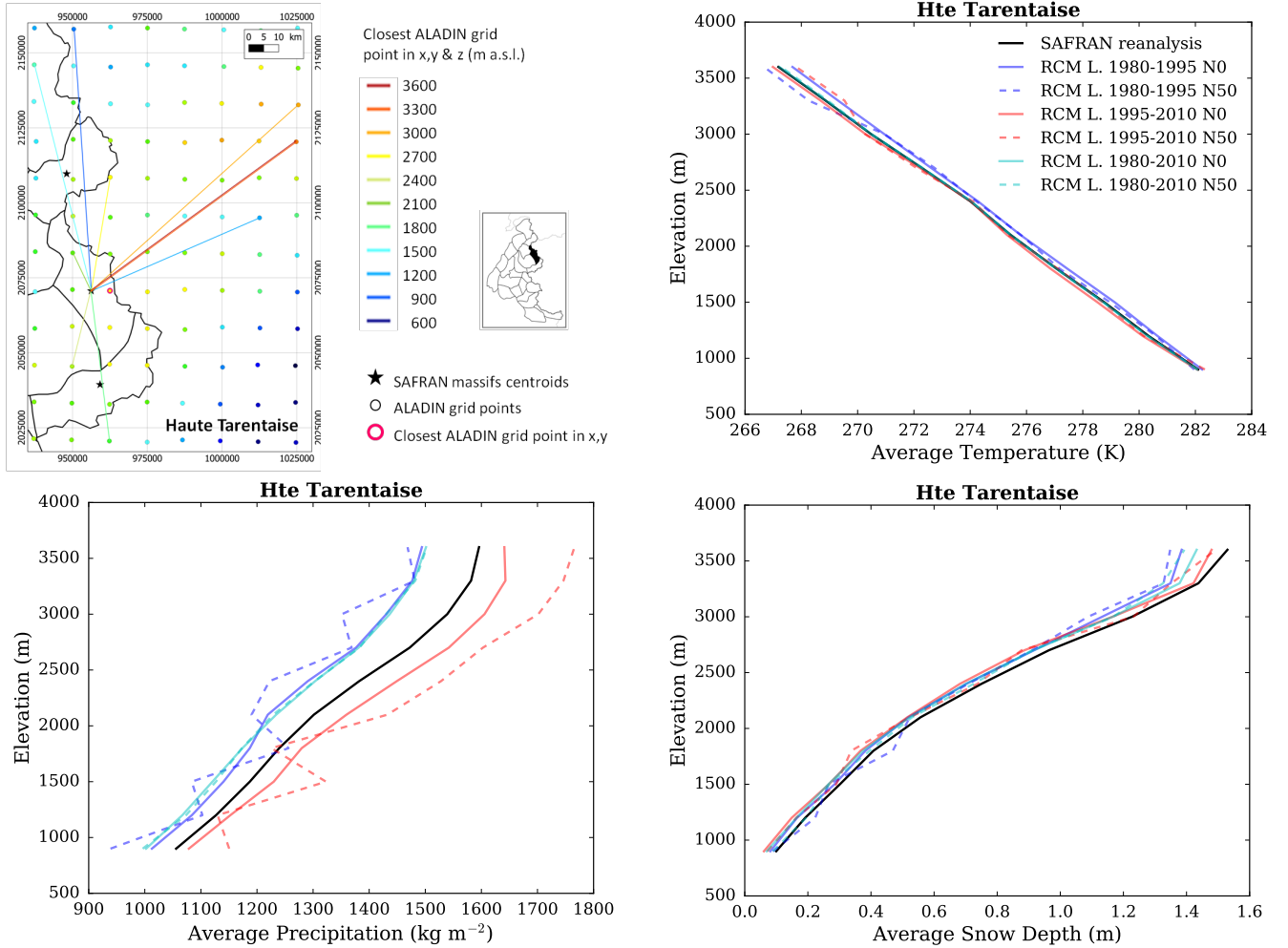


Figure S46: (top left) Location of the Haute Tarentaise massif, with ALADIN RCM grid points chosen as the closest in x, y ($N = 0$, pink contour) and in x, y and z (using $N \neq 0$). Coloured lines link each SAFRAN massif centre point with the corresponding grid point in ALADIN for the different elevations considered (in m above sea level (a.s.l.)). (top right) Mean temperature, (bottom left) precipitation and (bottom right) snow depth (using Crocus in this case) for each elevation band for the Haute Tarentaise massif, over the evaluation period in each adjusted RCM simulation (different learning periods and 2 neighbour selection methods) and in SAFRAN (1980-2010).

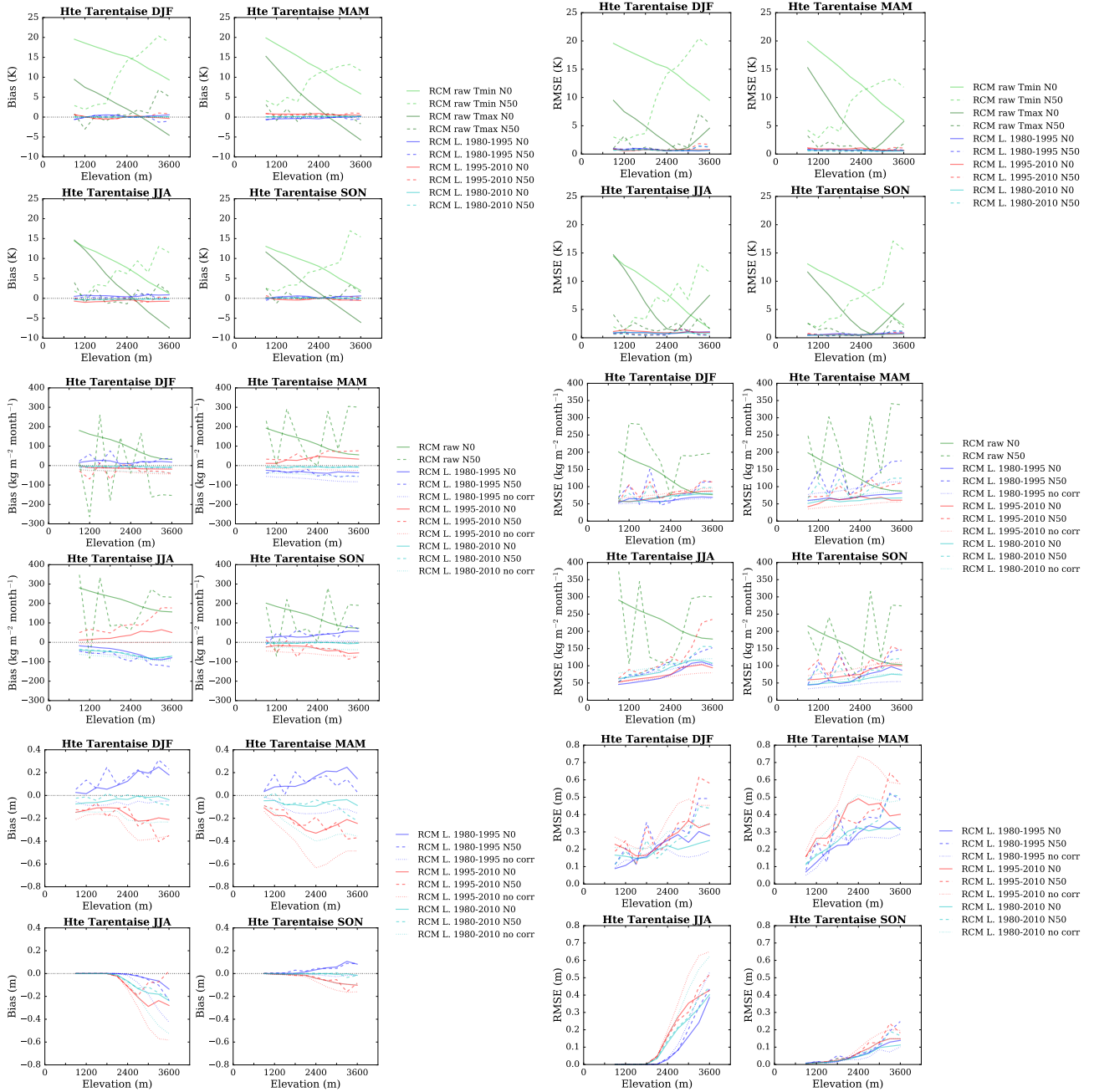


Figure S47: (top) Temperature, (middle) precipitation and (bottom) snow depth (using Crocus in this case) mean bias and root mean square error of each raw and adjusted RCM simulation compared to the SAFRAN reanalysis over the evaluation period for the Haute Tarentaise massif as a function of elevation. Scores computed for the raw RCM simulations concern minimum and maximum daily temperatures.

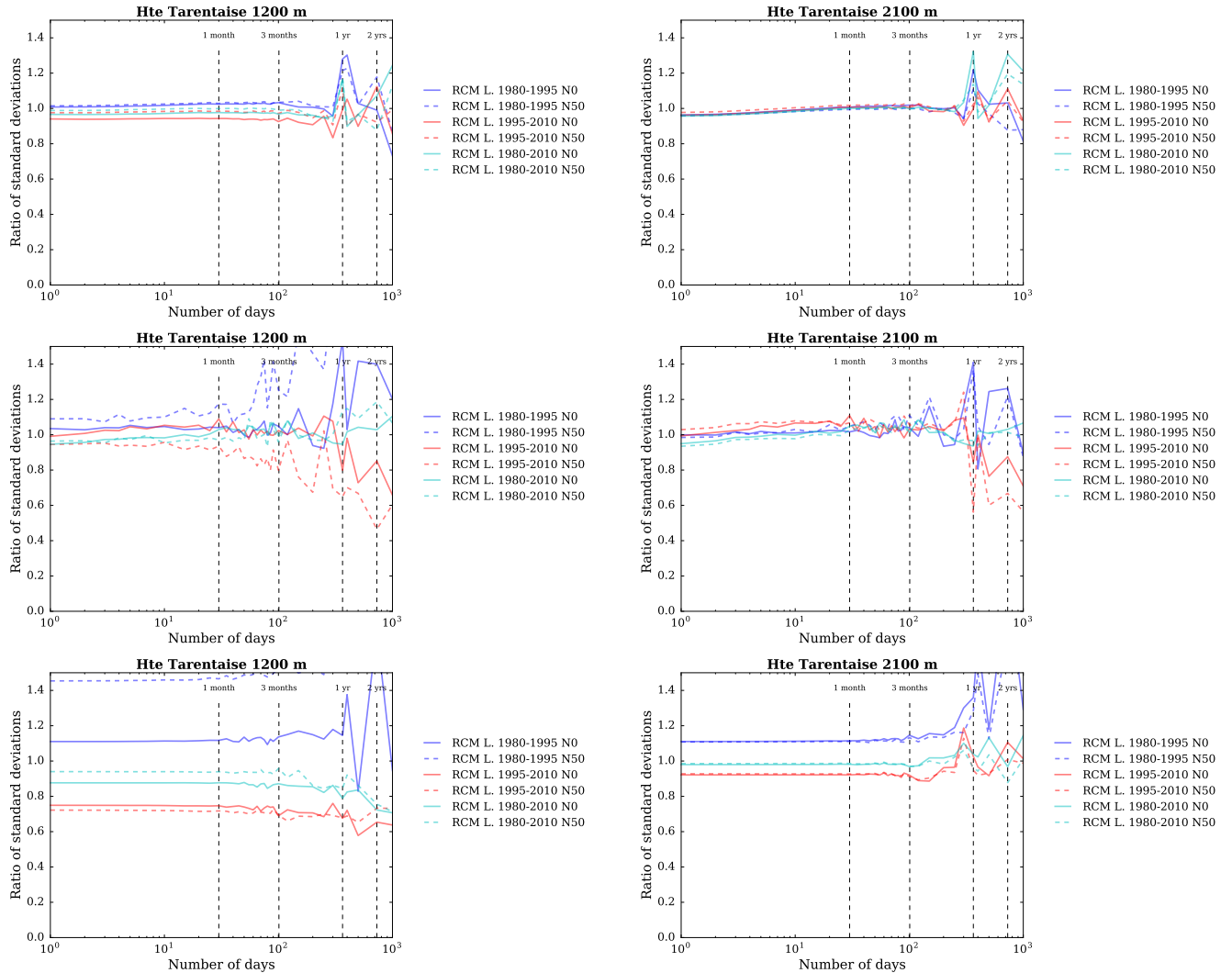


Figure S48: Ratios of standard deviations between the SAFRAN reanalysis and adjusted RCM (top) temperature, (middle) precipitation and (bottom) snow depth (using Crocus in this case) as a function of the integration window over the evaluation period, for the Haute Tarentaise massif, at (left) 1200 m a.s.l. and (right) 2100 m a.s.l..

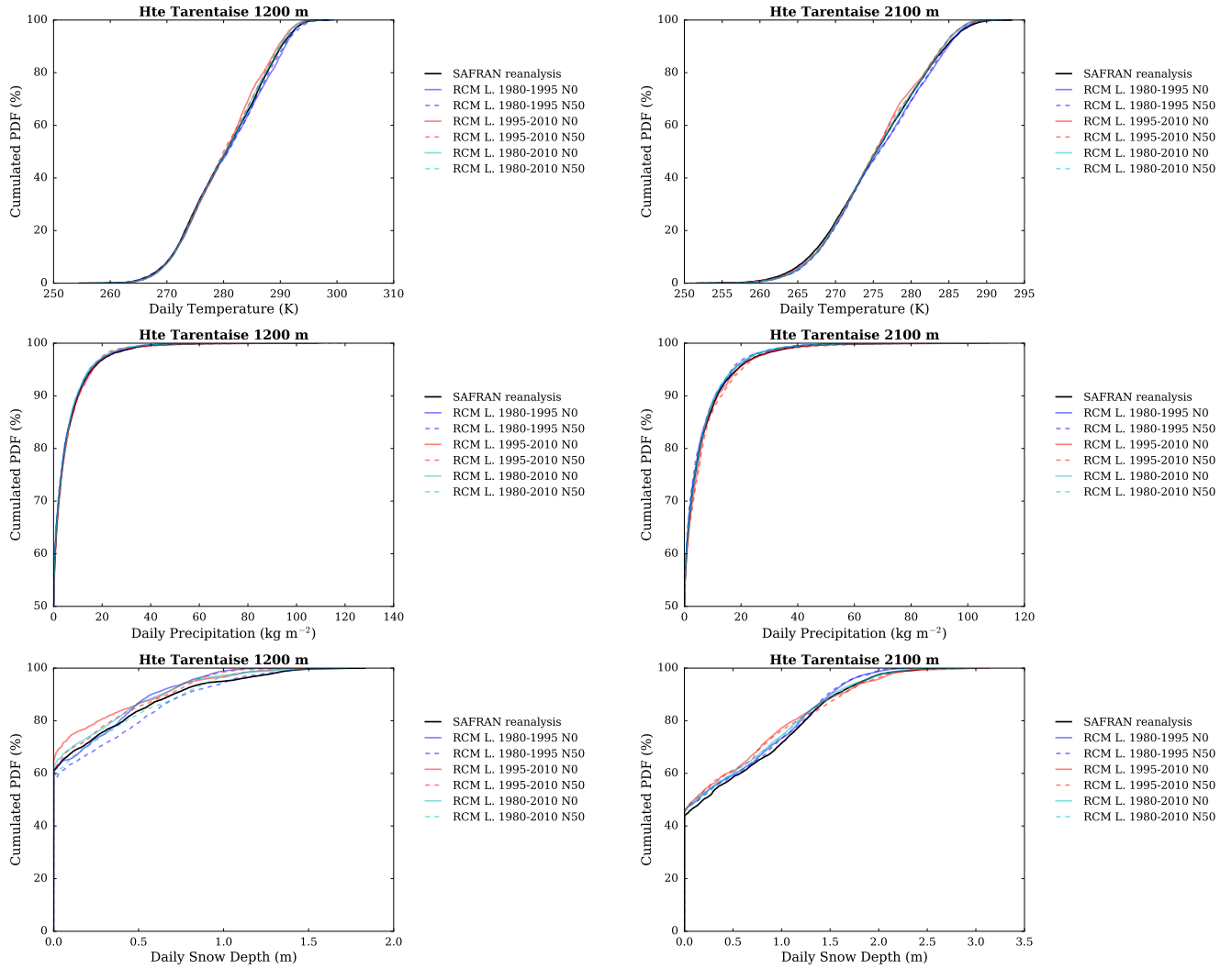


Figure S49: Cumulated probability density functions (PDFs) of daily (top) temperature, (middle) precipitation and (bottom) snow depth (using Crocus in this case) in each adjusted RCM simulation and in the SAFRAN reanalysis (1980-2010) over the evaluation period, for the Haute Tarentaise massif, at (left) 1200 m a.s.l. and (right) 2100 m a.s.l..

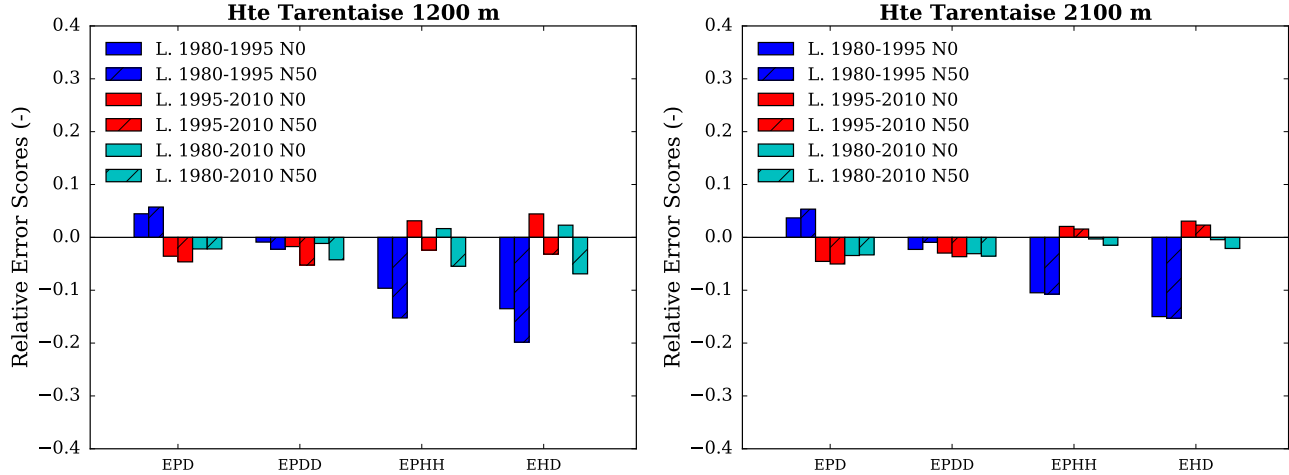


Figure S50: Scores for the duration and persistence of precipitation events in each adjusted RCM simulation compared to the SAFRAN reanalysis over the evaluation period, for the Haute Tarentaise massif, at (left) 1200 m a.s.l. and (right) 2100 m a.s.l.. EPD = relative error on the probability of a dry day, EPDD = relative error on the probability of a dry day following a dry day, EPHH = relative error on the probability of a wet day following a wet day, EHD = relative error on the mean duration of wet periods.

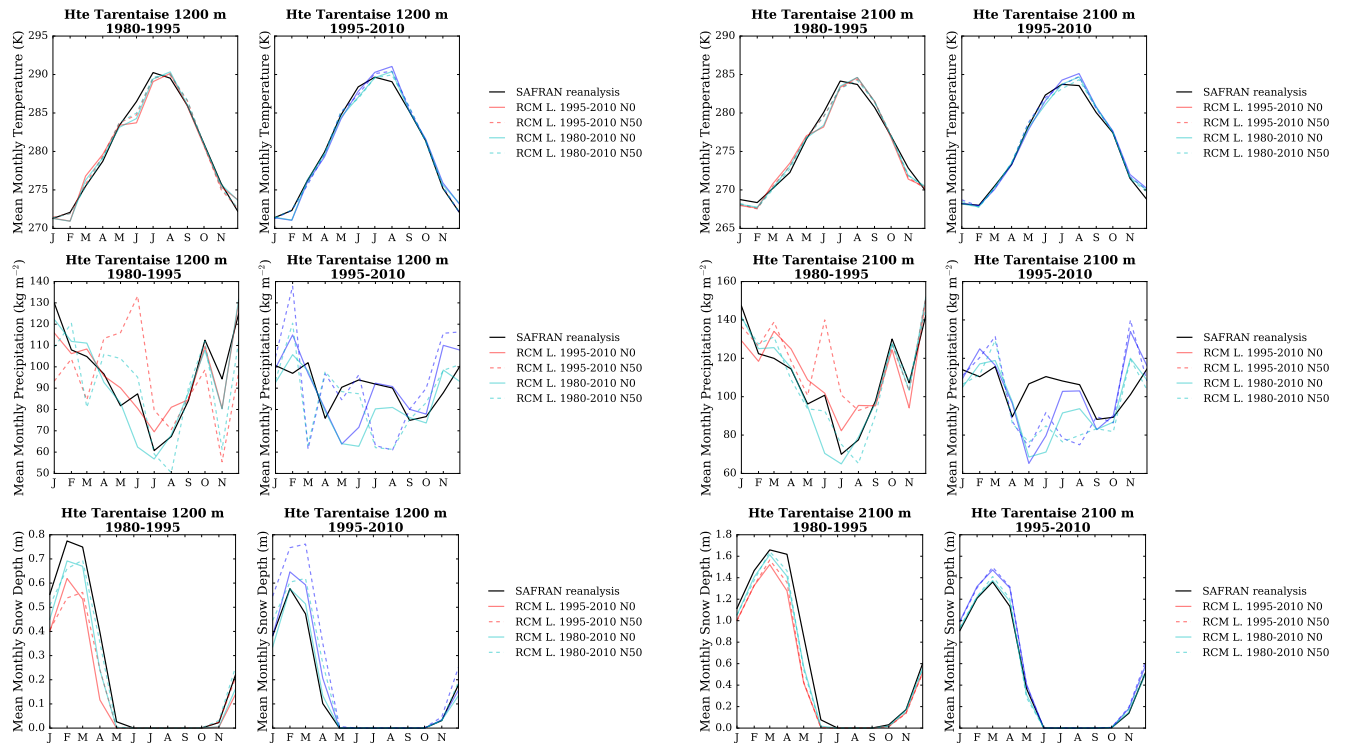


Figure S51: (top) Temperature, (middle) precipitation and (bottom) snow depth (using Crocus in this case) mean annual cycle in each adjusted RCM simulation and in the SAFRAN reanalysis over the period 1980-1995 and 1995-2010, for the Haute Tarentaise massif, and at (left) 1200 m a.s.l. and (right) 2100 m a.s.l.. Letters on the x-axis correspond to the different months of the calendar (J = January, F = February, etc.).

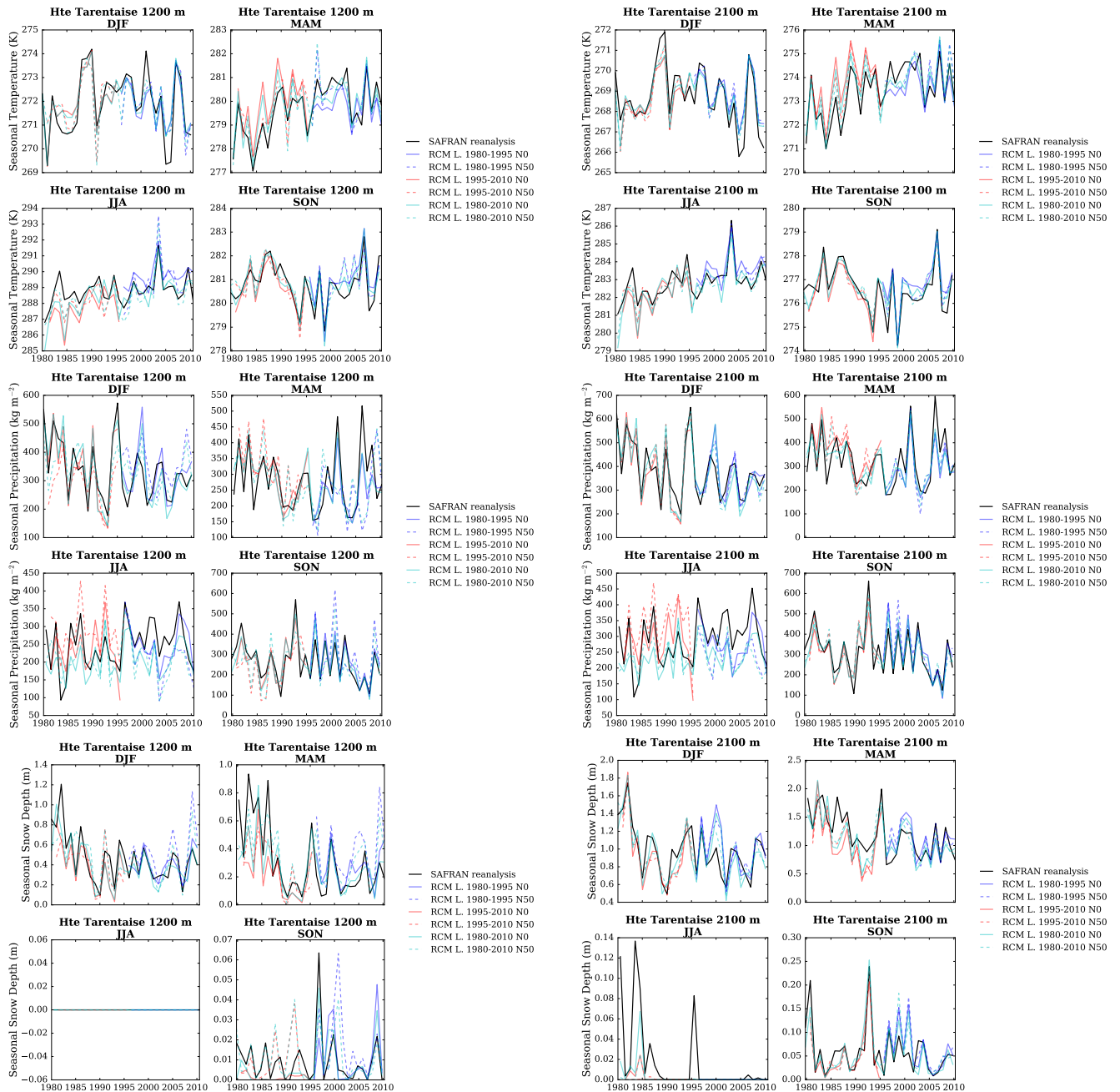


Figure S52: (top) Temperature, (middle) precipitation and (bottom) snow depth (using Crocus in this case) seasonal average time series from 1980 to 2010 in each adjusted RCM simulation and in the SAFRAN reanalysis, for the Haute Tarentaise massif, and at (left) 1200 m a.s.l. and (right) 2100 m a.s.l..

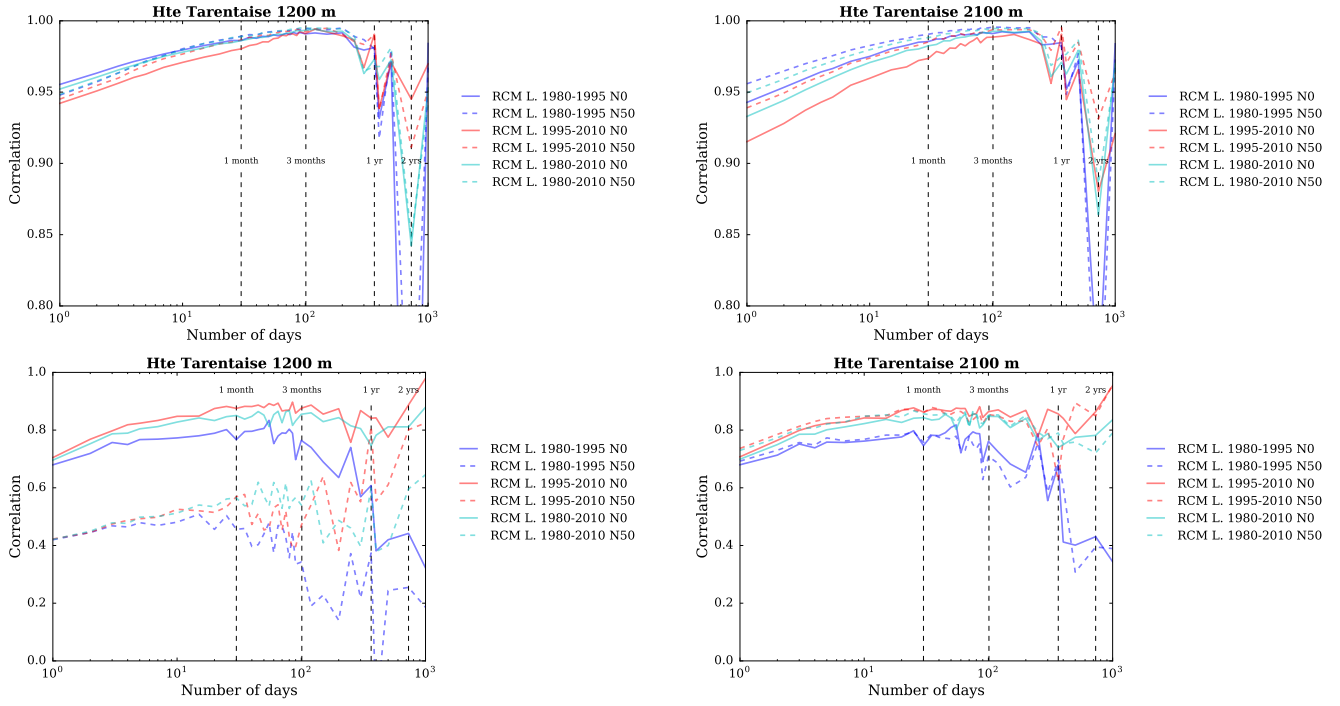


Figure S53: Correlation between the SAFRAN reanalysis and adjusted RCM (top) temperature and (bottom) precipitation as a function of the integration window over the evaluation period, for the Haute Tarentaise massif, and at (left) 1200 m a.s.l. and (right) 2100 m a.s.l..

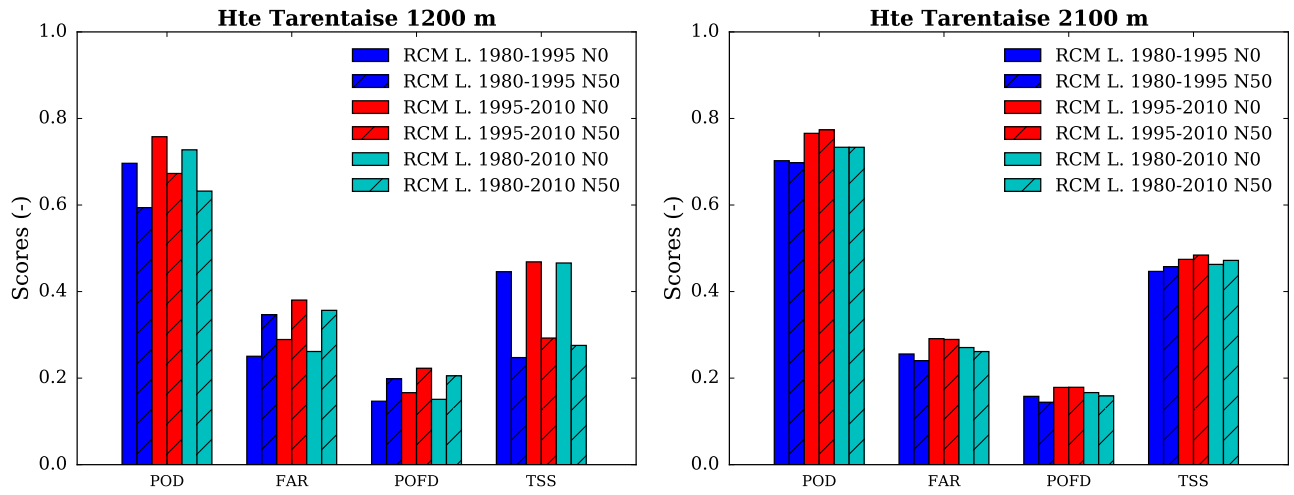


Figure S54: Scores for the detection of precipitation events in each adjusted RCM simulation compared to the SAFRAN reanalysis over the evaluation period, for the Haute Tarentaise massif, at (left) 1200 m a.s.l. and (right) 2100 m a.s.l.. POD = probability of detection, FAR = false alarm rate, POFD = probability of false detection, TSS = true skill score.

Chartreuse

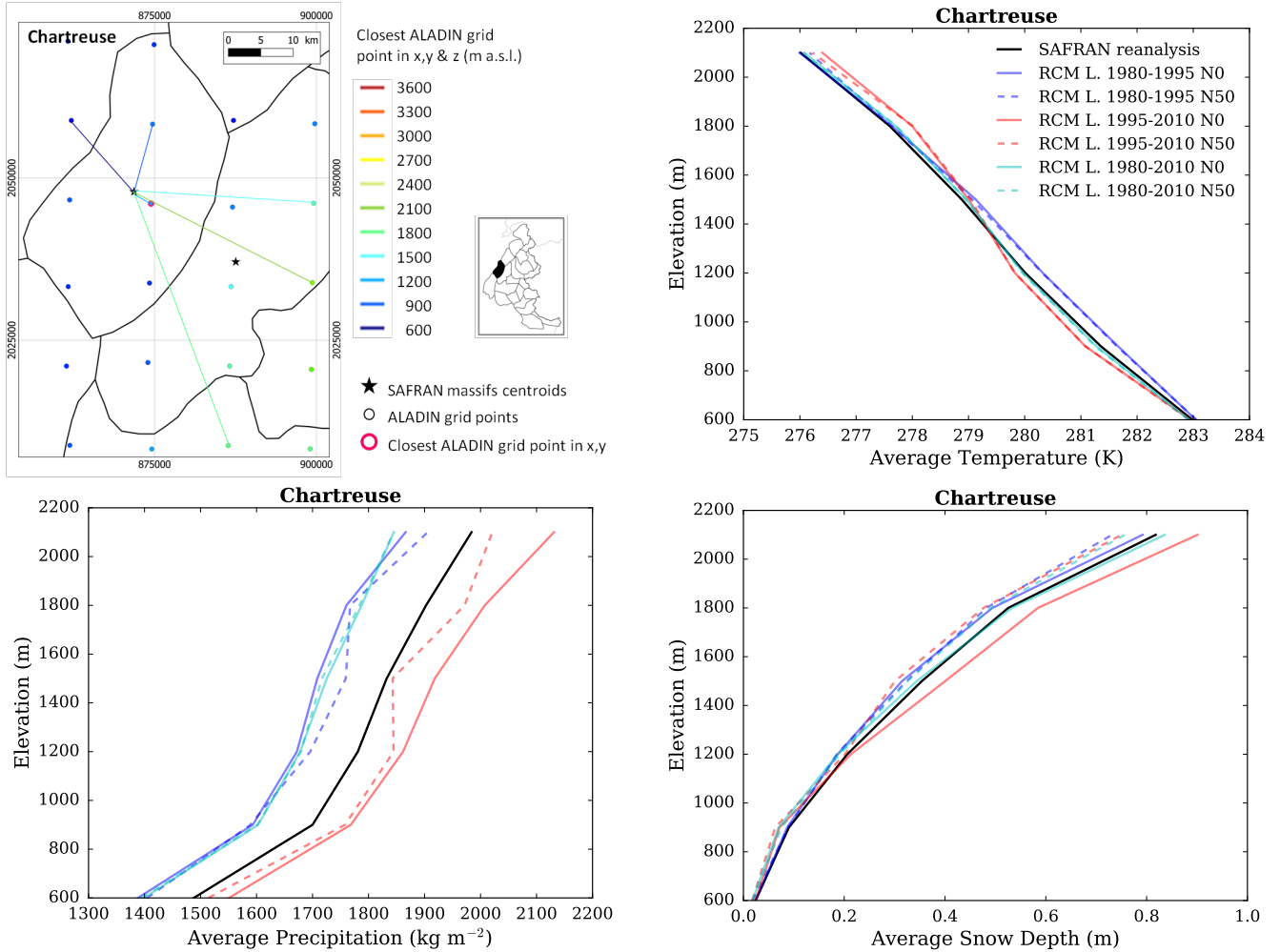


Figure S55: (top left) Location of the Chartreuse massif, with ALADIN RCM grid points chosen as the closest in x, y ($N = 0$, pink contour) and in x, y and z (using $N \neq 0$). Coloured lines link each SAFRAN massif centre point with the corresponding grid point in ALADIN for the different elevations considered (in m above sea level (a.s.l.)). (top right) Mean temperature, (bottom left) precipitation and (bottom right) snow depth (using Crocus in this case) for each elevation band for the Chartreuse massif, over the evaluation period in each adjusted RCM simulation (different learning periods and 2 neighbour selection methods) and in SAFRAN (1980-2010).

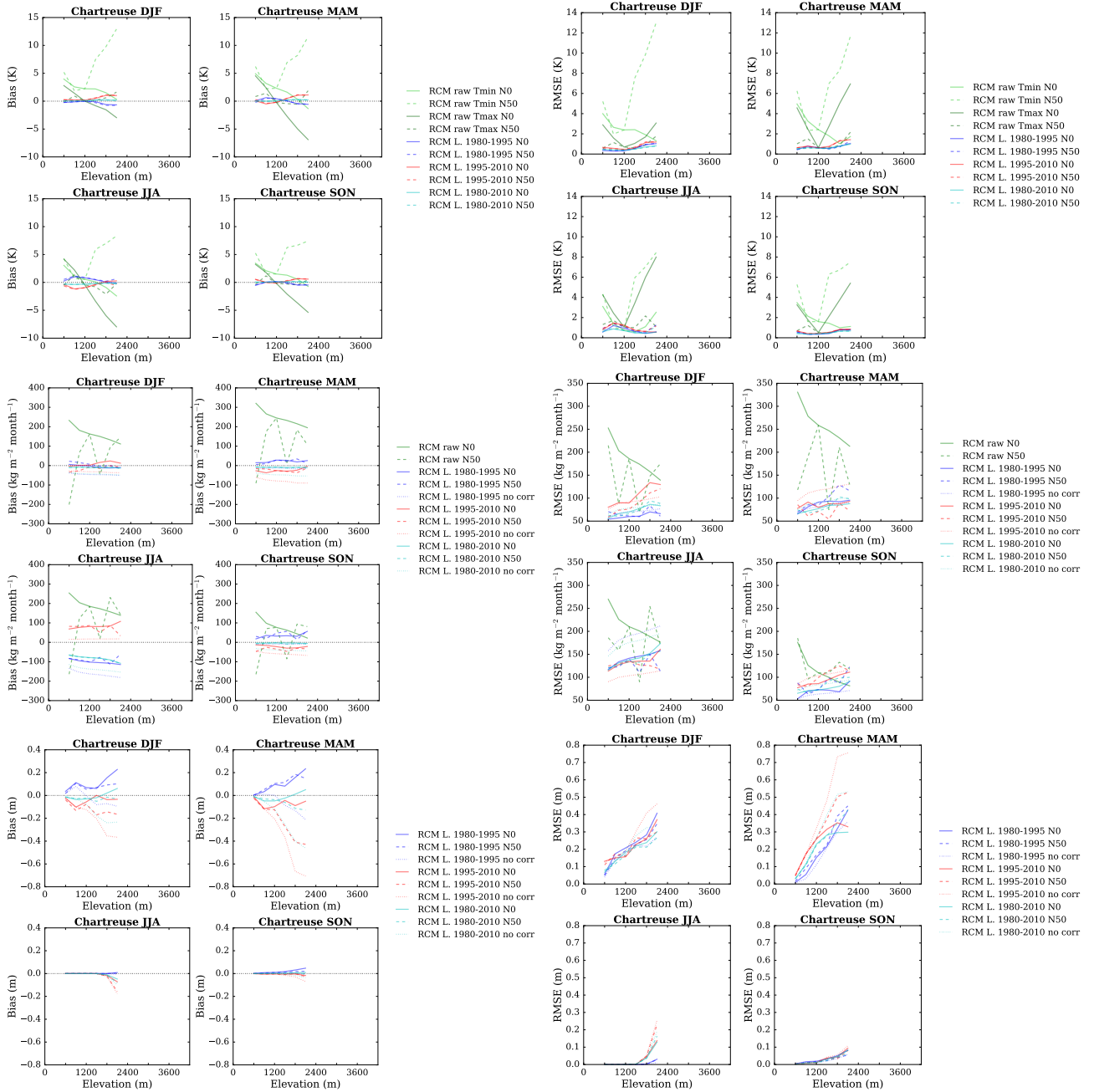


Figure S56: (top) Temperature, (middle) precipitation and (bottom) snow depth (using Crocus in this case) mean bias and root mean square error of each raw and adjusted RCM simulation compared to the SAFRAN reanalysis over the evaluation period for the Chartreuse massif as a function of elevation. Scores computed for the raw RCM simulations concern minimum and maximum daily temperatures.

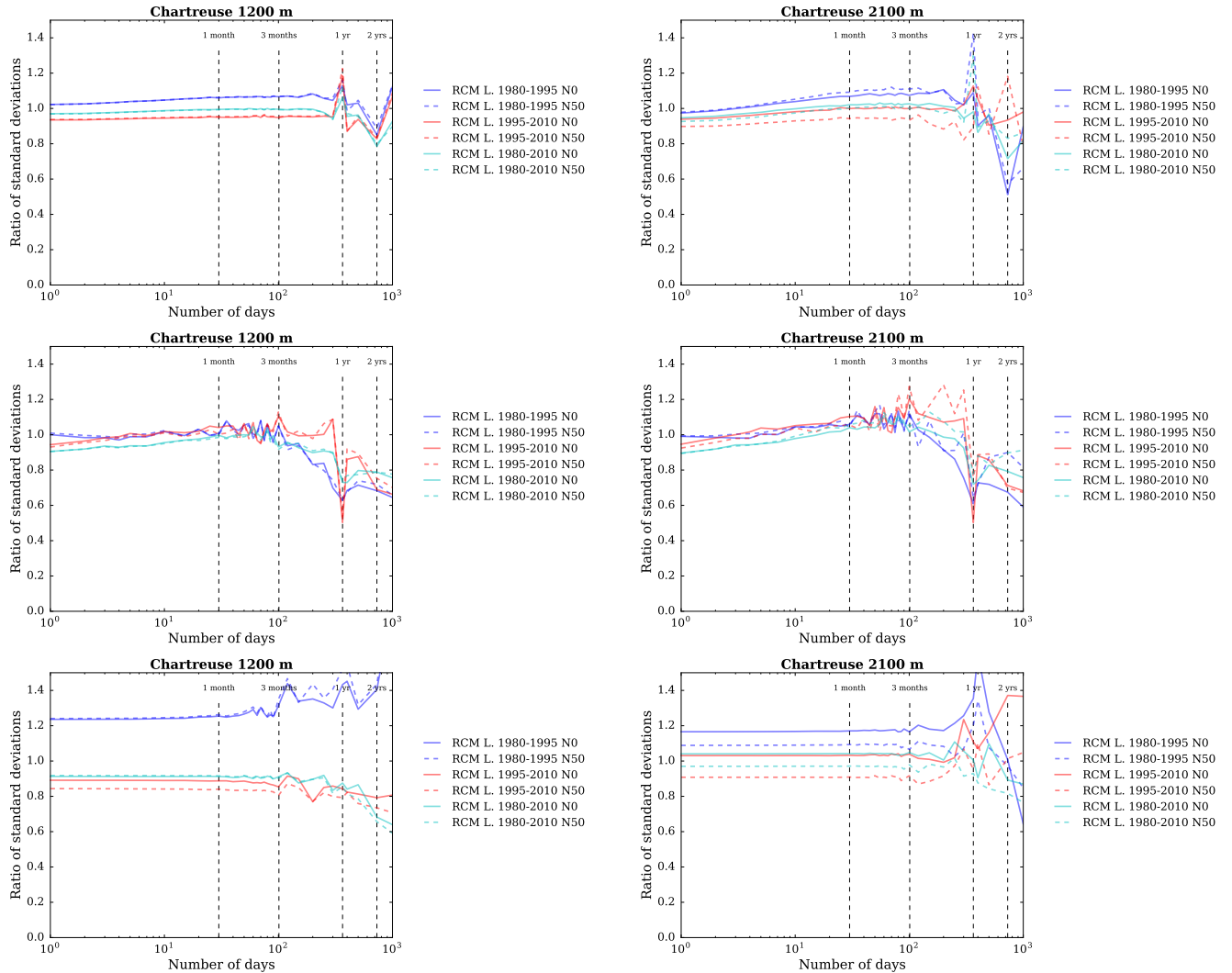


Figure S57: Ratios of standard deviations between the SAFRAN ranalysis and adjusted RCM (top) temperature, (middle) precipitation and (bottom) snow depth (using Crocus in this case) as a function of the integration window over the evaluation period, for the Chartreuse massif, at (left) 1200 m a.s.l. and (right) 2100 m a.s.l..

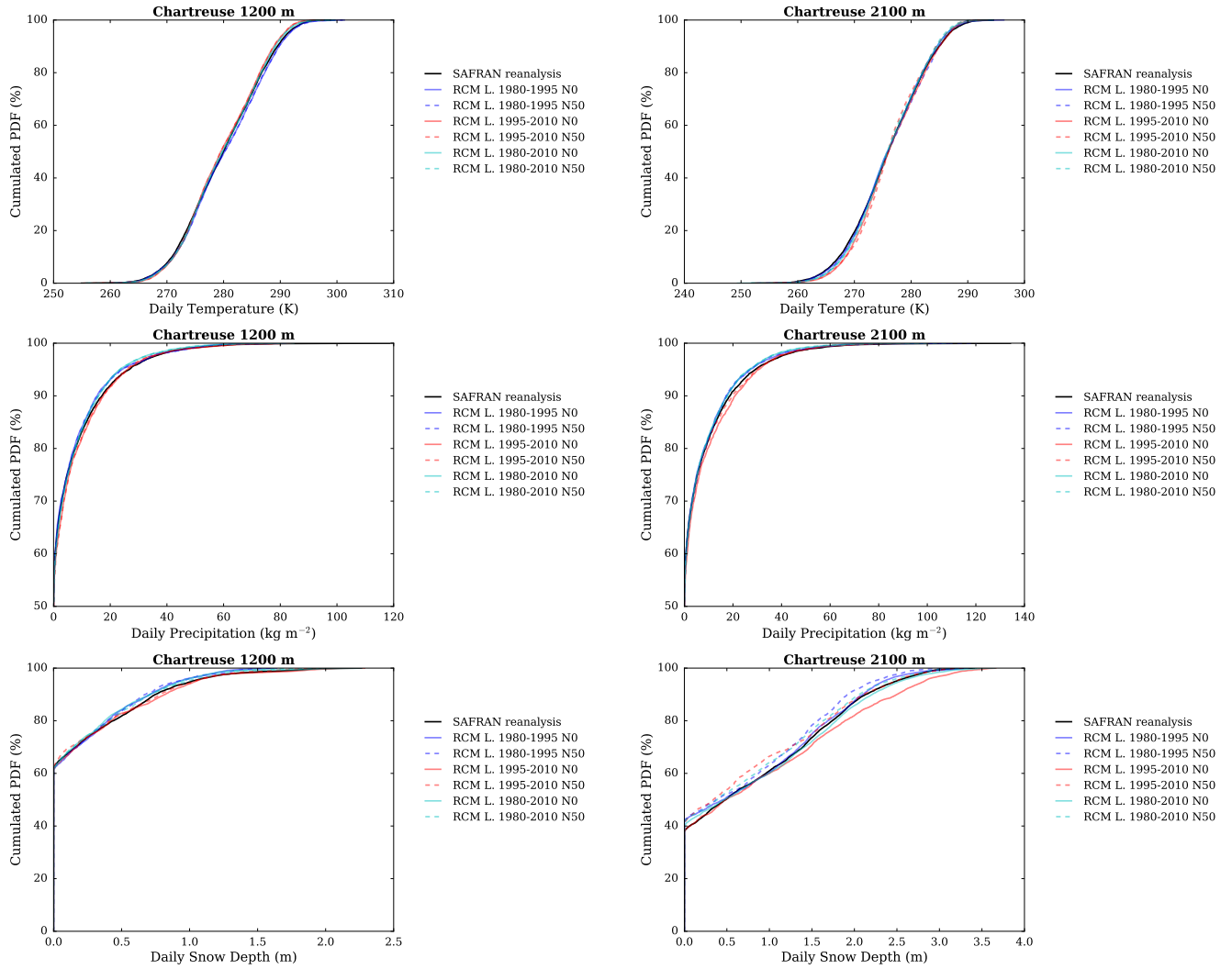


Figure S58: Cumulated probability density functions (PDFs) of daily (top) temperature, (middle) precipitation and (bottom) snow depth (using Crocus in this case) in each adjusted RCM simulation and in the SAFRAN reanalysis (1980-2010) over the evaluation period, for the Chartreuse massif, at (left) 1200 m a.s.l. and (right) 2100 m a.s.l..

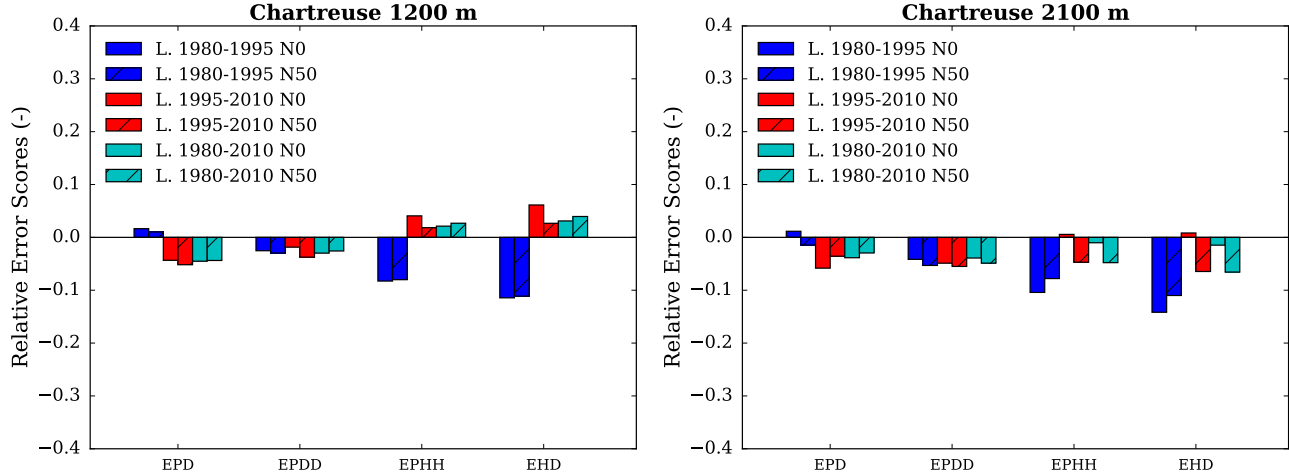


Figure S59: Scores for the duration and persistence of precipitation events in each adjusted RCM simulation compared to the SAFRAN reanalysis over the evaluation period, for the Chartreuse massif, at (left) 1200 m a.s.l. and (right) 2100 m a.s.l.. EPD = relative error on the probability of a dry day, EPDD = relative error on the probability of a dry day following a dry day, EPHH = relative error on the probability of a wet day following a wet day, EHD = relative error on the mean duration of wet periods.

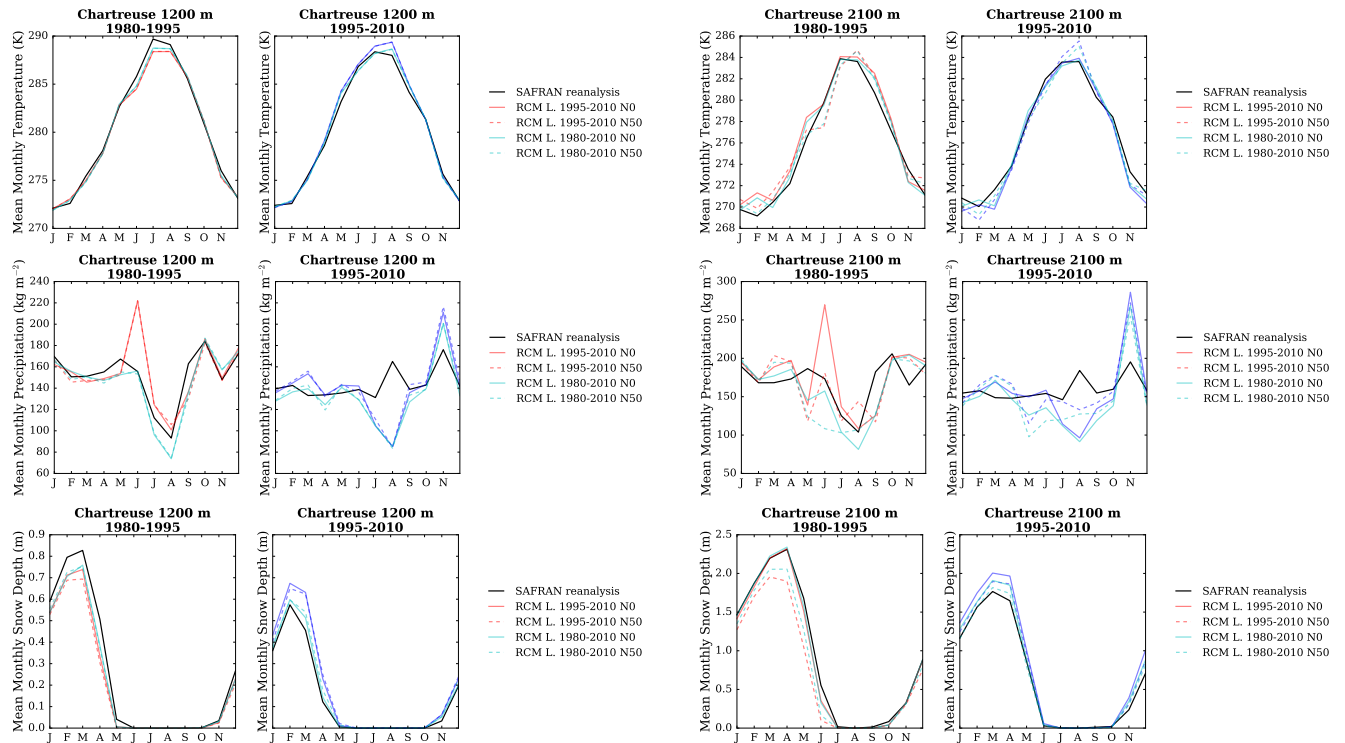


Figure S60: (top) Temperature, (middle) precipitation and (bottom) snow depth (using Crocus in this case) mean annual cycle in each adjusted RCM simulation and in the SAFRAN reanalysis over the period 1980-1995 and 1995-2010, for the Chartreuse massif, and at (left) 1200 m a.s.l. and (right) 2100 m a.s.l.. Letters on the x-axis correspond to the different months of the calendar (J = January, F = February, etc.).

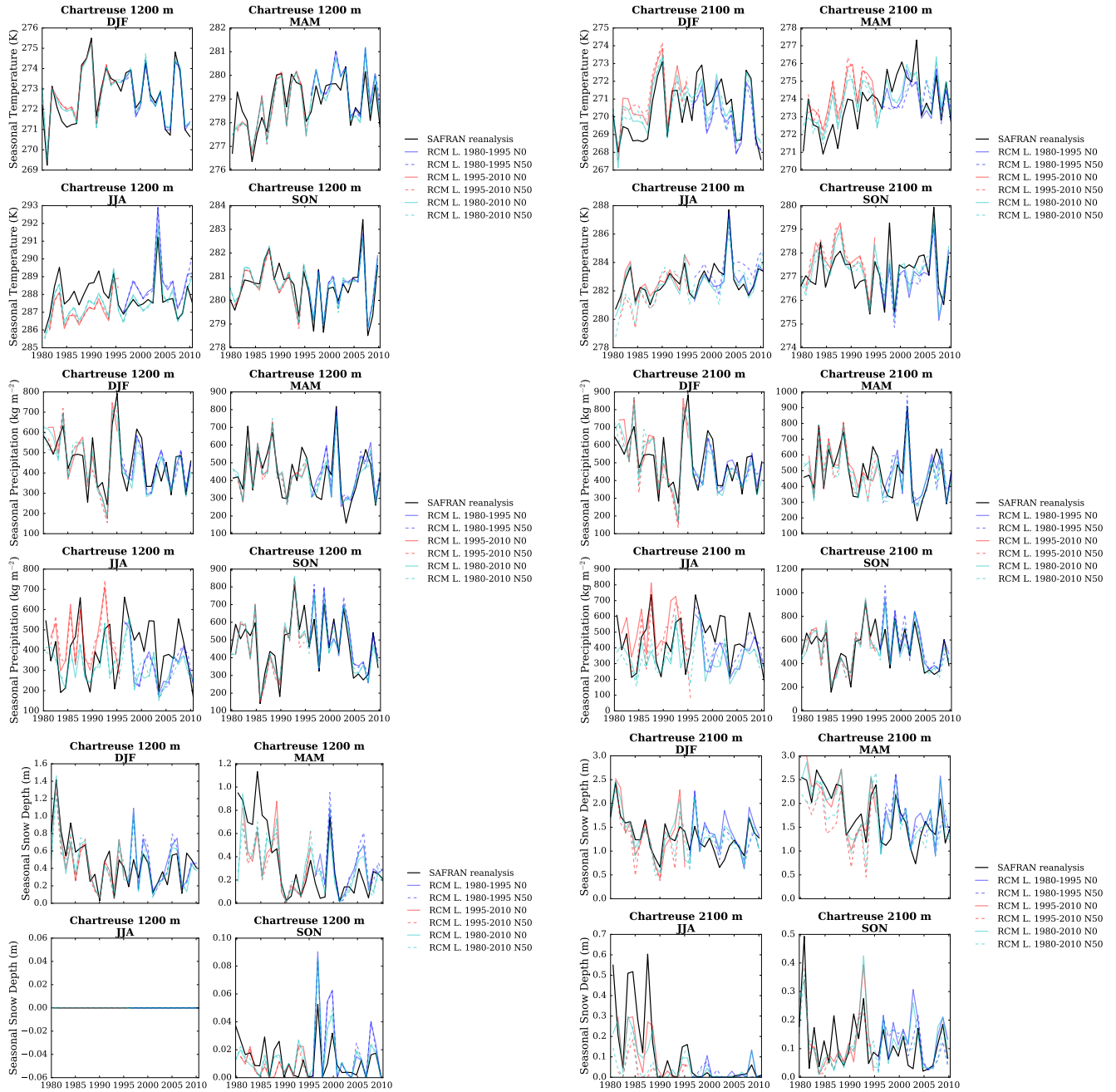


Figure S61: (top) Temperature, (middle) precipitation and (bottom) snow depth (using Crocus in this case) seasonal average time series from 1980 to 2010 in each adjusted RCM simulation and in the SAFRAN reanalysis, for the Chartreuse massif, and at (left) 1200 m a.s.l. and (right) 2100 m a.s.l..

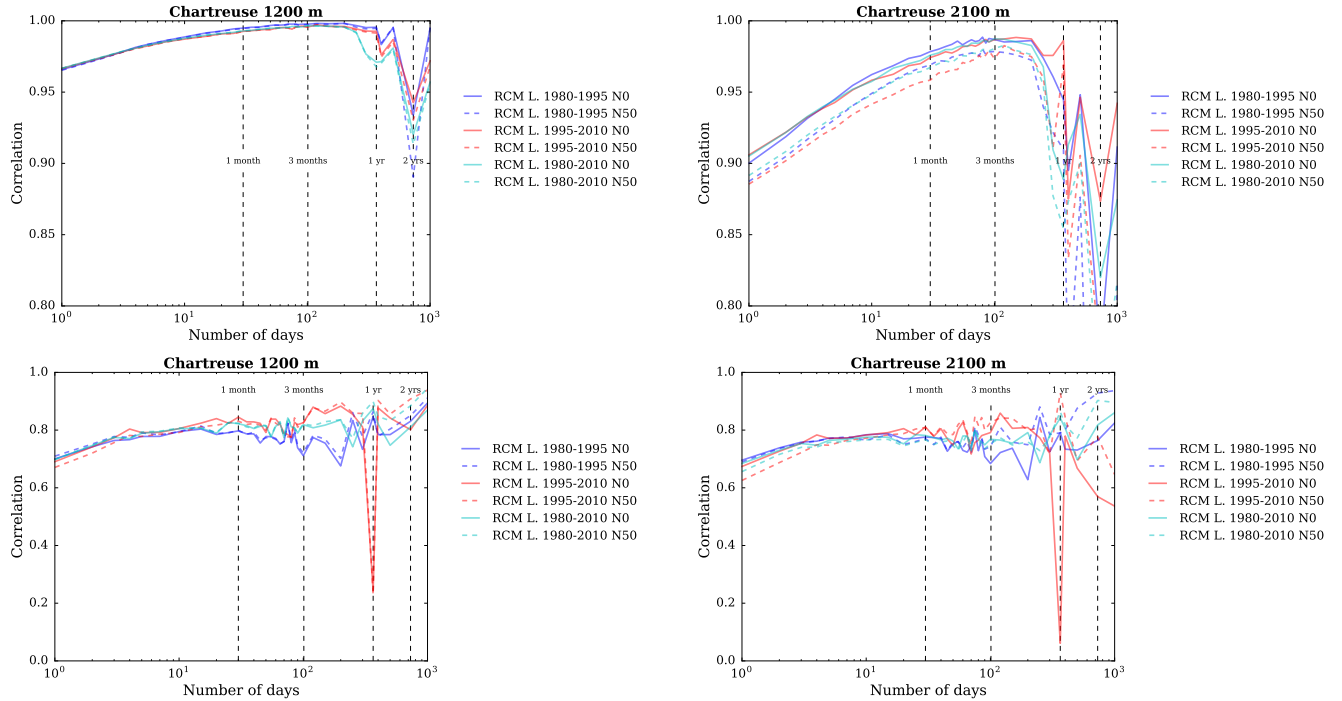


Figure S62: Correlation between the SAFRAN reanalysis and adjusted RCM (top) temperature and (bottom) precipitation as a function of the integration window over the evaluation period, for the Chartreuse massif, and at (left) 1200 m a.s.l. and (right) 2100 m a.s.l..

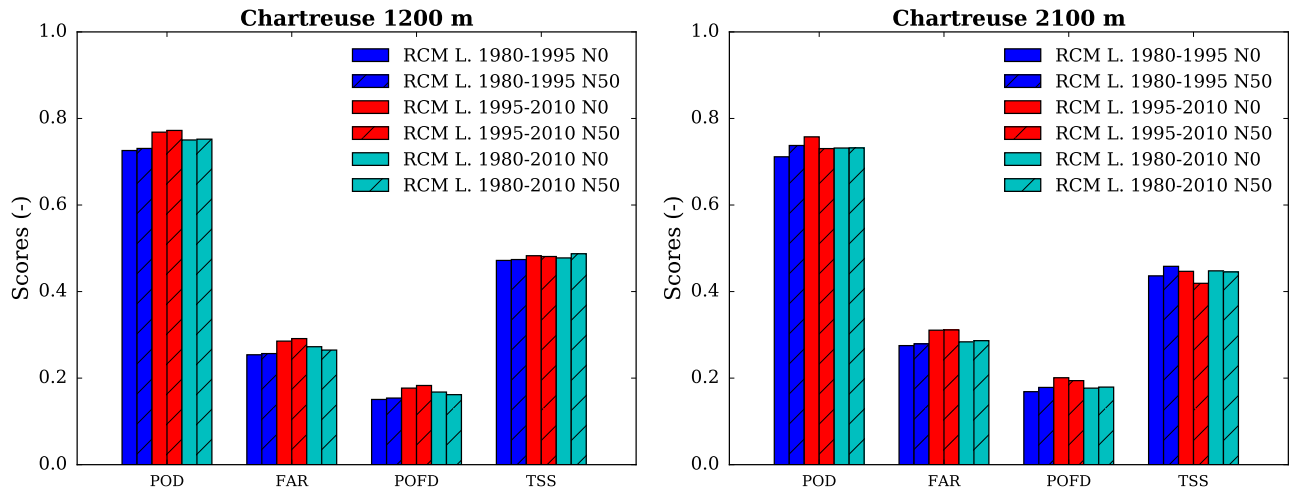


Figure S63: Scores for the detection of precipitation events in each adjusted RCM simulation compared to the SAFRAN reanalysis over the evaluation period, for the Chartreuse massif, at (left) 1200 m a.s.l. and (right) 2100 m a.s.l.. POD = probability of detection, FAR = false alarm rate, POFD = probability of false detection, TSS = true skill score.

Belledonne

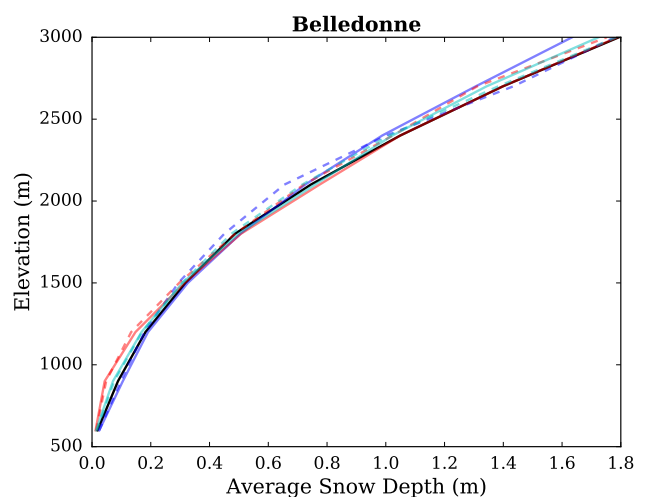
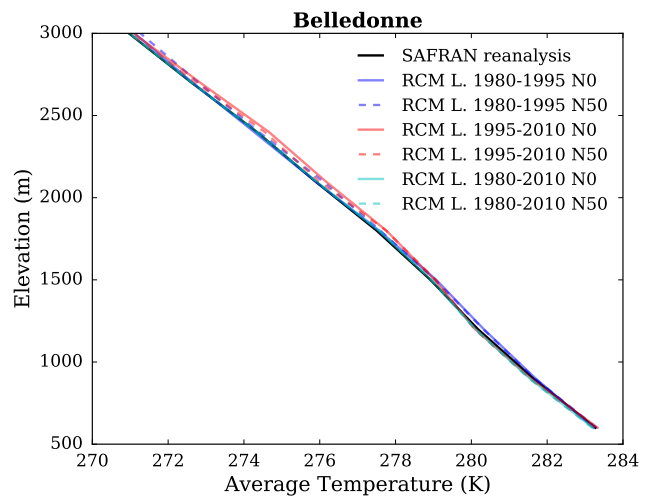
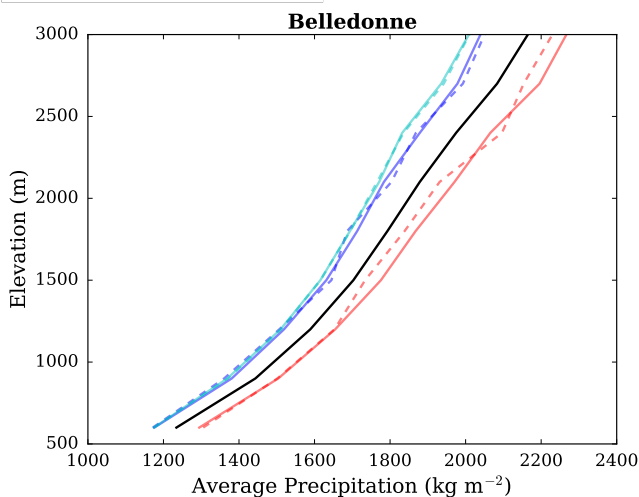
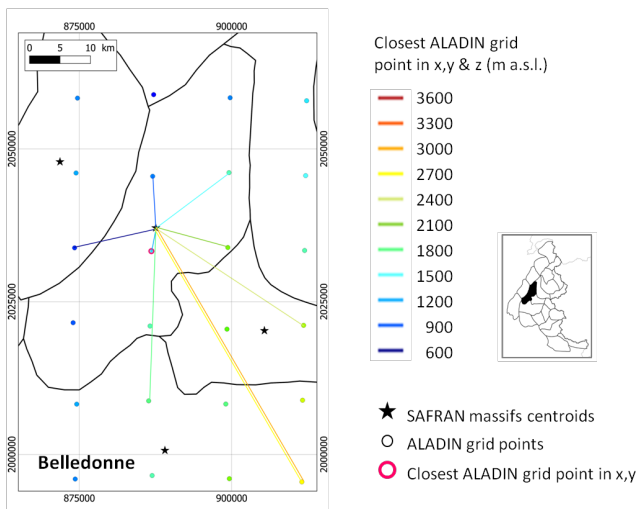


Figure S64: (top left) Location of the Belledonne massif, with ALADIN RCM grid points chosen as the closest in x , y ($N = 0$, pink contour) and in x , y and z (using $N \neq 0$). Coloured lines link each SAFRAN massif centre point with the corresponding grid point in ALADIN for the different elevations considered (in m above sea level (a.s.l.)). (top right) Mean temperature, (bottom left) precipitation and (bottom right) snow depth (using Crocus in this case) for each elevation band for the Belledonne massif, over the evaluation period in each adjusted RCM simulation (different learning periods and 2 neighbour selection methods) and in SAFRAN (1980-2010).

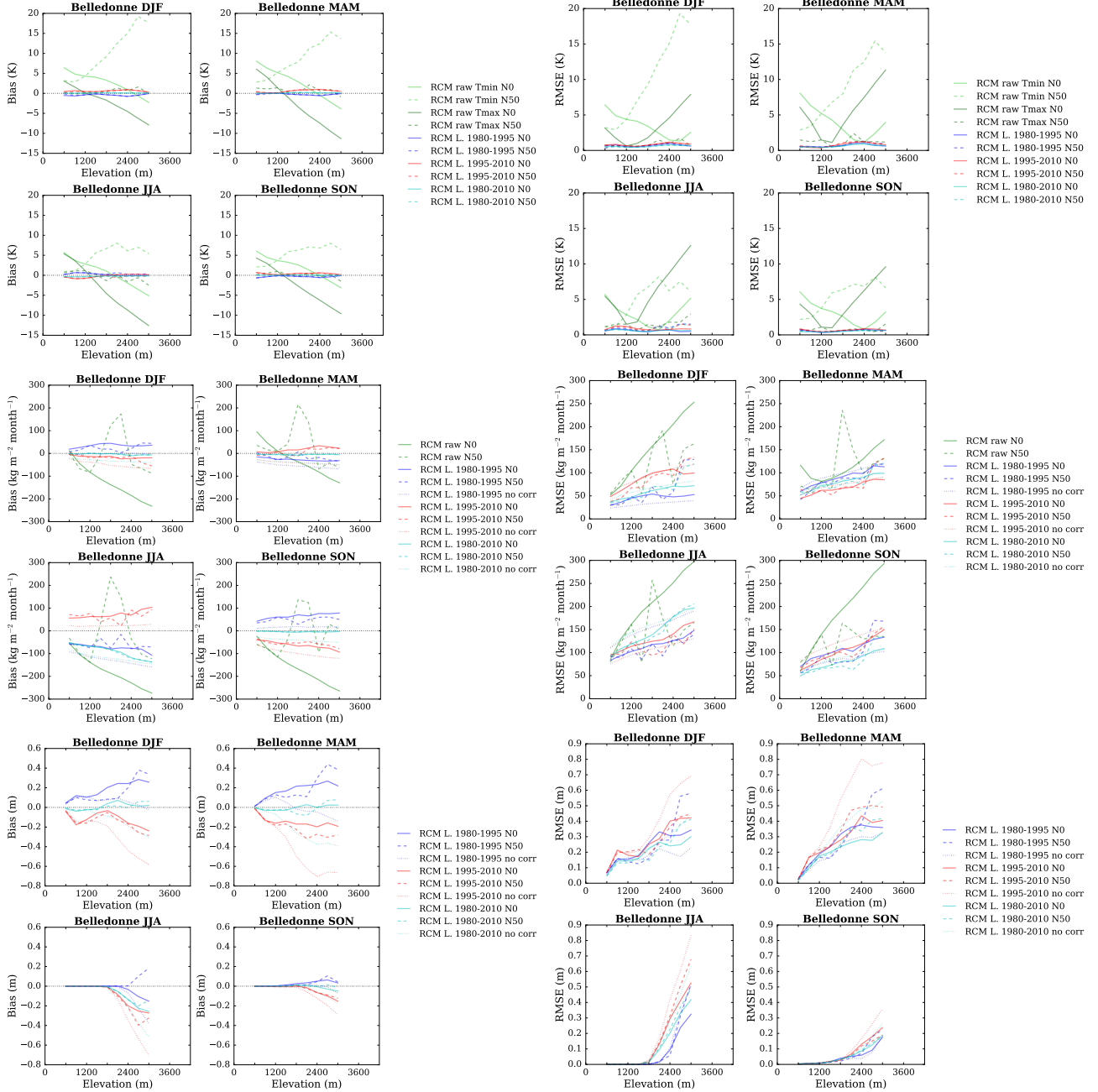


Figure S65: (top) Temperature, (middle) precipitation and (bottom) snow depth (using Crocus in this case) mean bias and root mean square error of each raw and adjusted RCM simulation compared to the SAFRAN reanalysis over the evaluation period for the Belledonne massif as a function of elevation. Scores computed for the raw RCM simulations concern minimum and maximum daily temperatures.

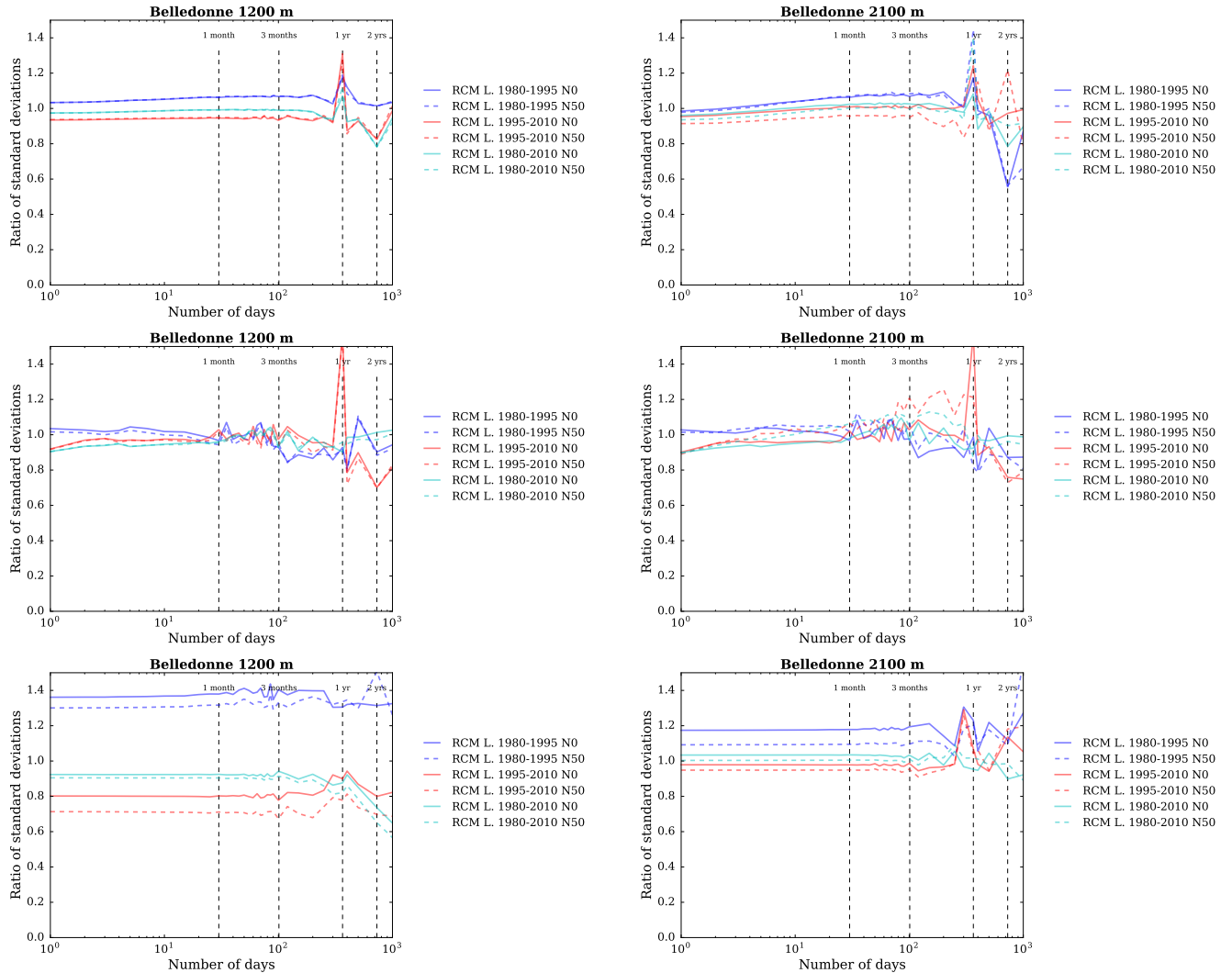


Figure S66: Ratios of standard deviations between the SAFRAN ranalysis and adjusted RCM (top) temperature, (middle) precipitation and (bottom) snow depth (using Crocus in this case) as a function of the integration window over the evaluation period, for the Belledonne massif, at (left) 1200 m a.s.l. and (right) 2100 m a.s.l..

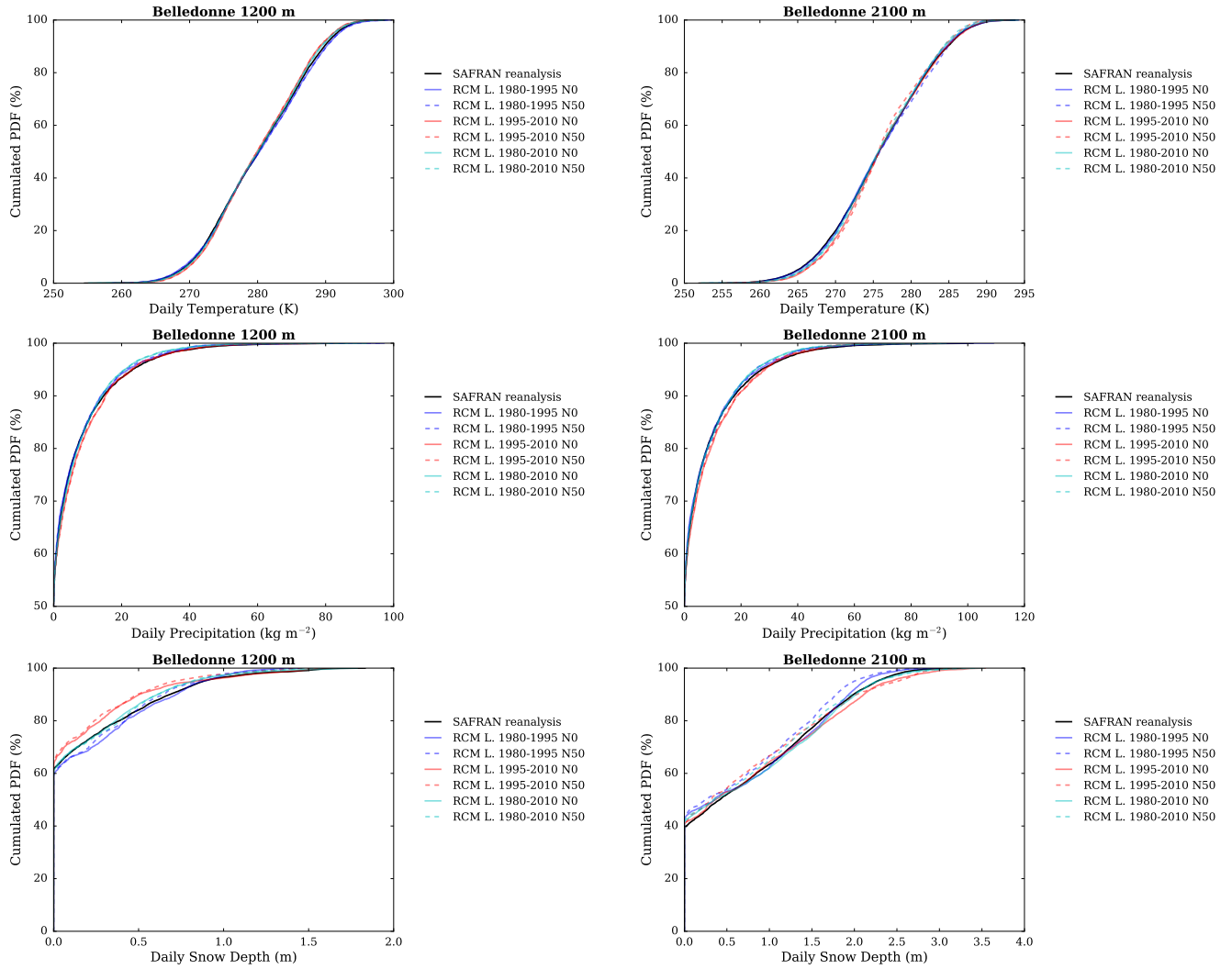


Figure S67: Cumulated probability density functions (PDFs) of daily (top) temperature, (middle) precipitation and (bottom) snow depth (using Crocus in this case) in each adjusted RCM simulation and in the SAFRAN reanalysis (1980-2010) over the evaluation period, for the Belledonne massif, at (left) 1200 m a.s.l. and (right) 2100 m a.s.l..

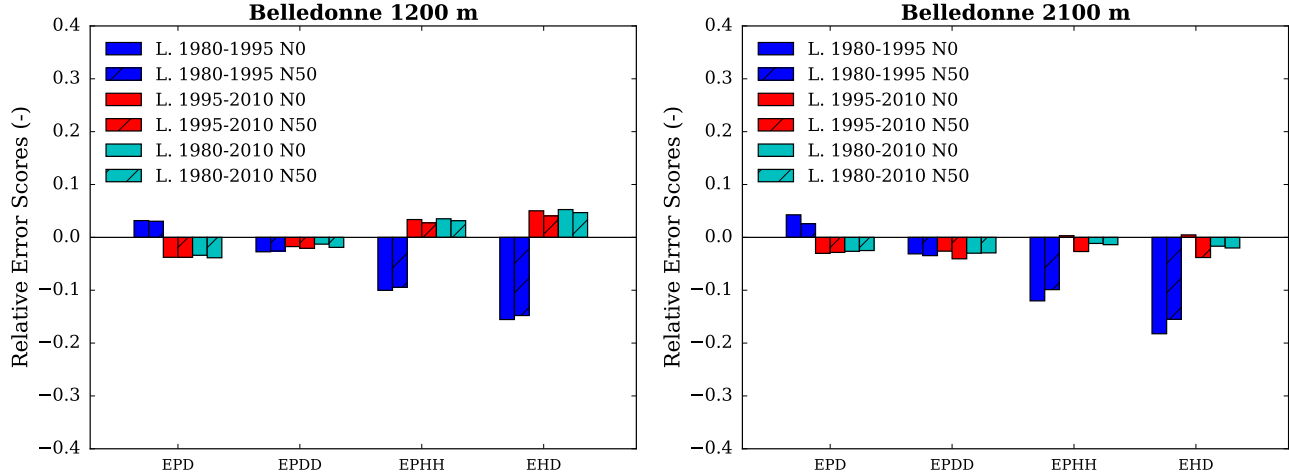


Figure S68: Scores for the duration and persistence of precipitation events in each adjusted RCM simulation compared to the SAFRAN reanalysis over the evaluation period, for the Belledonne massif, at (left) 1200 m a.s.l. and (right) 2100 m a.s.l.. EPD = relative error on the probability of a dry day, EPDD = relative error on the probability of a dry day following a dry day, EPHH = relative error on the probability of a wet day following a wet day, EHD = relative error on the mean duration of wet periods.

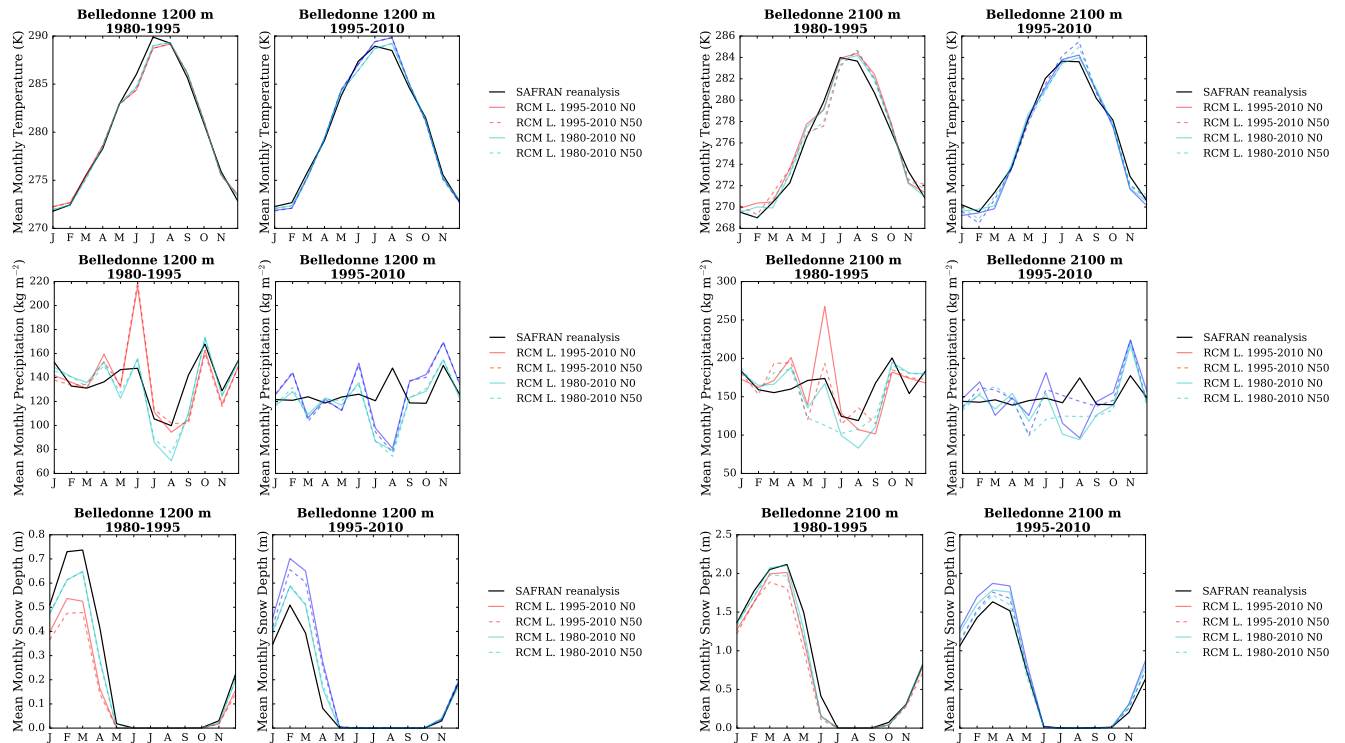


Figure S69: (top) Temperature, (middle) precipitation and (bottom) snow depth (using Crocus in this case) mean annual cycle in each adjusted RCM simulation and in the SAFRAN reanalysis over the period 1980-1995 and 1995-2010, for the Belledonne massif, and at (left) 1200 m a.s.l. and (right) 2100 m a.s.l.. Letters on the x-axis correspond to the different months of the calendar (J = January, F = February, etc.).

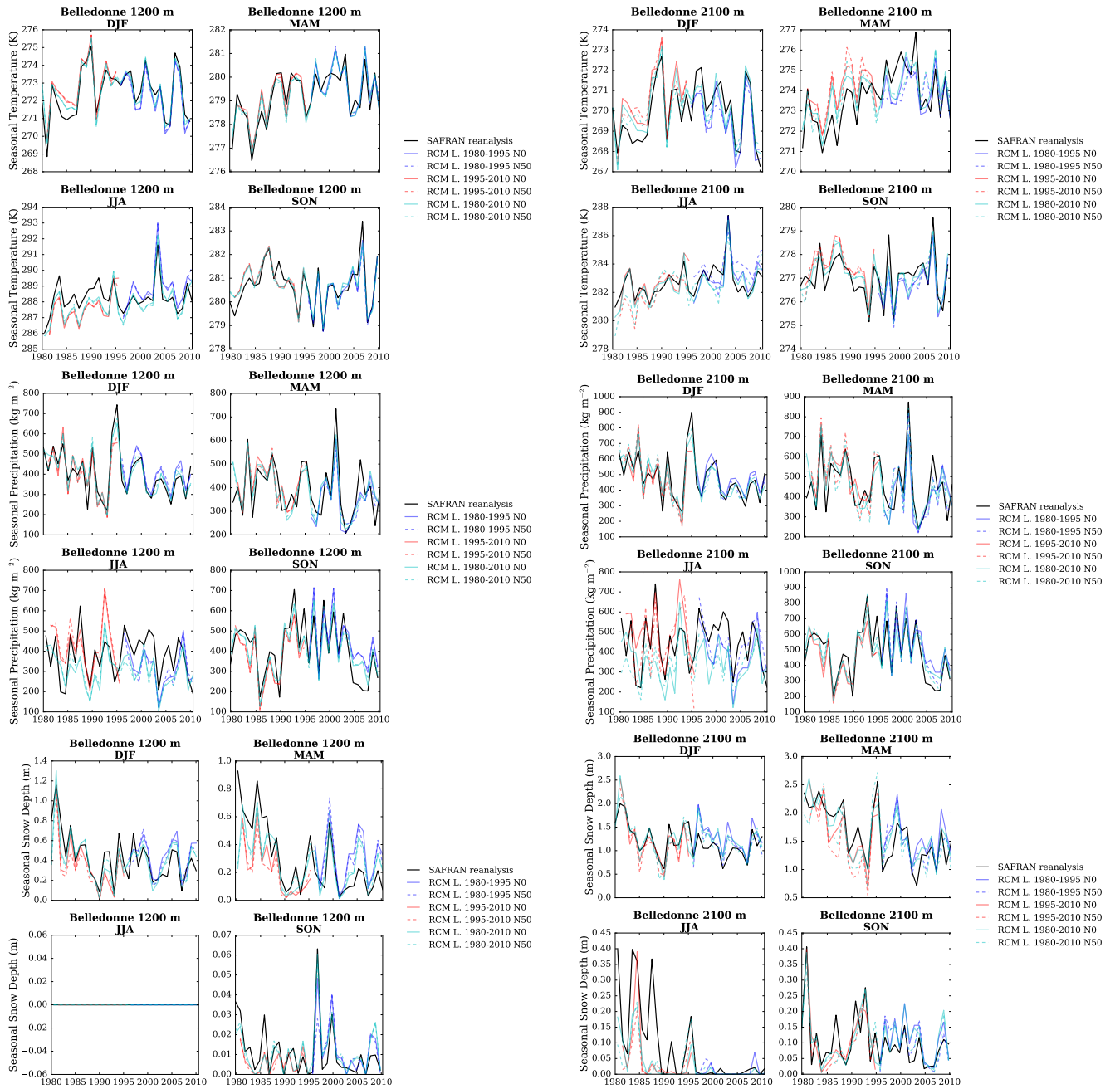


Figure S70: (top) Temperature, (middle) precipitation and (bottom) snow depth (using Crocus in this case) seasonal average time series from 1980 to 2010 in each adjusted RCM simulation and in the SAFRAN reanalysis, for the Belledonne massif, and at (left) 1200 m a.s.l. and (right) 2100 m a.s.l..

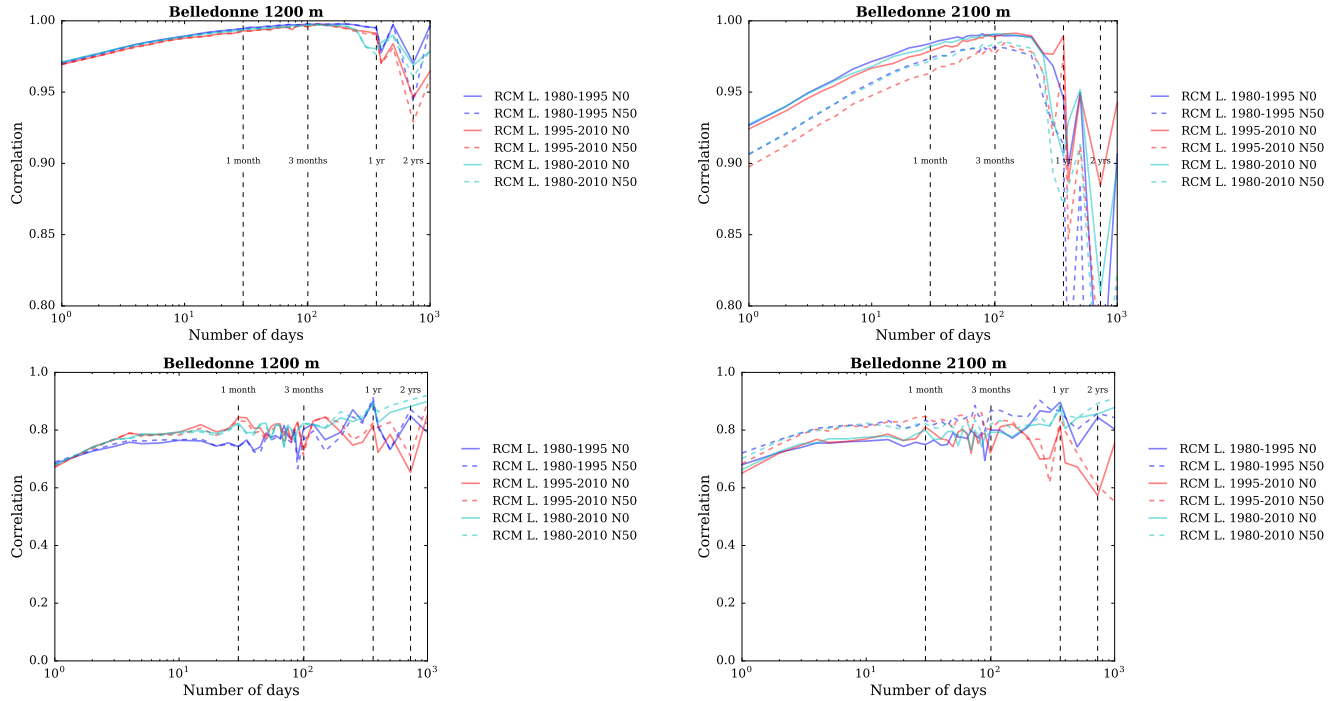


Figure S71: Correlation between the SAFRAN reanalysis and adjusted RCM (top) temperature and (bottom) precipitation as a function of the integration window over the evaluation period, for the Belledonne massif, and at (left) 1200 m a.s.l. and (right) 2100 m a.s.l..

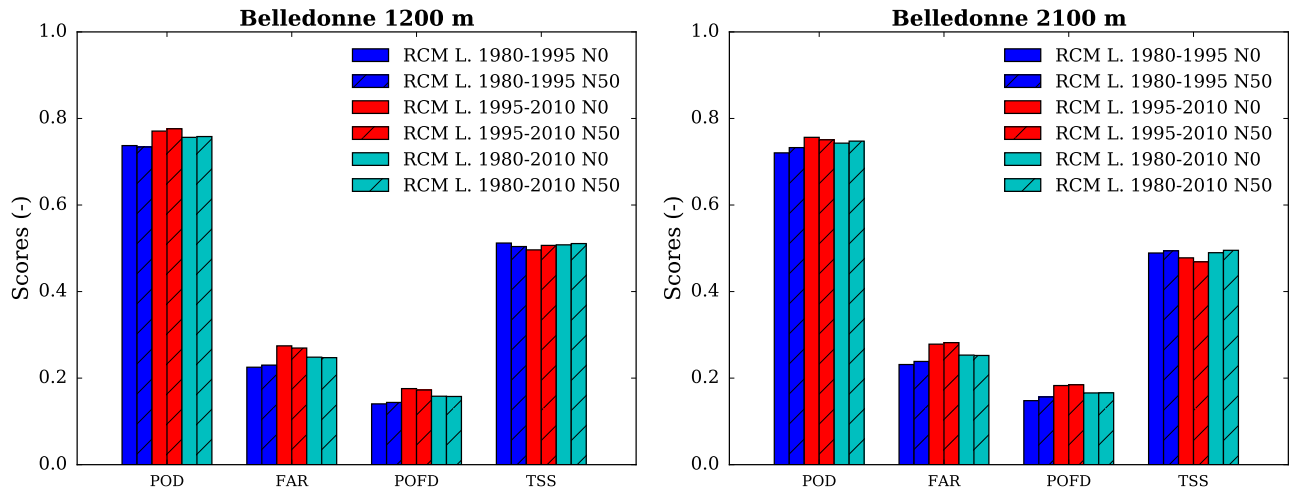


Figure S72: Scores for the detection of precipitation events in each adjusted RCM simulation compared to the SAFRAN reanalysis over the evaluation period, for the Belledonne massif, at (left) 1200 m a.s.l. and (right) 2100 m a.s.l.. POD = probability of detection, FAR = false alarm rate, POFD = probability of false detection, TSS = true skill score.

Maurienne

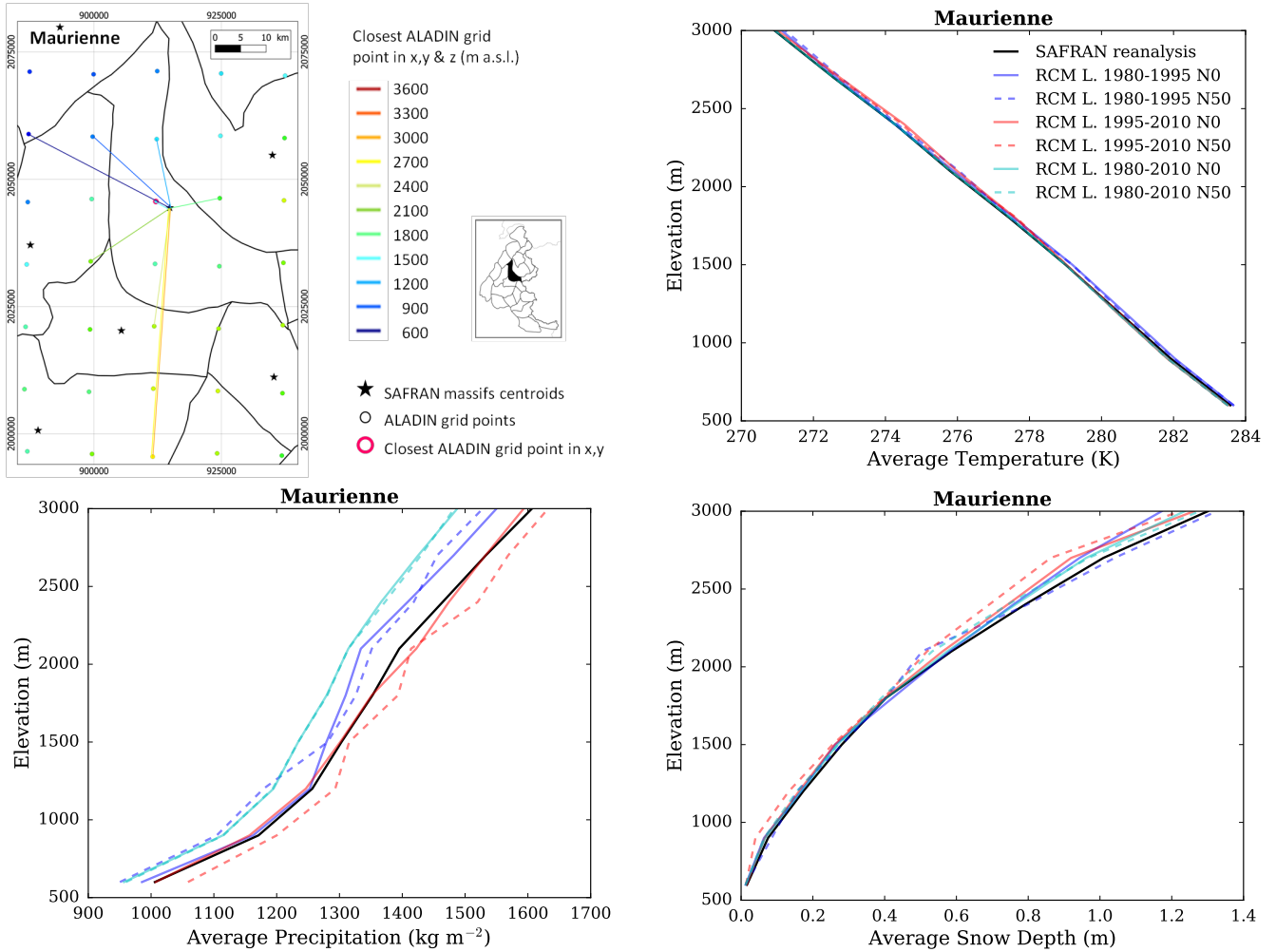


Figure S73: (top left) Location of the Maurienne massif, with ALADIN RCM grid points chosen as the closest in x, y ($N = 0$, pink contour) and in x, y and z (using $N \neq 0$). Coloured lines link each SAFRAN massif centre point with the corresponding grid point in ALADIN for the different elevations considered (in m above sea level (a.s.l.)). (top right) Mean temperature, (bottom left) precipitation and (bottom right) snow depth (using Crocus in this case) for each elevation band for the Maurienne massif, over the evaluation period in each adjusted RCM simulation (different learning periods and 2 neighbour selection methods) and in SAFRAN (1980-2010).

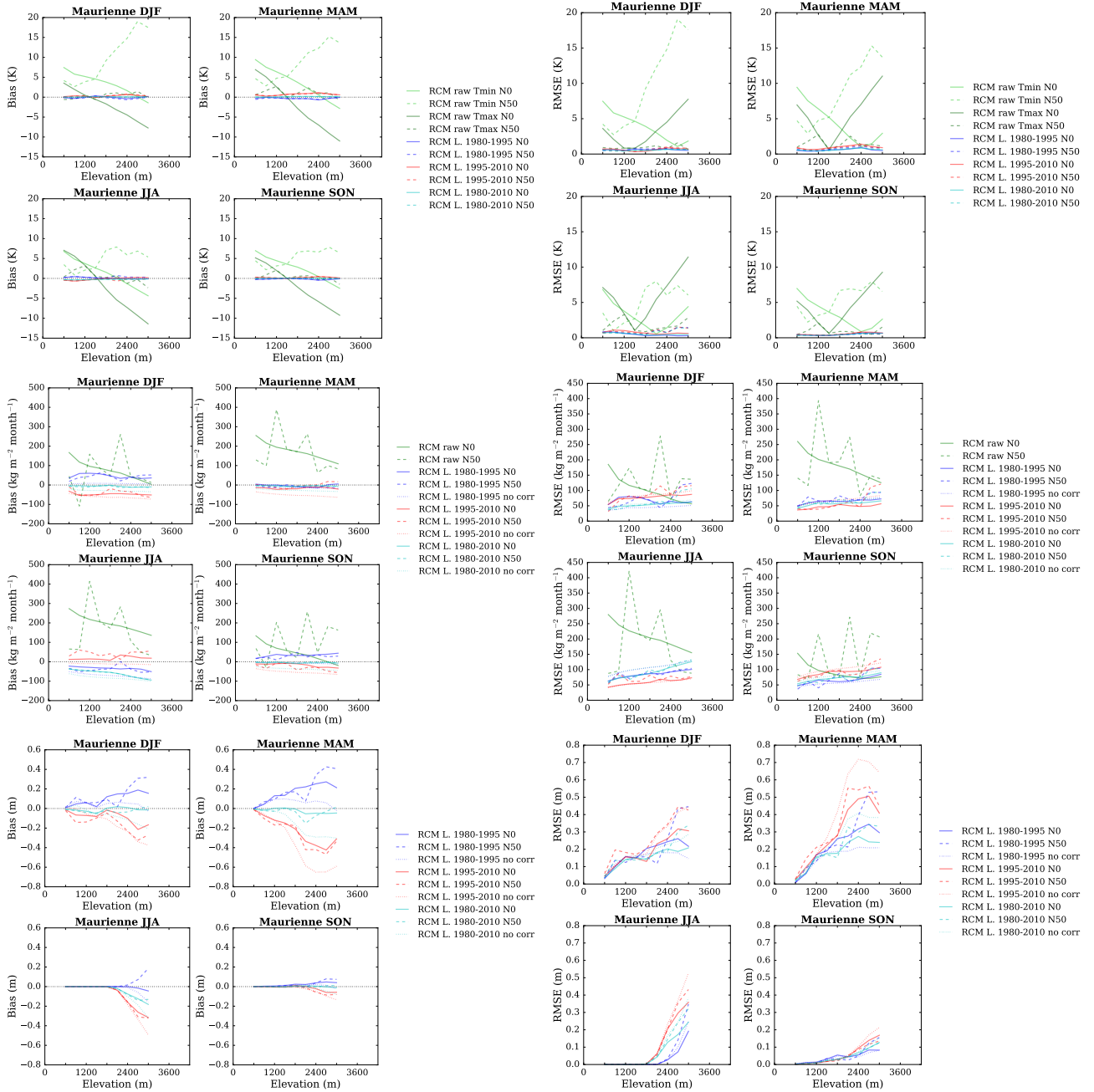


Figure S74: (top) Temperature, (middle) precipitation and (bottom) snow depth (using Crocus in this case) mean bias and root mean square error of each raw and adjusted RCM simulation compared to the SAFRAN reanalysis over the evaluation period for the Maurienne massif as a function of elevation. Scores computed for the raw RCM simulations concern minimum and maximum daily temperatures.

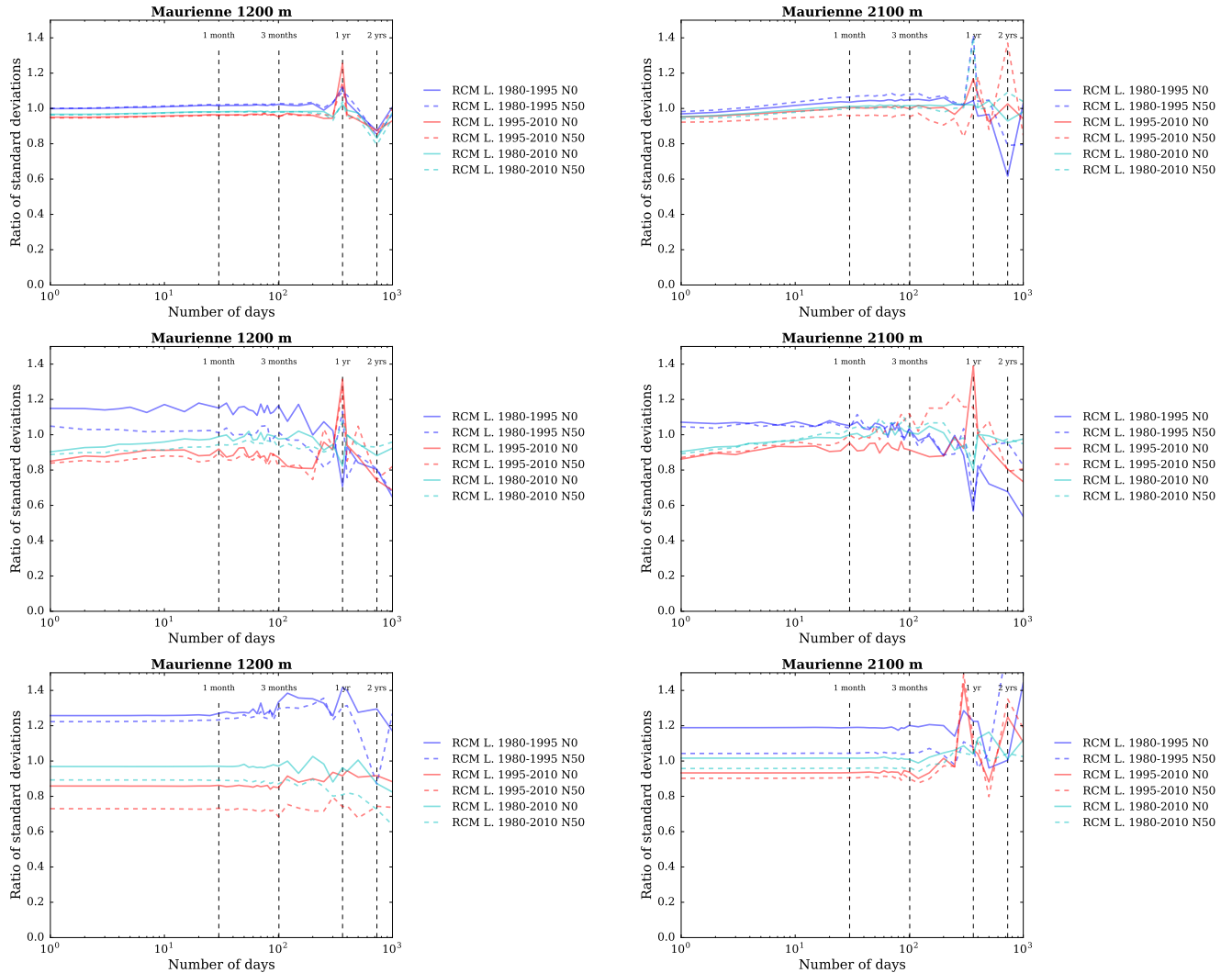


Figure S75: Ratios of standard deviations between the SAFRAN reanalysis and adjusted RCM (top) temperature, (middle) precipitation and (bottom) snow depth (using Crocus in this case) as a function of the integration window over the evaluation period, for the Maurienne massif, at (left) 1200 m a.s.l. and (right) 2100 m a.s.l..

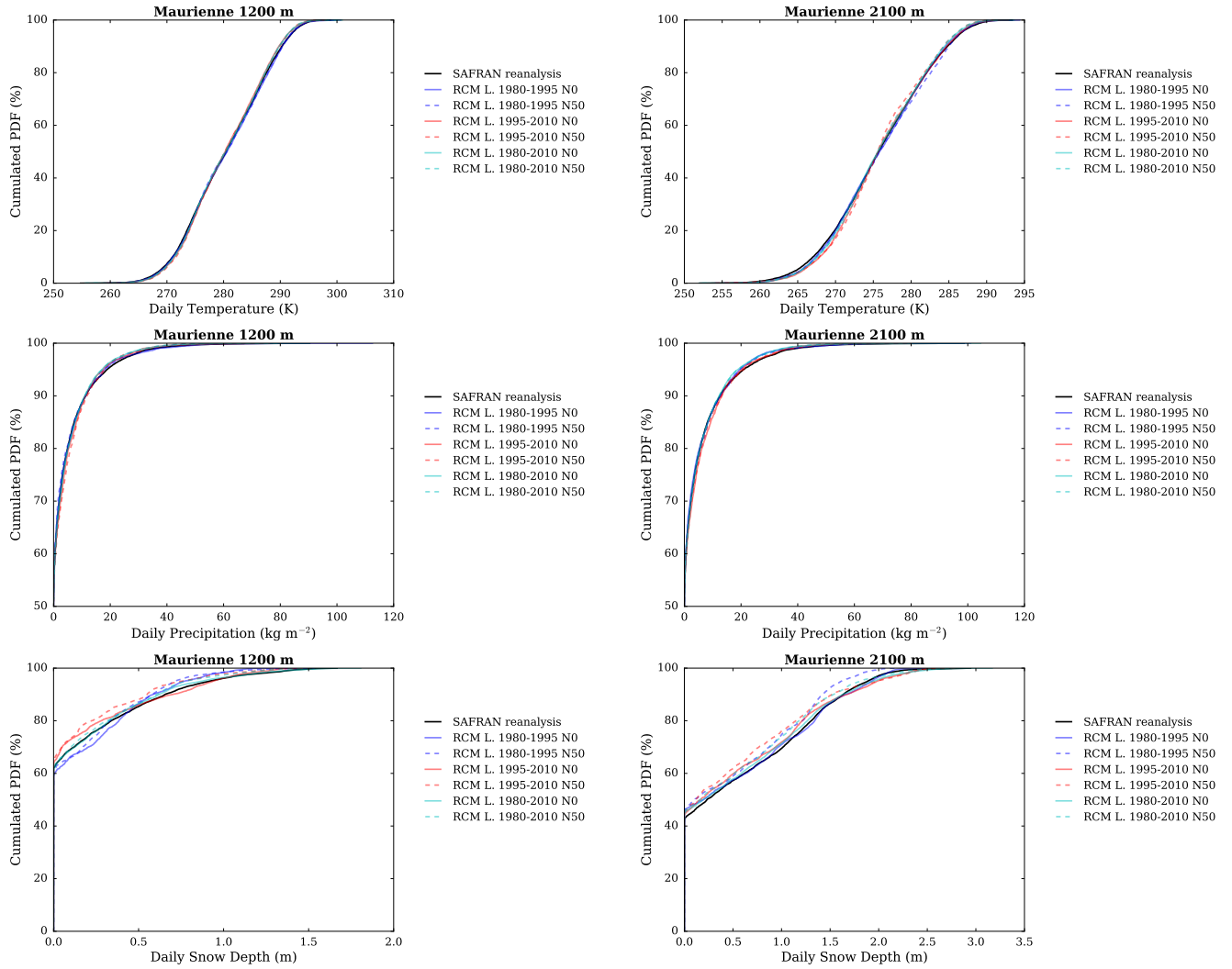


Figure S76: Cumulated probability density functions (PDFs) of daily (top) temperature, (middle) precipitation and (bottom) snow depth (using Crocus in this case) in each adjusted RCM simulation and in the SAFRAN reanalysis (1980-2010) over the evaluation period, for the Maurienne massif, at (left) 1200 m a.s.l. and (right) 2100 m a.s.l..

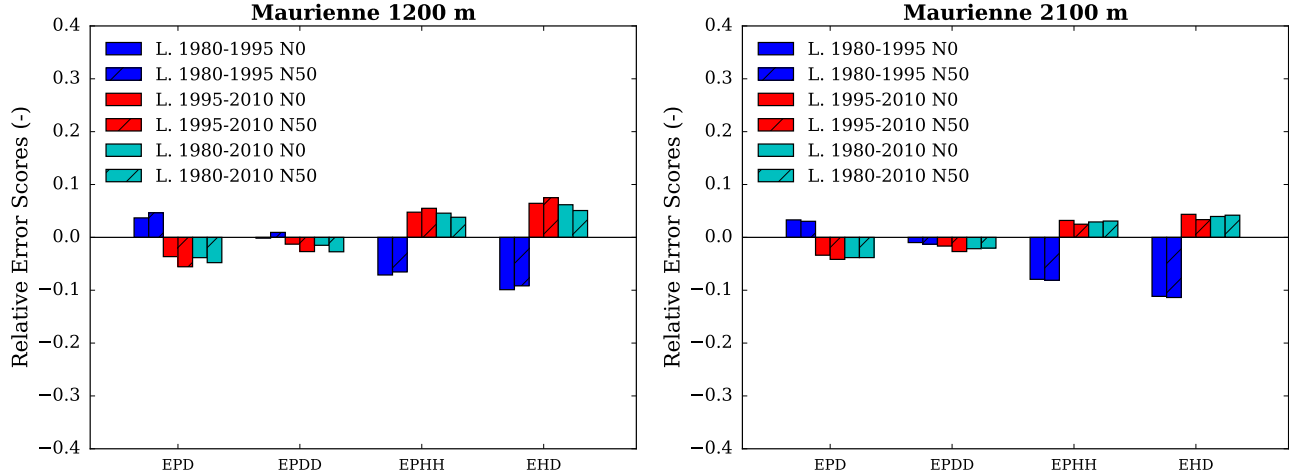


Figure S77: Scores for the duration and persistence of precipitation events in each adjusted RCM simulation compared to the SAFRAN reanalysis over the evaluation period, for the Maurienne massif, at (left) 1200 m a.s.l. and (right) 2100 m a.s.l.. EPD = relative error on the probability of a dry day, EPDD = relative error on the probability of a dry day following a dry day, EPHH = relative error on the probability of a wet day following a wet day, EHD = relative error on the mean duration of wet periods.

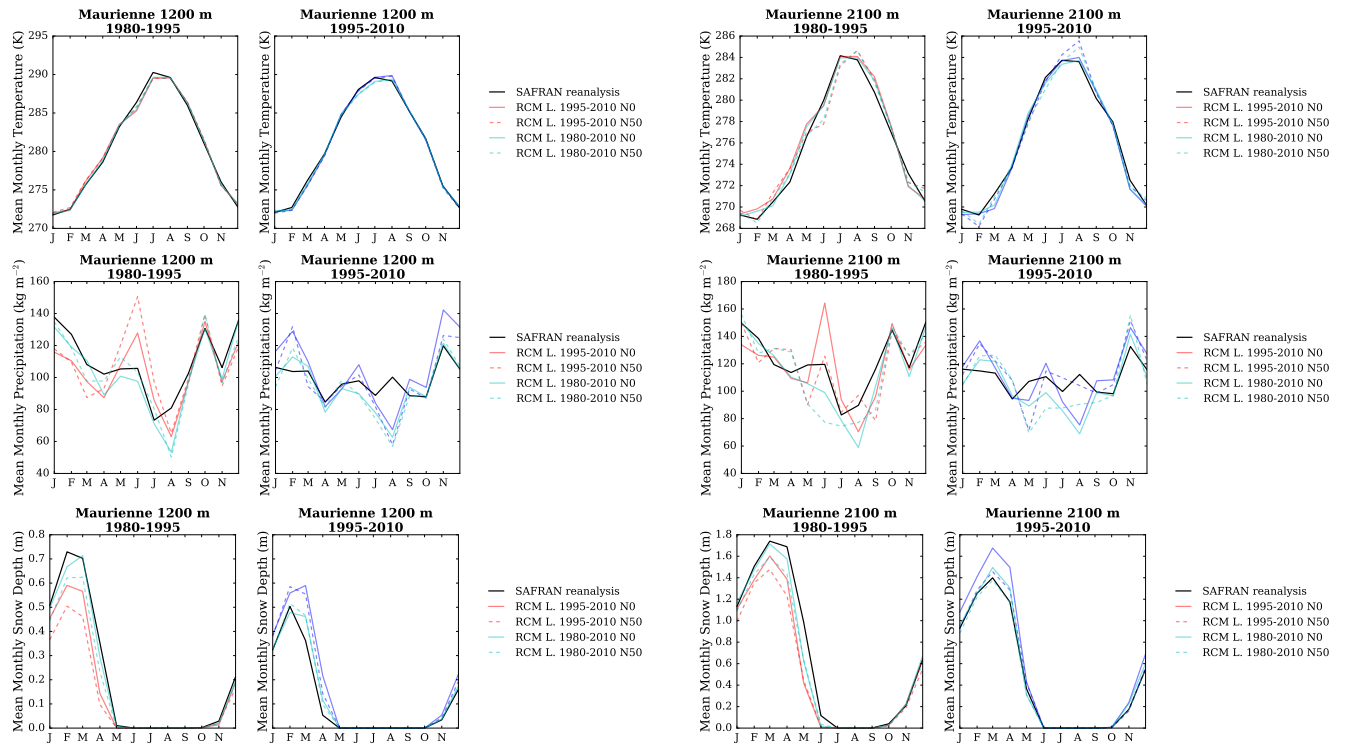


Figure S78: (top) Temperature, (middle) precipitation and (bottom) snow depth (using Crocus in this case) mean annual cycle in each adjusted RCM simulation and in the SAFRAN reanalysis over the period 1980-1995 and 1995-2010, for the Maurienne massif, and at (left) 1200 m a.s.l. and (right) 2100 m a.s.l.. Letters on the x-axis correspond to the different months of the calendar (J = January, F = February, etc.).

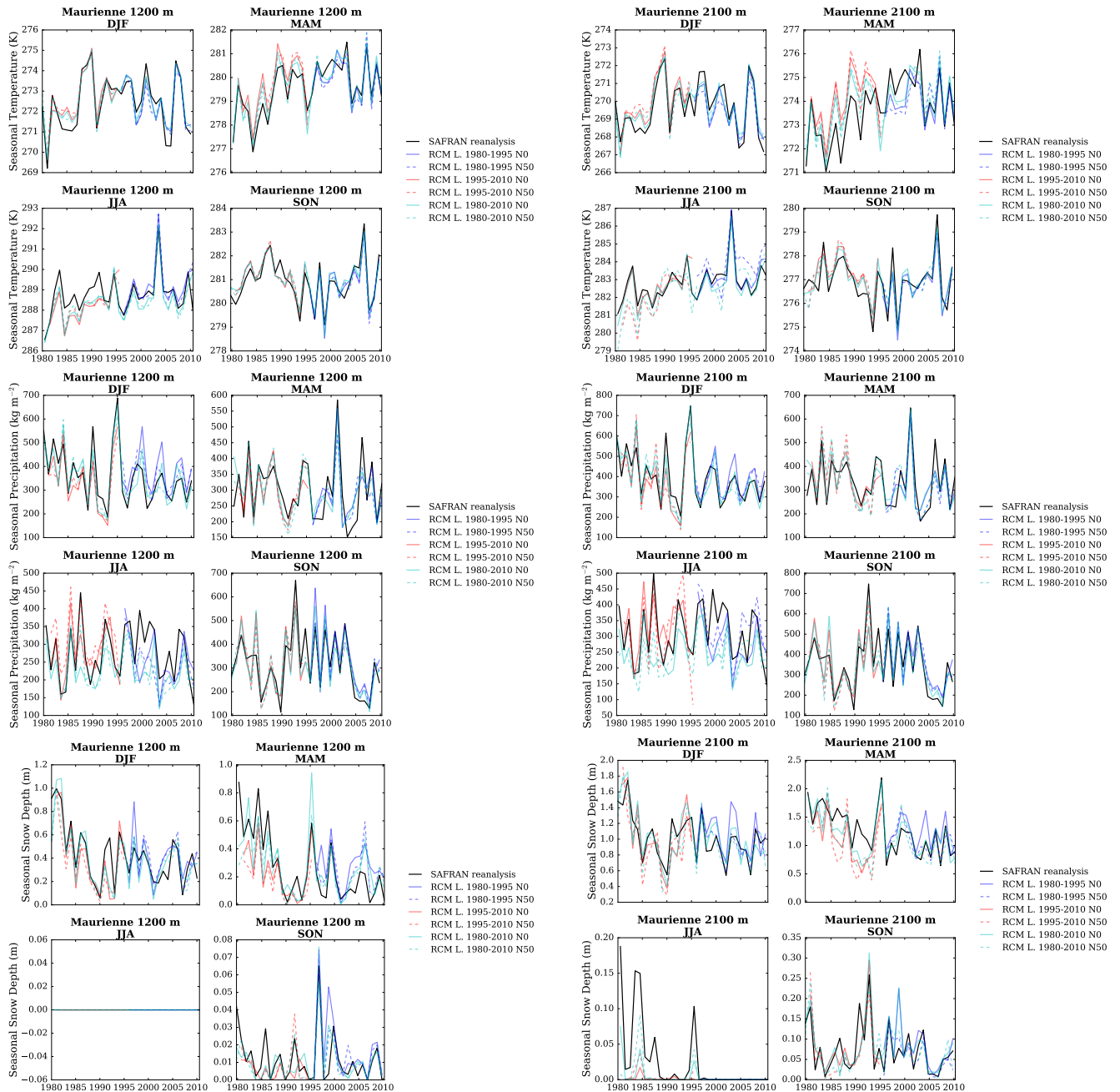


Figure S79: (top) Temperature, (middle) precipitation and (bottom) snow depth (using Crocus in this case) seasonal average time series from 1980 to 2010 in each adjusted RCM simulation and in the SAFRAN reanalysis, for the Maurienne massif, and at (left) 1200 m a.s.l. and (right) 2100 m a.s.l..

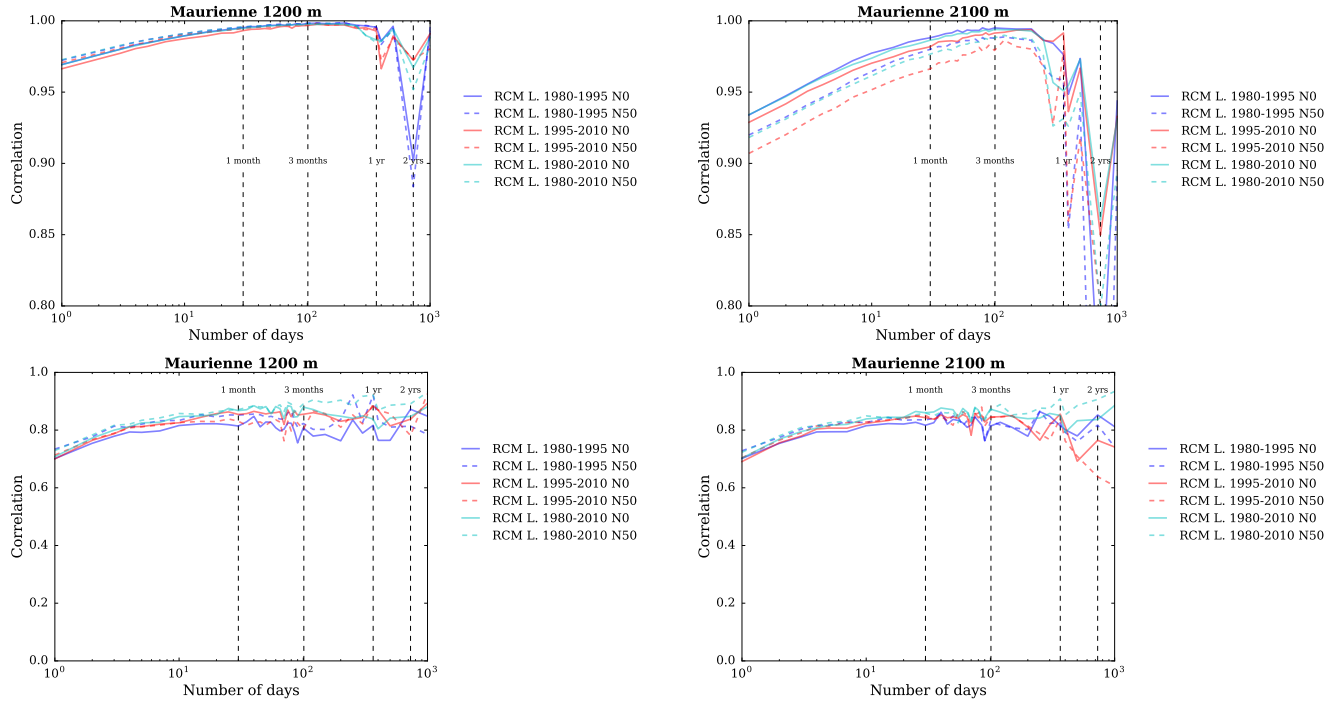


Figure S80: Correlation between the SAFRAN reanalysis and adjusted RCM (top) temperature and (bottom) precipitation as a function of the integration window over the evaluation period, for the Maurienne massif, and at (left) 1200 m a.s.l. and (right) 2100 m a.s.l..

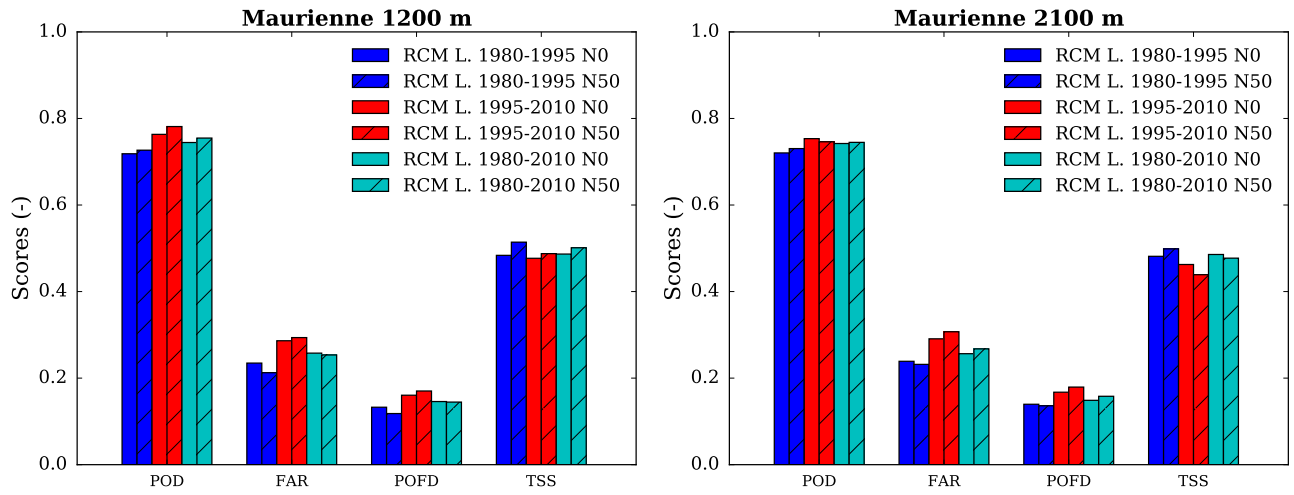


Figure S81: Scores for the detection of precipitation events in each adjusted RCM simulation compared to the SAFRAN reanalysis over the evaluation period, for the Maurienne massif, at (left) 1200 m a.s.l. and (right) 2100 m a.s.l.. POD = probability of detection, FAR = false alarm rate, POFD = probability of false detection, TSS = true skill score.

Vanoise

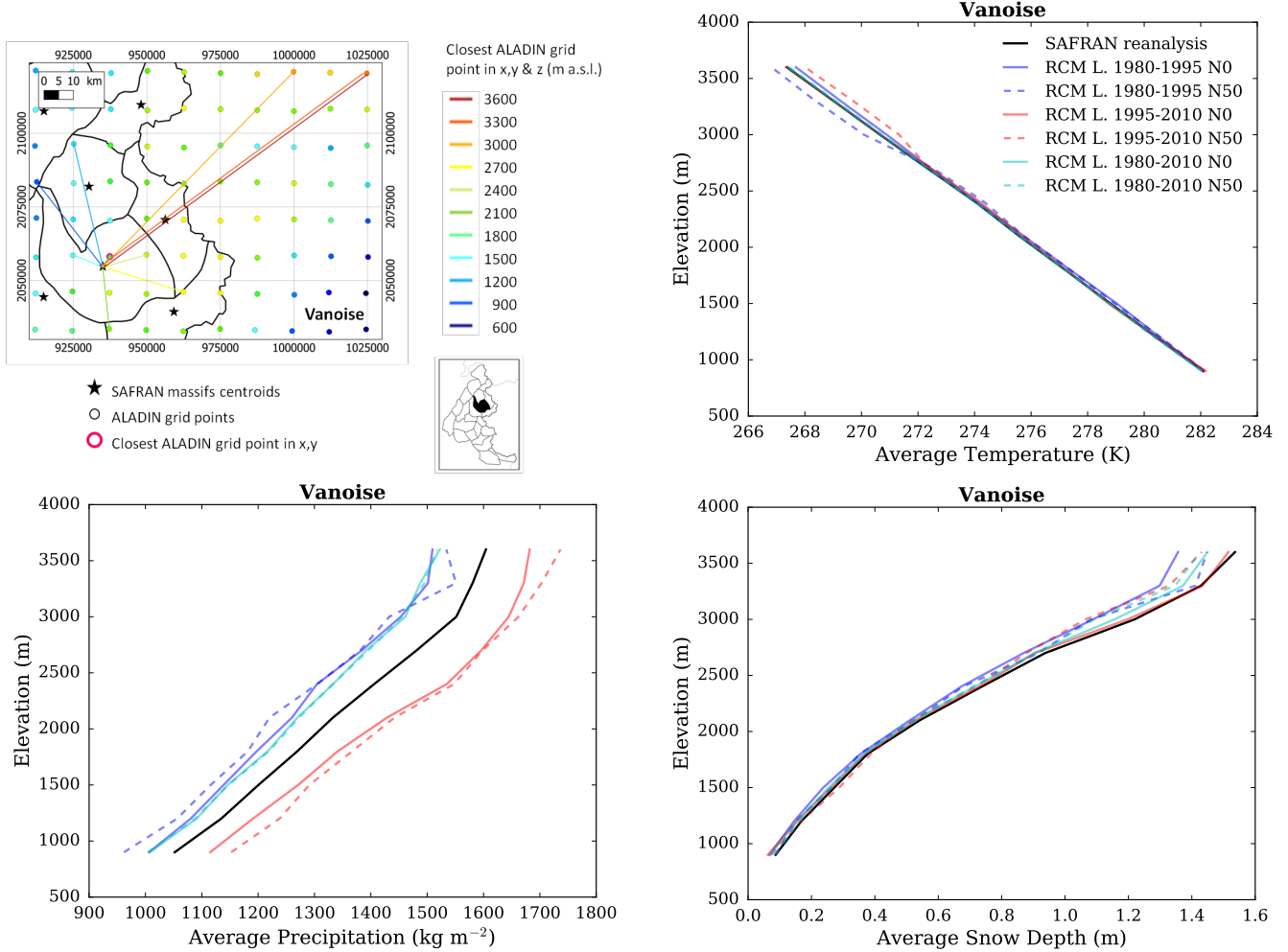


Figure S82: (top left) Location of the Vanoise massif, with ALADIN RCM grid points chosen as the closest in x, y ($N = 0$, pink contour) and in x, y and z (using $N \neq 0$). Coloured lines link each SAFRAN massif centre point with the corresponding grid point in ALADIN for the different elevations considered (in m above sea level (a.s.l.)). (top right) Mean temperature, (bottom left) precipitation and (bottom right) snow depth (using Crocus in this case) for each elevation band for the Vanoise massif, over the evaluation period in each adjusted RCM simulation (different learning periods and 2 neighbour selection methods) and in SAFRAN (1980-2010).

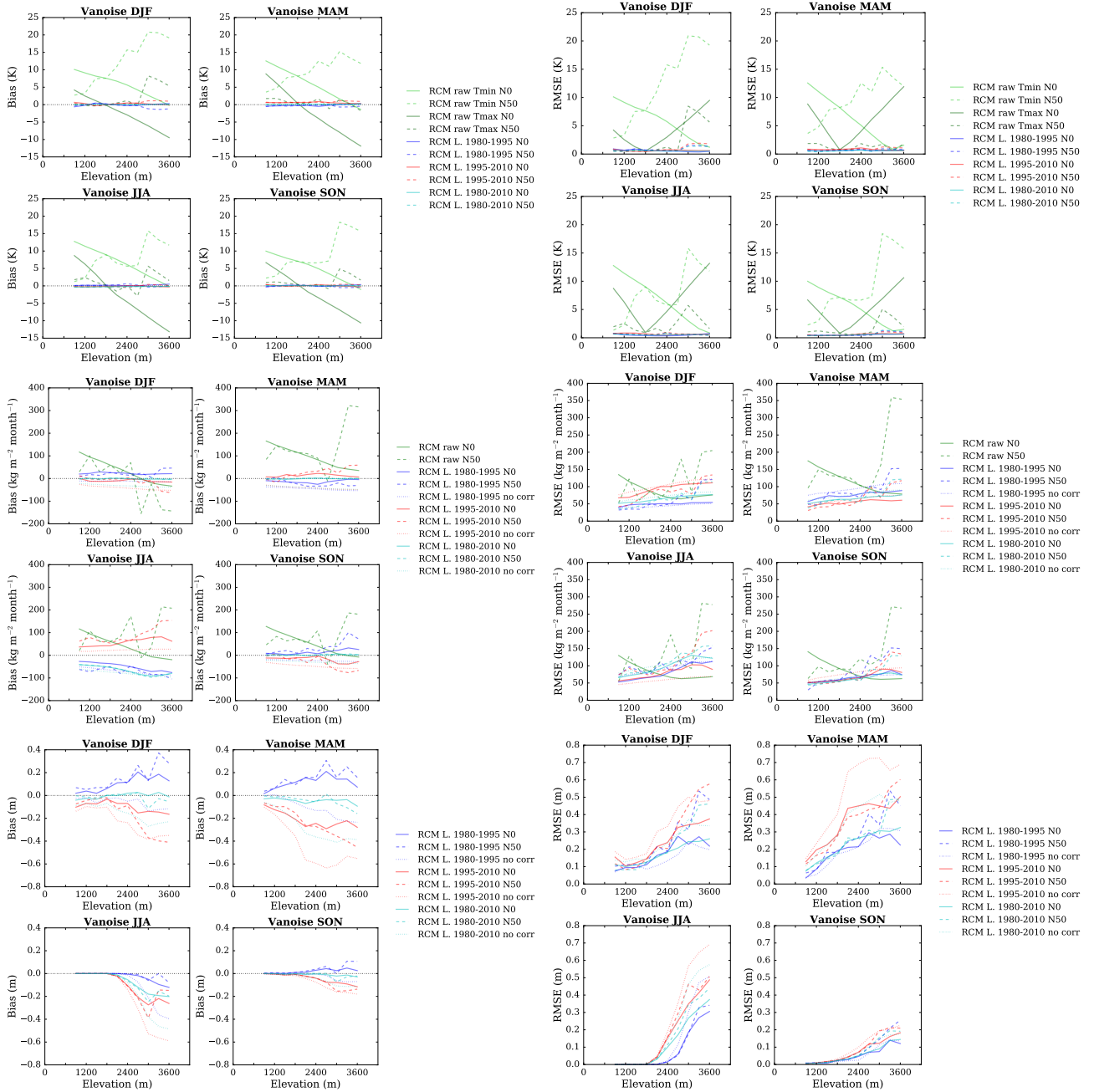


Figure S83: (top) Temperature, (middle) precipitation and (bottom) snow depth (using Crocus in this case) mean bias and root mean square error of each raw and adjusted RCM simulation compared to the SAFRAN reanalysis over the evaluation period for the Vanoise massif as a function of elevation. Scores computed for the raw RCM simulations concern minimum and maximum daily temperatures.

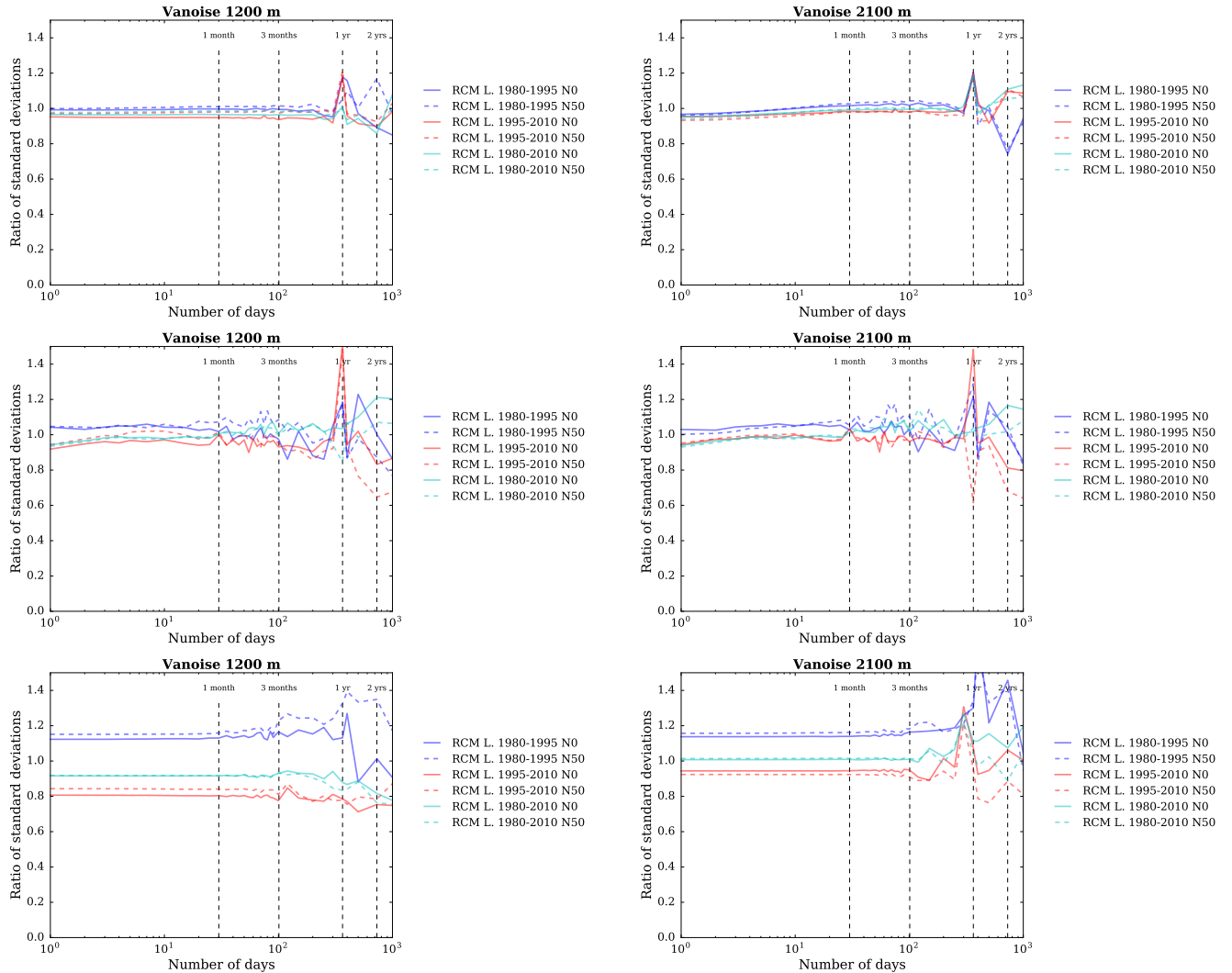


Figure S84: Ratios of standard deviations between the SAFRAN reanalysis and adjusted RCM (top) temperature, (middle) precipitation and (bottom) snow depth (using Crocus in this case) as a function of the integration window over the evaluation period, for the Vanoise massif, at (left) 1200 m a.s.l. and (right) 2100 m a.s.l..

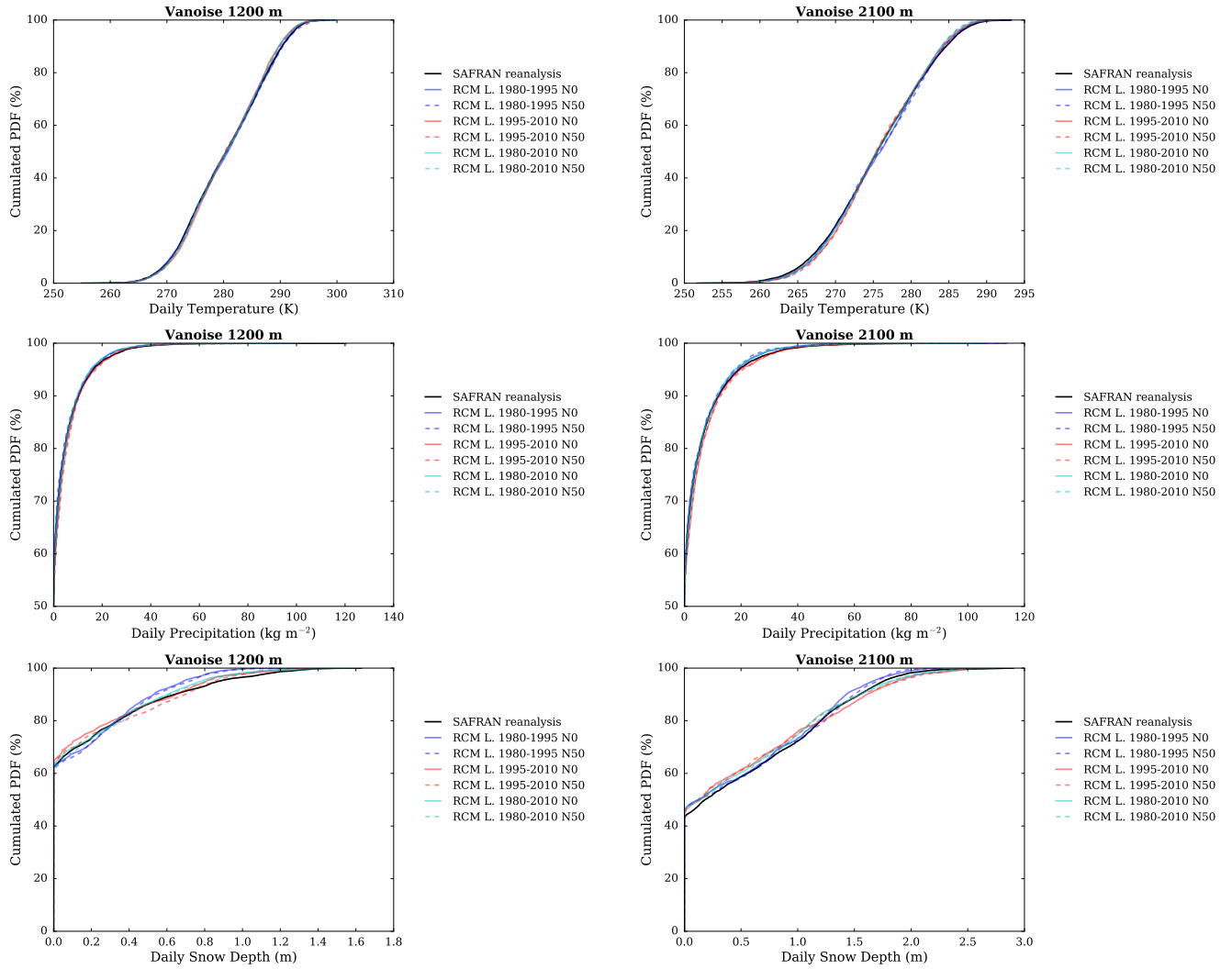


Figure S85: Cumulated probability density functions (PDFs) of daily (top) temperature, (middle) precipitation and (bottom) snow depth (using Crocus in this case) in each adjusted RCM simulation and in the SAFRAN reanalysis (1980-2010) over the evaluation period, for the Vanoise massif, at (left) 1200 m a.s.l. and (right) 2100 m a.s.l..

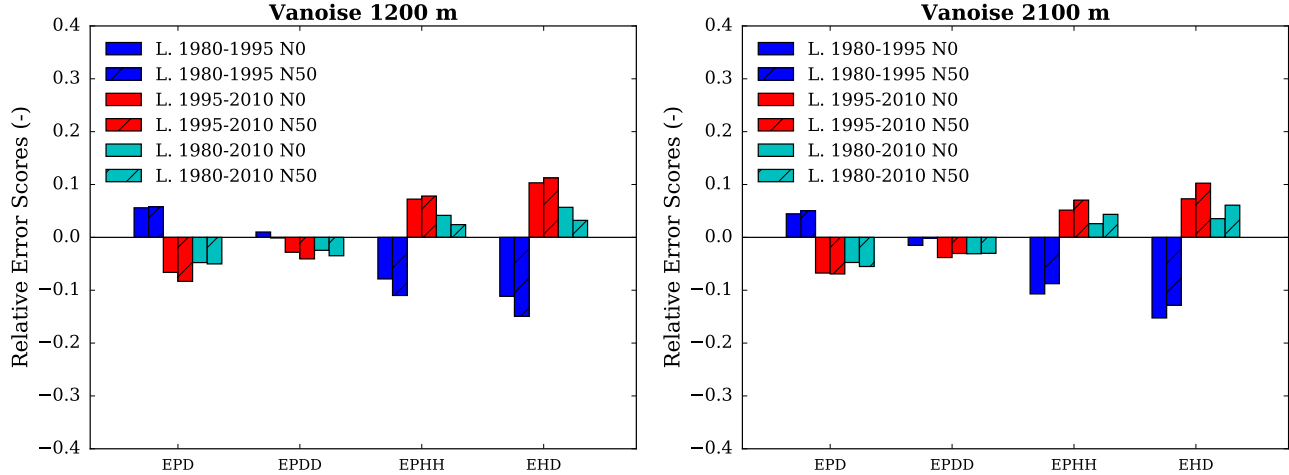


Figure S86: Scores for the duration and persistence of precipitation events in each adjusted RCM simulation compared to the SAFRAN reanalysis over the evaluation period, for the Vanoise massif, at (left) 1200 m a.s.l. and (right) 2100 m a.s.l.. EPD = relative error on the probability of a dry day, EPDD = relative error on the probability of a dry day following a dry day, EPHH = relative error on the probability of a wet day following a wet day, EHD = relative error on the mean duration of wet periods.

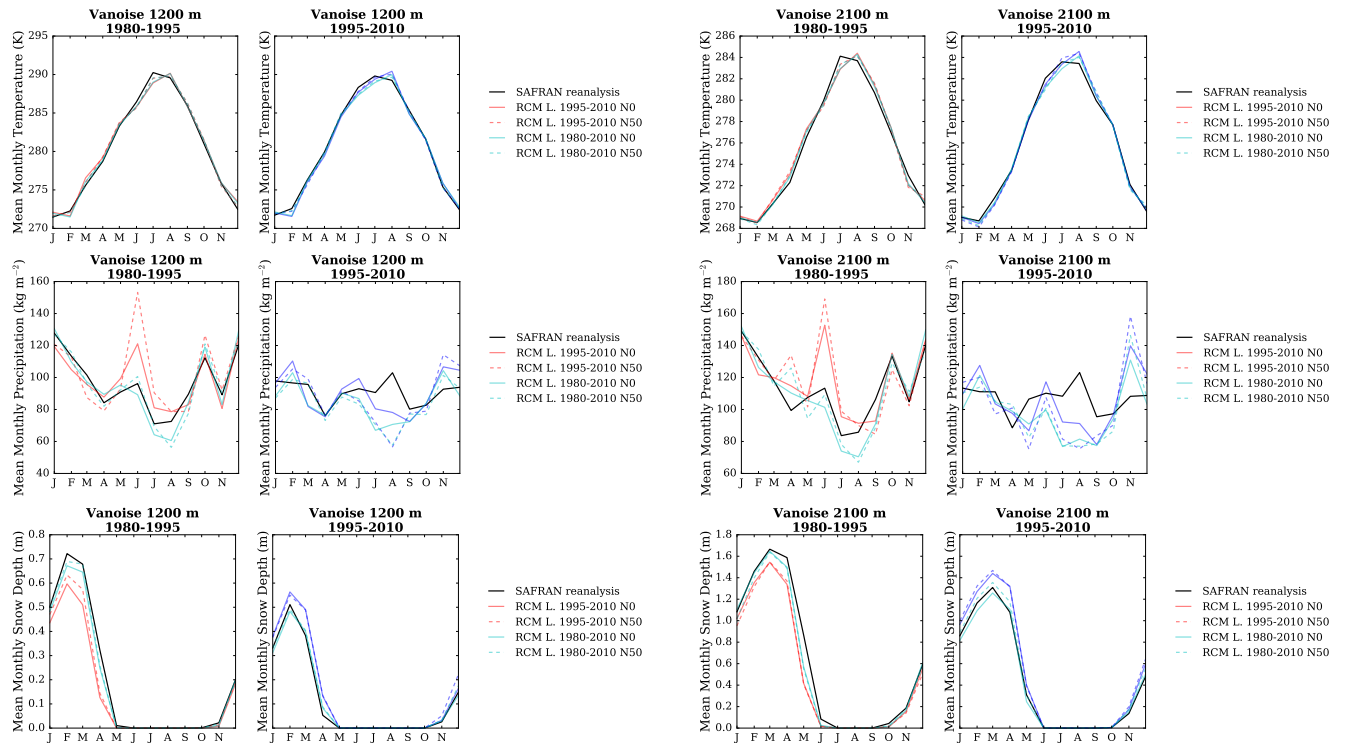


Figure S87: (top) Temperature, (middle) precipitation and (bottom) snow depth (using Crocus in this case) mean annual cycle in each adjusted RCM simulation and in the SAFRAN reanalysis over the period 1980-1995 and 1995-2010, for the Vanoise massif, and at (left) 1200 m a.s.l. and (right) 2100 m a.s.l.. Letters on the x-axis correspond to the different months of the calendar (J = January, F = February, etc.).

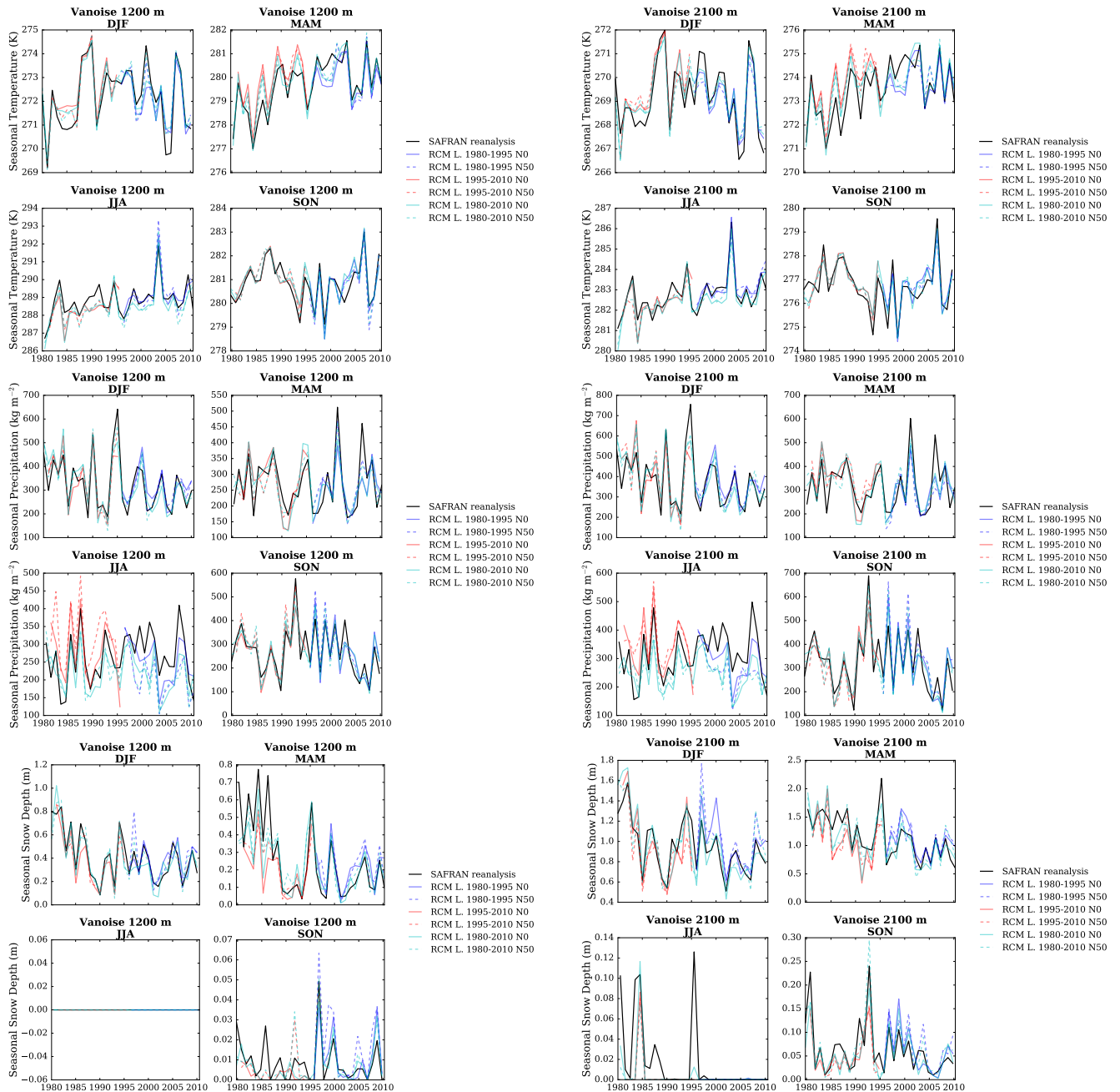


Figure S88: (top) Temperature, (middle) precipitation and (bottom) snow depth (using Crocus in this case) seasonal average time series from 1980 to 2010 in each adjusted RCM simulation and in the SAFRAN reanalysis, for the Vanoise massif, and at (left) 1200 m a.s.l. and (right) 2100 m a.s.l..

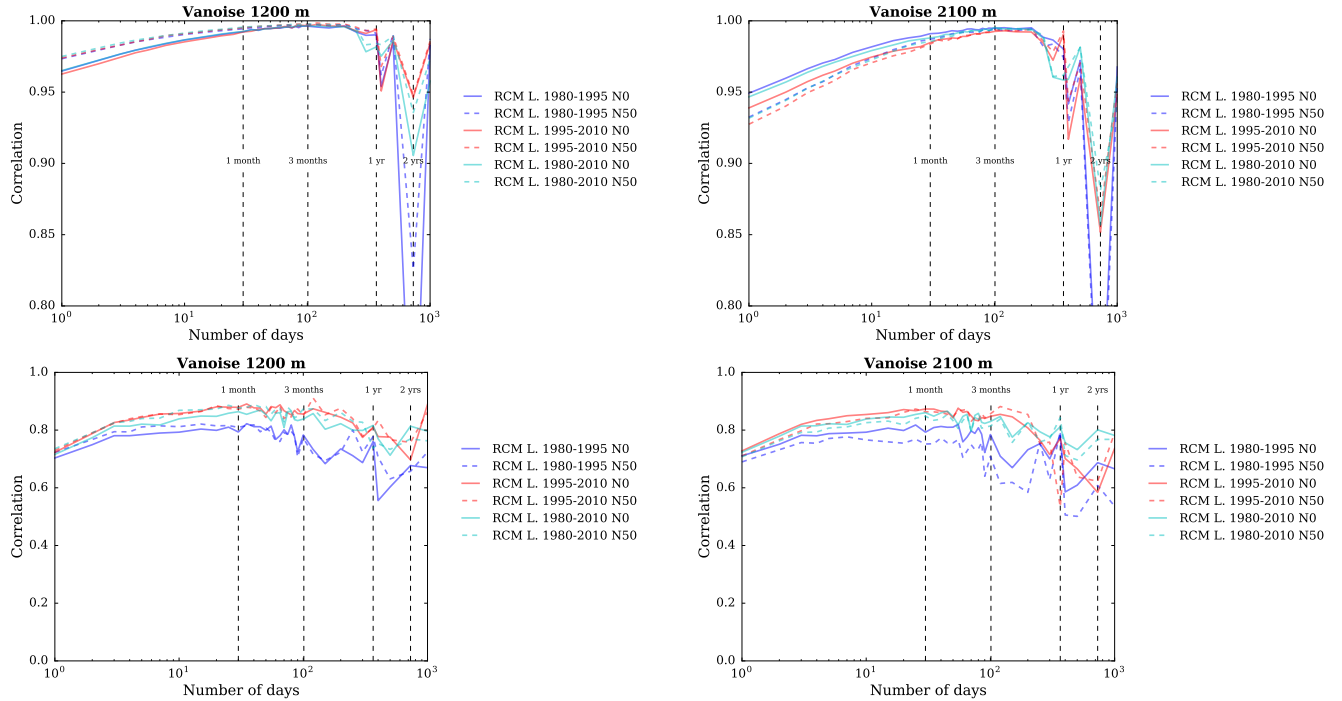


Figure S89: Correlation between the SAFRAN reanalysis and adjusted RCM (top) temperature and (bottom) precipitation as a function of the integration window over the evaluation period, for the Vanoise massif, and at (left) 1200 m a.s.l. and (right) 2100 m a.s.l..

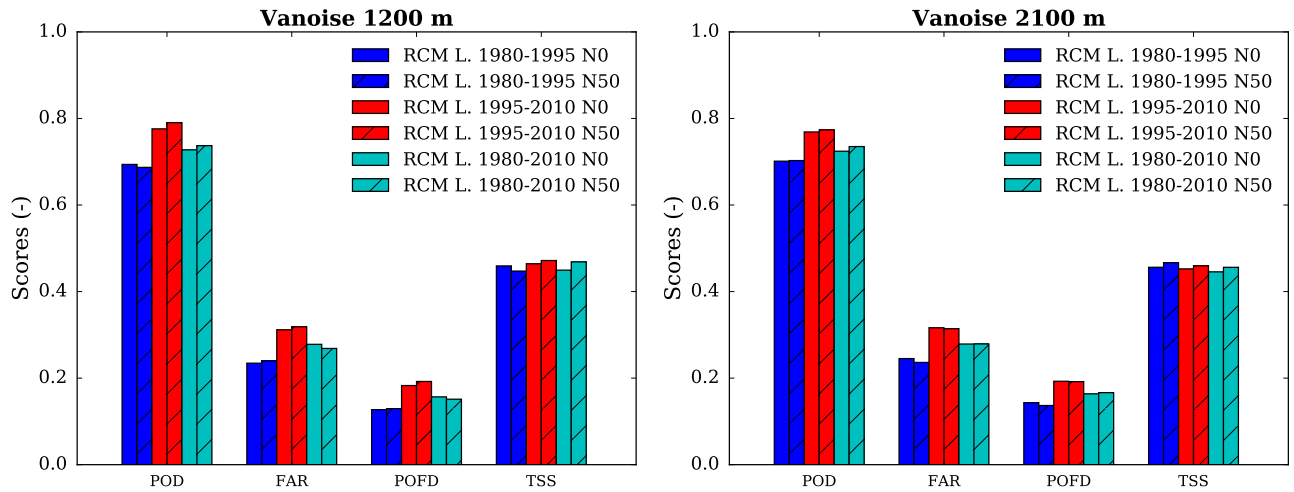


Figure S90: Scores for the detection of precipitation events in each adjusted RCM simulation compared to the SAFRAN reanalysis over the evaluation period, for the Vanoise massif, at (left) 1200 m a.s.l. and (right) 2100 m a.s.l.. POD = probability of detection, FAR = false alarm rate, POFD = probability of false detection, TSS = true skill score.

Haute Maurienne

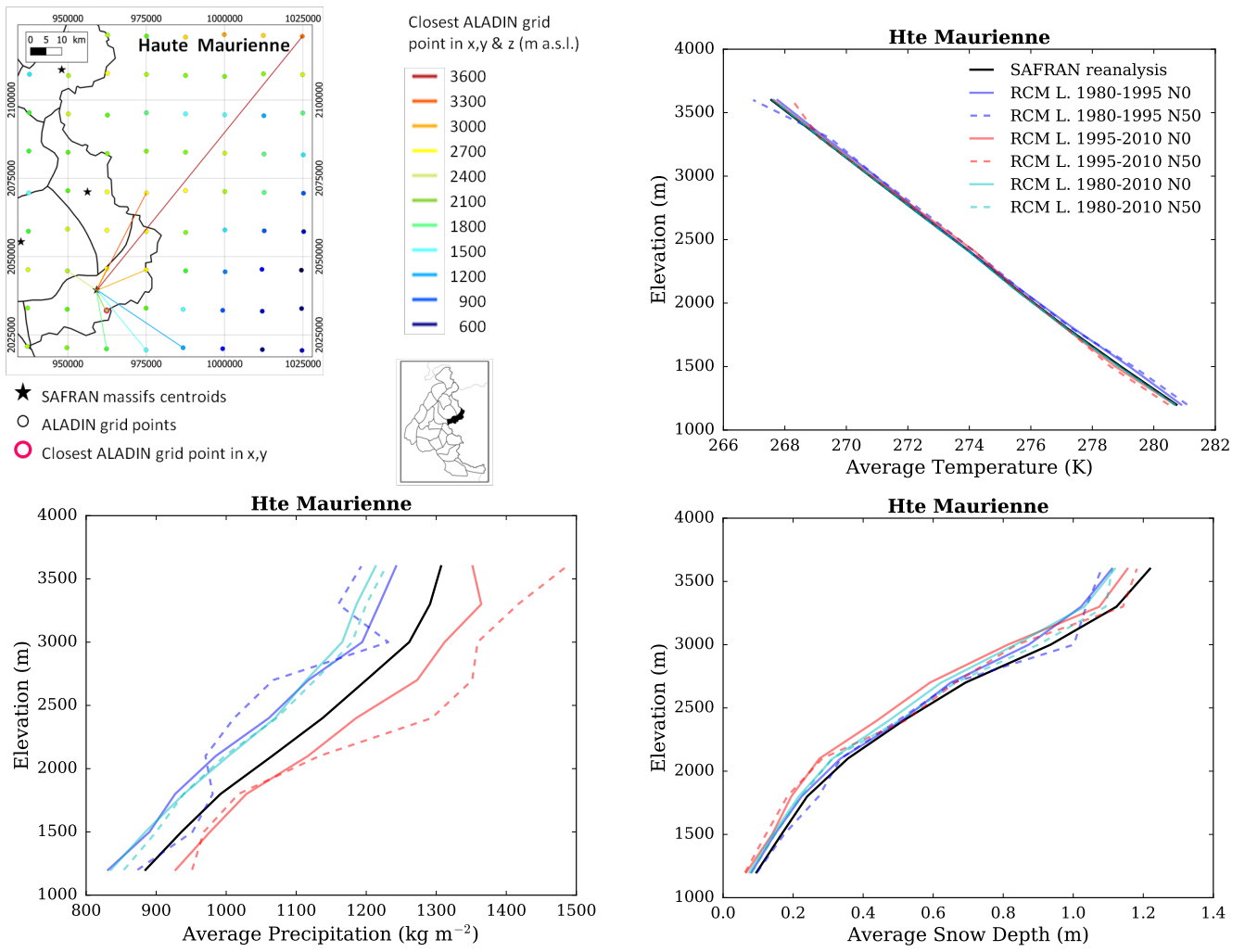


Figure S91: (top left) Location of the Haute Maurienne massif, with ALADIN RCM grid points chosen as the closest in x, y ($N = 0$, pink contour) and in x, y and z (using $N \neq 0$). Coloured lines link each SAFRAN massif centre point with the corresponding grid point in ALADIN for the different elevations considered (in m above sea level (a.s.l.)). (top right) Mean temperature, (bottom left) precipitation and (bottom right) snow depth (using Crocus in this case) for each elevation band for the Haute Maurienne massif, over the evaluation period in each adjusted RCM simulation (different learning periods and 2 neighbour selection methods) and in SAFRAN (1980-2010).

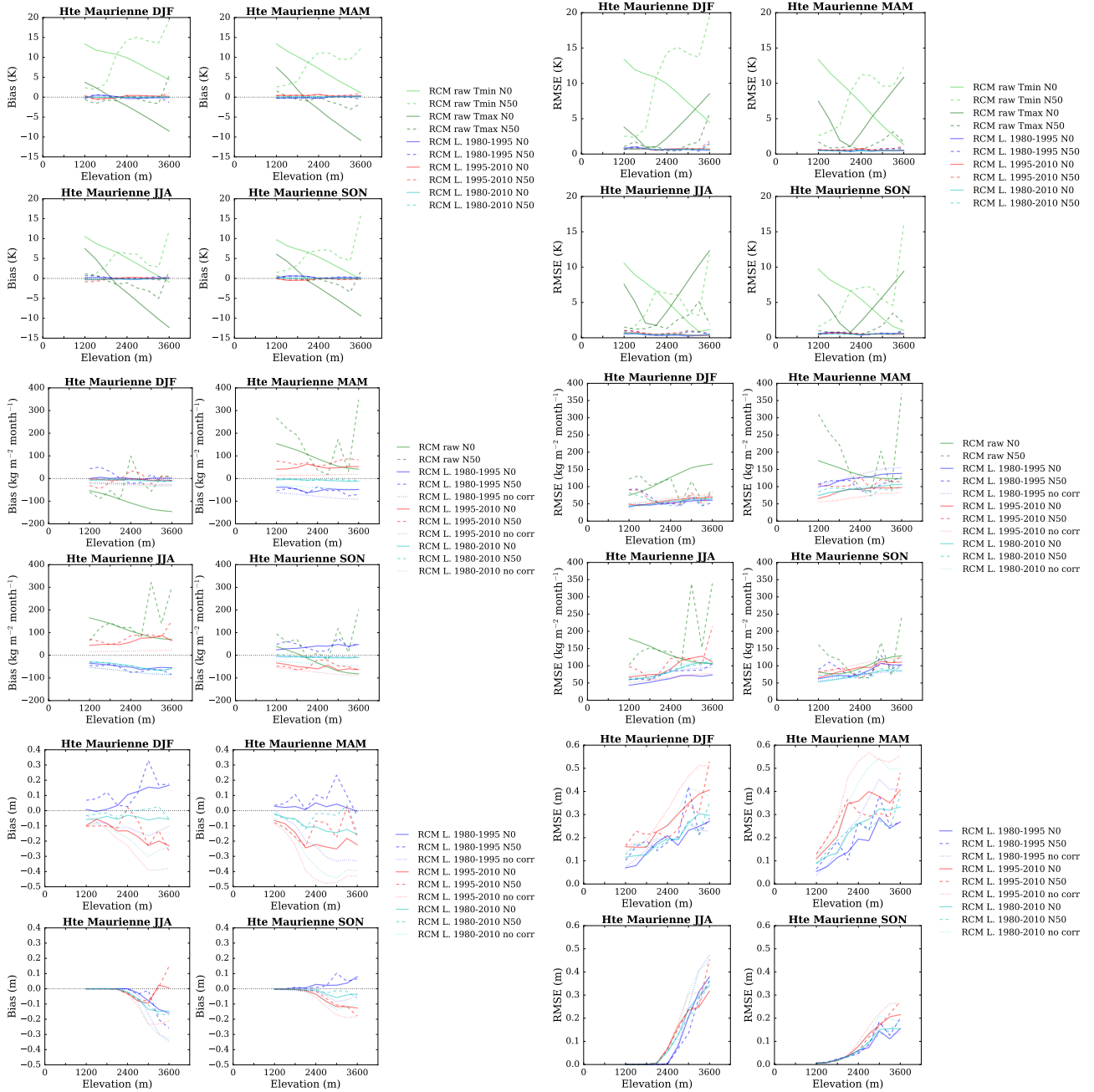


Figure S92: (top) Temperature, (middle) precipitation and (bottom) snow depth (using Crocus in this case) mean bias and root mean square error of each raw and adjusted RCM simulation compared to the SAFRAN reanalysis over the evaluation period for the Haute Maurienne massif as a function of elevation. Scores computed for the raw RCM simulations concern minimum and maximum daily temperatures.

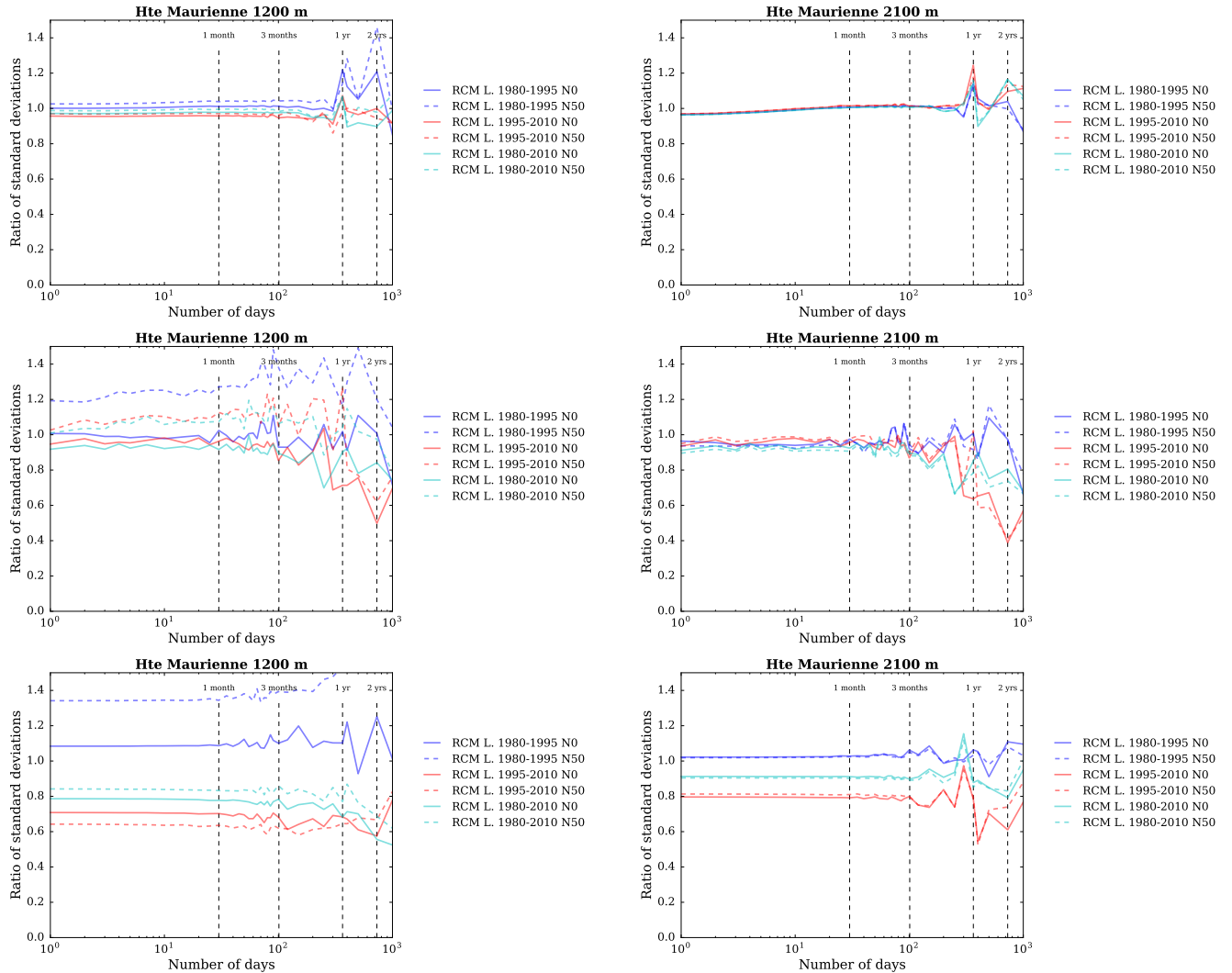


Figure S93: Ratios of standard deviations between the SAFRAN reanalysis and adjusted RCM (top) temperature, (middle) precipitation and (bottom) snow depth (using Crocus in this case) as a function of the integration window over the evaluation period, for the Haute Maurienne massif, at (left) 1200 m a.s.l. and (right) 2100 m a.s.l..

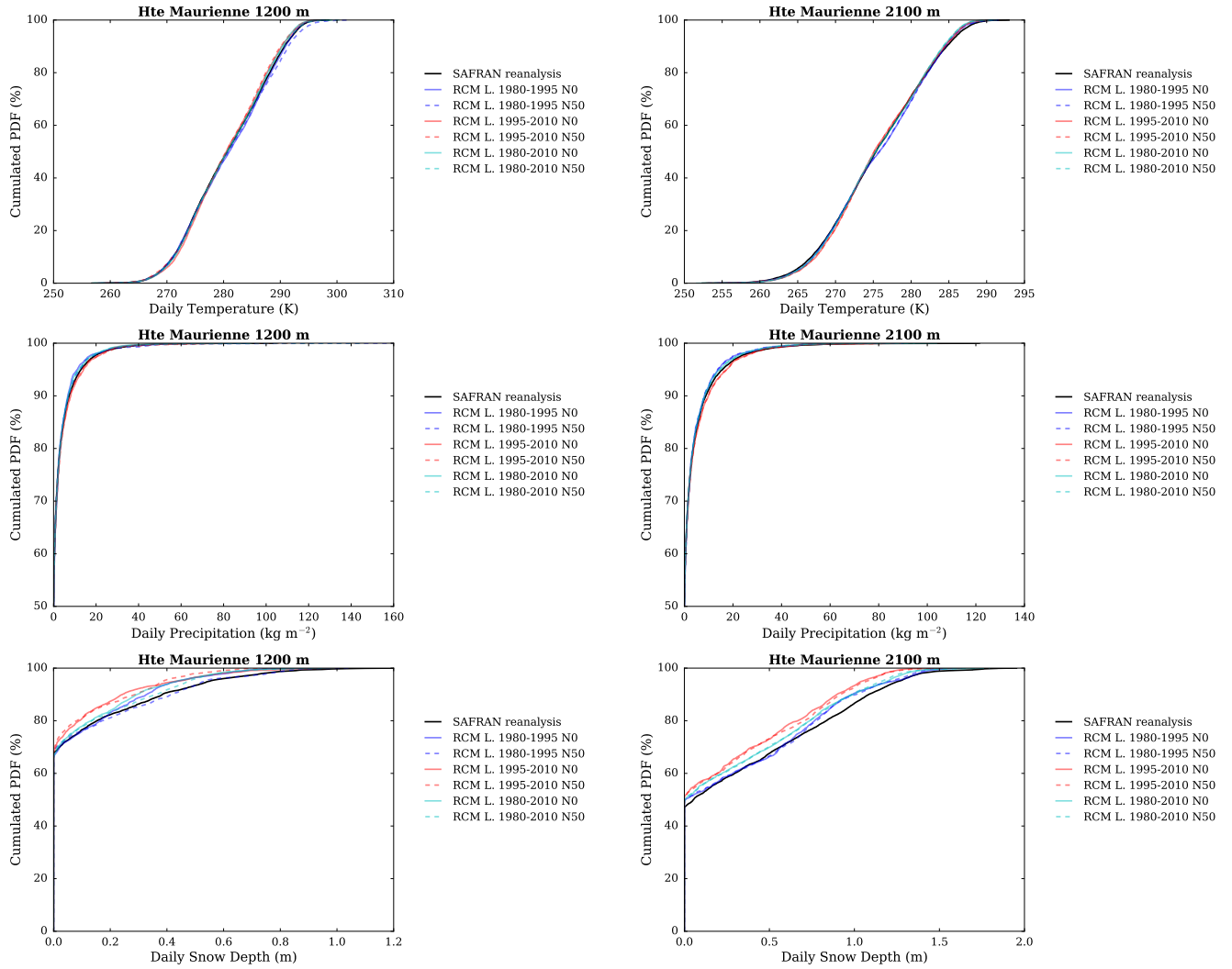


Figure S94: Cumulated probability density functions (PDFs) of daily (top) temperature, (middle) precipitation and (bottom) snow depth (using Crocus in this case) in each adjusted RCM simulation and in the SAFRAN reanalysis (1980-2010) over the evaluation period, for the Haute Maurienne massif, at (left) 1200 m a.s.l. and (right) 2100 m a.s.l..

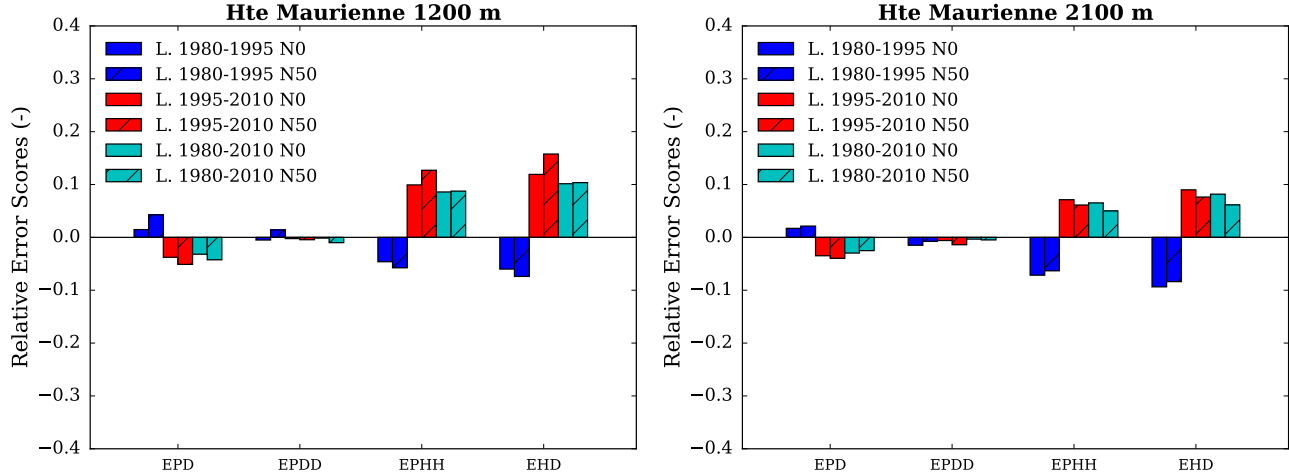


Figure S95: Scores for the duration and persistence of precipitation events in each adjusted RCM simulation compared to the SAFRAN reanalysis over the evaluation period, for the Haute Maurienne massif, at (left) 1200 m a.s.l. and (right) 2100 m a.s.l.. EPD = relative error on the probability of a dry day, EPDD = relative error on the probability of a dry day following a dry day, EPHH = relative error on the probability of a wet day following a wet day, EHD = relative error on the mean duration of wet periods.

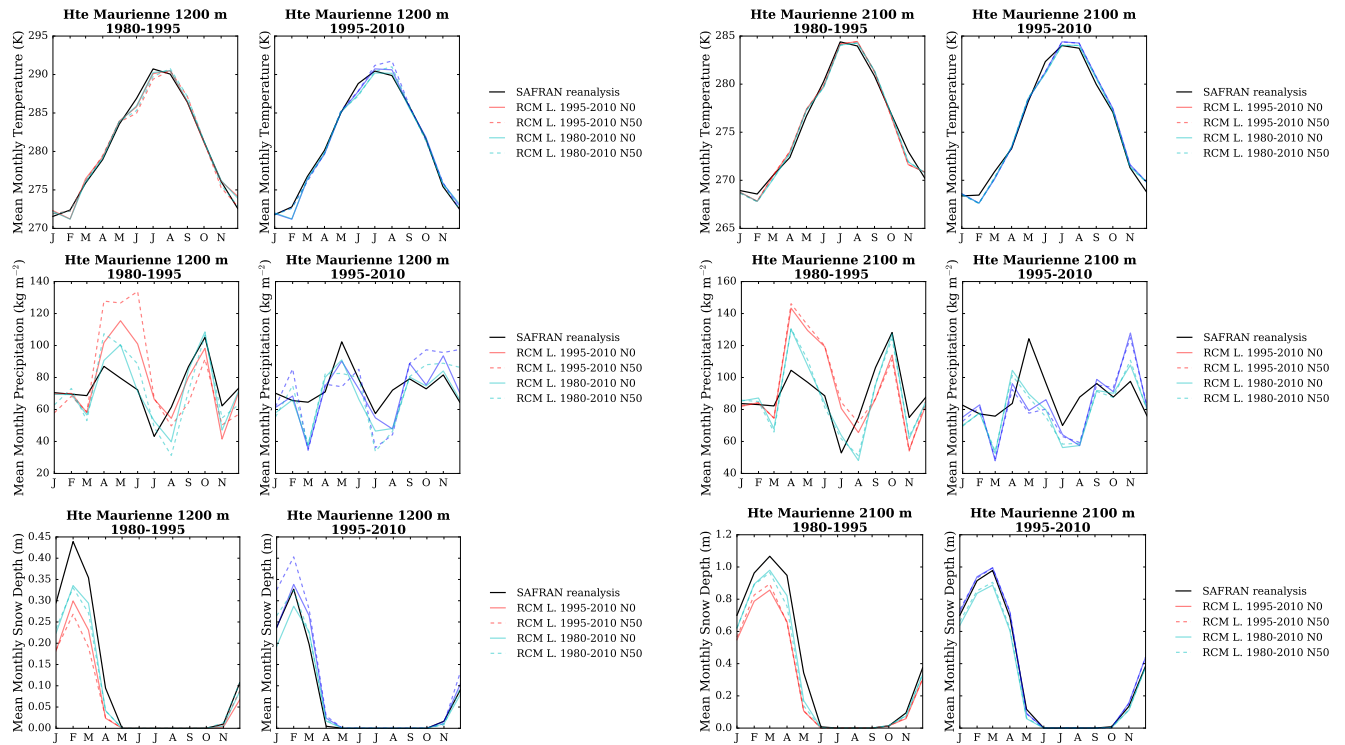


Figure S96: (top) Temperature, (middle) precipitation and (bottom) snow depth (using Crocus in this case) mean annual cycle in each adjusted RCM simulation and in the SAFRAN reanalysis over the period 1980-1995 and 1995-2010, for the Haute Maurienne massif, and at (left) 1200 m a.s.l. and (right) 2100 m a.s.l.. Letters on the x-axis correspond to the different months of the calendar (J = January, F = February, etc.).

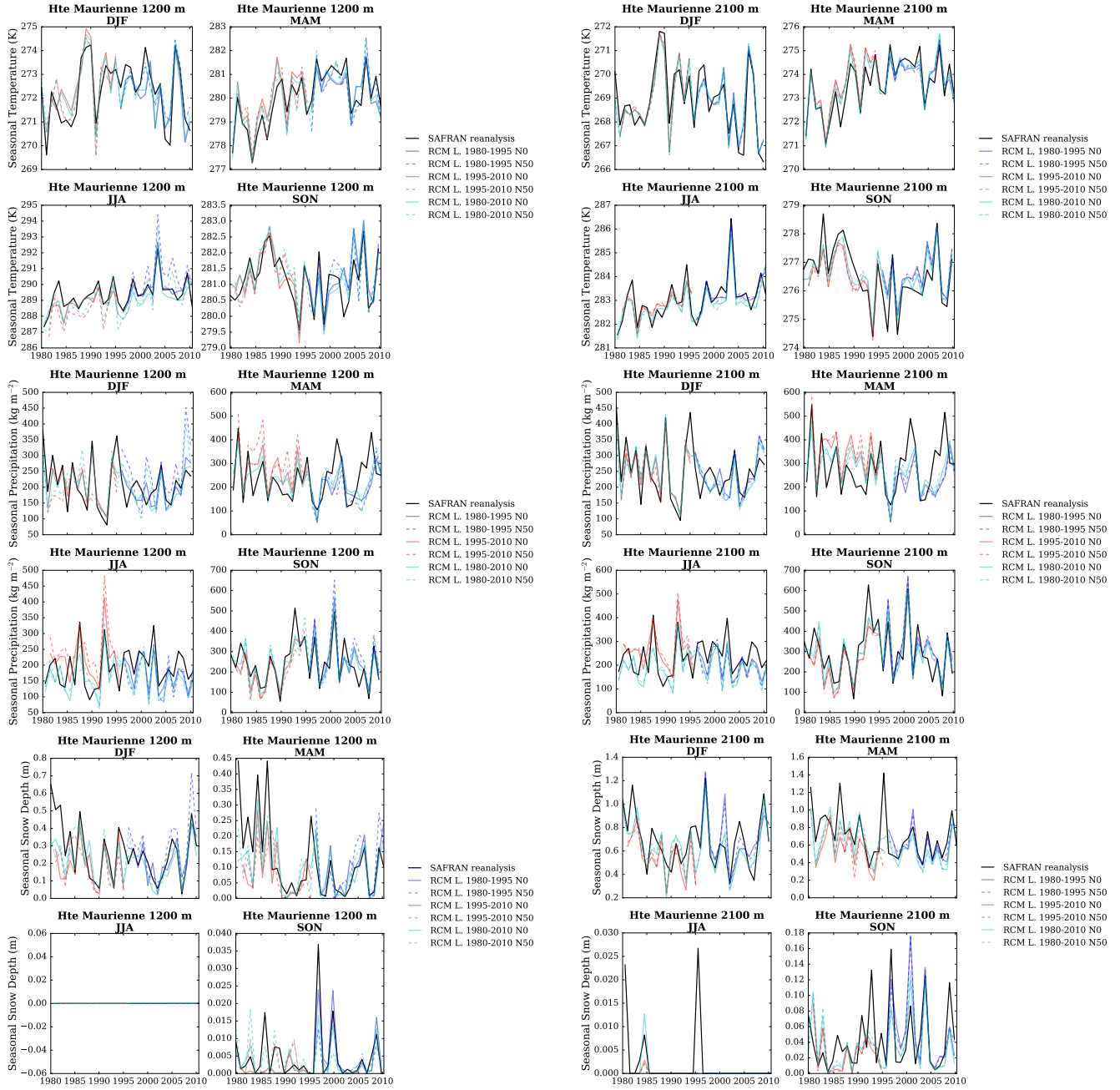


Figure S97: (top) Temperature, (middle) precipitation and (bottom) snow depth (using Crocus in this case) seasonal average time series from 1980 to 2010 in each adjusted RCM simulation and in the SAFRAN reanalysis, for the Haute Maurienne massif, and at (left) 1200 m a.s.l. and (right) 2100 m a.s.l..

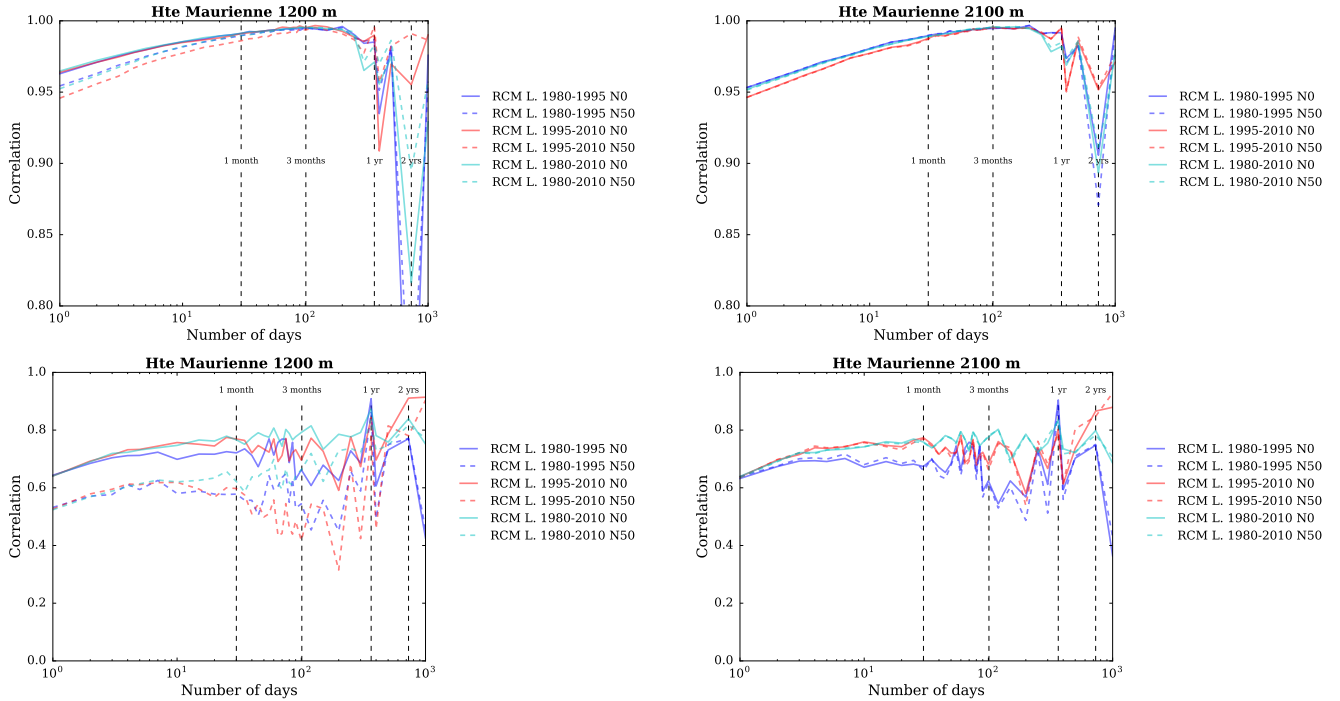


Figure S98: Correlation between the SAFRAN reanalysis and adjusted RCM (top) temperature and (bottom) precipitation as a function of the integration window over the evaluation period, for the Haute Maurienne massif, and at (left) 1200 m a.s.l. and (right) 2100 m a.s.l..

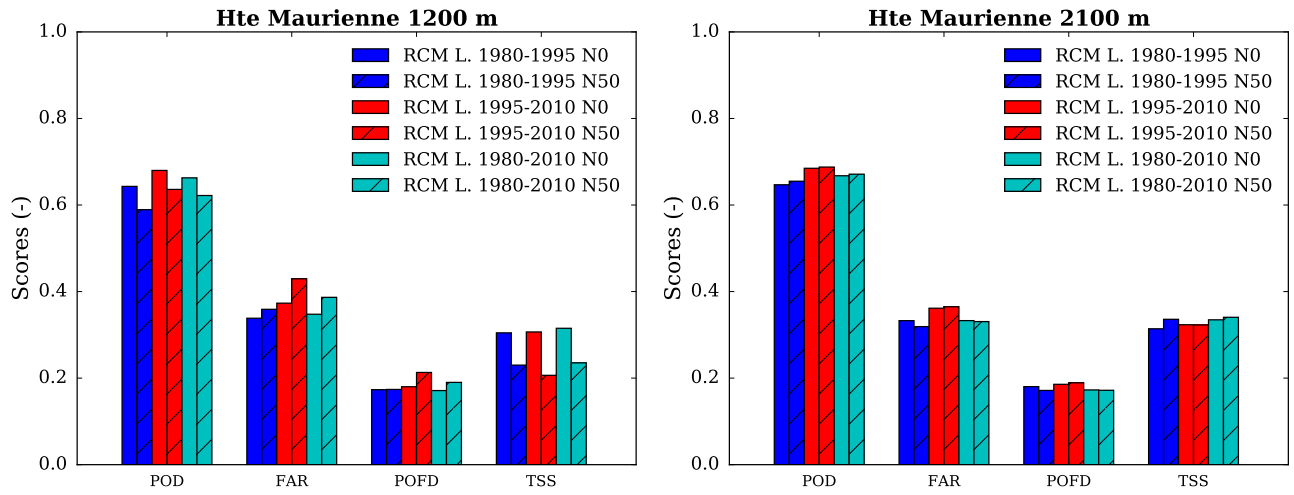


Figure S99: Scores for the detection of precipitation events in each adjusted RCM simulation compared to the SAFRAN reanalysis over the evaluation period, for the Haute Maurienne massif, at (left) 1200 m a.s.l. and (right) 2100 m a.s.l.. POD = probability of detection, FAR = false alarm rate, POFD = probability of false detection, TSS = true skill score.

Grandes Rousses

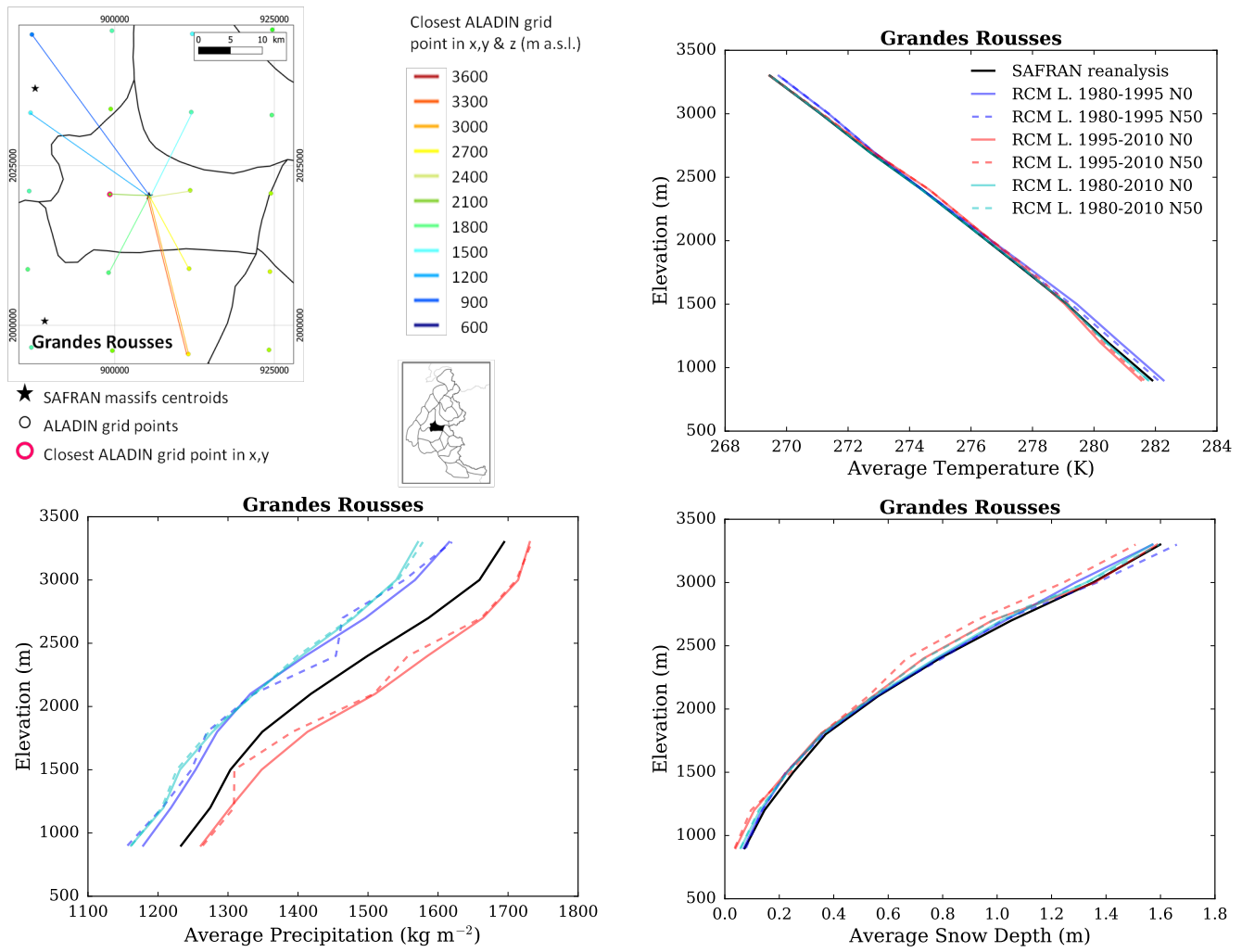


Figure S100: (top left) Location of the Grandes Rousses massif, with ALADIN RCM grid points chosen as the closest in x, y ($N = 0$, pink contour) and in x, y and z (using $N \neq 0$). Coloured lines link each SAFRAN massif centre point with the corresponding grid point in ALADIN for the different elevations considered (in m above sea level (a.s.l.)). (top right) Mean temperature, (bottom left) precipitation and (bottom right) snow depth (using Crocus in this case) for each elevation band for the Grandes Rousses massif, over the evaluation period in each adjusted RCM simulation (different learning periods and 2 neighbour selection methods) and in SAFRAN (1980-2010).

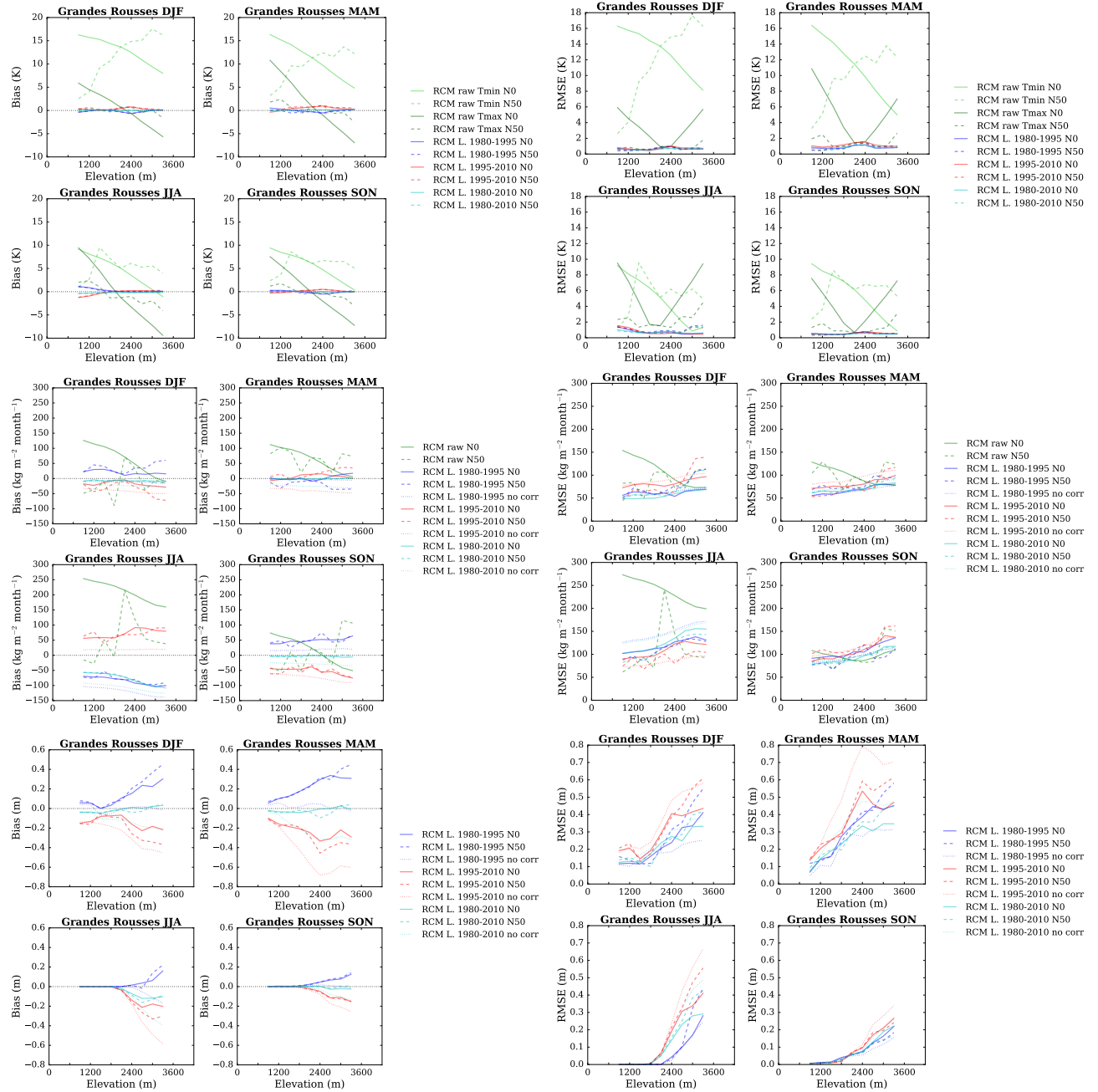


Figure S101: (top) Temperature, (middle) precipitation and (bottom) snow depth (using Crocus in this case) mean bias and root mean square error of each raw and adjusted RCM simulation compared to the SAFRAN reanalysis over the evaluation period for the Grandes Rousses massif as a function of elevation. Scores computed for the raw RCM simulations concern minimum and maximum daily temperatures.

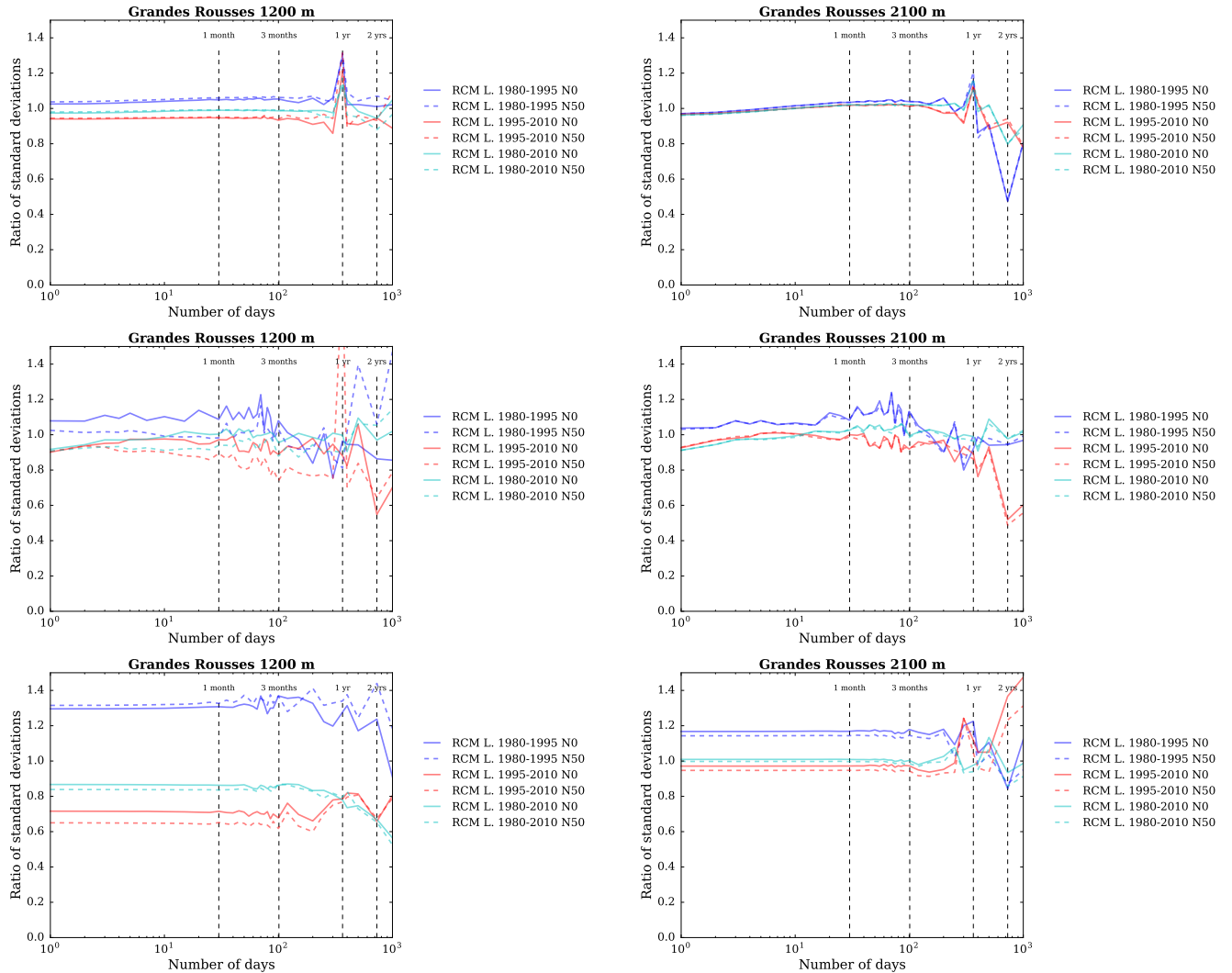


Figure S102: Ratios of standard deviations between the SAFRAN reanalysis and adjusted RCM (top) temperature, (middle) precipitation and (bottom) snow depth (using Crocus in this case) as a function of the integration window over the evaluation period, for the Grandes Rousses massif, at (left) 1200 m a.s.l. and (right) 2100 m a.s.l..

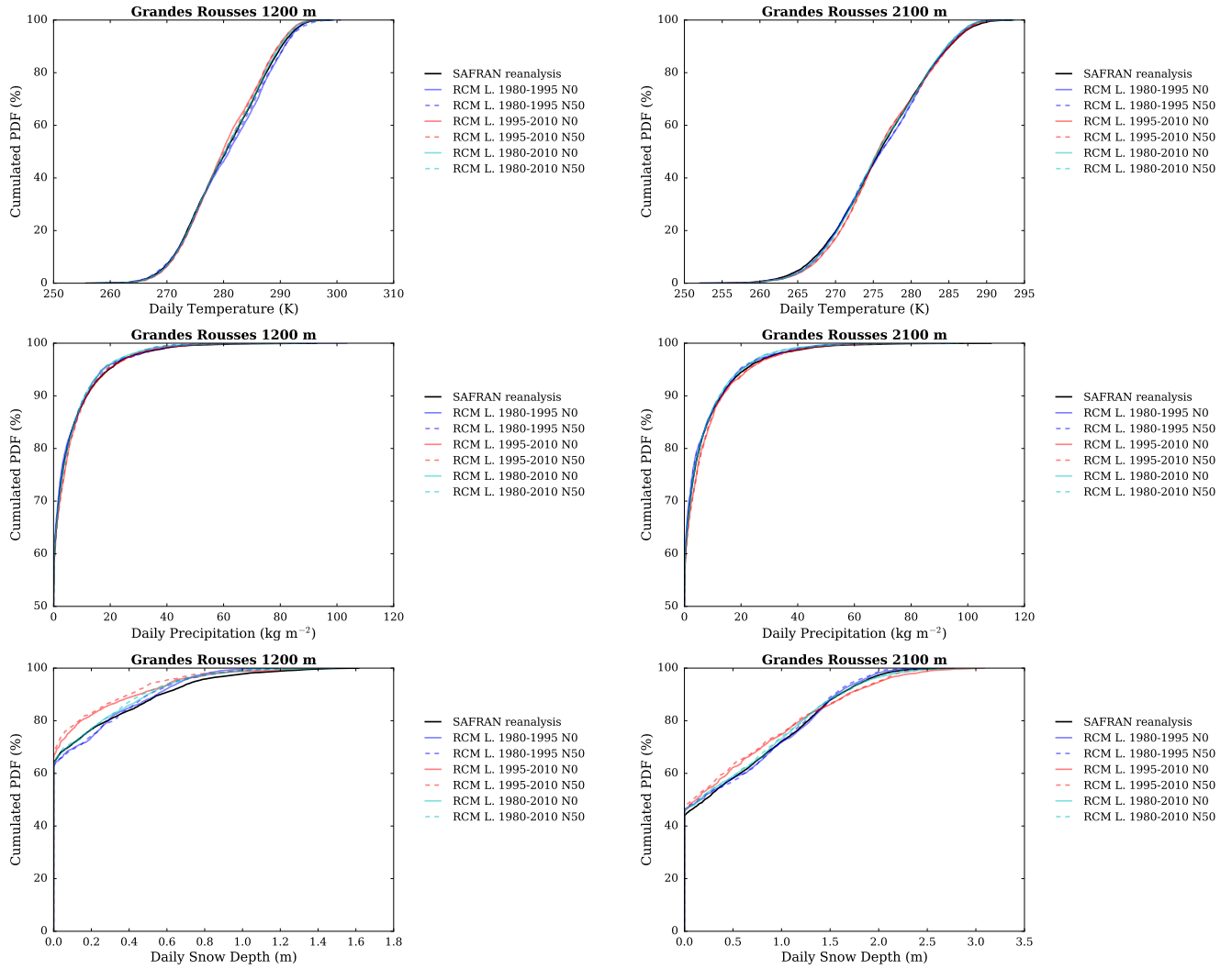


Figure S103: Cumulated probability density functions (PDFs) of daily (top) temperature, (middle) precipitation and (bottom) snow depth (using Crocus in this case) in each adjusted RCM simulation and in the SAFRAN reanalysis (1980-2010) over the evaluation period, for the Grandes Rousses massif, at (left) 1200 m a.s.l. and (right) 2100 m a.s.l..

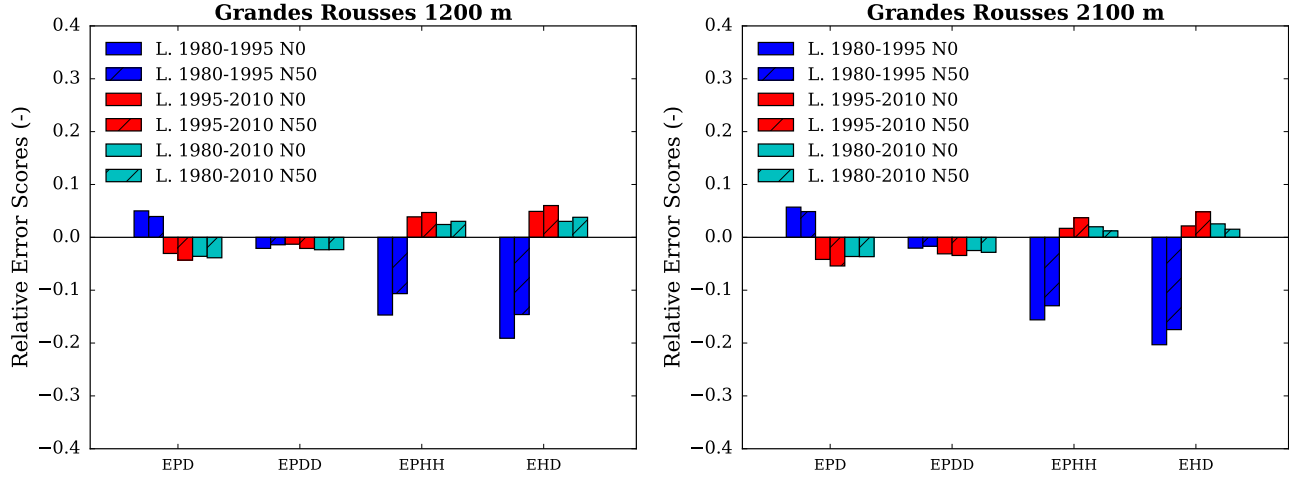


Figure S104: Scores for the duration and persistence of precipitation events in each adjusted RCM simulation compared to the SAFRAN reanalysis over the evaluation period, for the Grandes Rousses massif, at (left) 1200 m a.s.l. and (right) 2100 m a.s.l.. EPD = relative error on the probability of a dry day, EPDD = relative error on the probability of a dry day following a dry day, EPHH = relative error on the probability of a wet day following a wet day, EHD = relative error on the mean duration of wet periods.

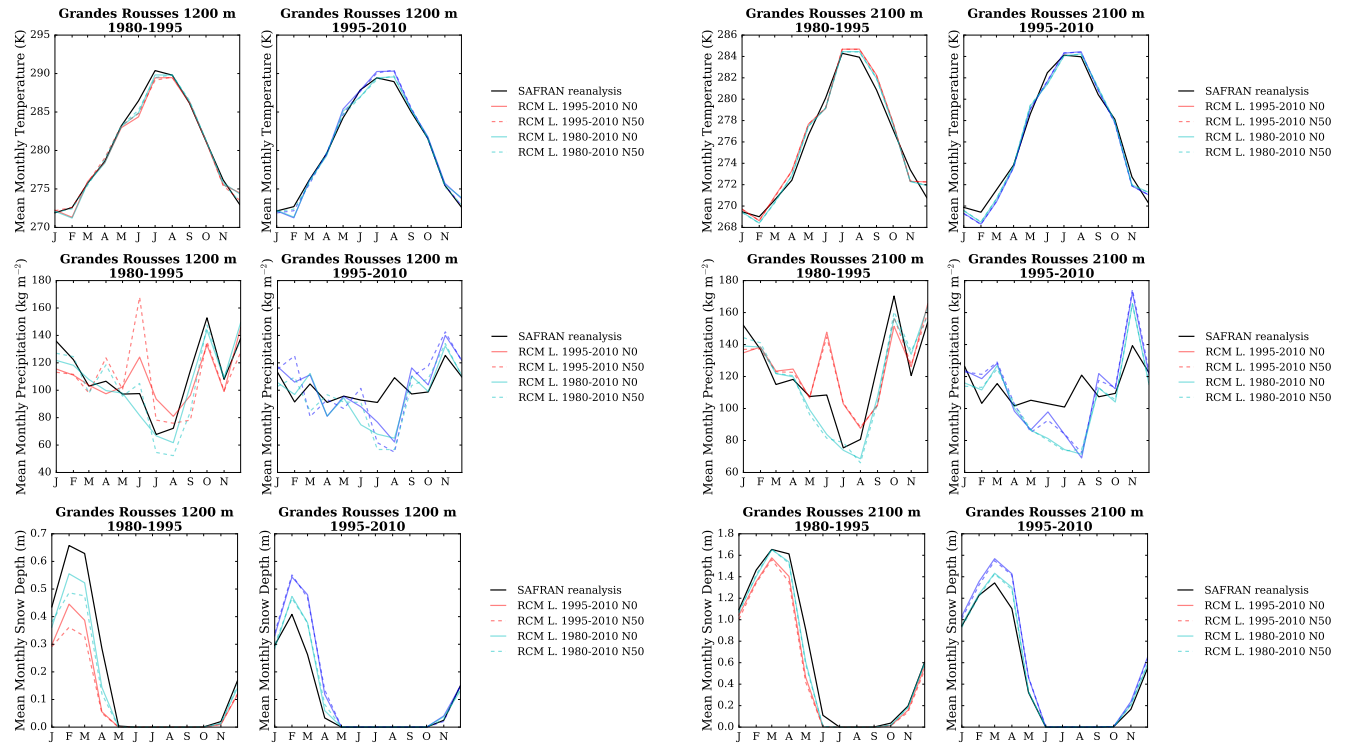


Figure S105: (top) Temperature, (middle) precipitation and (bottom) snow depth (using Crocus in this case) mean annual cycle in each adjusted RCM simulation and in the SAFRAN reanalysis over the period 1980-1995 and 1995-2010, for the Grandes Rousses massif, and at (left) 1200 m a.s.l. and (right) 2100 m a.s.l.. Letters on the x-axis correspond to the different months of the calendar (J = January, F = February, etc.).

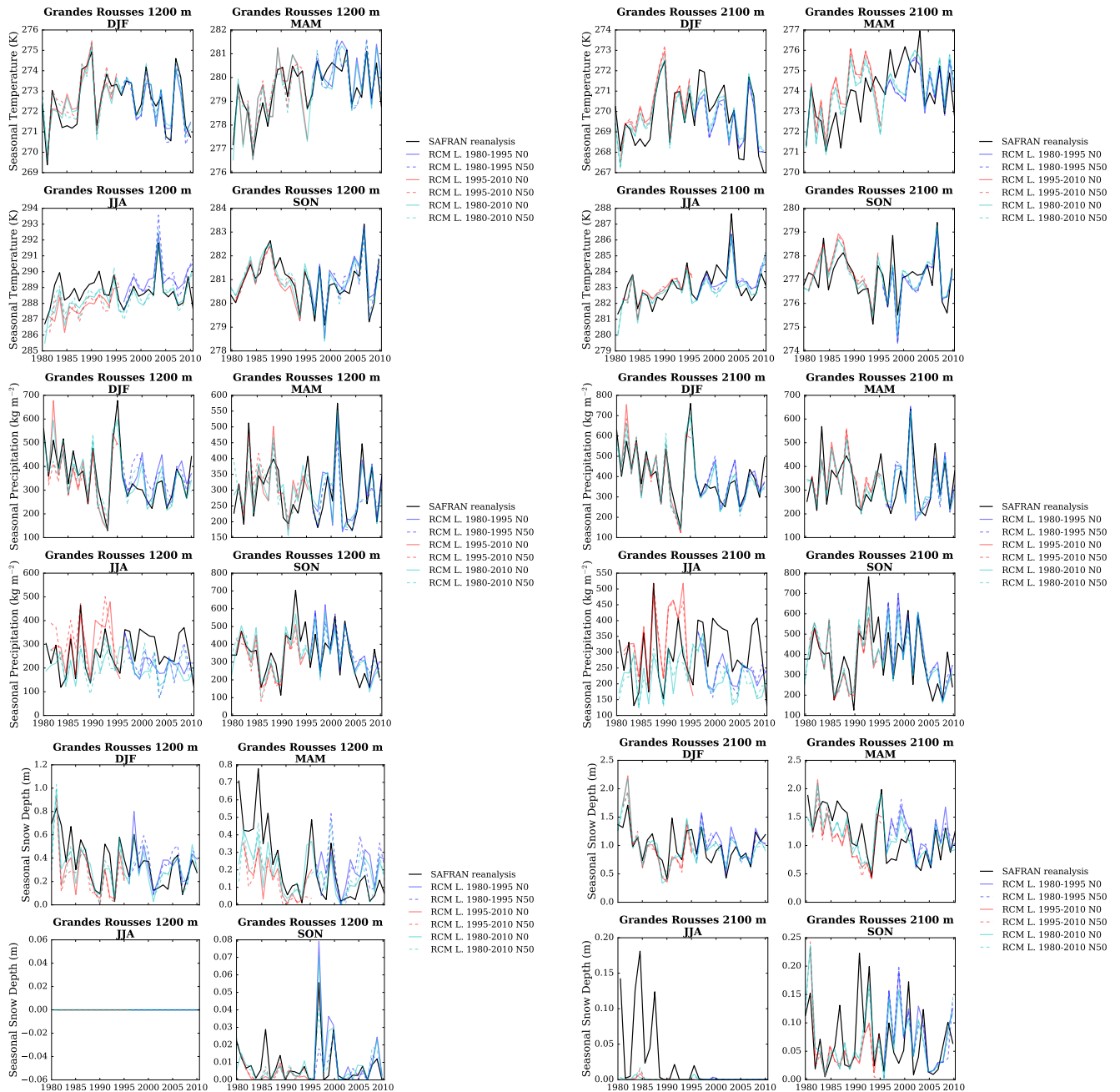


Figure S106: (top) Temperature, (middle) precipitation and (bottom) snow depth (using Crocus in this case) seasonal average time series from 1980 to 2010 in each adjusted RCM simulation and in the SAFRAN reanalysis, for the Grandes Rousses massif, and at (left) 1200 m a.s.l. and (right) 2100 m a.s.l..

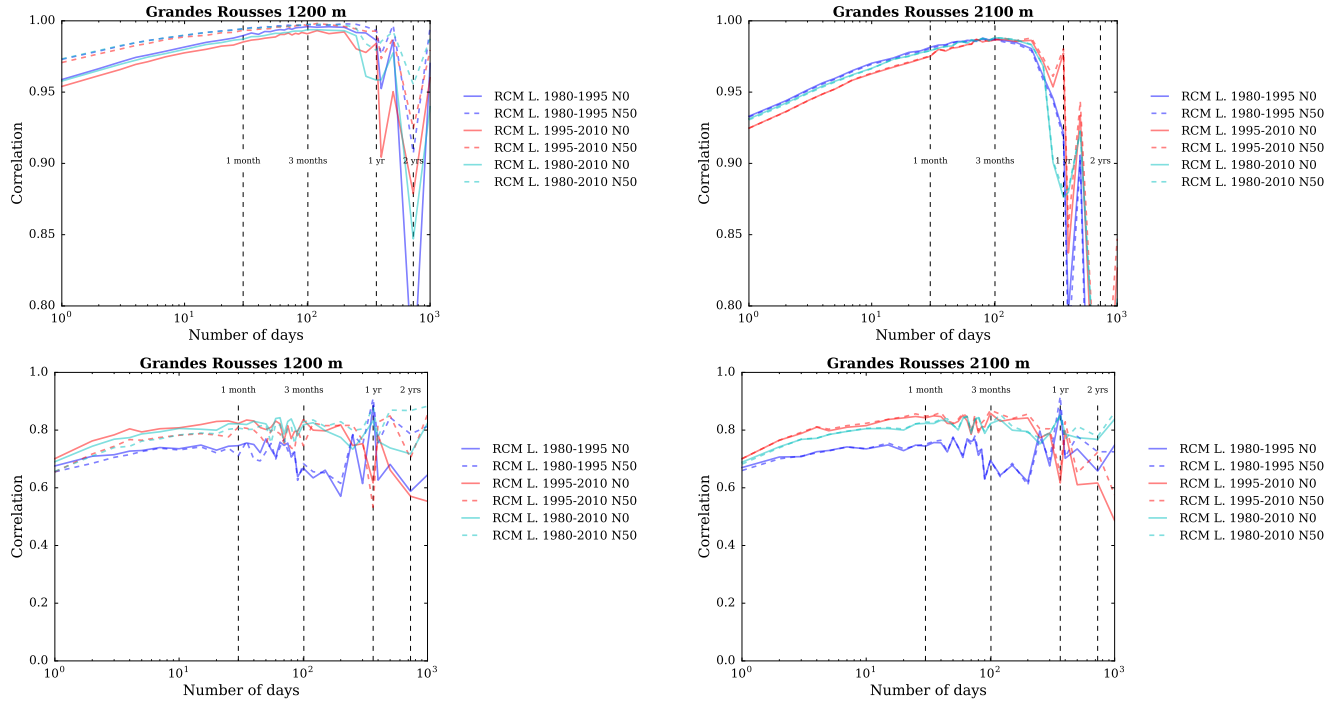


Figure S107: Correlation between the SAFRAN reanalysis and adjusted RCM (top) temperature and (bottom) precipitation as a function of the integration window over the evaluation period, for the Grandes Rousses massif, and at (left) 1200 m a.s.l. and (right) 2100 m a.s.l..

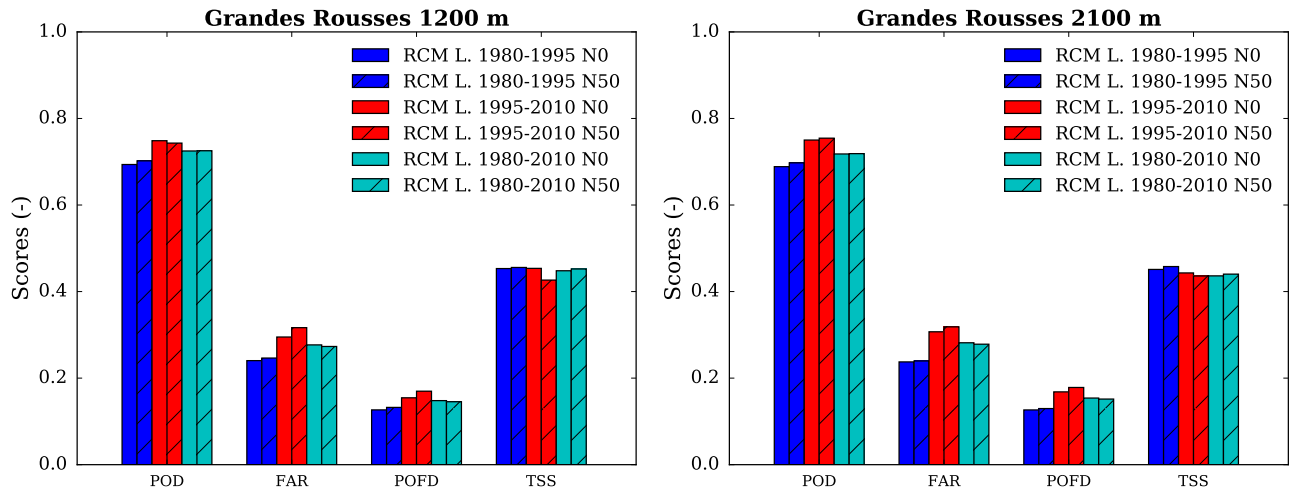


Figure S108: Scores for the detection of precipitation events in each adjusted RCM simulation compared to the SAFRAN reanalysis over the evaluation period, for the Grandes Rousses massif, at (left) 1200 m a.s.l. and (right) 2100 m a.s.l.. POD = probability of detection, FAR = false alarm rate, POFD = probability of false detection, TSS = true skill score.

Thabor

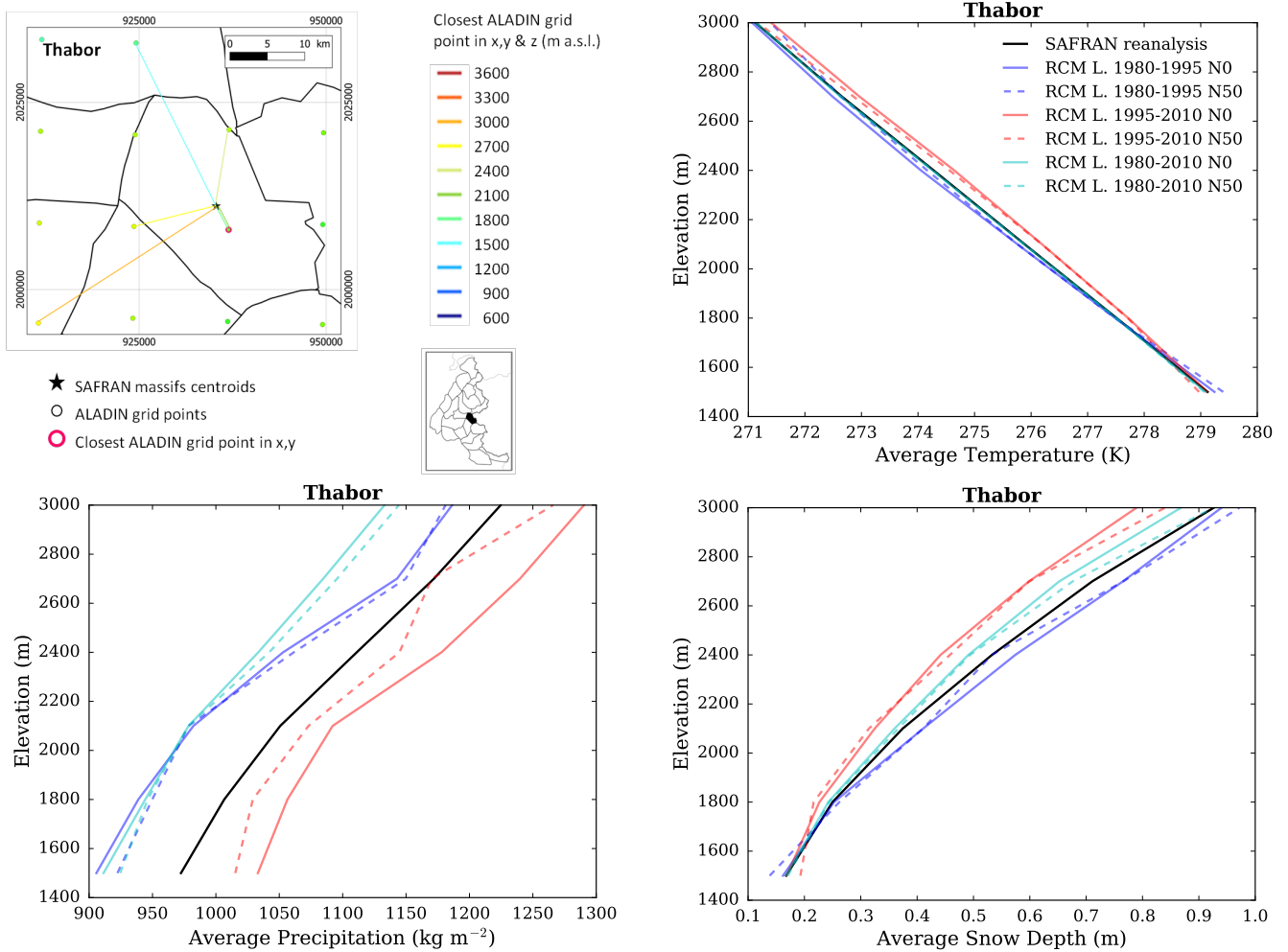


Figure S109: (top left) Location of the Thabor massif, with ALADIN RCM grid points chosen as the closest in x, y ($N = 0$, pink contour) and in x, y and z (using $N \neq 0$). Coloured lines link each SAFRAN massif centre point with the corresponding grid point in ALADIN for the different elevations considered (in m above sea level (a.s.l.)). (top right) Mean temperature, (bottom left) precipitation and (bottom right) snow depth (using Crocus in this case) for each elevation band for the Thabor massif, over the evaluation period in each adjusted RCM simulation (different learning periods and 2 neighbour selection methods) and in SAFRAN (1980-2010).

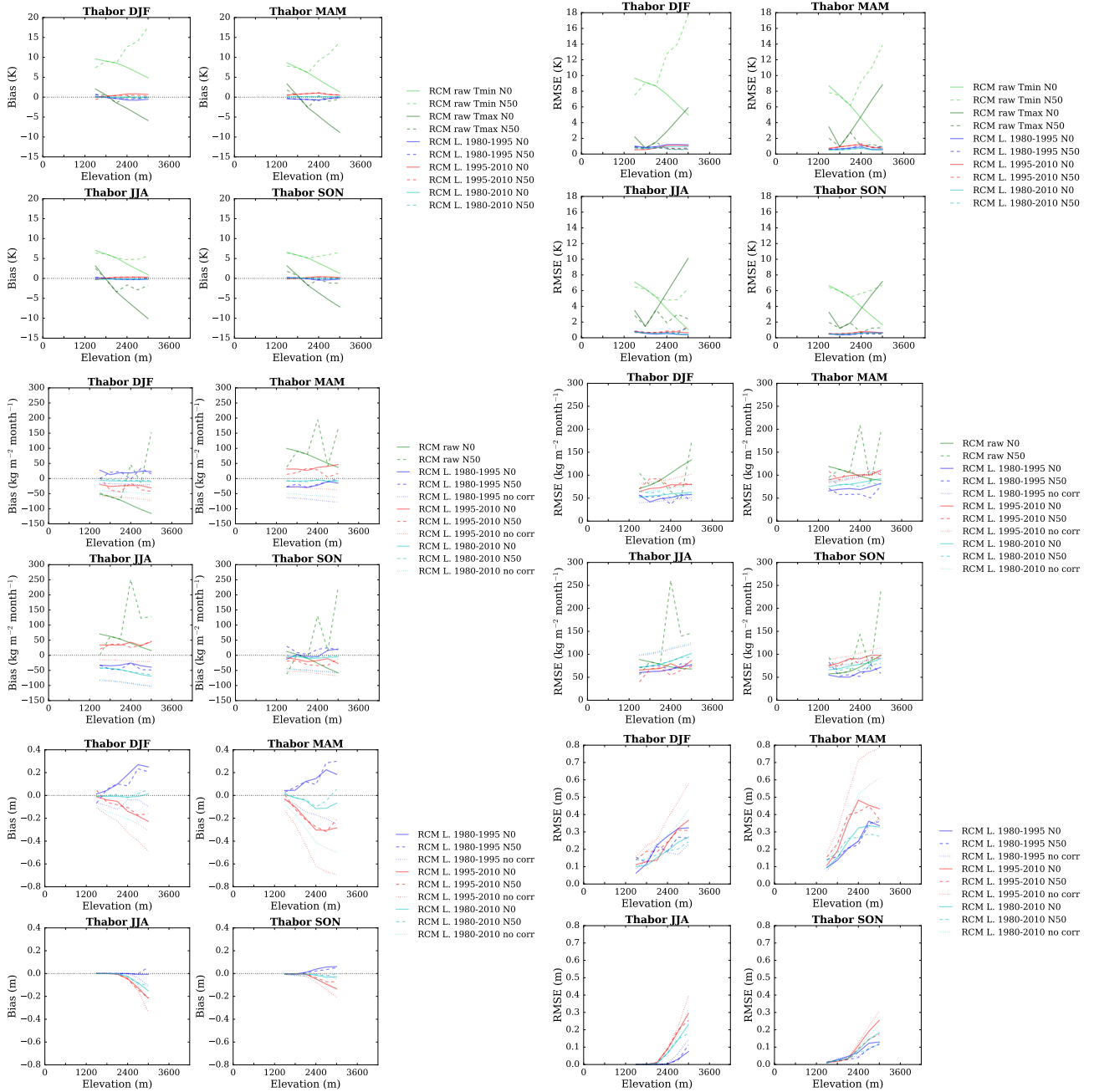


Figure S110: (top) Temperature, (middle) precipitation and (bottom) snow depth (using Crocus in this case) mean bias and root mean square error of each raw and adjusted RCM simulation compared to the SAFRAN reanalysis over the evaluation period for the Thabor massif as a function of elevation. Scores computed for the raw RCM simulations concern minimum and maximum daily temperatures.

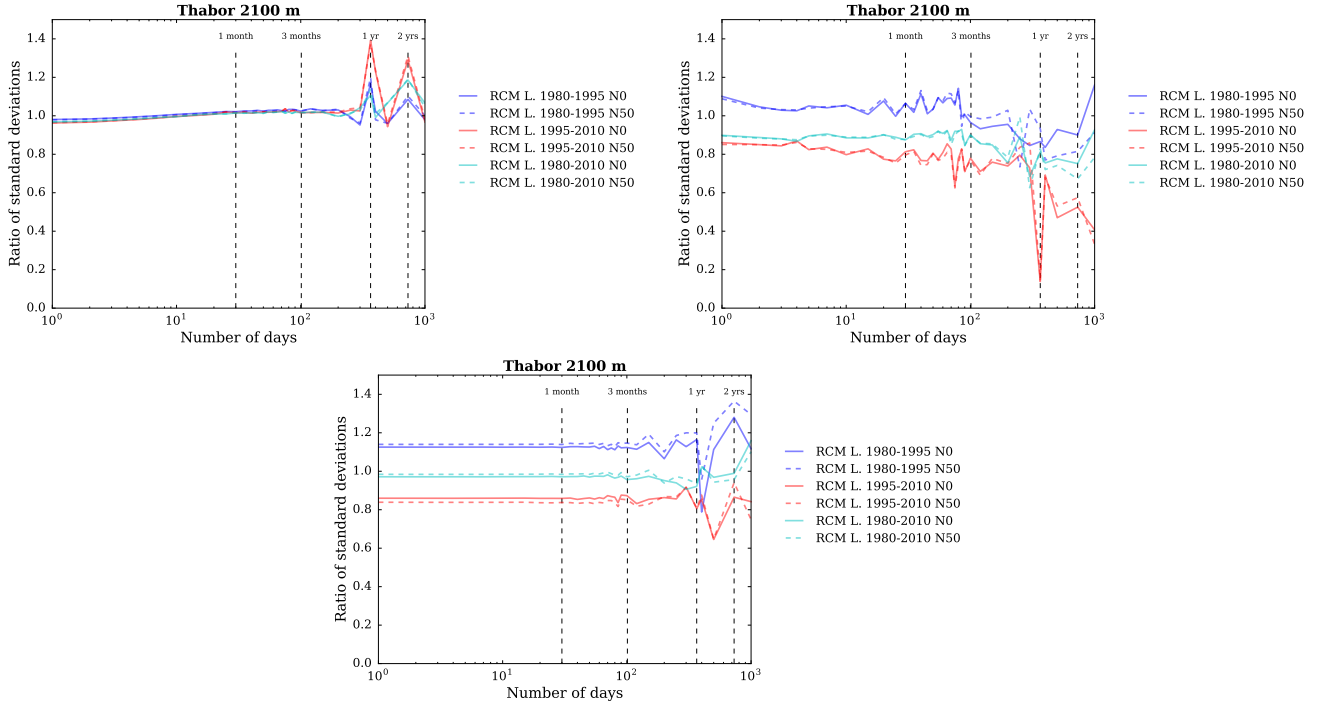


Figure S111: Ratios of standard deviations between the SAFRAN reanalysis and adjusted RCM (top left) temperature, (top right) precipitation and (bottom) snow depth (using Crocus in this case) as a function of the integration window over the evaluation period, for the Thabor massif, at 2100 m a.s.l..

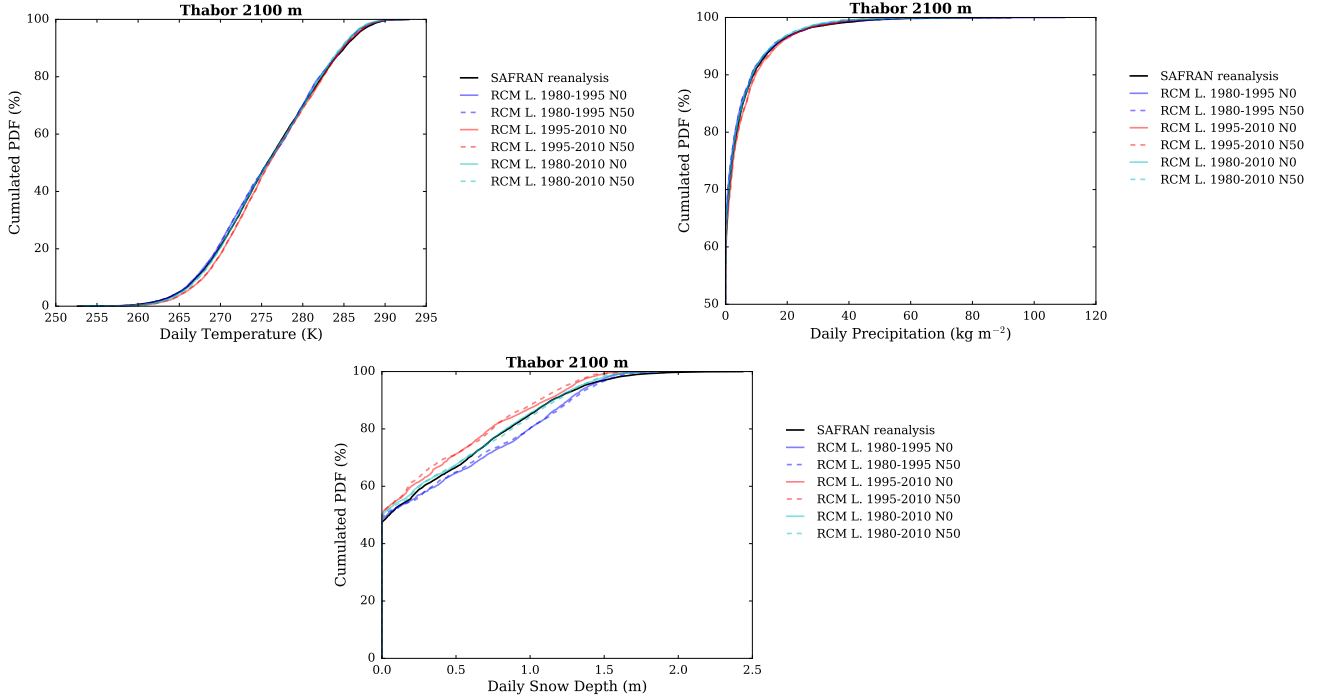


Figure S112: Cumulated probability density functions (PDFs) of daily (top left) temperature, (top right) precipitation and (bottom) snow depth (using Crocus in this case) in each adjusted RCM simulation and in the SAFRAN reanalysis (1980-2010) over the evaluation period, for the Thabor massif, at 2100 m a.s.l..

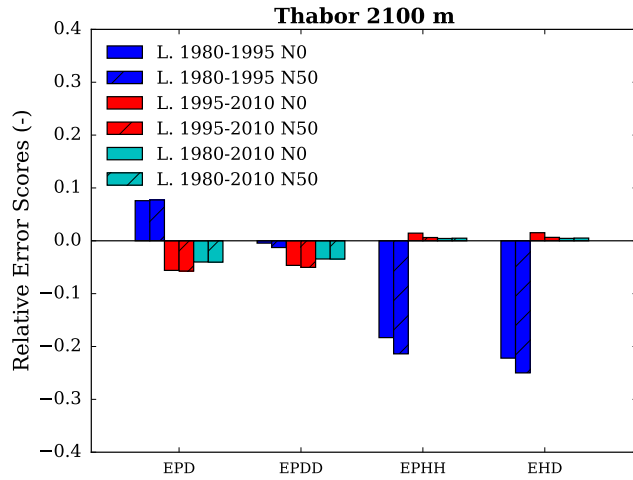


Figure S113: Scores for the duration and persistence of precipitation events in each adjusted RCM simulation compared to the SAFRAN reanalysis over the evaluation period, for the Thabor massif, at 2100 m a.s.l.. EPD = relative error on the probability of a dry day, EPDD = relative error on the probability of a dry day following a dry day, EPHH = relative error on the probability of a wet day following a wet day, EHD = relative error on the mean duration of wet periods.

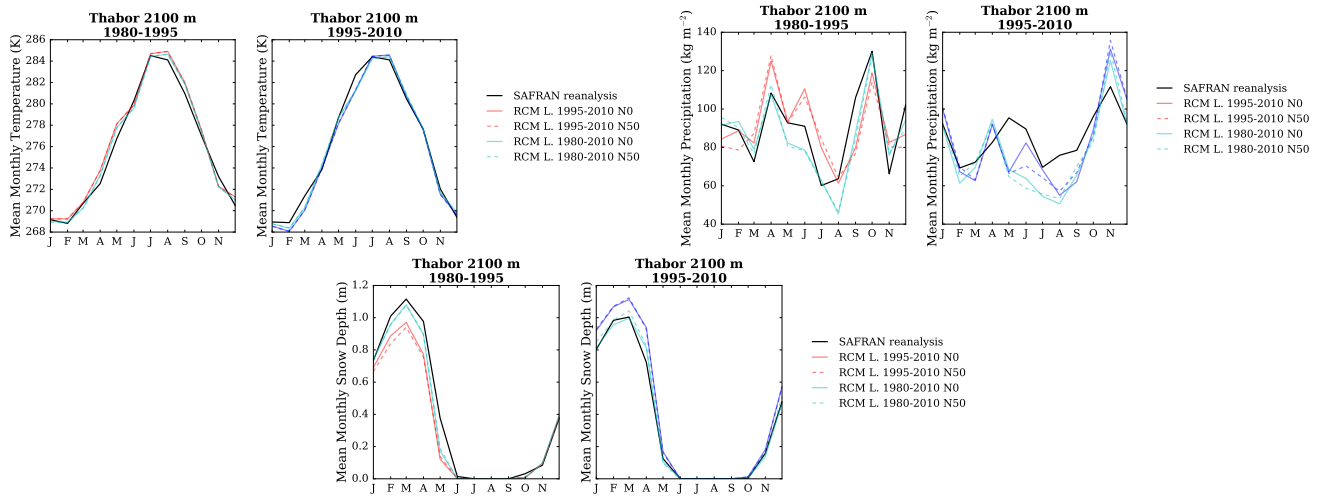


Figure S114: (top left) Temperature, (top right) precipitation and (bottom) snow depth (using Crocus in this case) mean annual cycle in each adjusted RCM simulation and in the SAFRAN reanalysis over the period 1980-1995 and 1995-2010, for the Thabor massif, and at 2100 m a.s.l.. Letters on the x-axis correspond to the different months of the calendar (J = January, F = February, etc.).

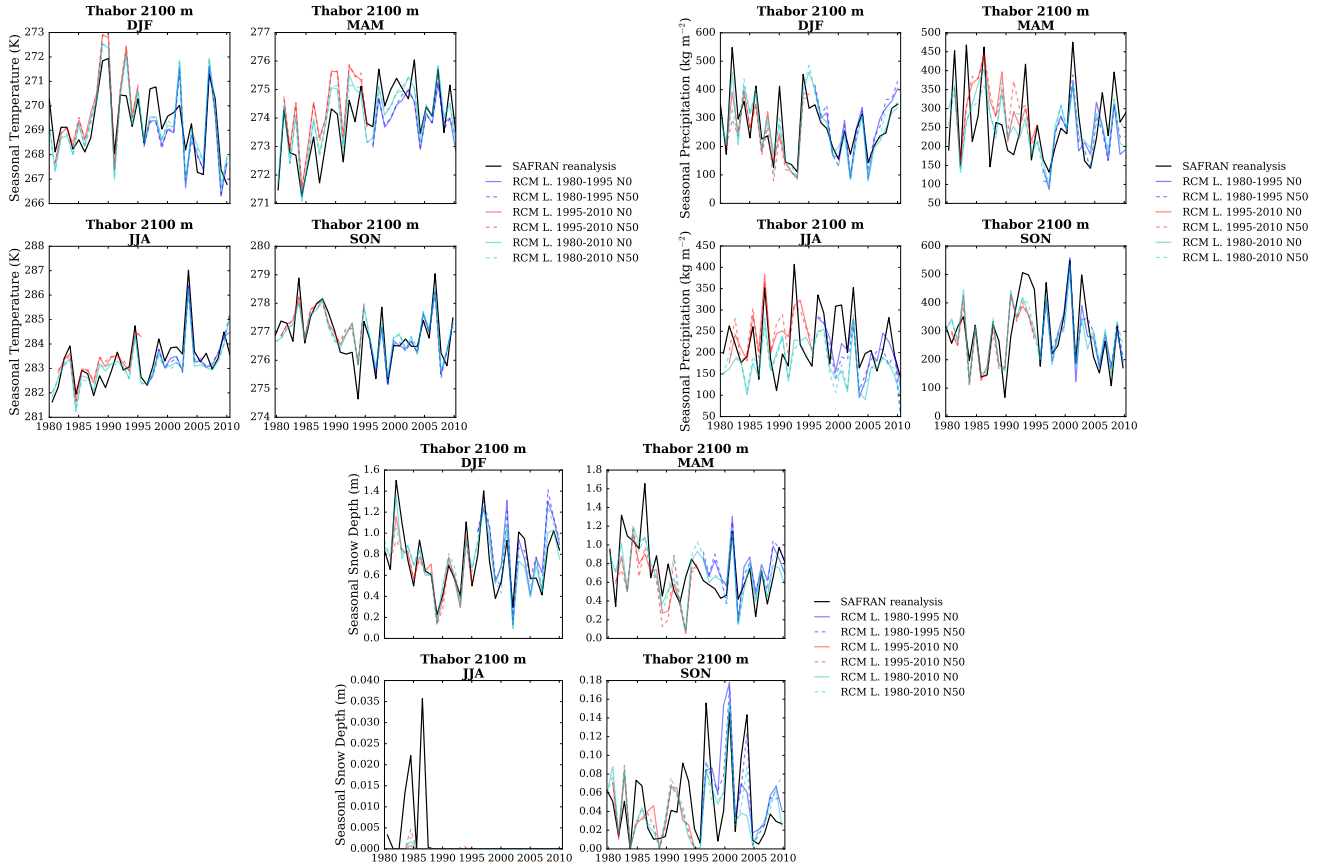


Figure S115: (top left) Temperature, (top right) precipitation and (bottom) snow depth (using Crocus in this case) seasonal average time series from 1980 to 2010 in each adjusted RCM simulation and in the SAFRAN reanalysis, for the Thabor massif, and at 2100 m a.s.l..

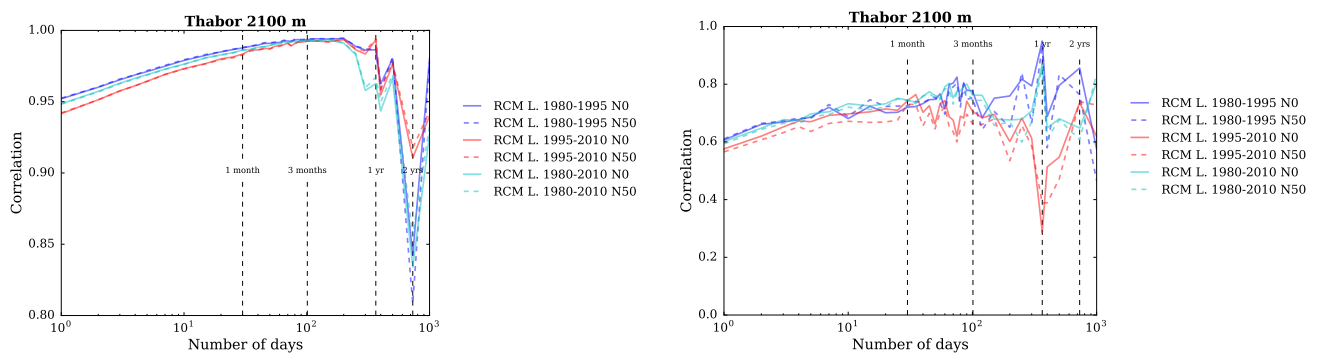


Figure S116: Correlation between the SAFRAN reanalysis and adjusted RCM (left) temperature and (right) precipitation as a function of the integration window over the evaluation period, for the Thabor massif, and at 2100 m a.s.l..

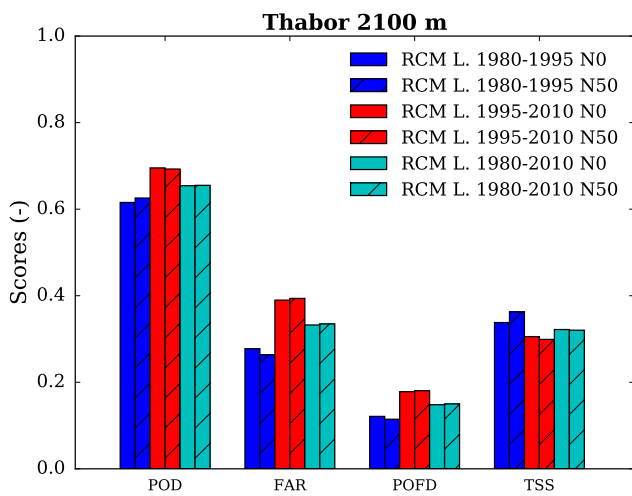


Figure S117: Scores for the detection of precipitation events in each adjusted RCM simulation compared to the SAFRAN reanalysis over the evaluation period, for the Thabor massif, at 2100 m a.s.l.. POD = probability of detection, FAR = false alarm rate, POFD = probability of false detection, TSS = true skill score.

Vercors

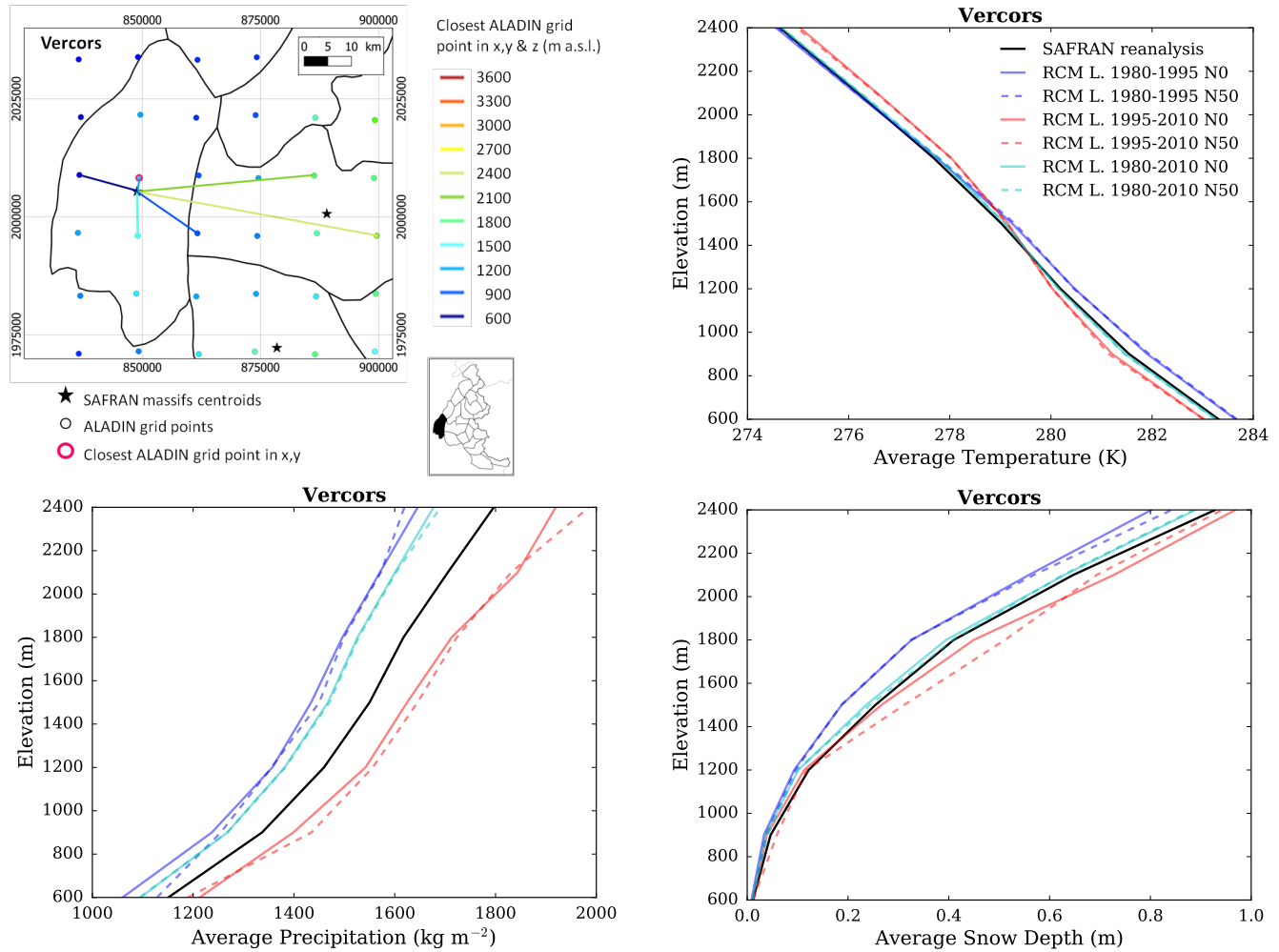


Figure S118: (top left) Location of the Vercors massif, with ALADIN RCM grid points chosen as the closest in x, y ($N = 0$, pink contour) and in x, y and z (using $N \neq 0$). Coloured lines link each SAFRAN massif centre point with the corresponding grid point in ALADIN for the different elevations considered (in m above sea level (a.s.l.)). (top right) Mean temperature, (bottom left) precipitation and (bottom right) snow depth (using Crocus in this case) for each elevation band for the Vercors massif, over the evaluation period in each adjusted RCM simulation (different learning periods and 2 neighbour selection methods) and in SAFRAN (1980-2010).

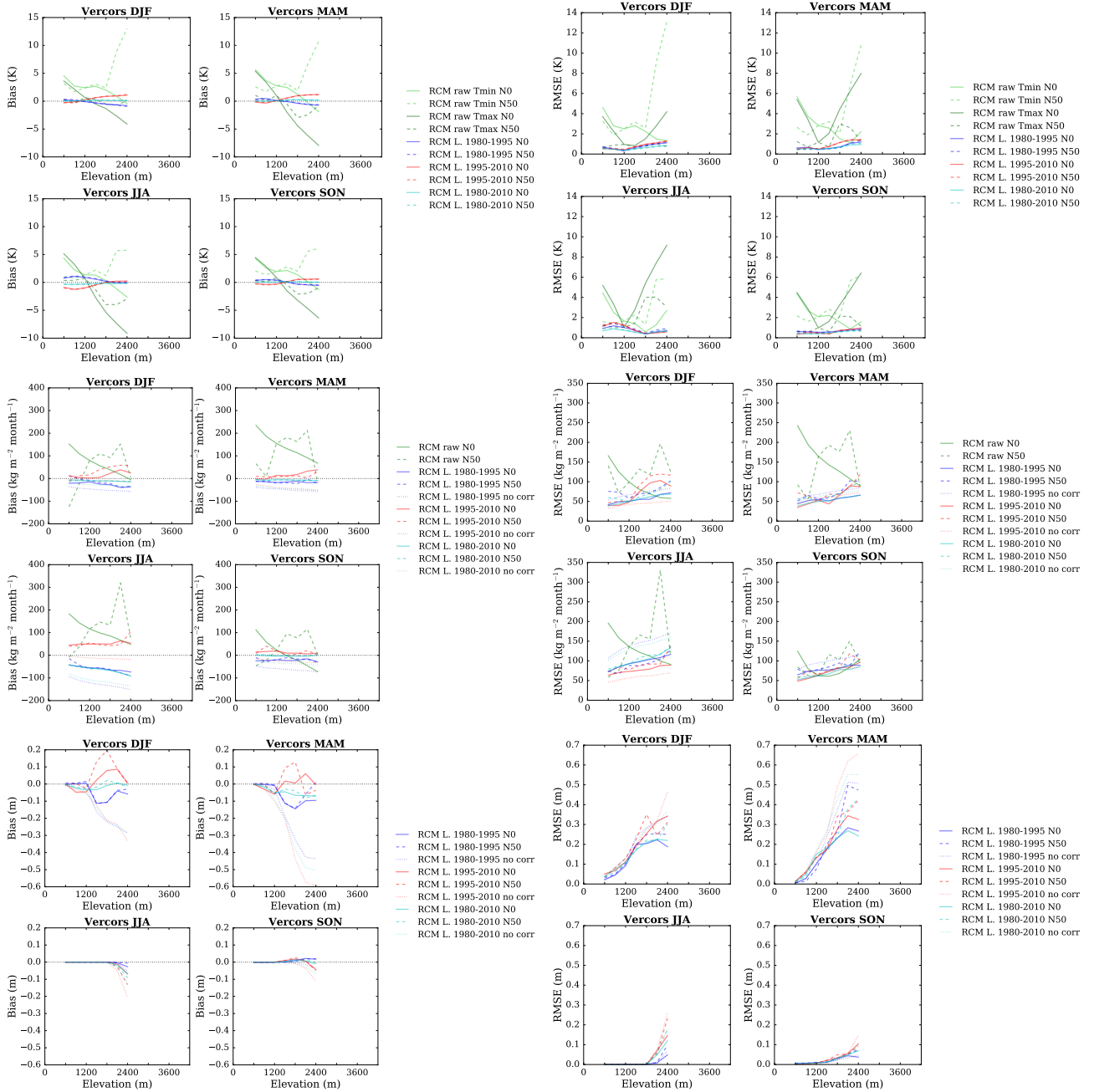


Figure S119: (top) Temperature, (middle) precipitation and (bottom) snow depth (using Crocus in this case) mean bias and root mean square error of each raw and adjusted RCM simulation compared to the SAFRAN reanalysis over the evaluation period for the Vercors massif as a function of elevation. Scores computed for the raw RCM simulations concern minimum and maximum daily temperatures.

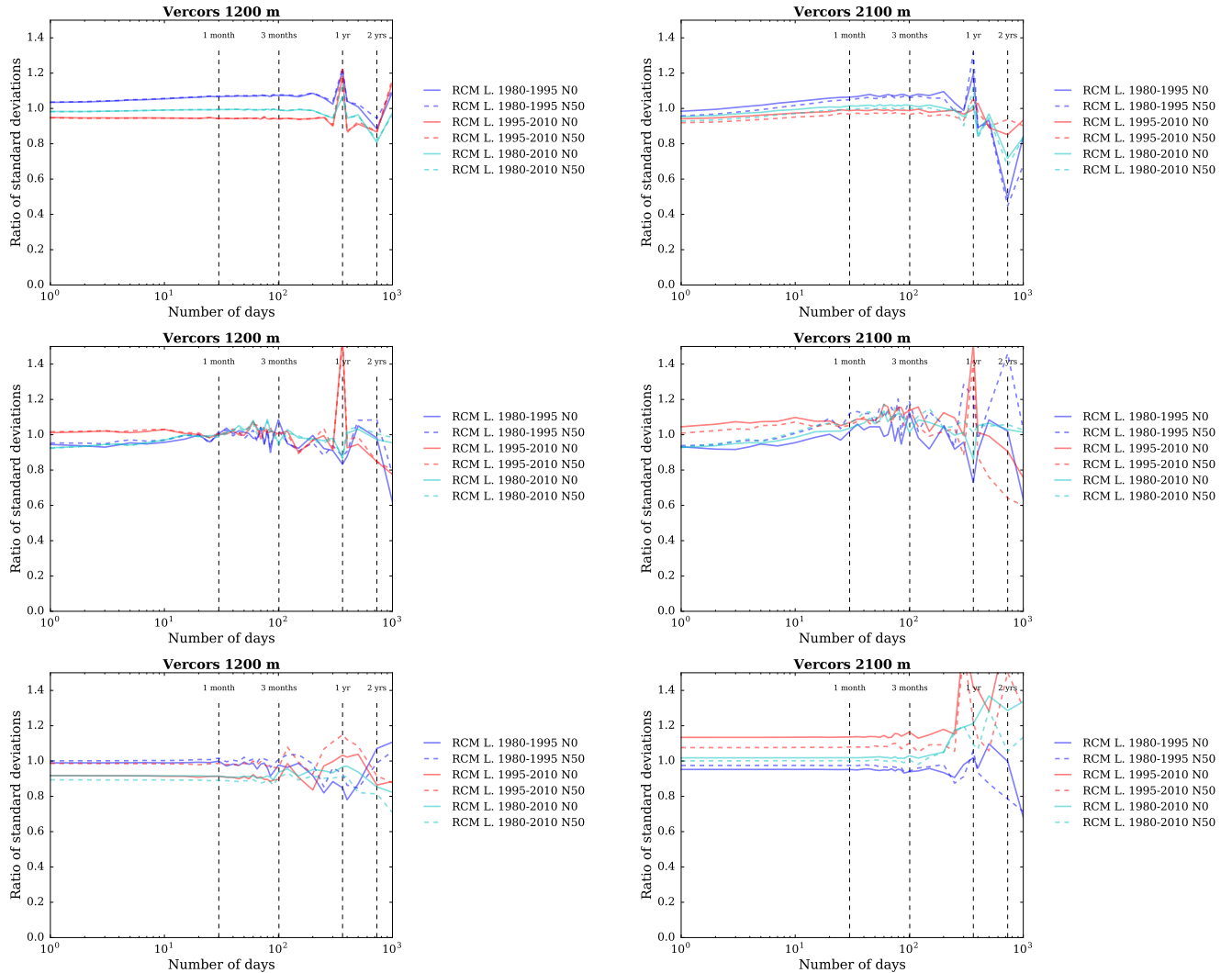


Figure S120: Ratios of standard deviations between the SAFRAN reanalysis and adjusted RCM (top) temperature, (middle) precipitation and (bottom) snow depth (using Crocus in this case) as a function of the integration window over the evaluation period, for the Vercors massif, at (left) 1200 m a.s.l. and (right) 2100 m a.s.l..

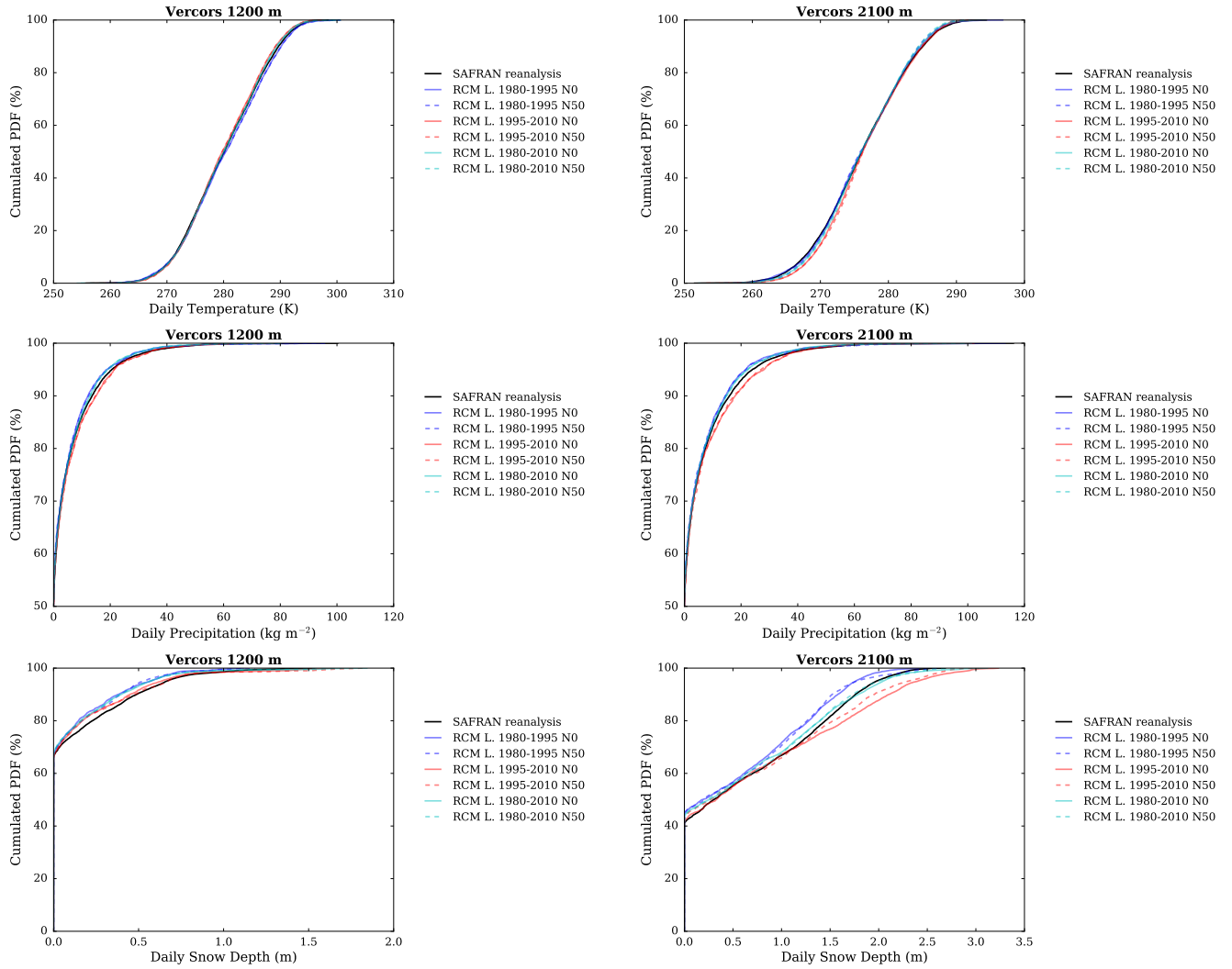


Figure S121: Cumulated probability density functions (PDFs) of daily (top) temperature, (middle) precipitation and (bottom) snow depth (using Crocus in this case) in each adjusted RCM simulation and in the SAFRAN reanalysis (1980-2010) over the evaluation period, for the Vercors massif, at (left) 1200 m a.s.l. and (right) 2100 m a.s.l..

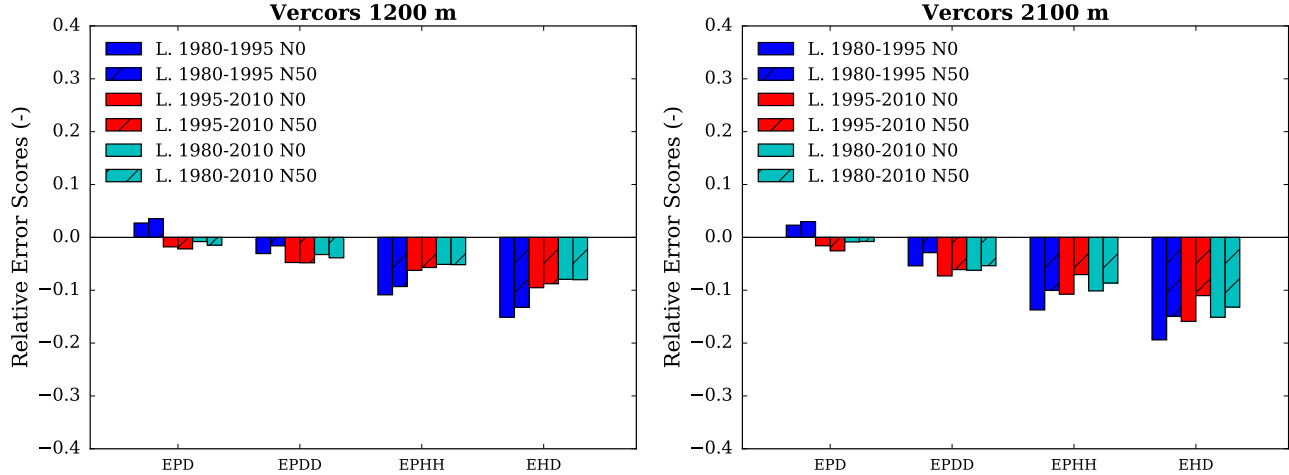


Figure S122: Scores for the duration and persistence of precipitation events in each adjusted RCM simulation compared to the SAFRAN reanalysis over the evaluation period, for the Vercors massif, at (left) 1200 m a.s.l. and (right) 2100 m a.s.l.. EPD = relative error on the probability of a dry day, EPDD = relative error on the probability of a dry day following a dry day, EPHH = relative error on the probability of a wet day following a wet day, EHD = relative error on the mean duration of wet periods.

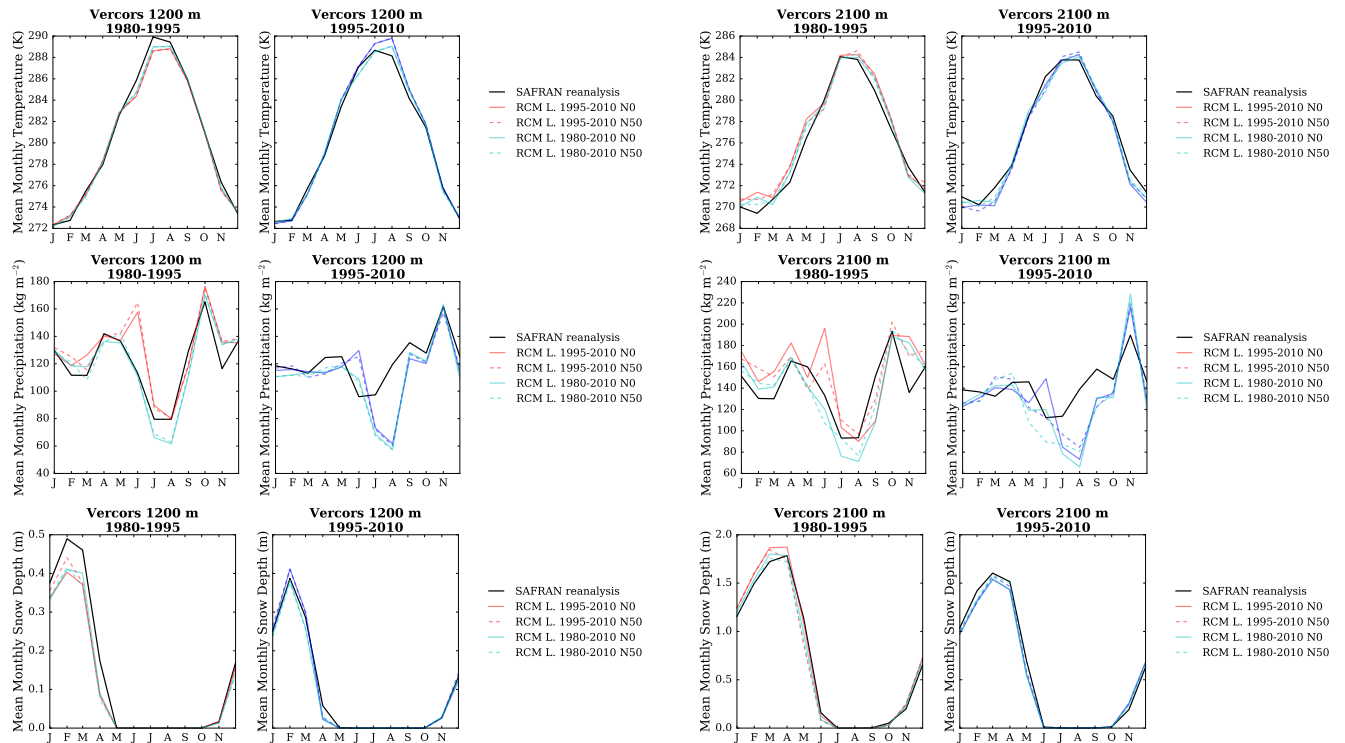


Figure S123: (top) Temperature, (middle) precipitation and (bottom) snow depth (using Crocus in this case) mean annual cycle in each adjusted RCM simulation and in the SAFRAN reanalysis over the period 1980-1995 and 1995-2010, for the Vercors massif, and at (left) 1200 m a.s.l. and (right) 2100 m a.s.l.. Letters on the x-axis correspond to the different months of the calendar (J = January, F = February, etc.).

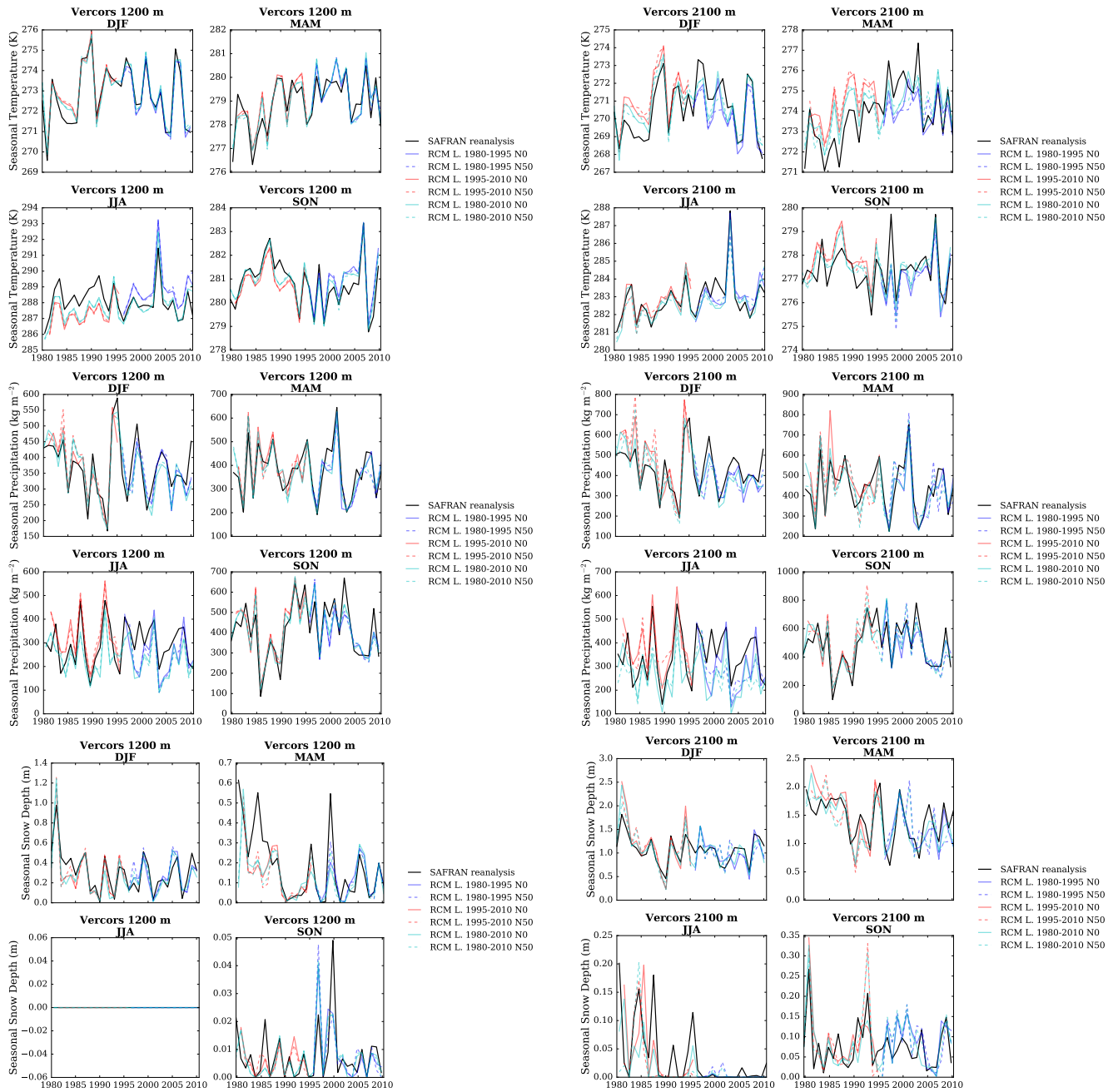


Figure S124: (top) Temperature, (middle) precipitation and (bottom) snow depth (using Crocus in this case) seasonal average time series from 1980 to 2010 in each adjusted RCM simulation and in the SAFRAN reanalysis, for the Vercors massif, and at (left) 1200 m a.s.l. and (right) 2100 m a.s.l..

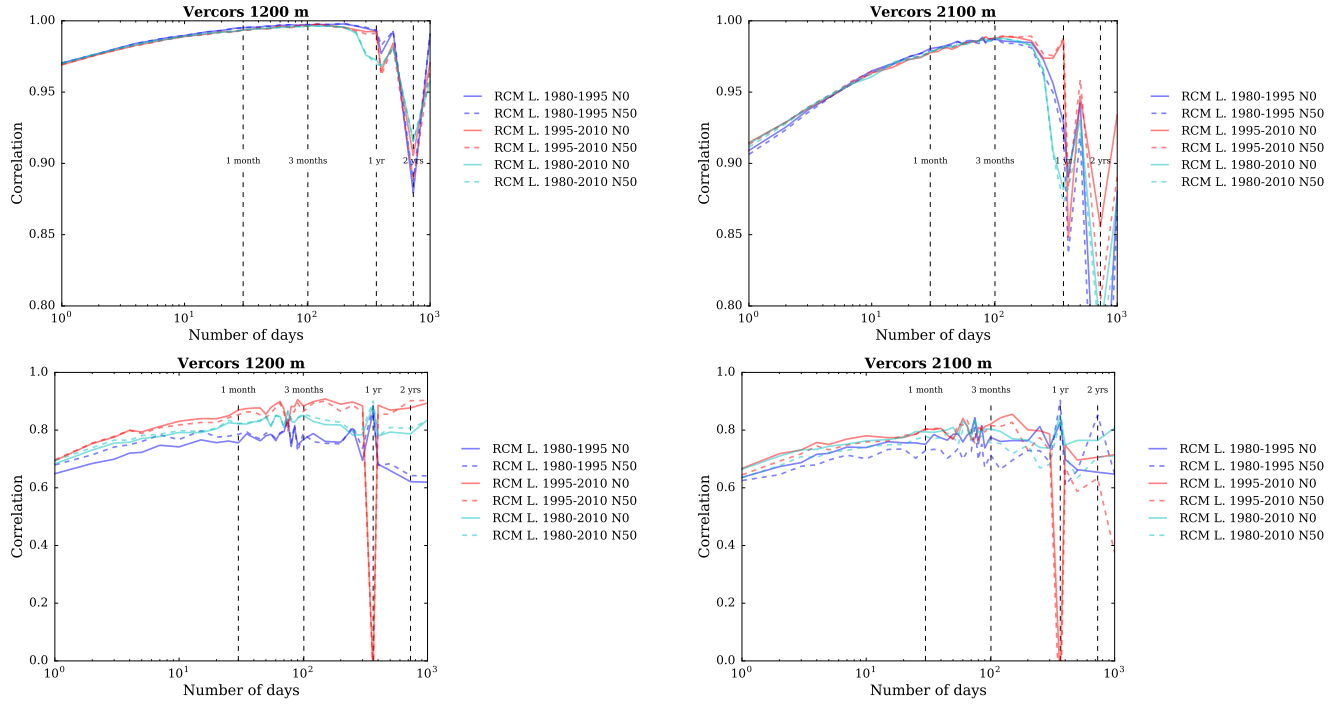


Figure S125: Correlation between the SAFRAN reanalysis and adjusted RCM (top) temperature and (bottom) precipitation as a function of the integration window over the evaluation period, for the Vercors massif, and at (left) 1200 m a.s.l. and (right) 2100 m a.s.l..

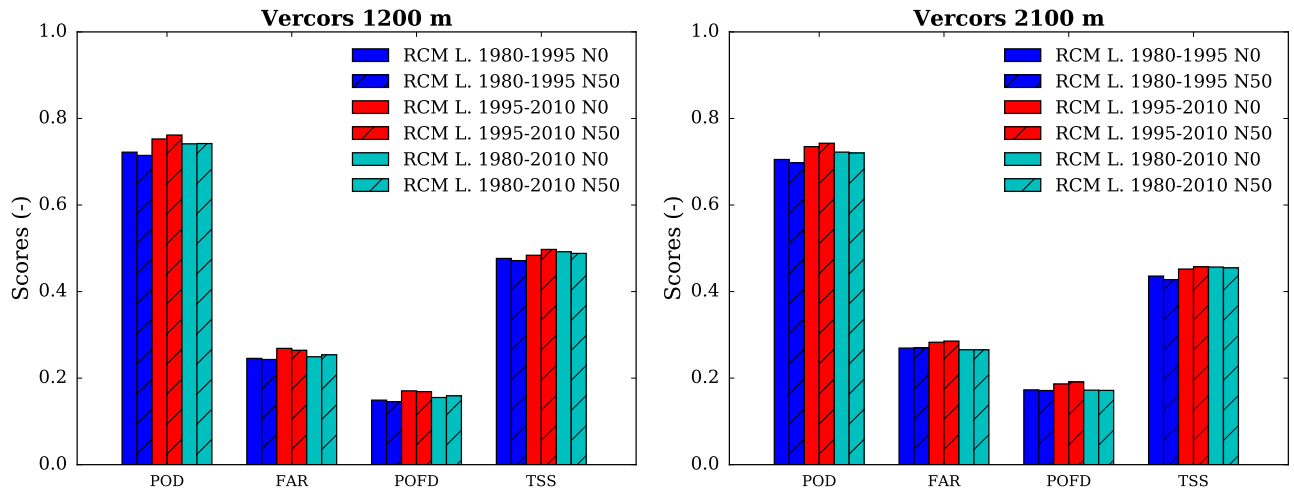


Figure S126: Scores for the detection of precipitation events in each adjusted RCM simulation compared to the SAFRAN reanalysis over the evaluation period, for the Vercors massif, at (left) 1200 m a.s.l. and (right) 2100 m a.s.l.. POD = probability of detection, FAR = false alarm rate, POFD = probability of false detection, TSS = true skill score.

Oisans

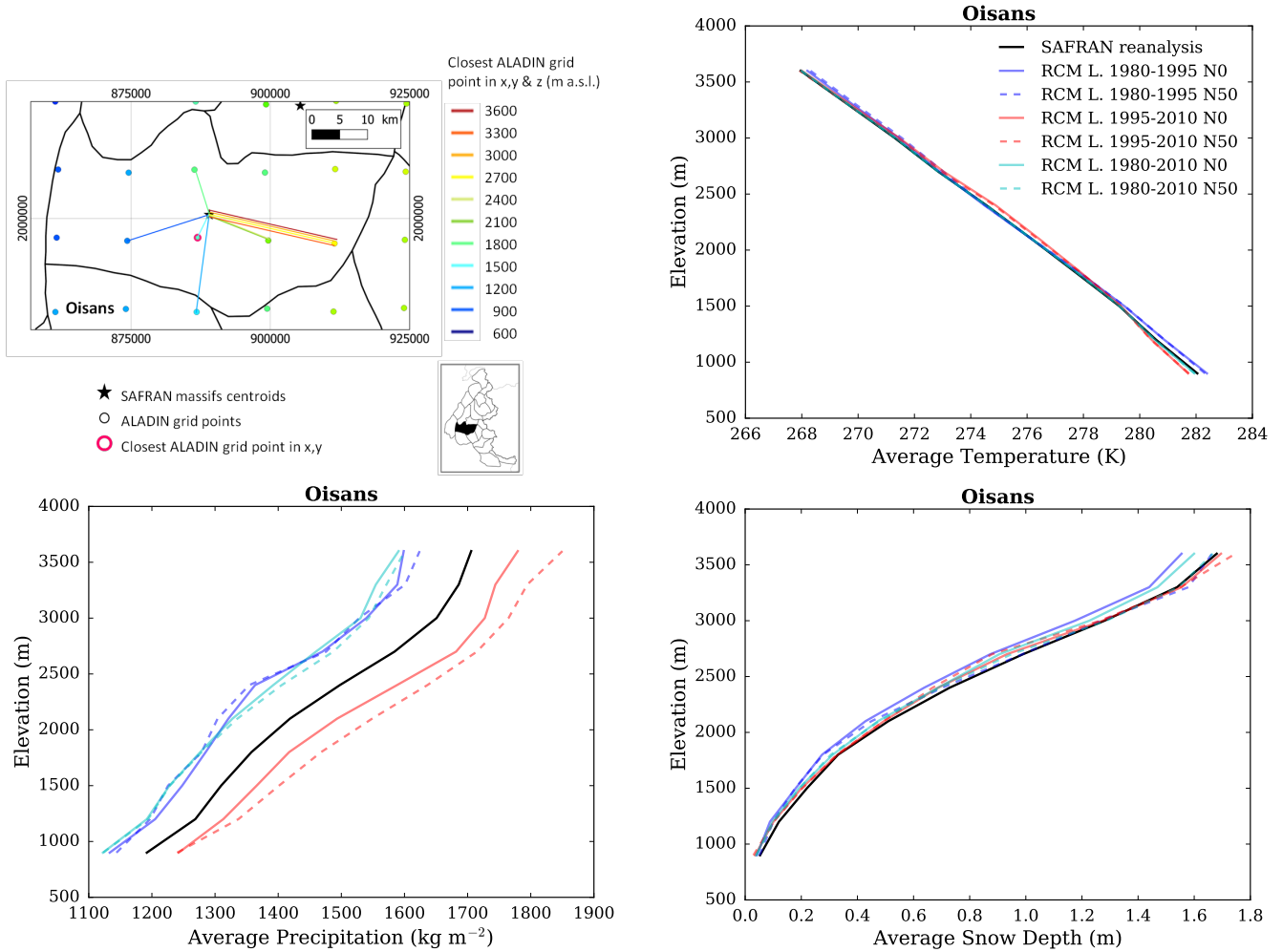


Figure S127: (top left) Location of the Oisans massif, with ALADIN RCM grid points chosen as the closest in x , y ($N = 0$, pink contour) and in x , y and z (using $N \neq 0$). Coloured lines link each SAFRAN massif centre point with the corresponding grid point in ALADIN for the different elevations considered (in m above sea level (a.s.l.)). (top right) Mean temperature, (bottom left) precipitation and (bottom right) snow depth (using Crocus in this case) for each elevation band for the Oisans massif, over the evaluation period in each adjusted RCM simulation (different learning periods and 2 neighbour selection methods) and in SAFRAN (1980-2010).

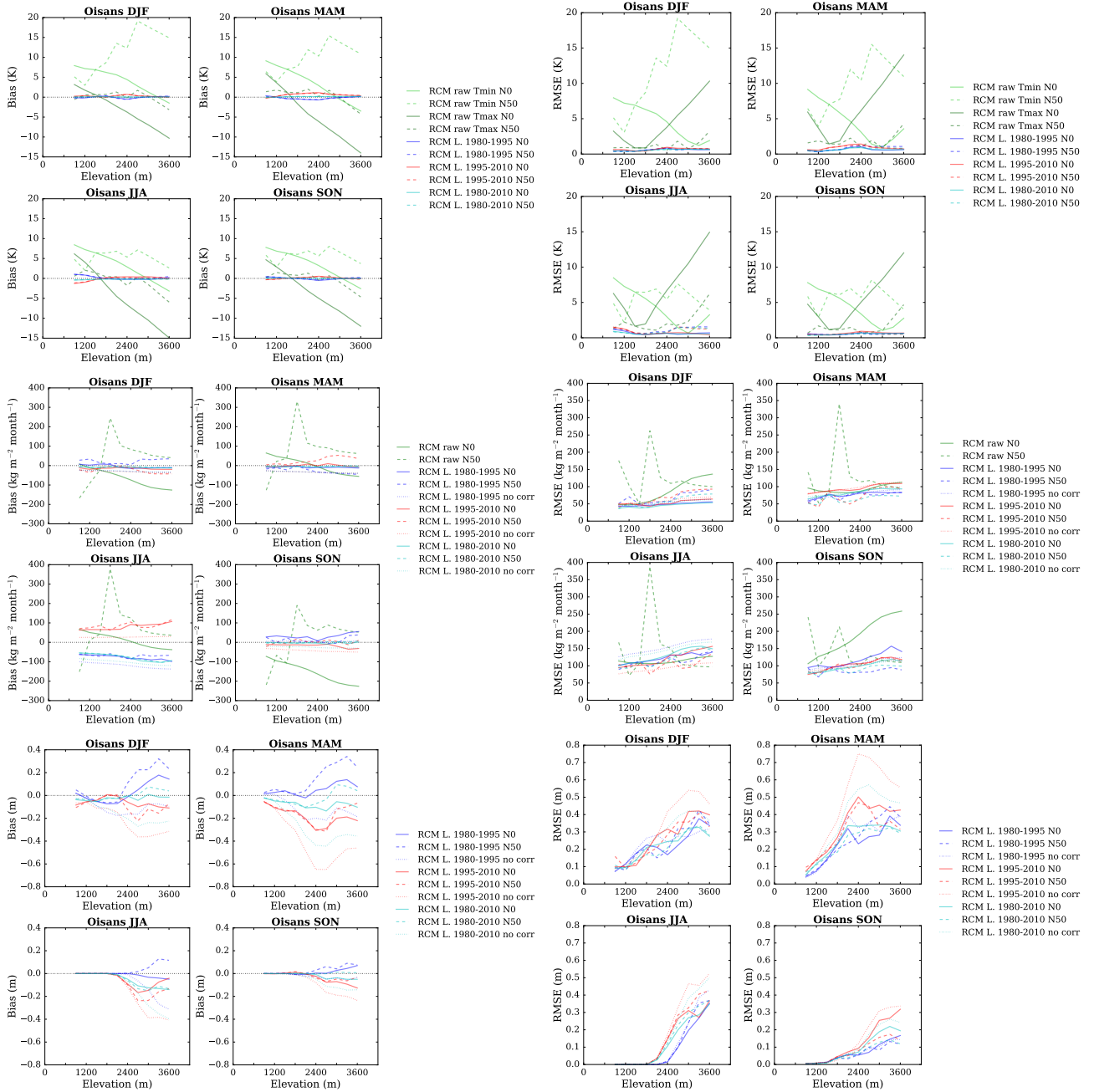


Figure S128: (top) Temperature, (middle) precipitation and (bottom) snow depth (using Crocus in this case) mean bias and root mean square error of each raw and adjusted RCM simulation compared to the SAFRAN reanalysis over the evaluation period for the Oisans massif as a function of elevation. Scores computed for the raw RCM simulations concern minimum and maximum daily temperatures.

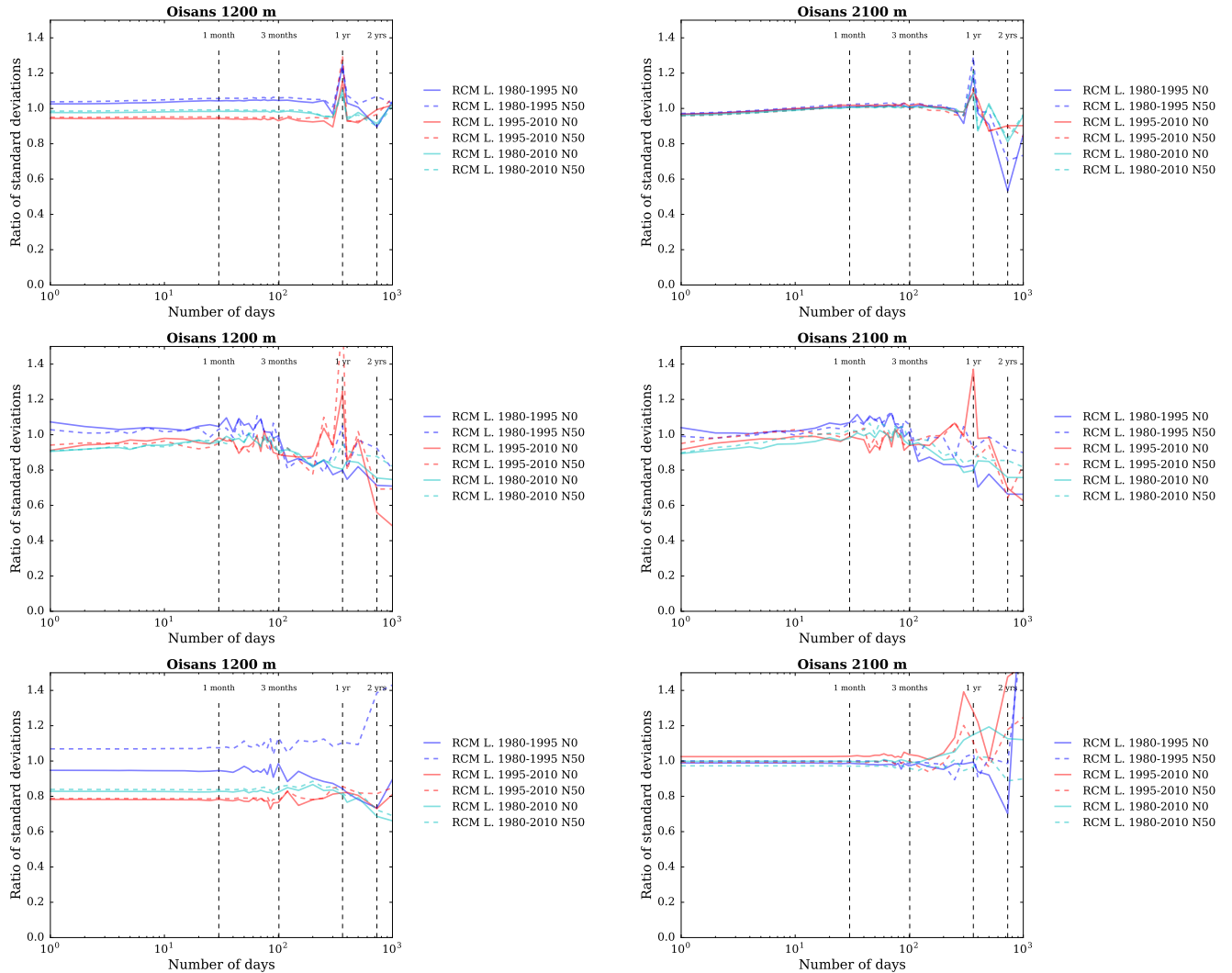


Figure S129: Ratios of standard deviations between the SAFRAN ranalysis and adjusted RCM (top) temperature, (middle) precipitation and (bottom) snow depth (using Crocus in this case) as a function of the integration window over the evaluation period, for the Oisans massif, at (left) 1200 m a.s.l. and (right) 2100 m a.s.l..

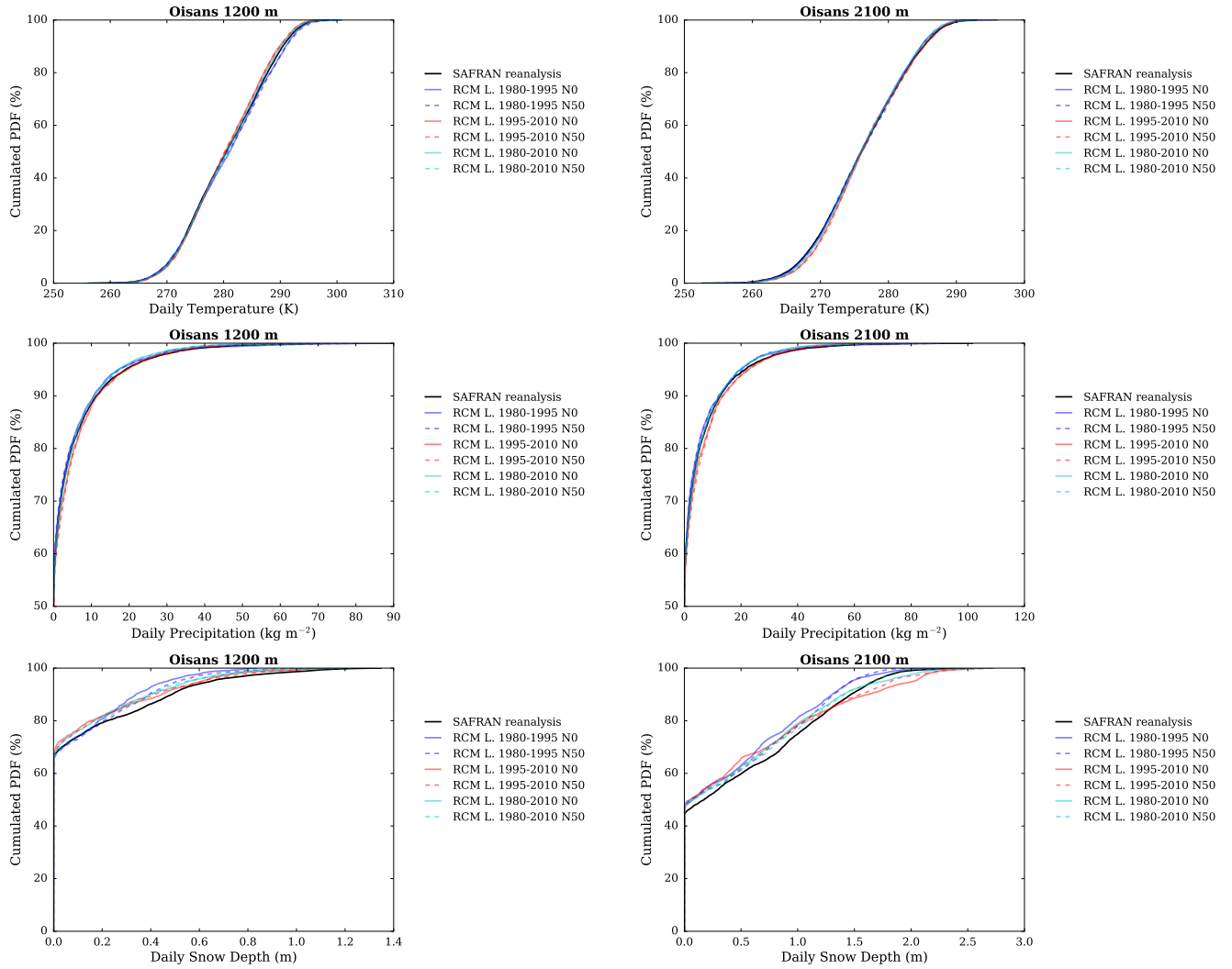


Figure S130: Cumulated probability density functions (PDFs) of daily (top) temperature, (middle) precipitation and (bottom) snow depth (using Crocus in this case) in each adjusted RCM simulation and in the SAFRAN reanalysis (1980-2010) over the evaluation period, for the Oisans massif, at (left) 1200 m a.s.l. and (right) 2100 m a.s.l..

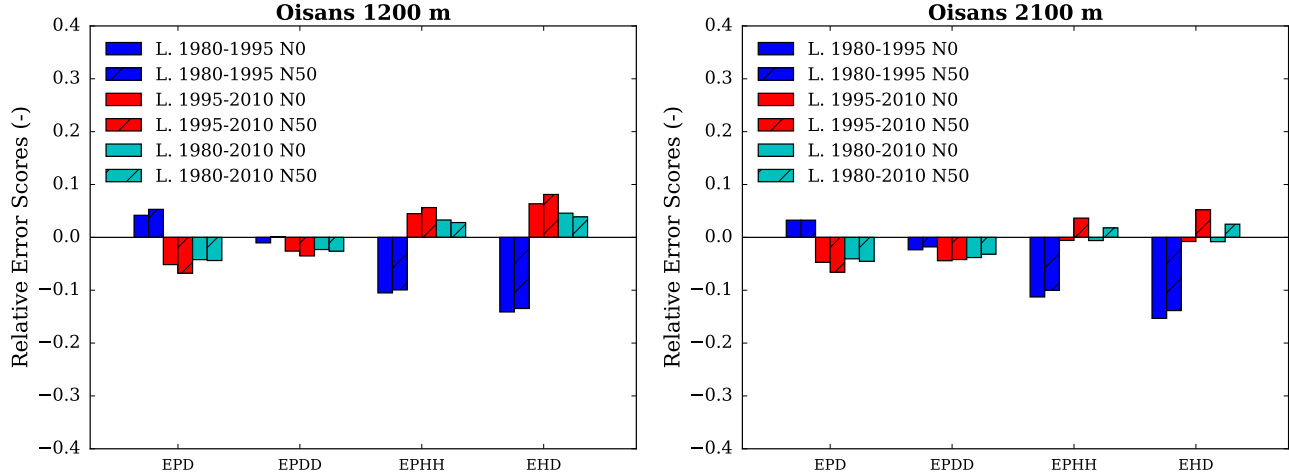


Figure S131: Scores for the duration and persistence of precipitation events in each adjusted RCM simulation compared to the SAFRAN reanalysis over the evaluation period, for the Oisans massif, at (left) 1200 m a.s.l. and (right) 2100 m a.s.l.. EPD = relative error on the probability of a dry day, EPDD = relative error on the probability of a dry day following a dry day, EPHH = relative error on the probability of a wet day following a wet day, EHD = relative error on the mean duration of wet periods.

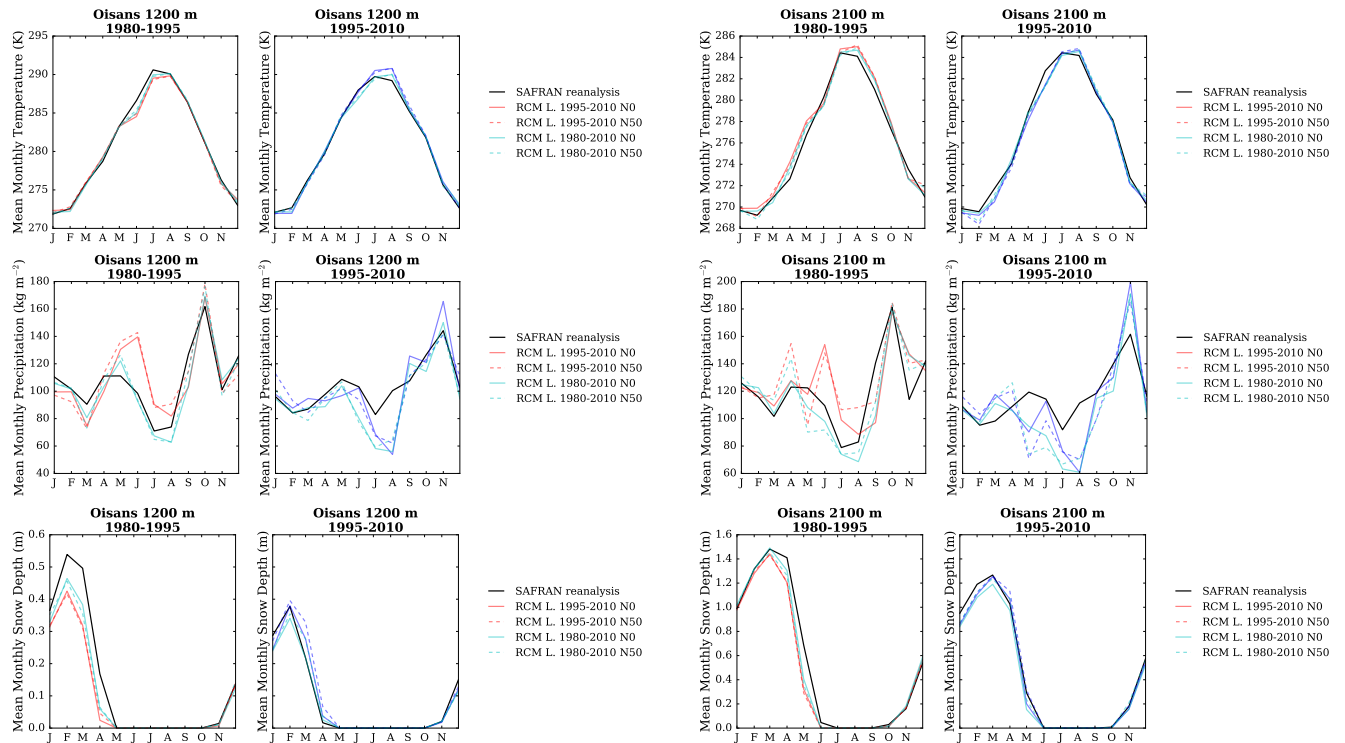


Figure S132: (top) Temperature, (middle) precipitation and (bottom) snow depth (using Crocus in this case) mean annual cycle in each adjusted RCM simulation and in the SAFRAN reanalysis over the period 1980-1995 and 1995-2010, for the Oisans massif, and at (left) 1200 m a.s.l. and (right) 2100 m a.s.l.. Letters on the x-axis correspond to the different months of the calendar (J = January, F = February, etc.).

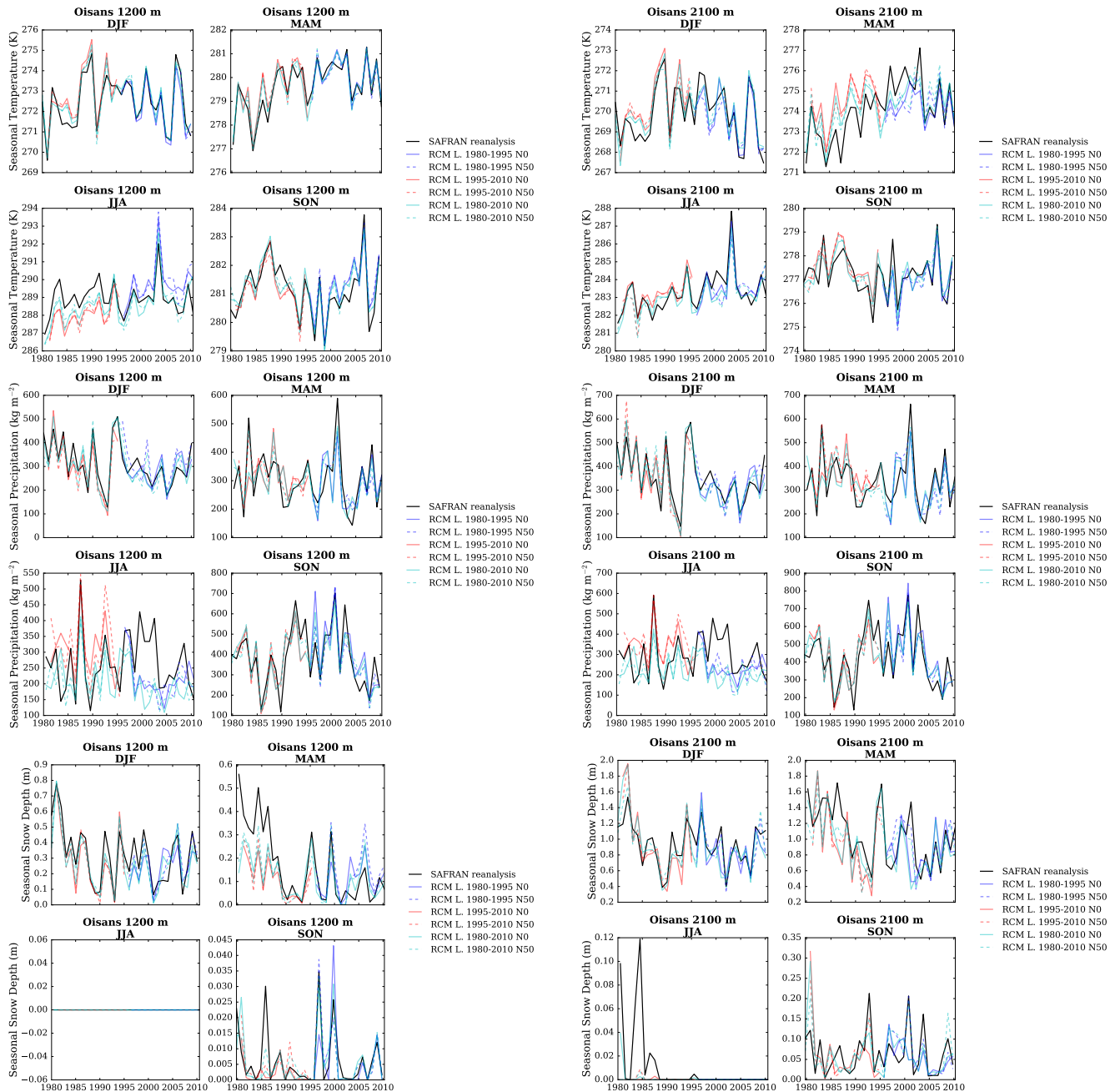


Figure S133: (top) Temperature, (middle) precipitation and (bottom) snow depth (using Crocus in this case) seasonal average time series from 1980 to 2010 in each adjusted RCM simulation and in the SAFRAN reanalysis, for the Oisans massif, and at (left) 1200 m a.s.l. and (right) 2100 m a.s.l..

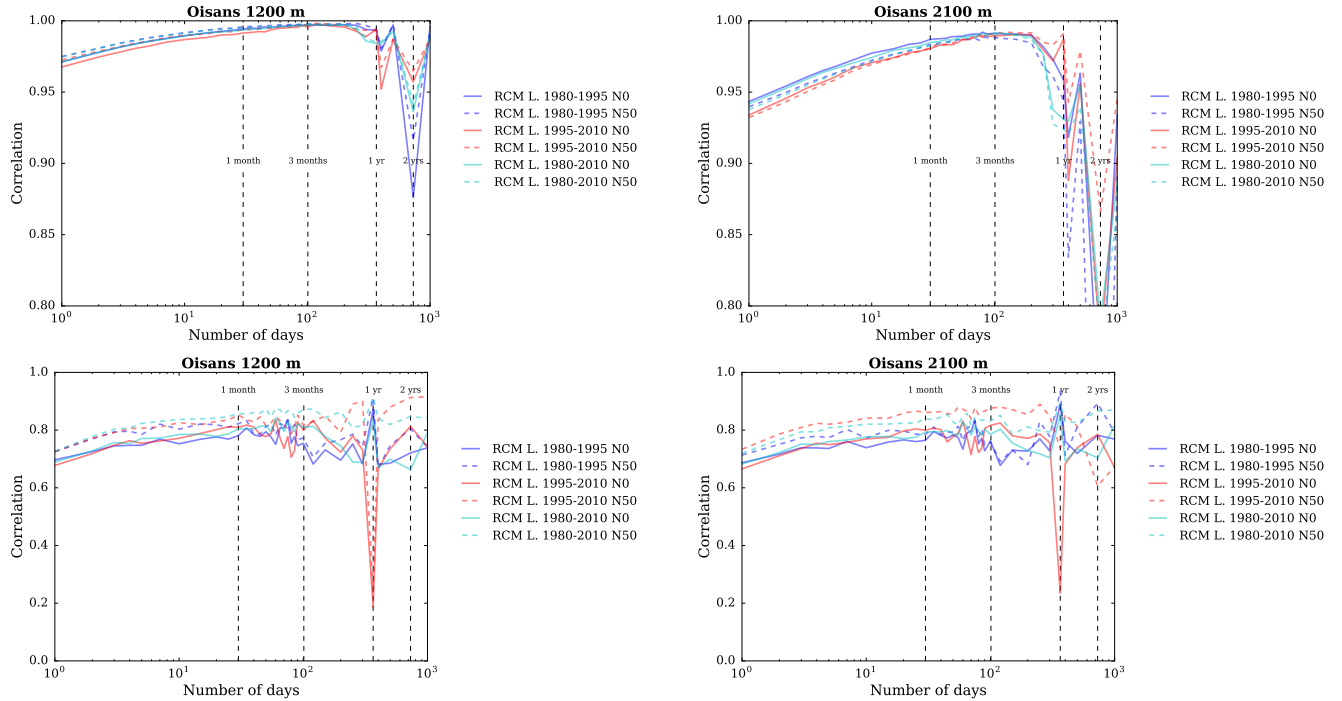


Figure S134: Correlation between the SAFRAN reanalysis and adjusted RCM (top) temperature and (bottom) precipitation as a function of the integration window over the evaluation period, for the Oisans massif, and at (left) 1200 m a.s.l. and (right) 2100 m a.s.l..

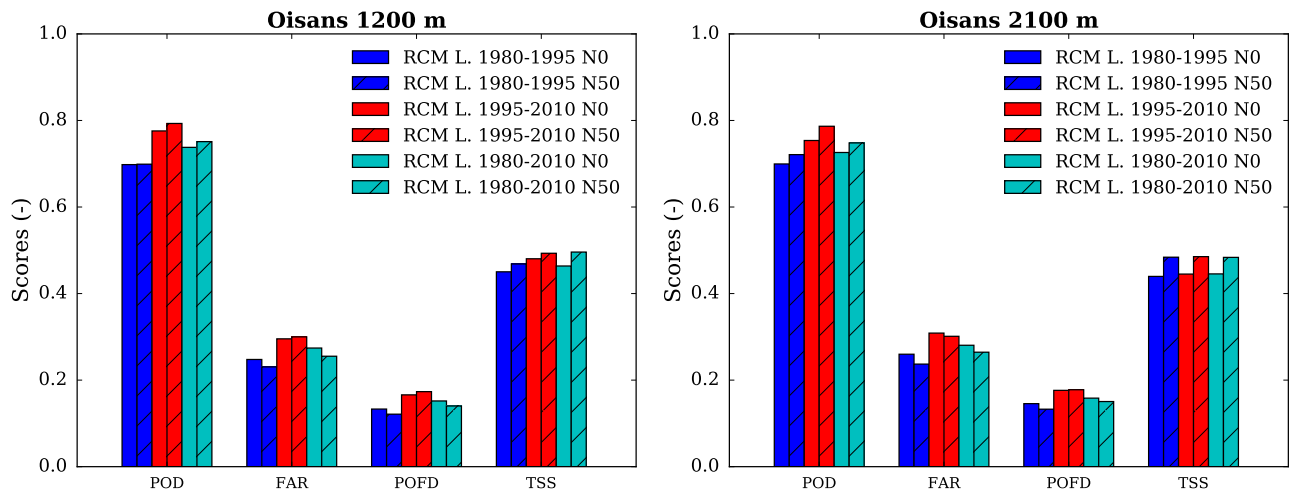


Figure S135: Scores for the detection of precipitation events in each adjusted RCM simulation compared to the SAFRAN reanalysis over the evaluation period, for the Oisans massif, at (left) 1200 m a.s.l. and (right) 2100 m a.s.l.. POD = probability of detection, FAR = false alarm rate, POFD = probability of false detection, TSS = true skill score.

Pelvoux

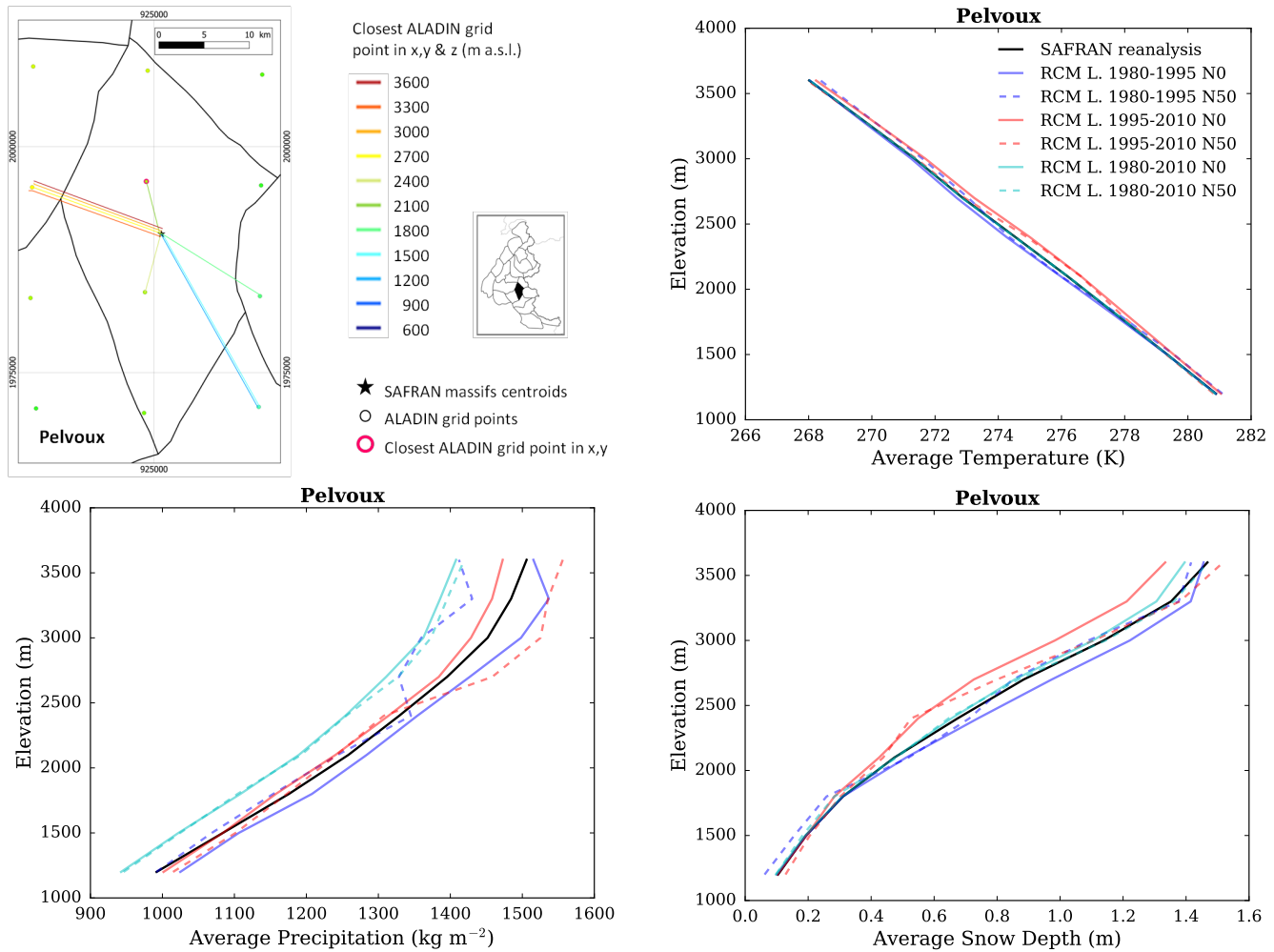


Figure S136: (top left) Location of the Pelvoux massif, with ALADIN RCM grid points chosen as the closest in x, y ($N = 0$, pink contour) and in x, y and z (using $N \neq 0$). Coloured lines link each SAFRAN massif centre point with the corresponding grid point in ALADIN for the different elevations considered (in m above sea level (a.s.l.)). (top right) Mean temperature, (bottom left) precipitation and (bottom right) snow depth (using Crocus in this case) for each elevation band for the Pelvoux massif, over the evaluation period in each adjusted RCM simulation (different learning periods and 2 neighbour selection methods) and in SAFRAN (1980-2010).

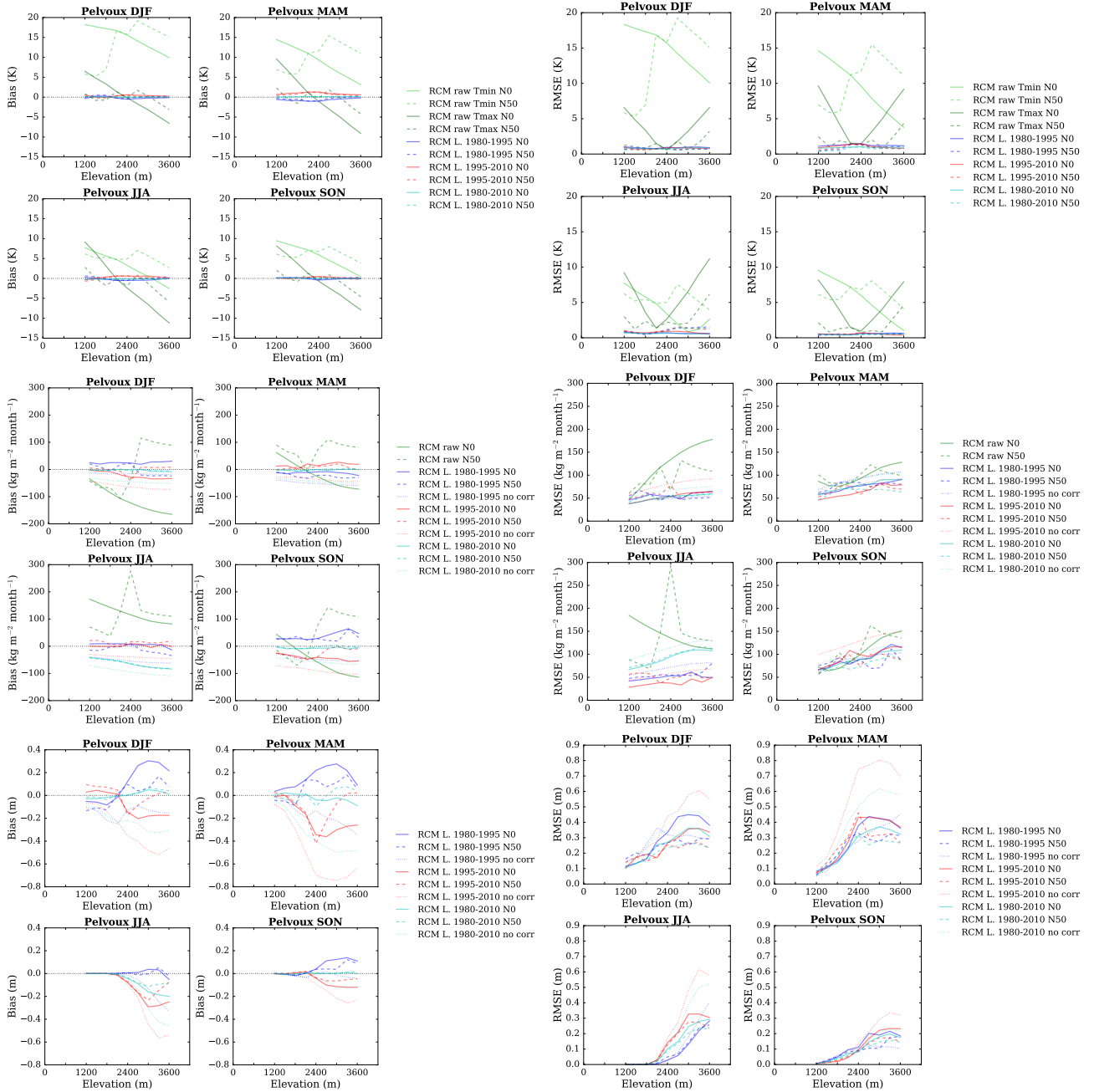


Figure S137: (top) Temperature, (middle) precipitation and (bottom) snow depth (using Crocus in this case) mean bias and root mean square error of each raw and adjusted RCM simulation compared to the SAFRAN reanalysis over the evaluation period for the Pelvoux massif as a function of elevation. Scores computed for the raw RCM simulations concern minimum and maximum daily temperatures.

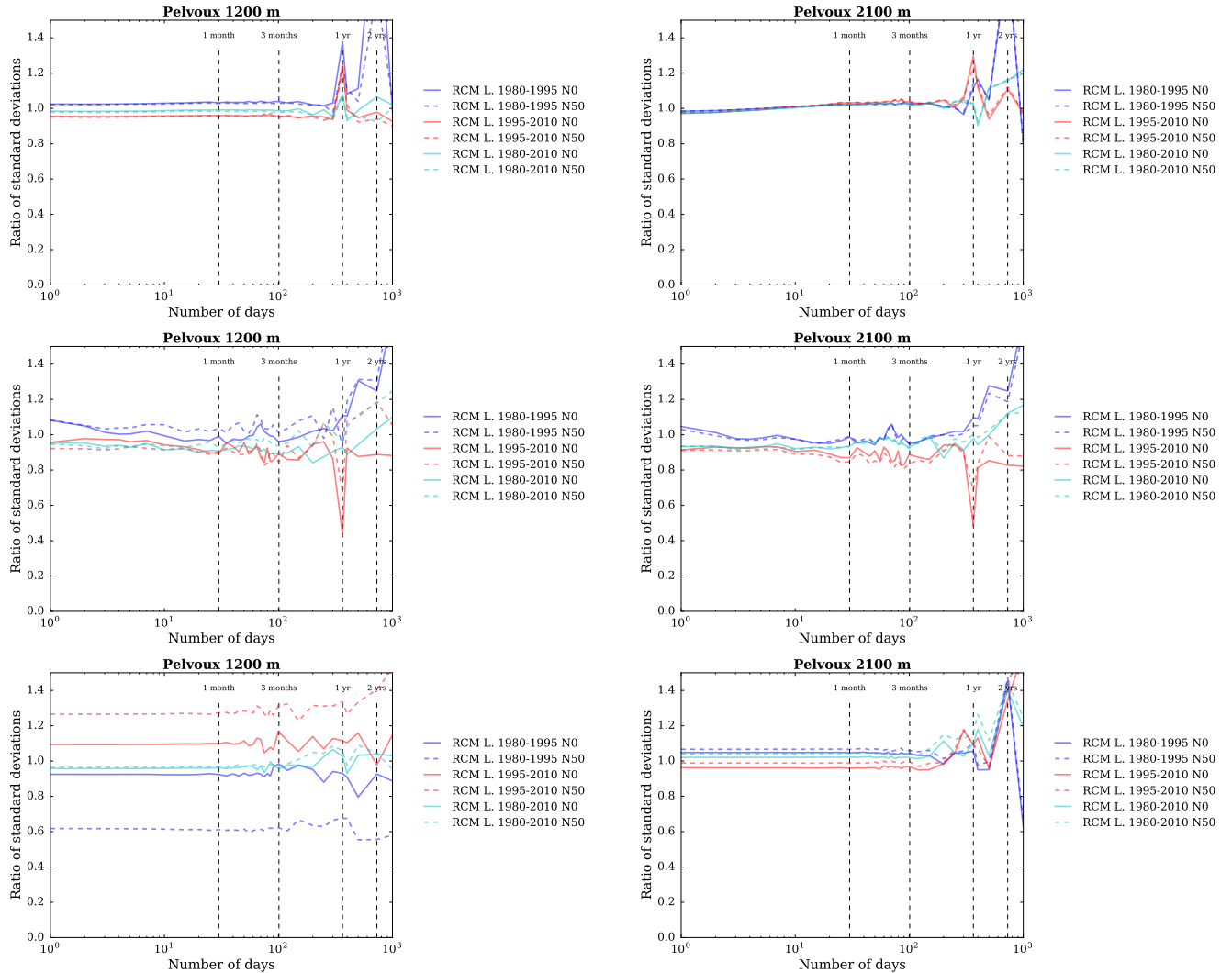


Figure S138: Ratios of standard deviations between the SAFRAN reanalysis and adjusted RCM (top) temperature, (middle) precipitation and (bottom) snow depth (using Crocus in this case) as a function of the integration window over the evaluation period, for the Pelvoux massif, at (left) 1200 m a.s.l. and (right) 2100 m a.s.l..

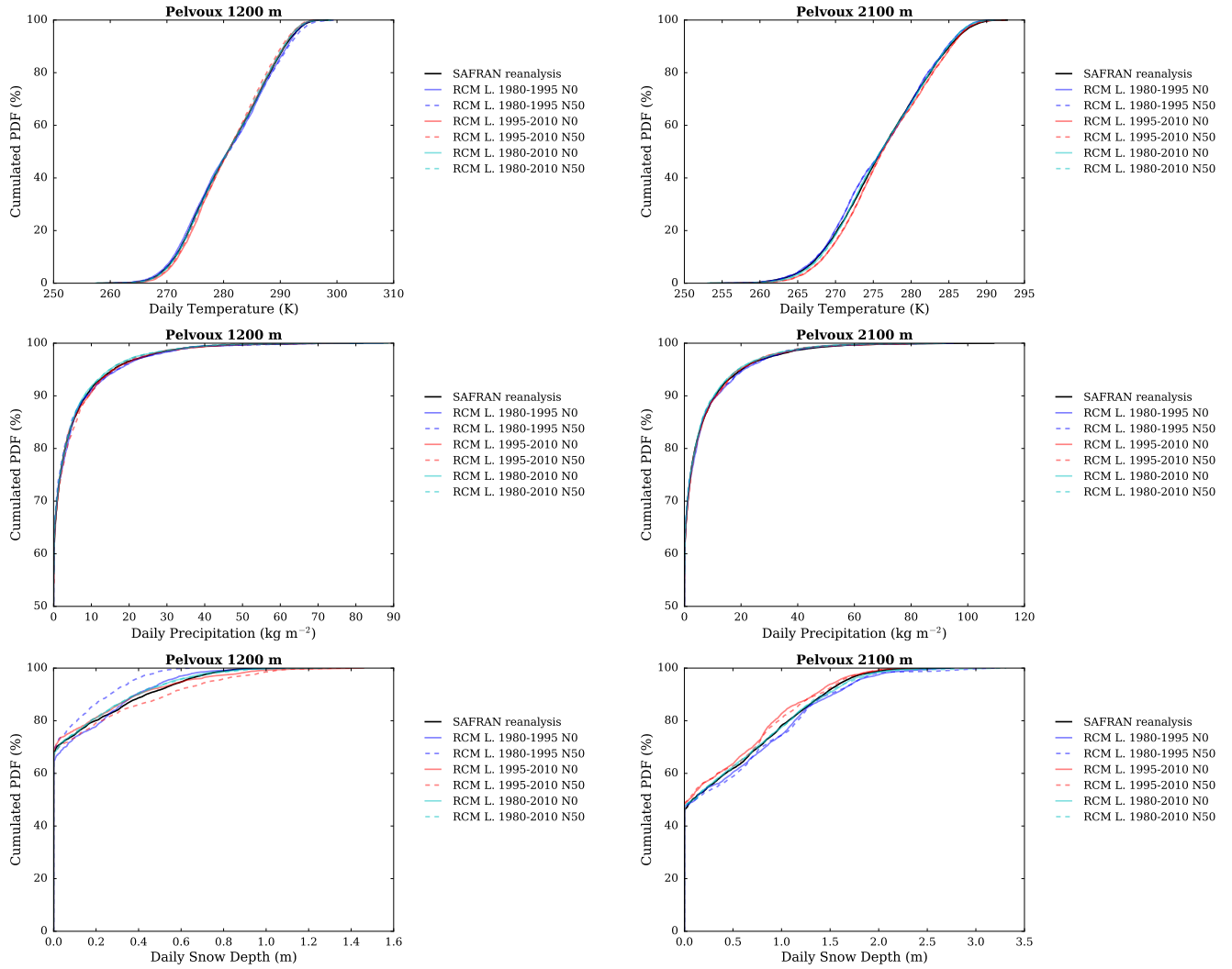


Figure S139: Cumulated probability density functions (PDFs) of daily (top) temperature, (middle) precipitation and (bottom) snow depth (using Crocus in this case) in each adjusted RCM simulation and in the SAFRAN reanalysis (1980-2010) over the evaluation period, for the Pelvoux massif, at (left) 1200 m a.s.l. and (right) 2100 m a.s.l..

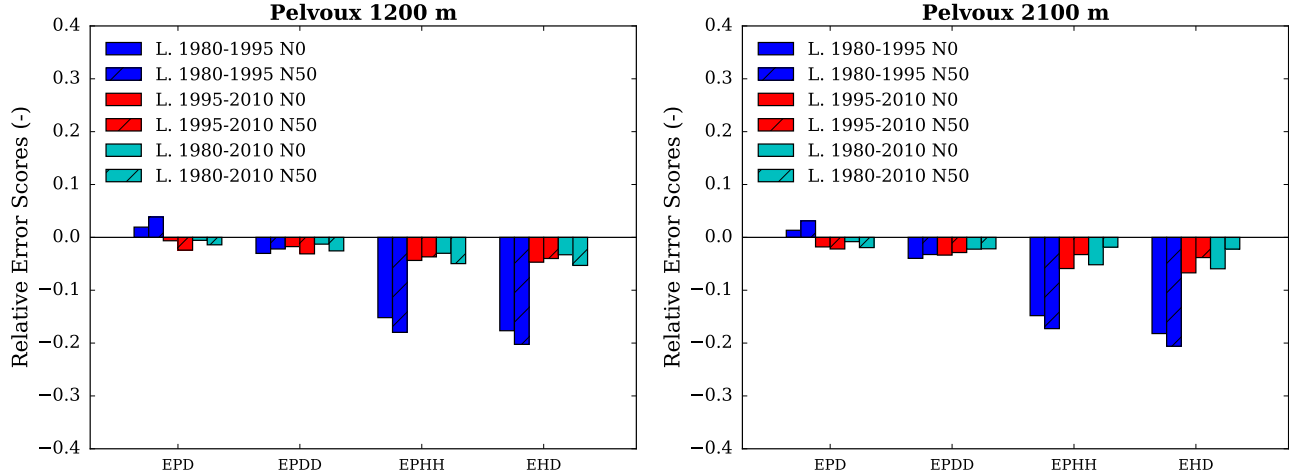


Figure S140: Scores for the duration and persistence of precipitation events in each adjusted RCM simulation compared to the SAFRAN reanalysis over the evaluation period, for the Pelvoux massif, at (left) 1200 m a.s.l. and (right) 2100 m a.s.l.. EPD = relative error on the probability of a dry day, EPDD = relative error on the probability of a dry day following a dry day, EPHH = relative error on the probability of a wet day following a wet day, EHD = relative error on the mean duration of wet periods.

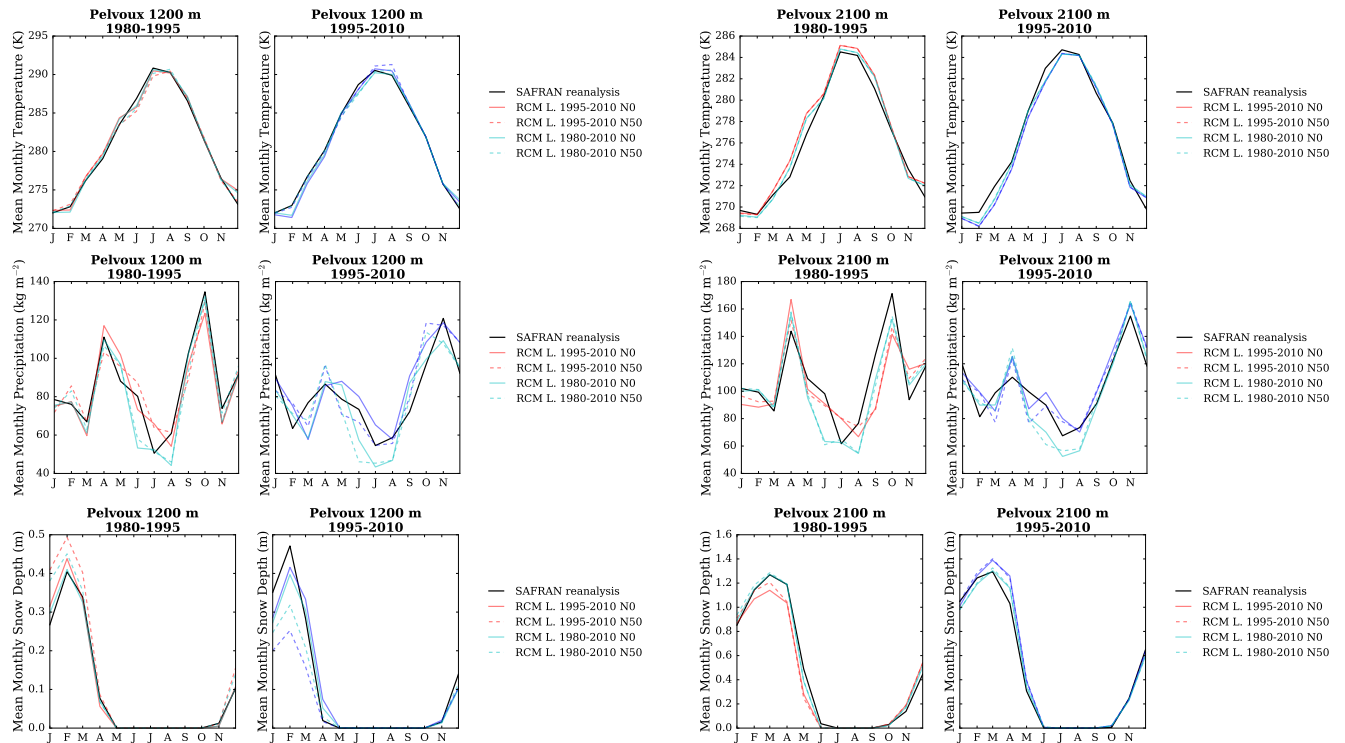


Figure S141: (top) Temperature, (middle) precipitation and (bottom) snow depth (using Crocus in this case) mean annual cycle in each adjusted RCM simulation and in the SAFRAN reanalysis over the period 1980-1995 and 1995-2010, for the Pelvoux massif, and at (left) 1200 m a.s.l. and (right) 2100 m a.s.l.. Letters on the x-axis correspond to the different months of the calendar (J = January, F = February, etc.).

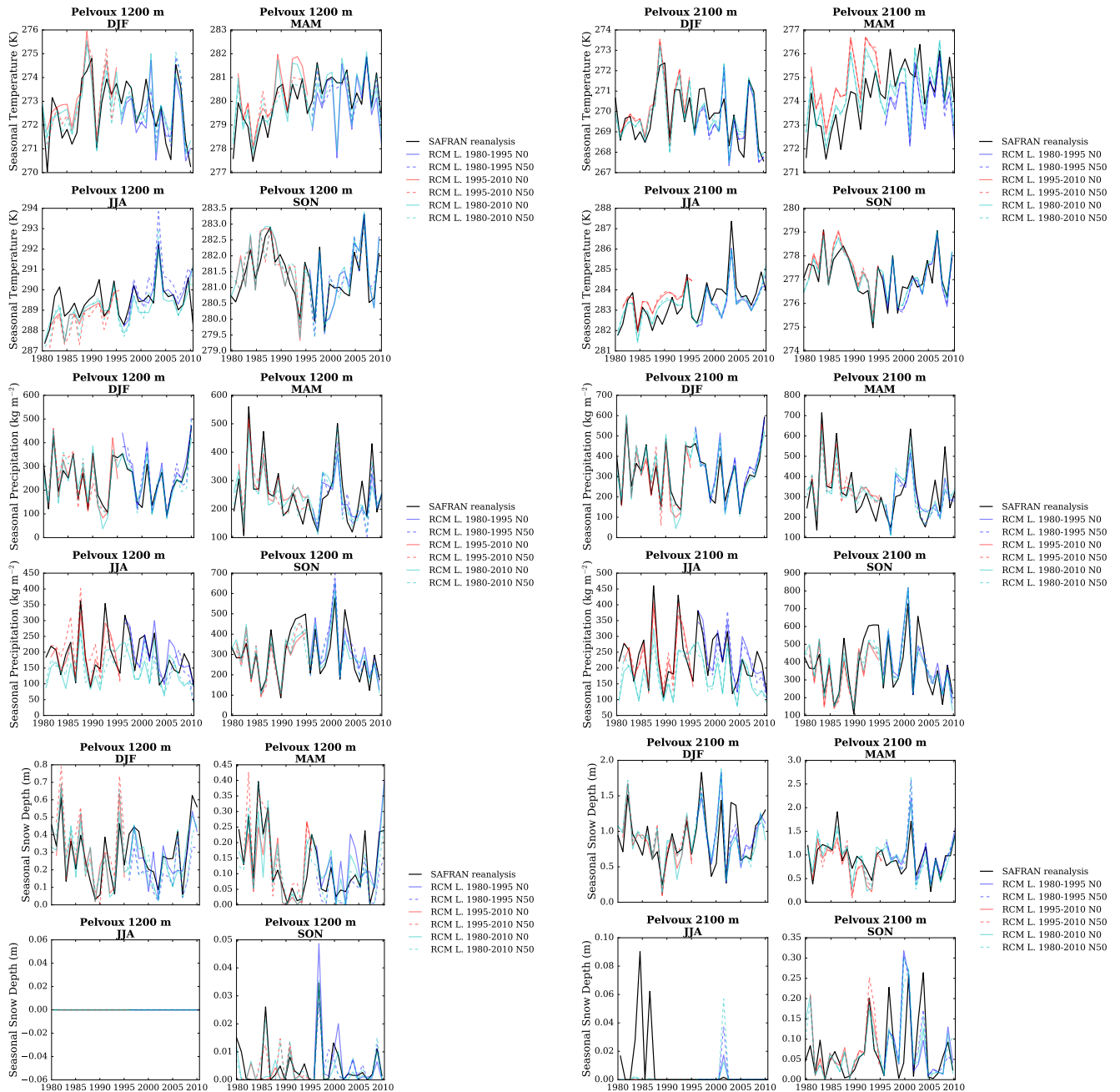


Figure S142: (top) Temperature, (middle) precipitation and (bottom) snow depth (using Crocus in this case) seasonal average time series from 1980 to 2010 in each adjusted RCM simulation and in the SAFRAN reanalysis, for the Pelvoux massif, and at (left) 1200 m a.s.l. and (right) 2100 m a.s.l..

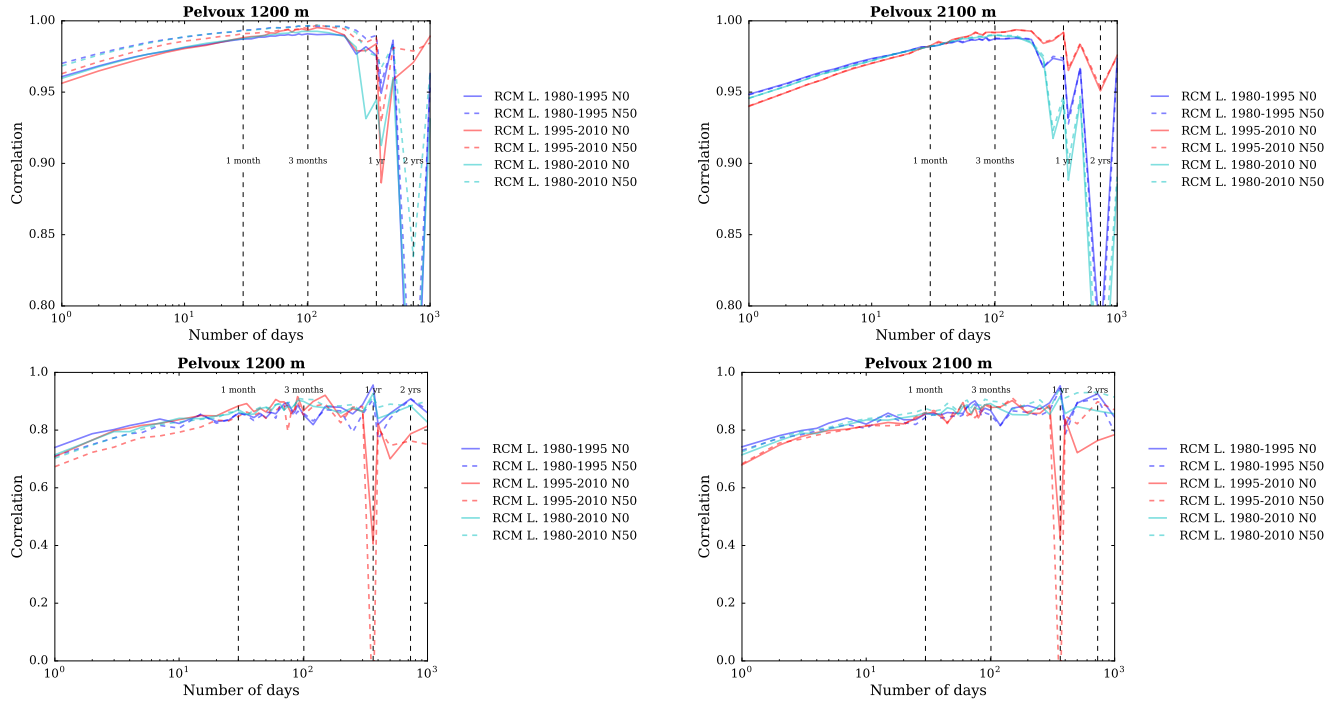


Figure S143: Correlation between the SAFRAN reanalysis and adjusted RCM (top) temperature and (bottom) precipitation as a function of the integration window over the evaluation period, for the Pelvoux massif, and at (left) 1200 m a.s.l. and (right) 2100 m a.s.l..

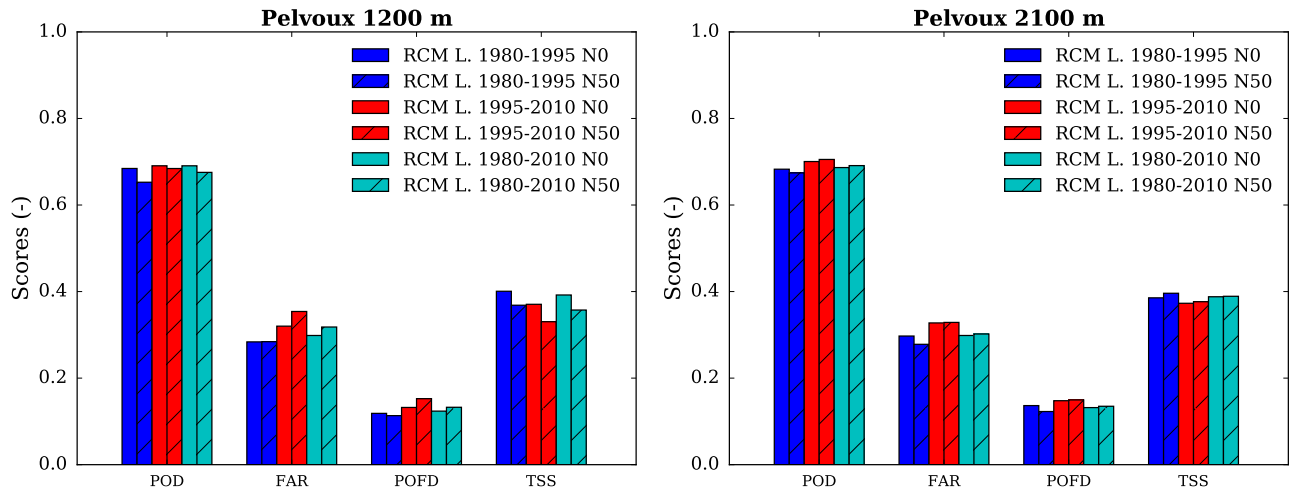


Figure S144: Scores for the detection of precipitation events in each adjusted RCM simulation compared to the SAFRAN reanalysis over the evaluation period, for the Pelvoux massif, at (left) 1200 m a.s.l. and (right) 2100 m a.s.l.. POD = probability of detection, FAR = false alarm rate, POFD = probability of false detection, TSS = true skill score.

Queyras

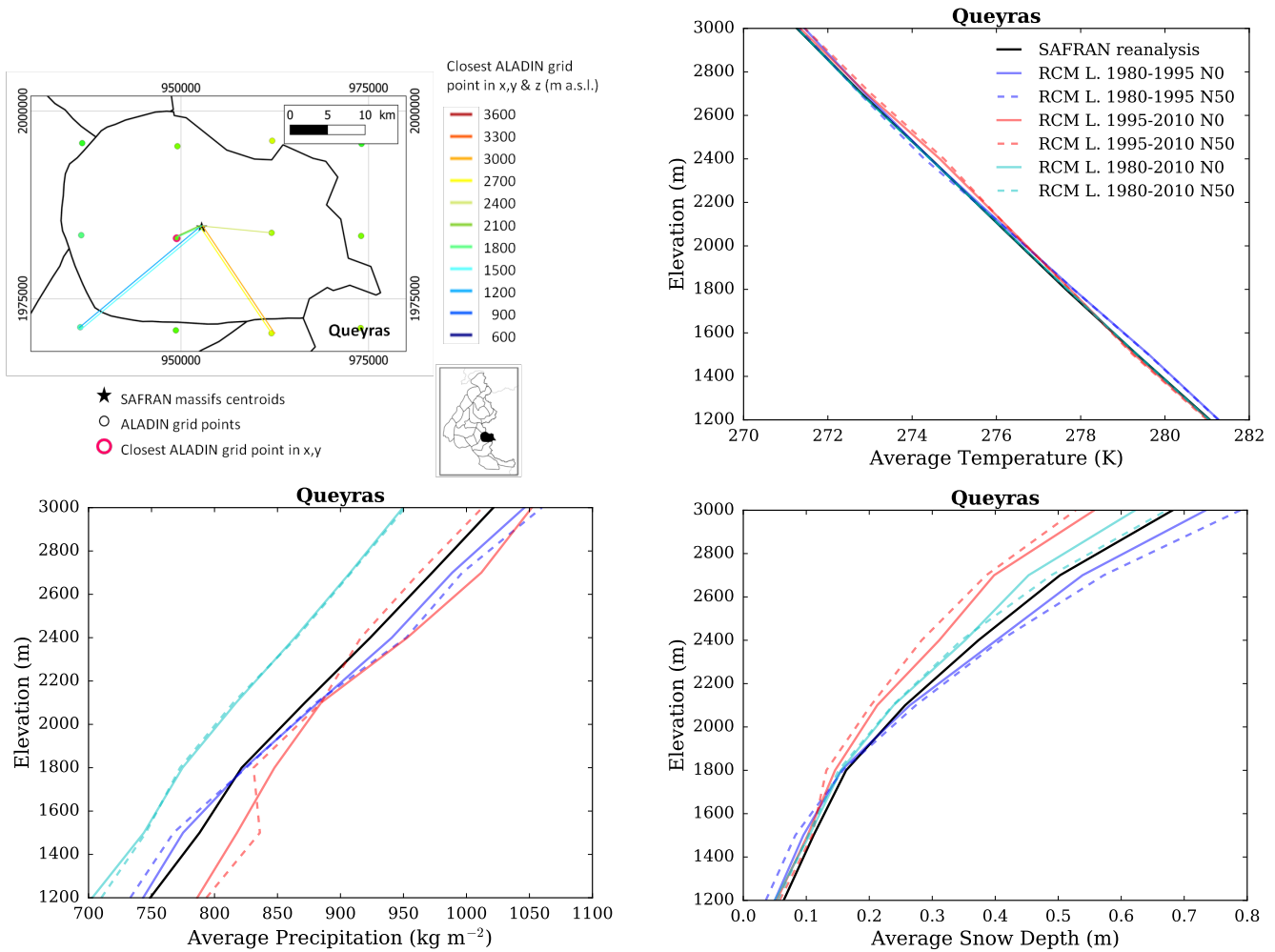


Figure S145: (top left) Location of the Queyras massif, with ALADIN RCM grid points chosen as the closest in x , y ($N = 0$, pink contour) and in x , y and z (using $N \neq 0$). Coloured lines link each SAFRAN massif centre point with the corresponding grid point in ALADIN for the different elevations considered (in m above sea level (a.s.l.)). (top right) Mean temperature, (bottom left) precipitation and (bottom right) snow depth (using Crocus in this case) for each elevation band for the Queyras massif, over the evaluation period in each adjusted RCM simulation (different learning periods and 2 neighbour selection methods) and in SAFRAN (1980-2010).

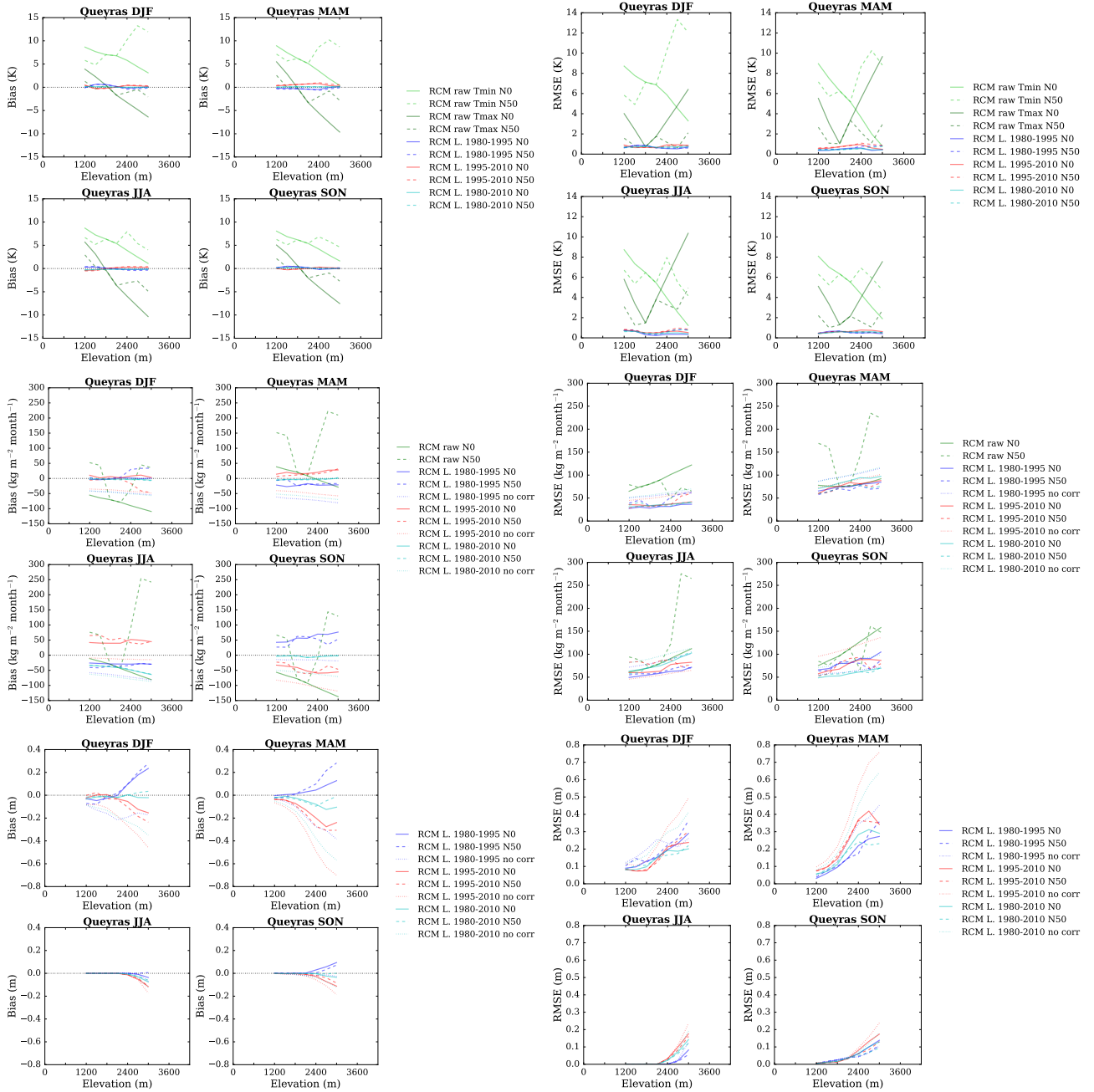


Figure S146: (top) Temperature, (middle) precipitation and (bottom) snow depth (using Crocus in this case) mean bias and root mean square error of each raw and adjusted RCM simulation compared to the SAFRAN reanalysis over the evaluation period for the Queyras massif as a function of elevation. Scores computed for the raw RCM simulations concern minimum and maximum daily temperatures.

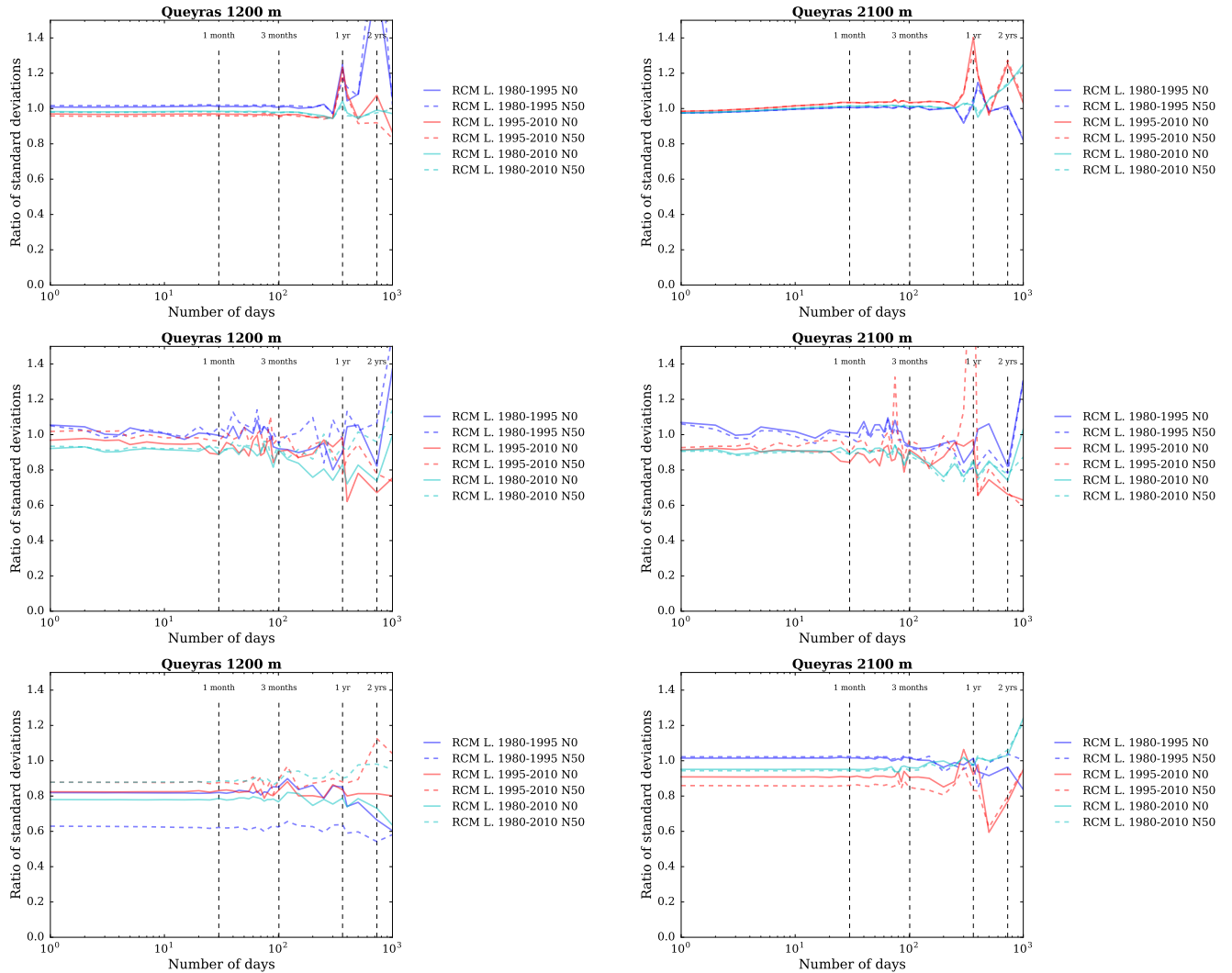


Figure S147: Ratios of standard deviations between the SAFRAN ranalysis and adjusted RCM (top) temperature, (middle) precipitation and (bottom) snow depth (using Crocus in this case) as a function of the integration window over the evaluation period, for the Queyras massif, at (left) 1200 m a.s.l. and (right) 2100 m a.s.l..

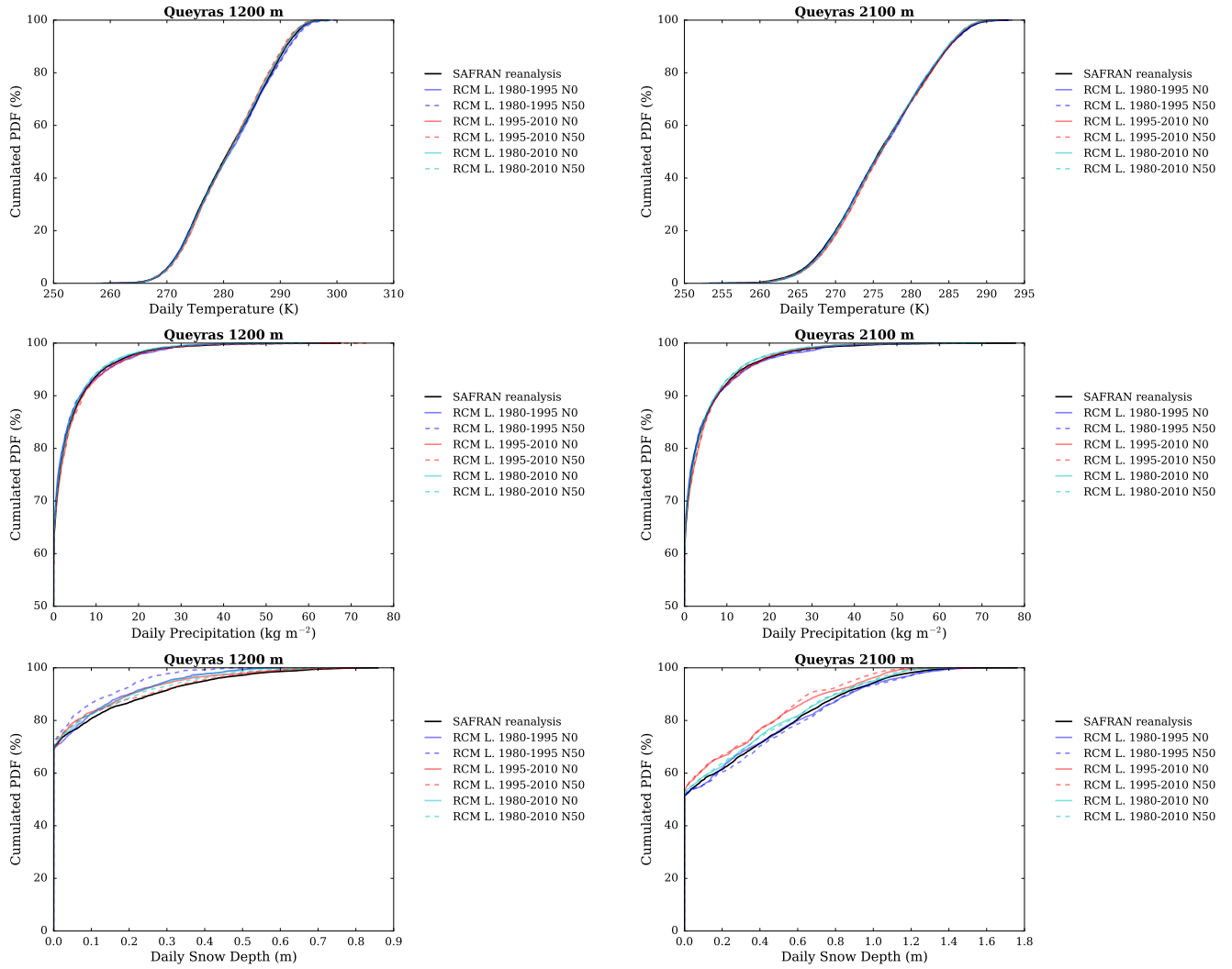


Figure S148: Cumulated probability density functions (PDFs) of daily (top) temperature, (middle) precipitation and (bottom) snow depth (using Crocus in this case) in each adjusted RCM simulation and in the SAFRAN reanalysis (1980-2010) over the evaluation period, for the Queyras massif, at (left) 1200 m a.s.l. and (right) 2100 m a.s.l..

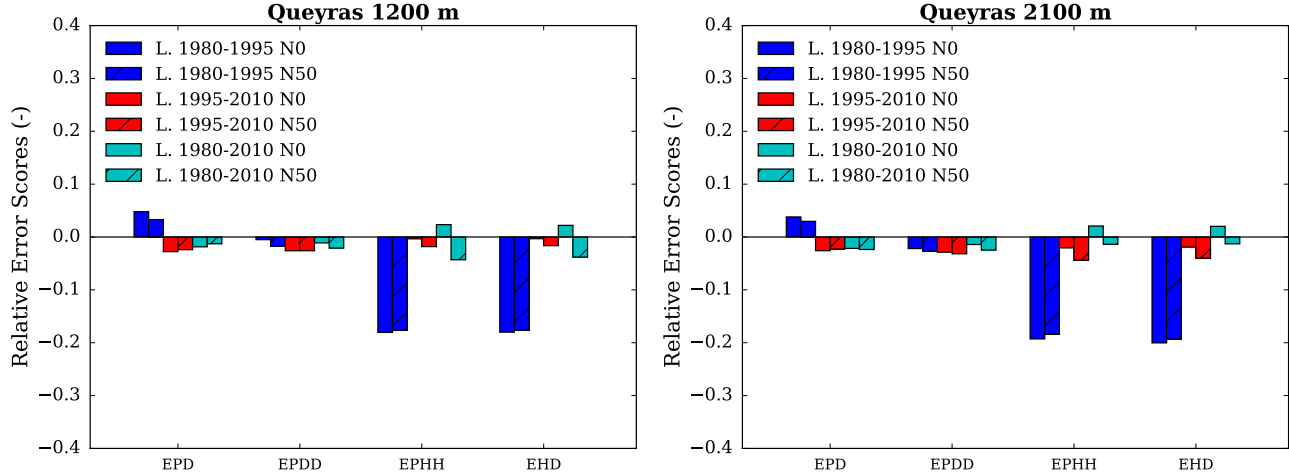


Figure S149: Scores for the duration and persistence of precipitation events in each adjusted RCM simulation compared to the SAFRAN reanalysis over the evaluation period, for the Queyras massif, at (left) 1200 m a.s.l. and (right) 2100 m a.s.l.. EPD = relative error on the probability of a dry day, EPDD = relative error on the probability of a dry day following a dry day, EPHH = relative error on the probability of a wet day following a wet day, EHD = relative error on the mean duration of wet periods.

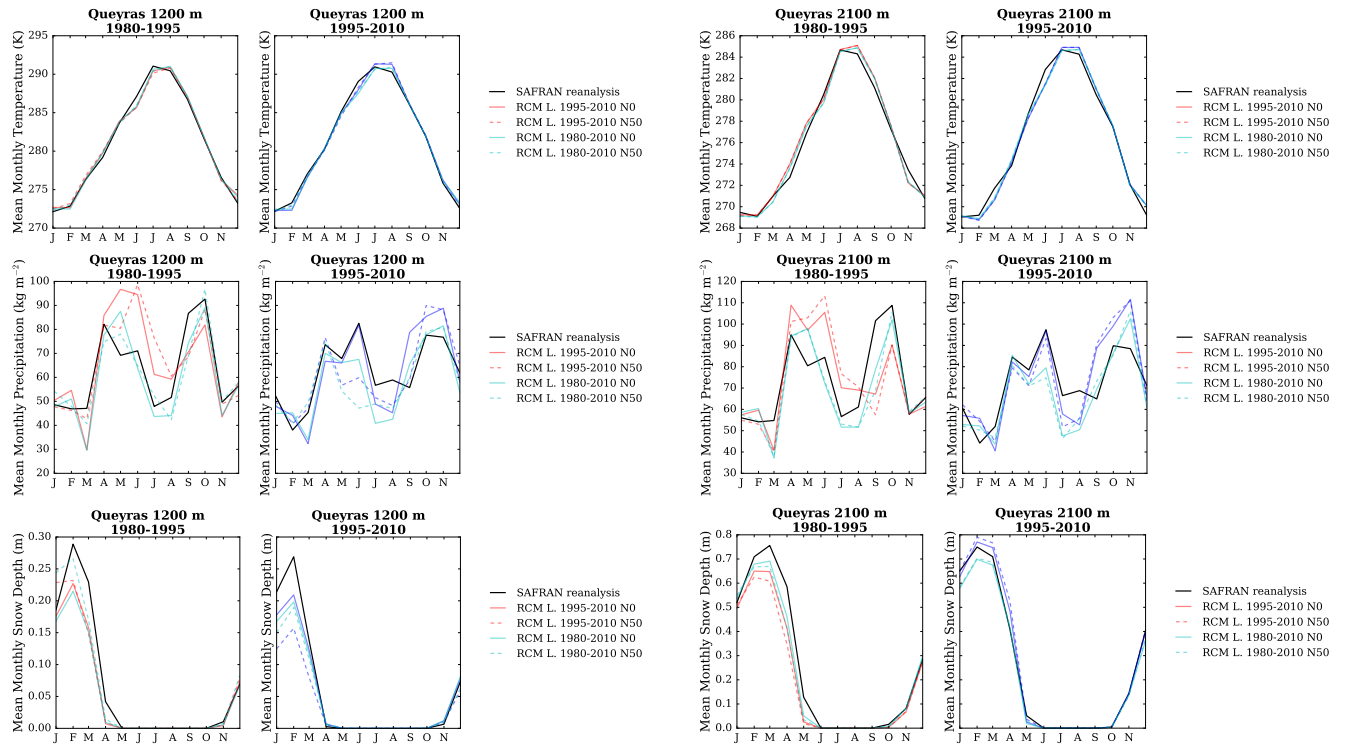


Figure S150: (top) Temperature, (middle) precipitation and (bottom) snow depth (using Crocus in this case) mean annual cycle in each adjusted RCM simulation and in the SAFRAN reanalysis over the period 1980-1995 and 1995-2010, for the Queyras massif, and at (left) 1200 m a.s.l. and (right) 2100 m a.s.l.. Letters on the x-axis correspond to the different months of the calendar (J = January, F = February, etc.).

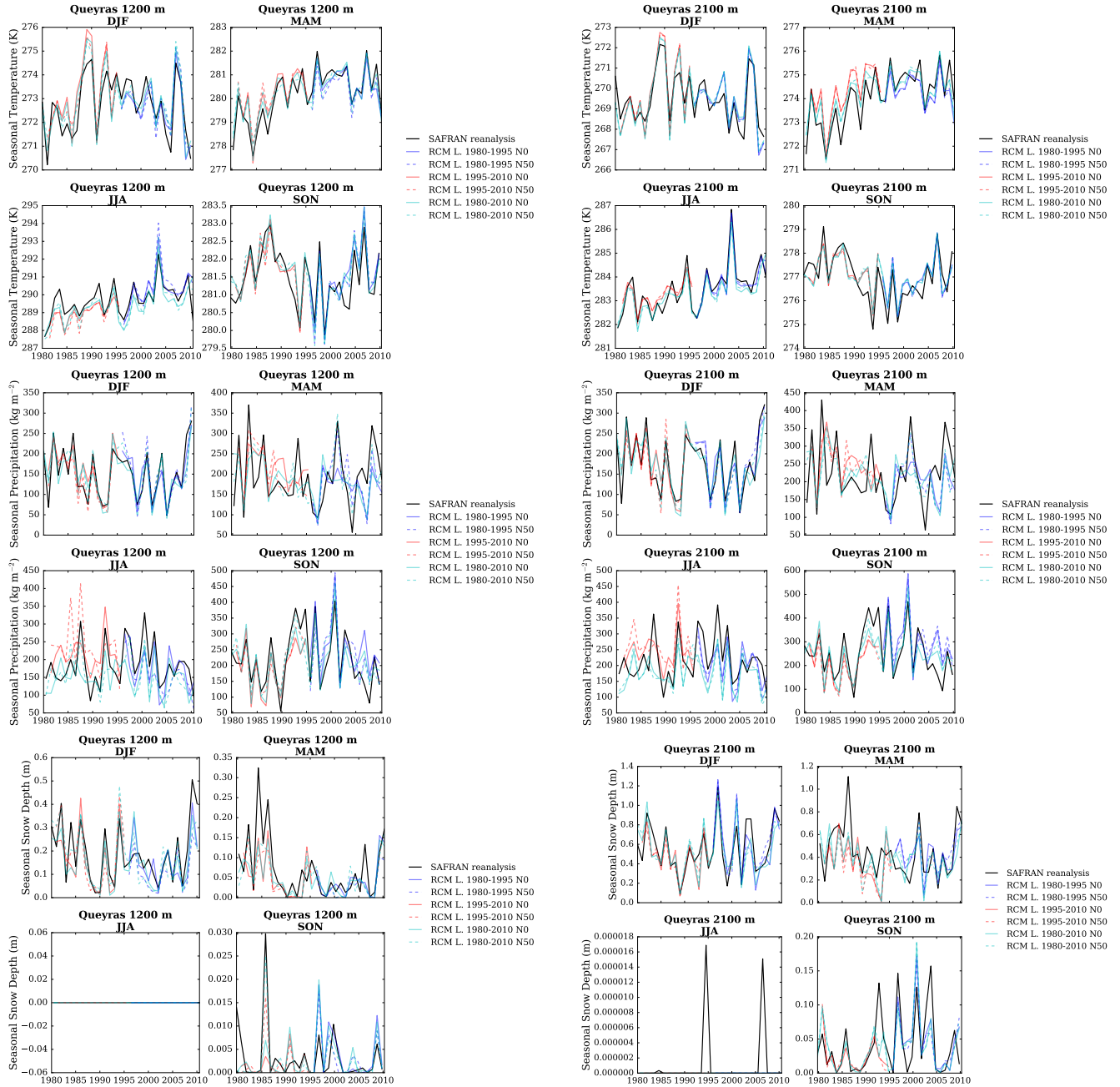


Figure S151: (top) Temperature, (middle) precipitation and (bottom) snow depth (using Crocus in this case) seasonal average time series from 1980 to 2010 in each adjusted RCM simulation and in the SAFRAN reanalysis, for the Queyras massif, and at (left) 1200 m a.s.l. and (right) 2100 m a.s.l..

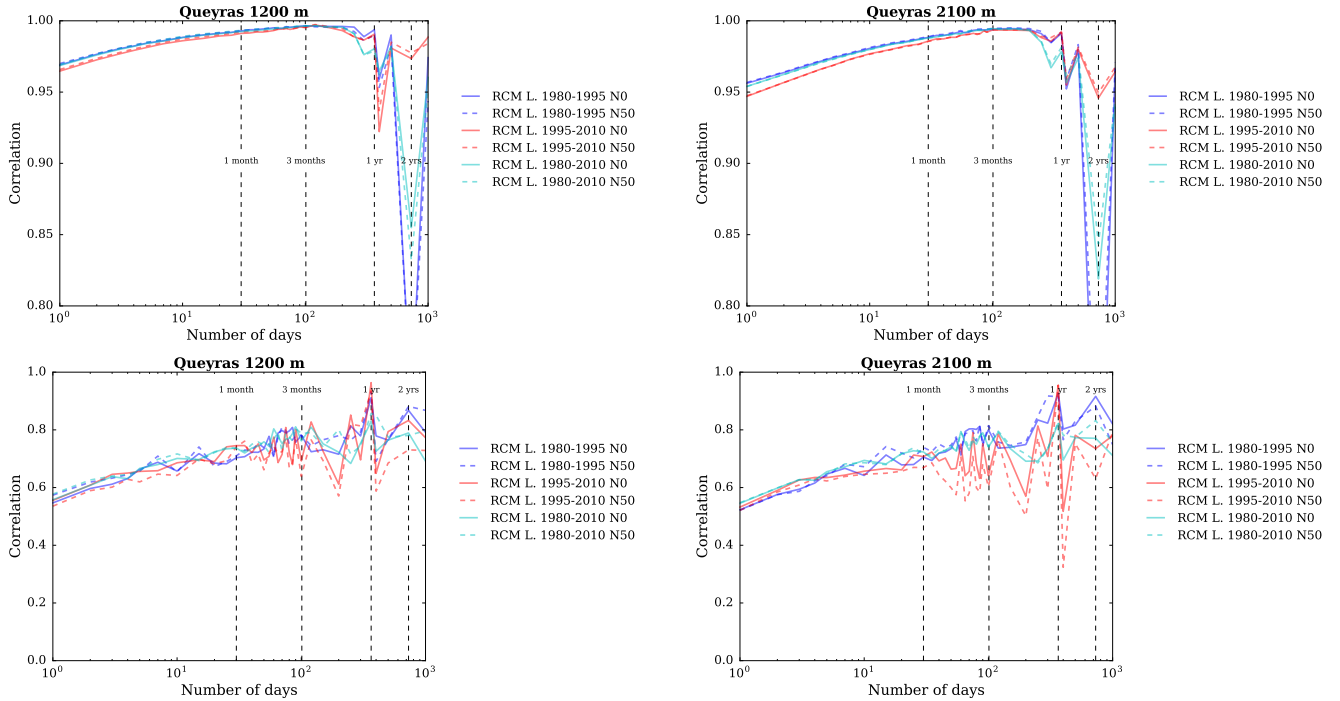


Figure S152: Correlation between the SAFRAN reanalysis and adjusted RCM (top) temperature and (bottom) precipitation as a function of the integration window over the evaluation period, for the Queyras massif, and at (left) 1200 m a.s.l. and (right) 2100 m a.s.l..

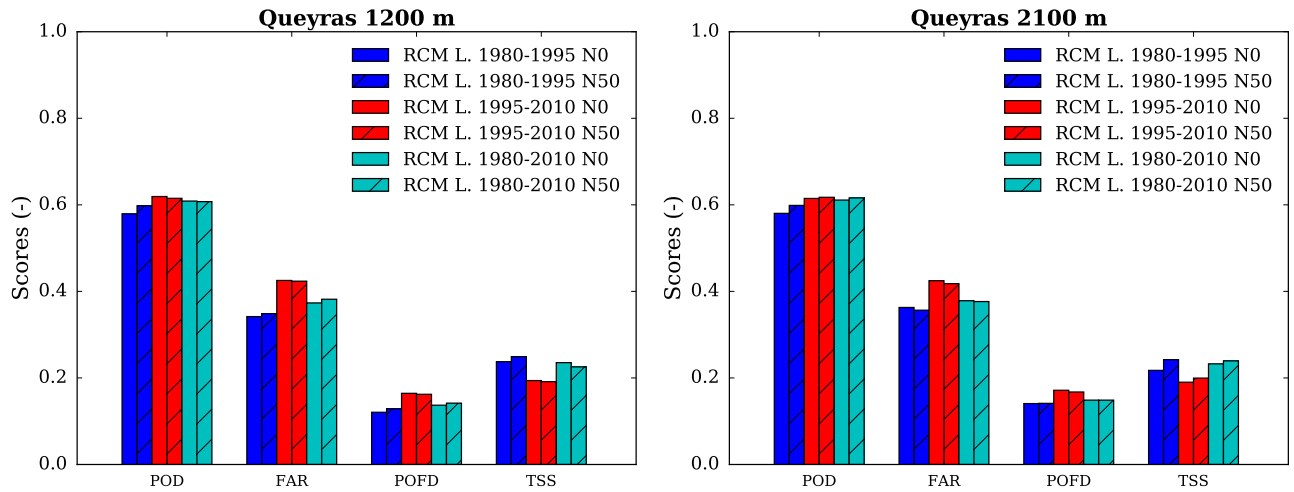


Figure S153: Scores for the detection of precipitation events in each adjusted RCM simulation compared to the SAFRAN reanalysis over the evaluation period, for the Queyras massif, at (left) 1200 m a.s.l. and (right) 2100 m a.s.l.. POD = probability of detection, FAR = false alarm rate, POFD = probability of false detection, TSS = true skill score.

Devoluy

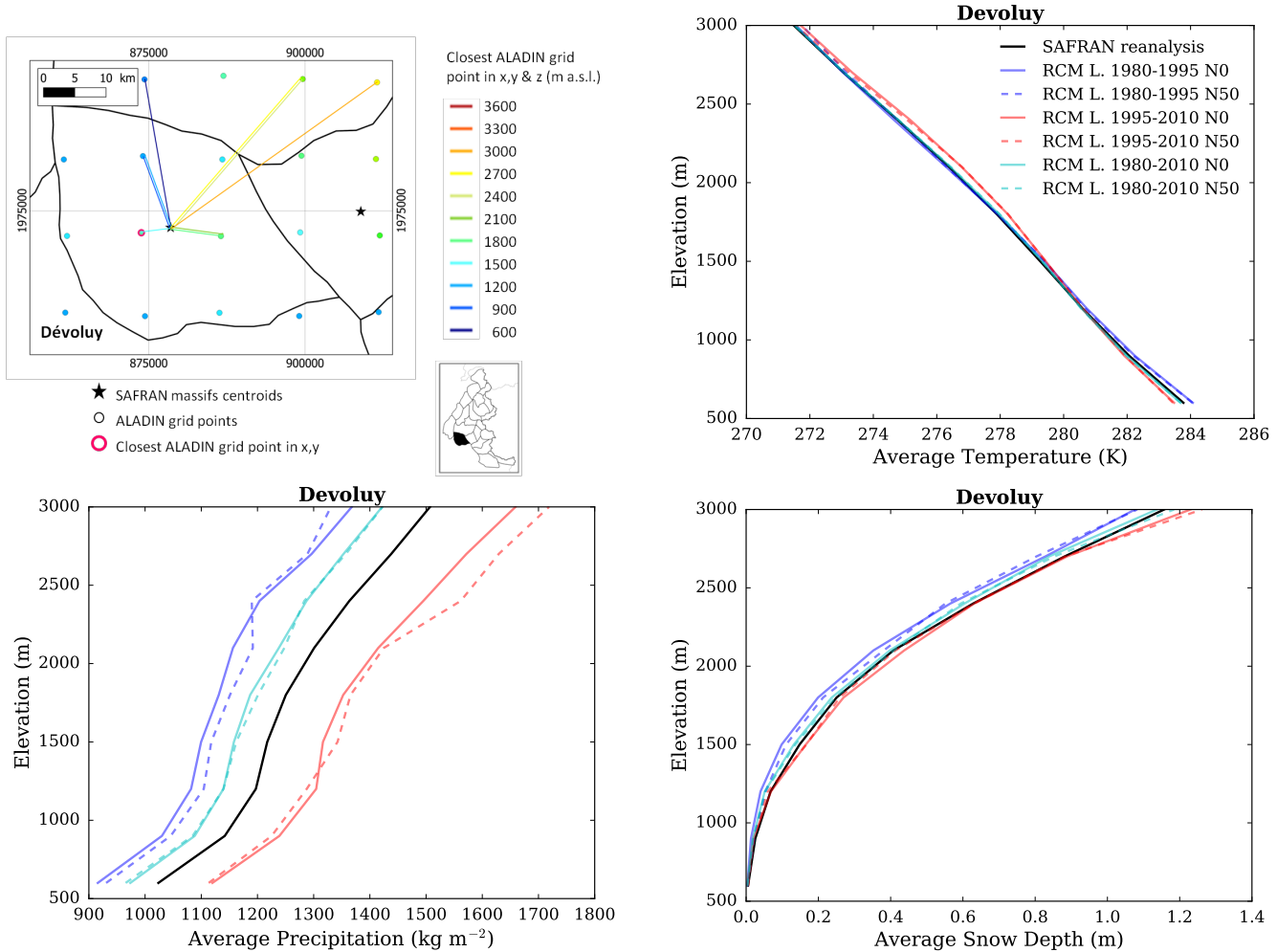


Figure S154: (top left) Location of the Devoluy massif, with ALADIN RCM grid points chosen as the closest in x, y ($N = 0$, pink contour) and in x, y and z (using $N \neq 0$). Coloured lines link each SAFRAN massif centre point with the corresponding grid point in ALADIN for the different elevations considered (in m above sea level (a.s.l.)). (top right) Mean temperature, (bottom left) precipitation and (bottom right) snow depth (using Crocus in this case) for each elevation band for the Devoluy massif, over the evaluation period in each adjusted RCM simulation (different learning periods and 2 neighbour selection methods) and in SAFRAN (1980-2010).

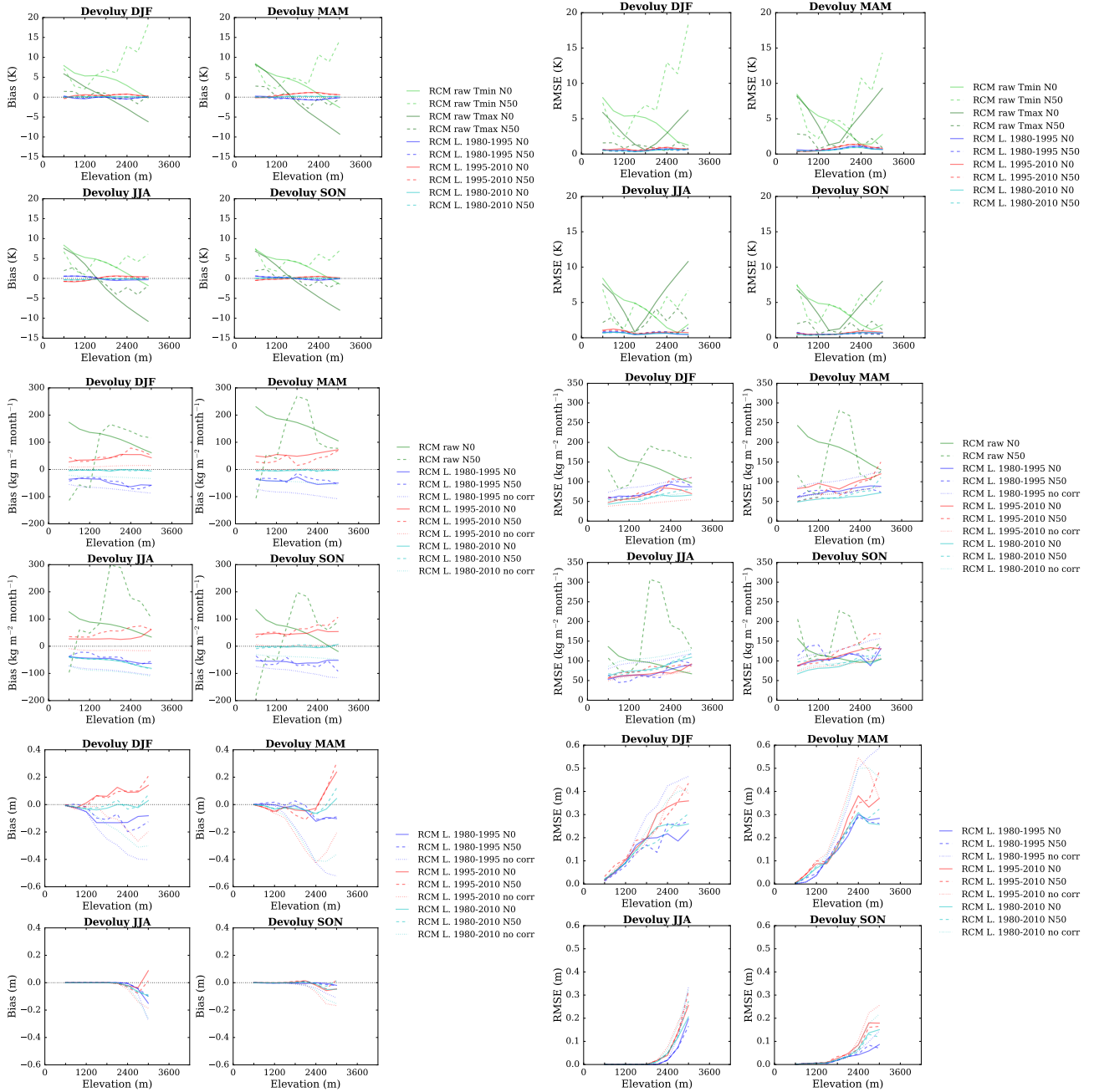


Figure S155: (top) Temperature, (middle) precipitation and (bottom) snow depth (using Crocus in this case) mean bias and root mean square error of each raw and adjusted RCM simulation compared to the SAFRAN reanalysis over the evaluation period for the Devoluy massif as a function of elevation. Scores computed for the raw RCM simulations concern minimum and maximum daily temperatures.

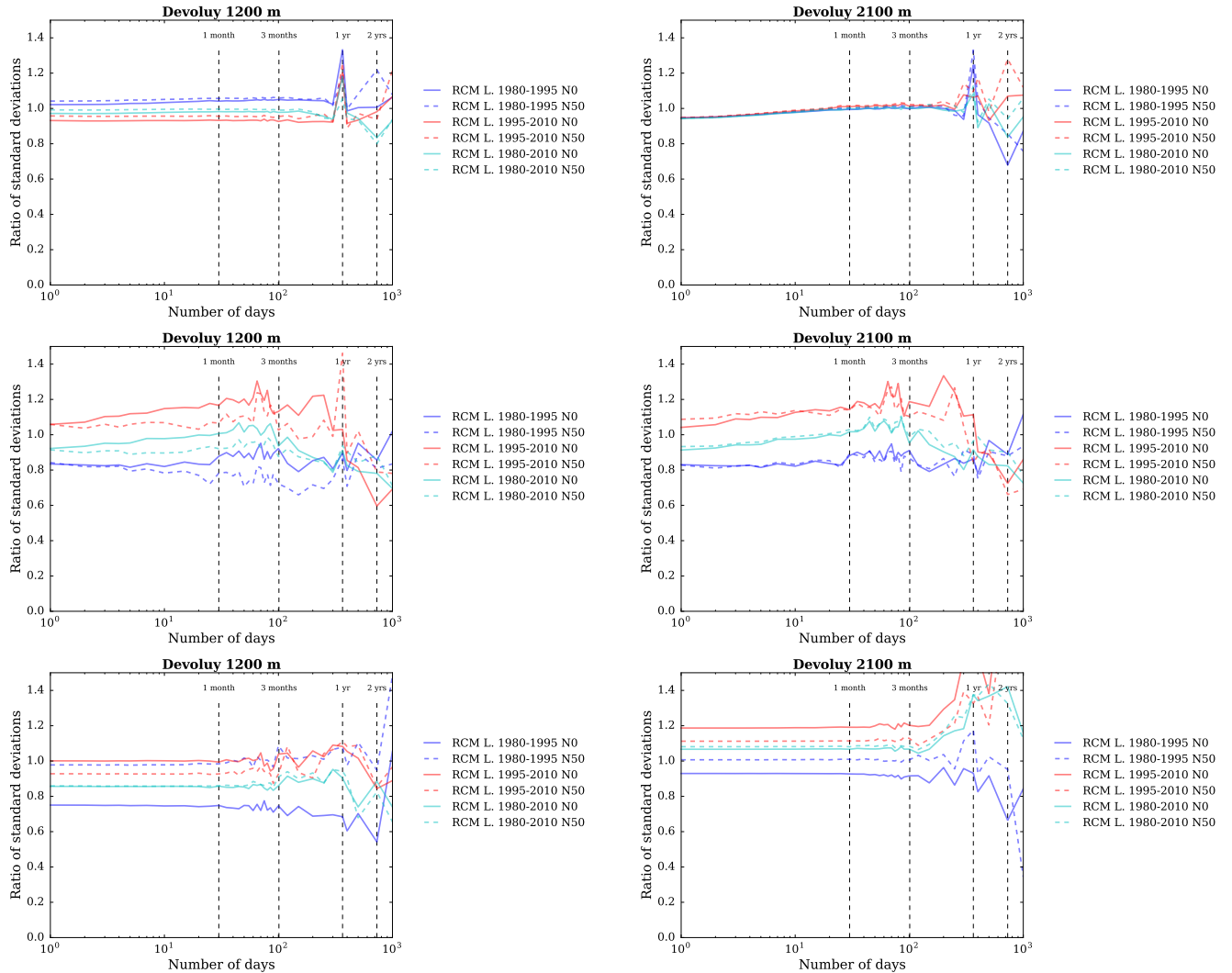


Figure S156: Ratios of standard deviations between the SAFRAN reanalysis and adjusted RCM (top) temperature, (middle) precipitation and (bottom) snow depth (using Crocus in this case) as a function of the integration window over the evaluation period, for the Devoluy massif, at (left) 1200 m a.s.l. and (right) 2100 m a.s.l..

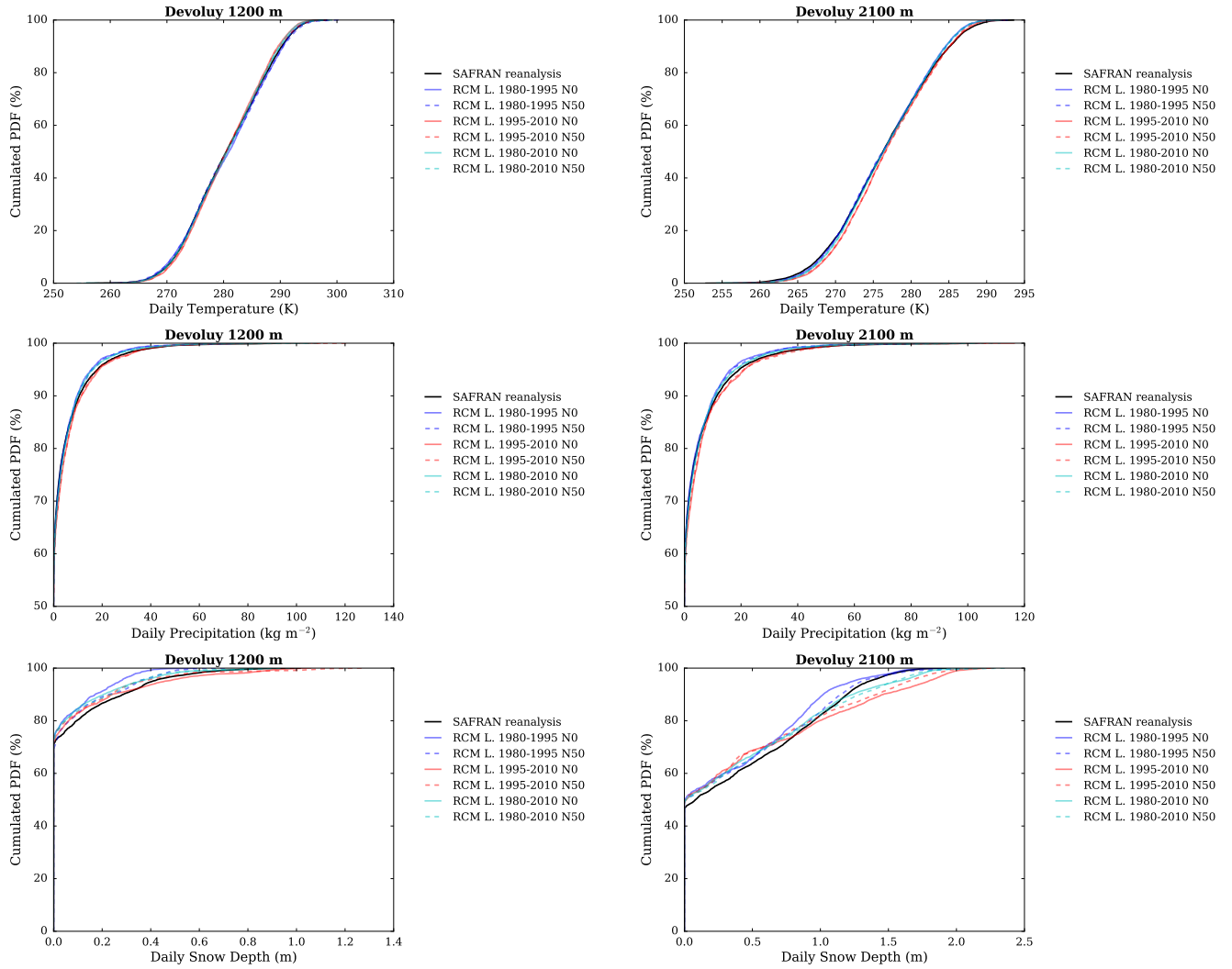


Figure S157: Cumulated probability density functions (PDFs) of daily (top) temperature, (middle) precipitation and (bottom) snow depth (using Crocus in this case) in each adjusted RCM simulation and in the SAFRAN reanalysis (1980-2010) over the evaluation period, for the Devoluy massif, at (left) 1200 m a.s.l. and (right) 2100 m a.s.l..

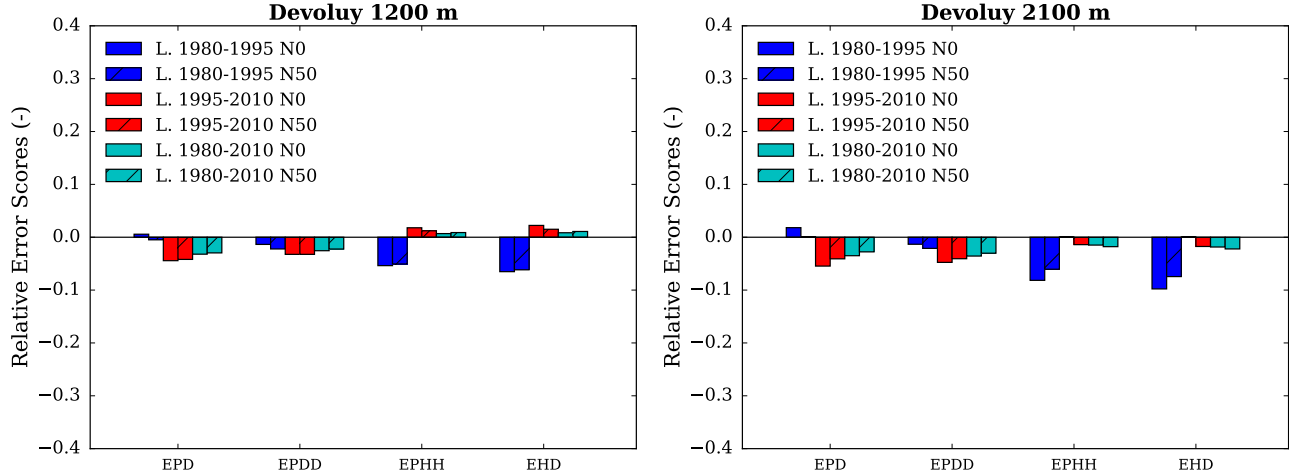


Figure S158: Scores for the duration and persistence of precipitation events in each adjusted RCM simulation compared to the SAFRAN reanalysis over the evaluation period, for the Devoluy massif, at (left) 1200 m a.s.l. and (right) 2100 m a.s.l.. EPD = relative error on the probability of a dry day, EPDD = relative error on the probability of a dry day following a dry day, EPHH = relative error on the probability of a wet day following a wet day, EHD = relative error on the mean duration of wet periods.

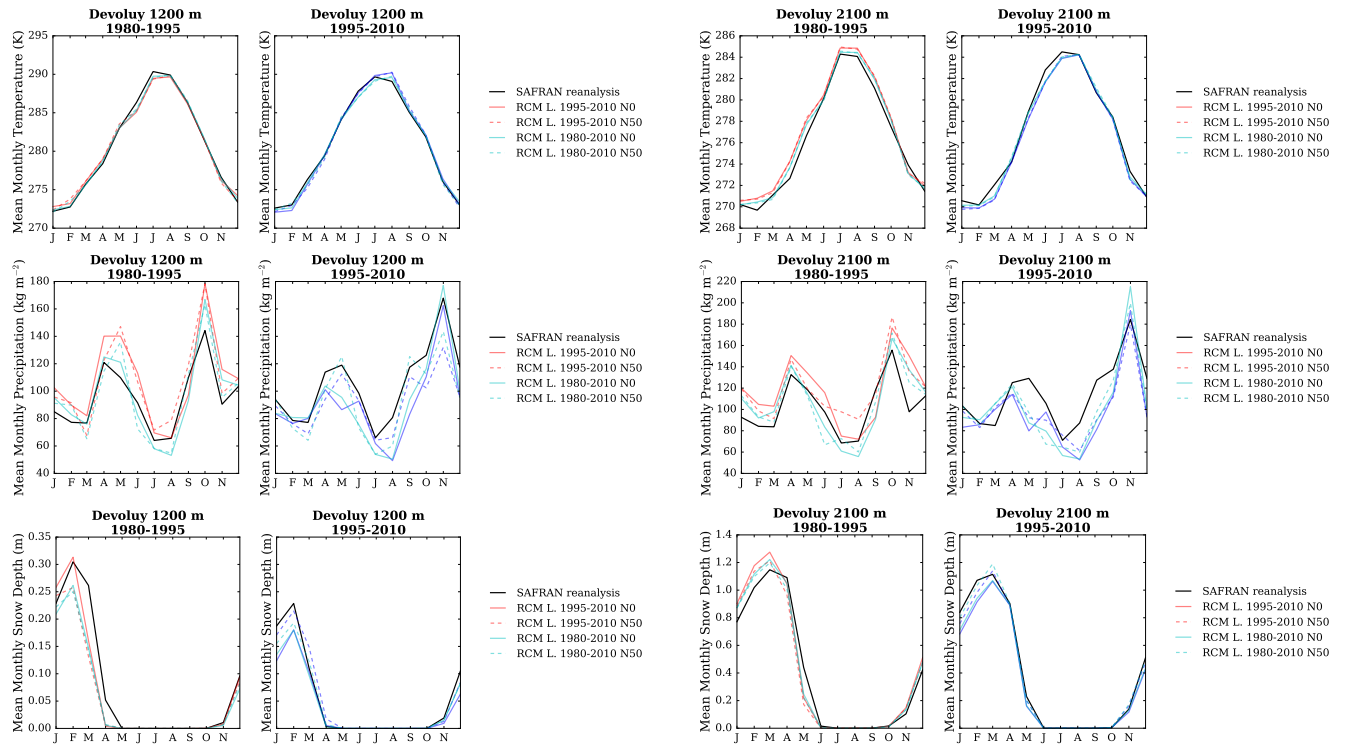


Figure S159: (top) Temperature, (middle) precipitation and (bottom) snow depth (using Crocus in this case) mean annual cycle in each adjusted RCM simulation and in the SAFRAN reanalysis over the period 1980-1995 and 1995-2010, for the Devoluy massif, and at (left) 1200 m a.s.l. and (right) 2100 m a.s.l.. Letters on the x-axis correspond to the different months of the calendar (J = January, F = February, etc.).

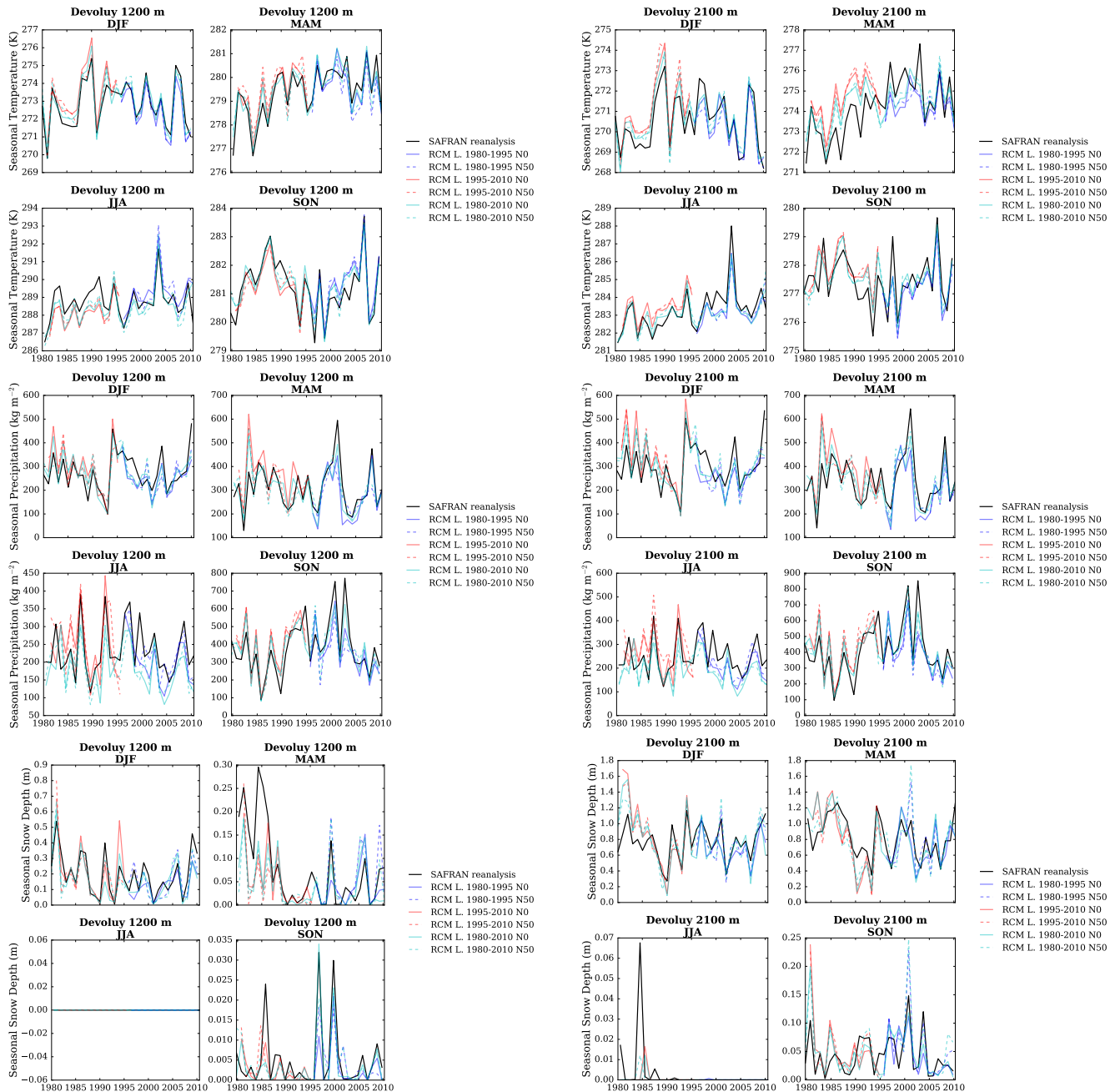


Figure S160: (top) Temperature, (middle) precipitation and (bottom) snow depth (using Crocus in this case) seasonal average time series from 1980 to 2010 in each adjusted RCM simulation and in the SAFRAN reanalysis, for the Devoluy massif, and at (left) 1200 m a.s.l. and (right) 2100 m a.s.l..

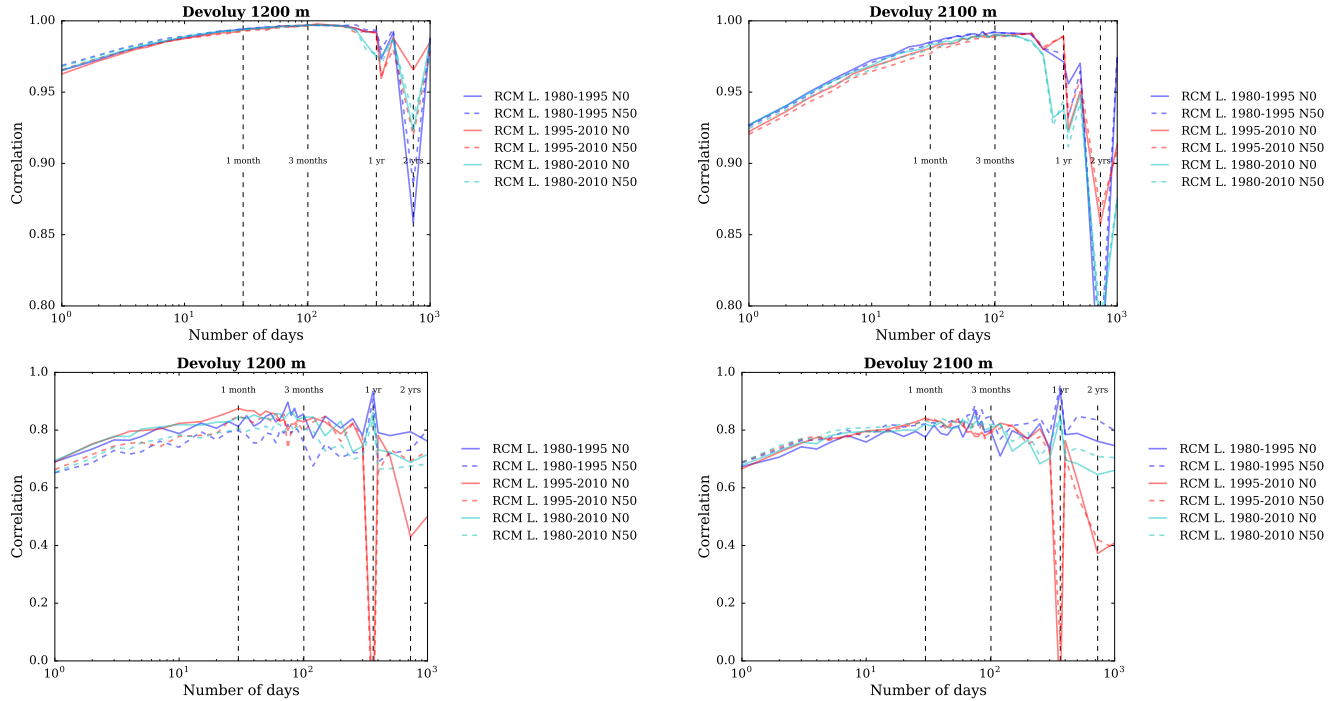


Figure S161: Correlation between the SAFRAN reanalysis and adjusted RCM (top) temperature and (bottom) precipitation as a function of the integration window over the evaluation period, for the Devoluy massif, and at (left) 1200 m a.s.l. and (right) 2100 m a.s.l..

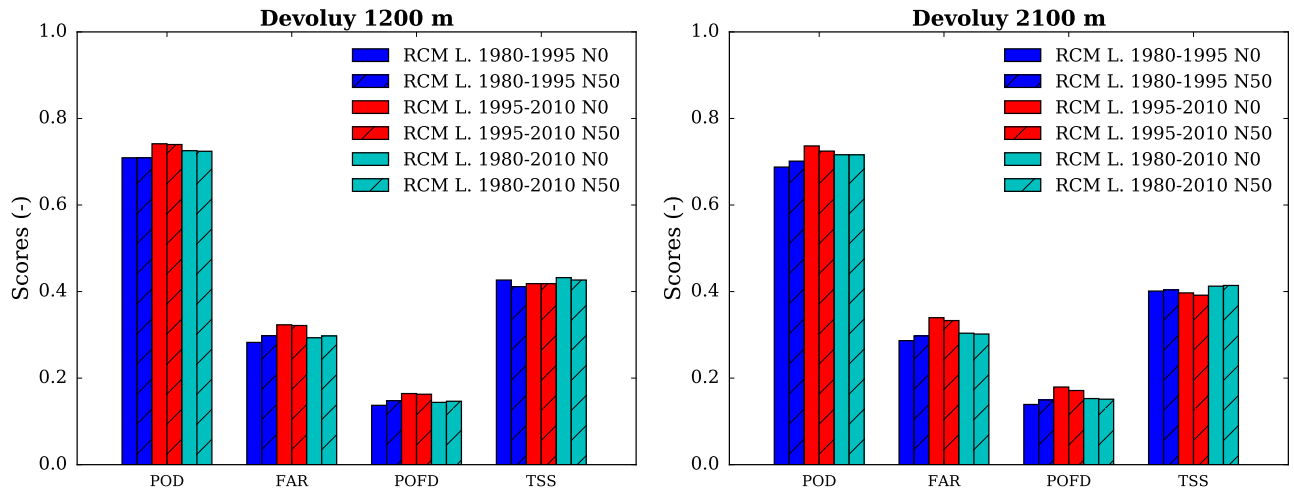


Figure S162: Scores for the detection of precipitation events in each adjusted RCM simulation compared to the SAFRAN reanalysis over the evaluation period, for the Devoluy massif, at (left) 1200 m a.s.l. and (right) 2100 m a.s.l.. POD = probability of detection, FAR = false alarm rate, POFD = probability of false detection, TSS = true skill score.

Champsaur

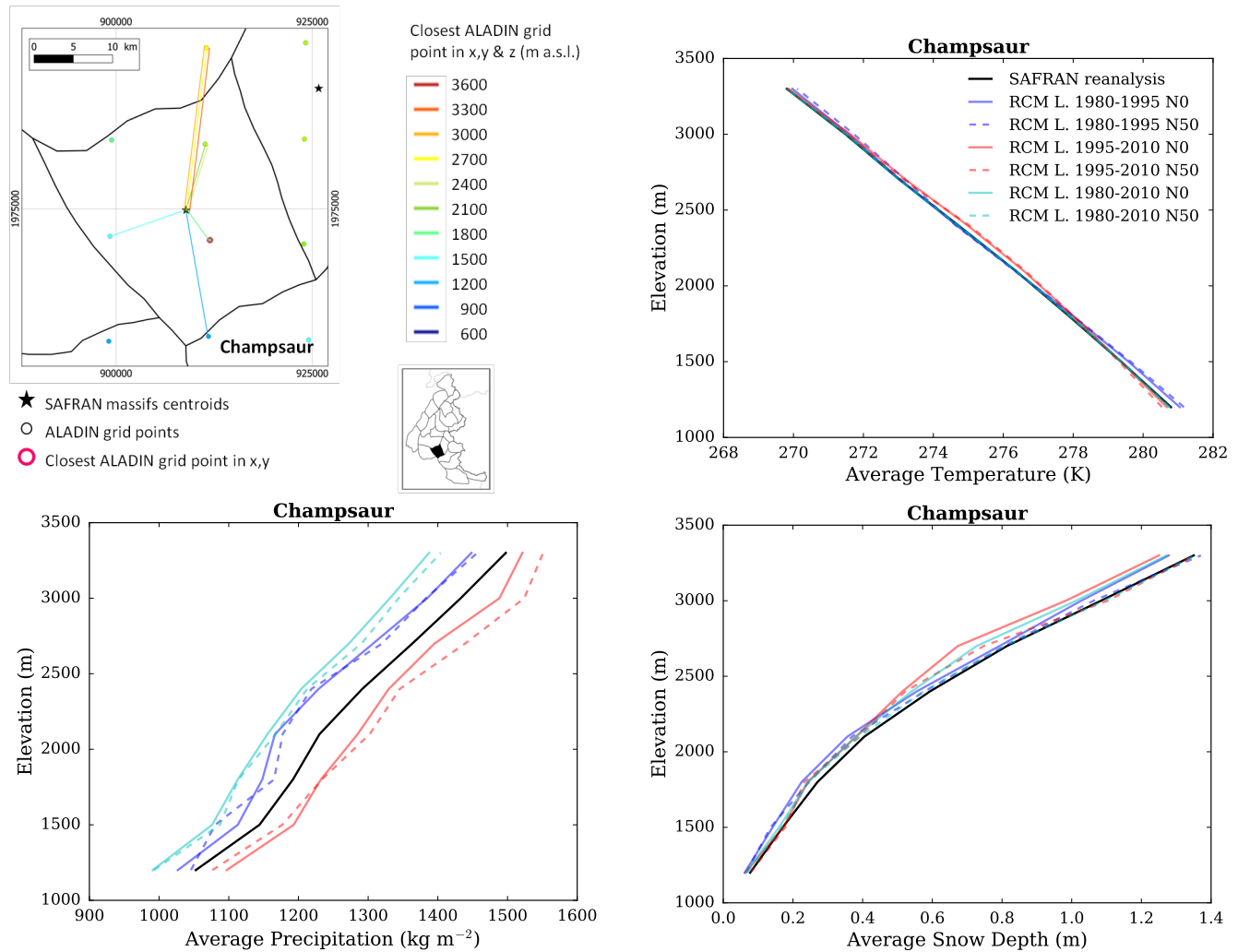


Figure S163: (top left) Location of the Champsaur massif, with ALADIN RCM grid points chosen as the closest in x, y ($N = 0$, pink contour) and in x, y and z (using $N \neq 0$). Coloured lines link each SAFRAN massif centre point with the corresponding grid point in ALADIN for the different elevations considered (in m above sea level (a.s.l.)). (top right) Mean temperature, (bottom left) precipitation and (bottom right) snow depth (using Crocus in this case) for each elevation band for the Champsaur massif, over the evaluation period in each adjusted RCM simulation (different learning periods and 2 neighbour selection methods) and in SAFRAN (1980-2010).

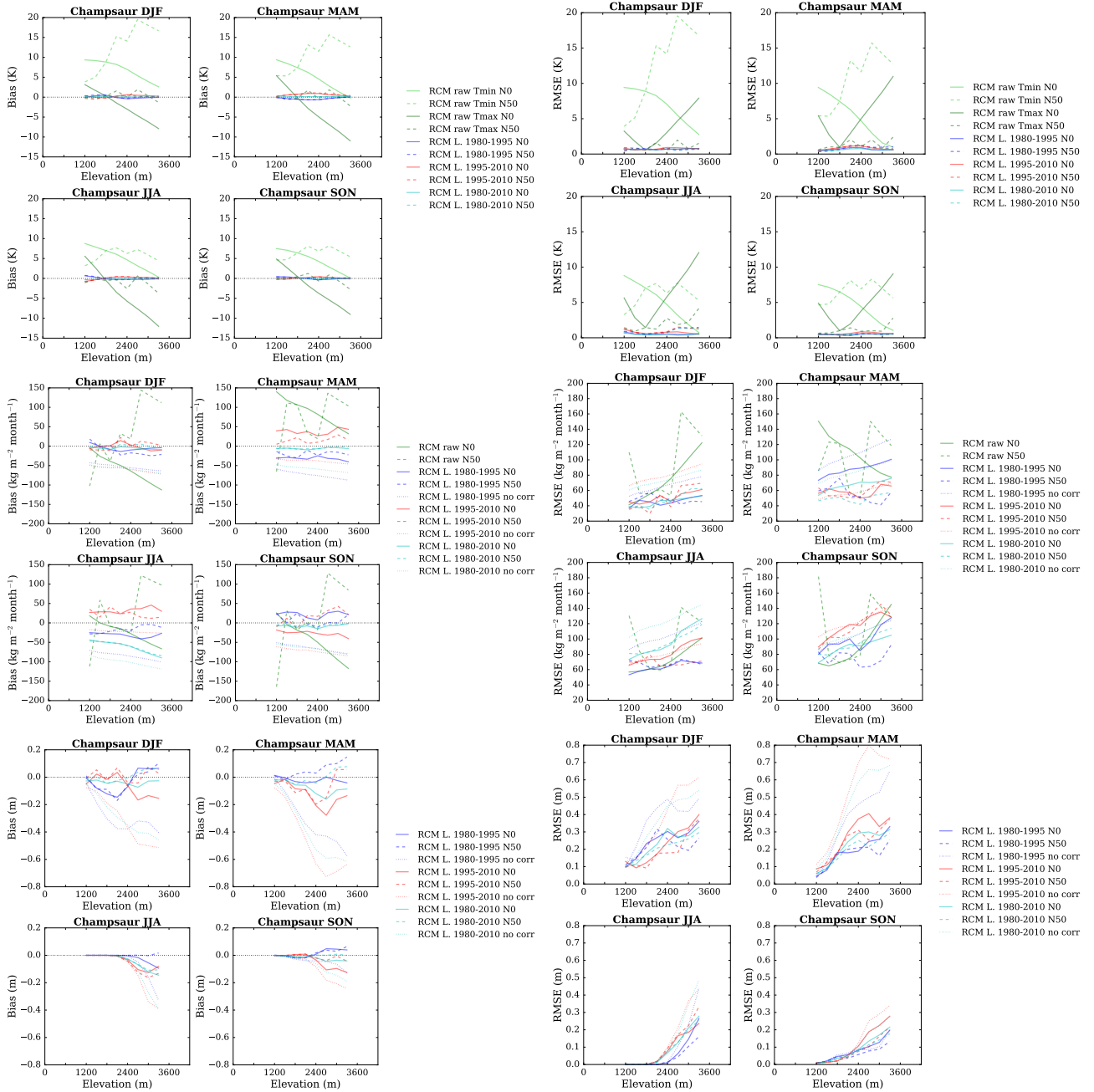


Figure S164: (top) Temperature, (middle) precipitation and (bottom) snow depth (using Crocus in this case) mean bias and root mean square error of each raw and adjusted RCM simulation compared to the SAFRAN reanalysis over the evaluation period for the Champsaur massif as a function of elevation. Scores computed for the raw RCM simulations concern minimum and maximum daily temperatures.

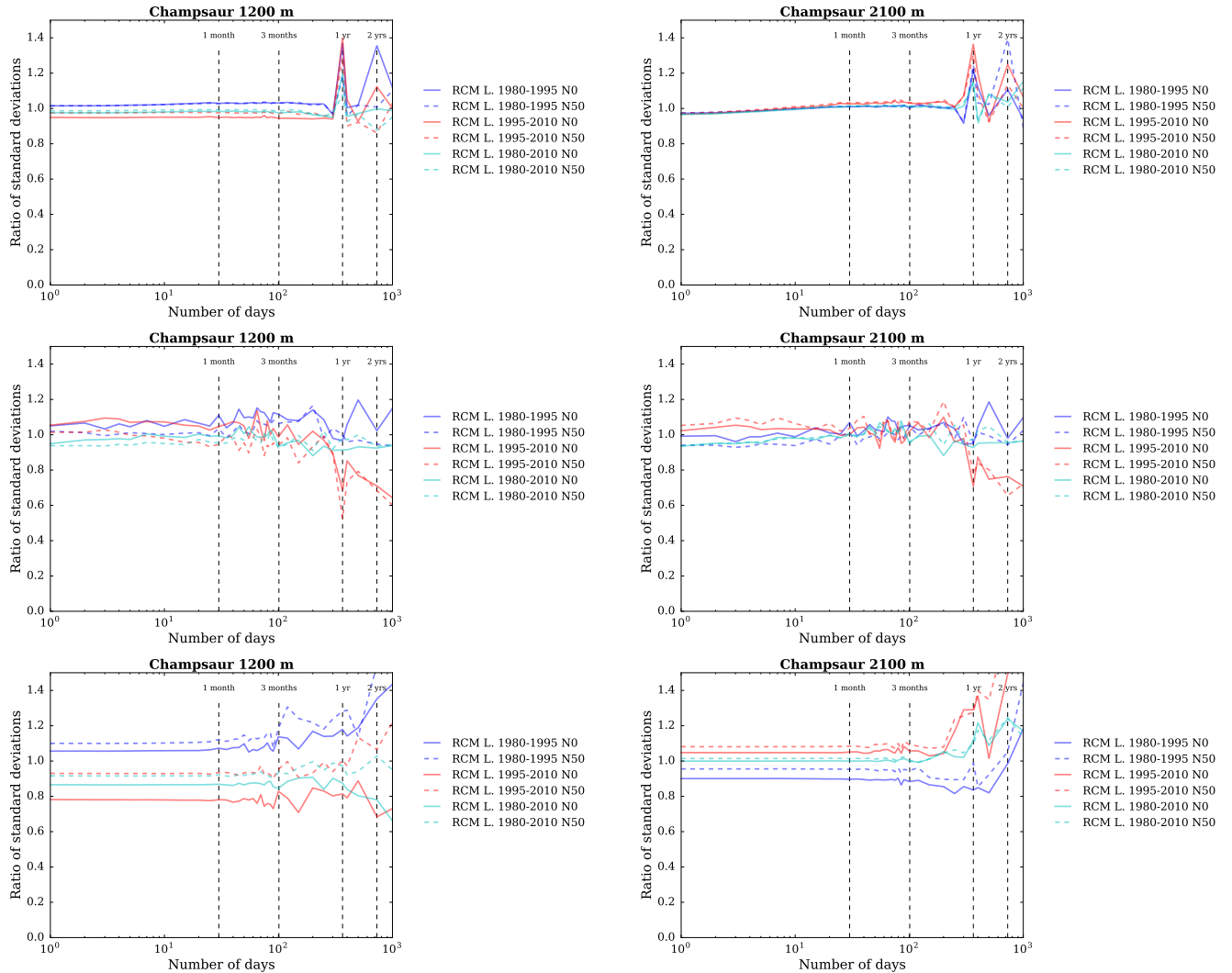


Figure S165: Ratios of standard deviations between the SAFRAN reanalysis and adjusted RCM (top) temperature, (middle) precipitation and (bottom) snow depth (using Crocus in this case) as a function of the integration window over the evaluation period, for the Champsaur massif, at (left) 1200 m a.s.l. and (right) 2100 m a.s.l..

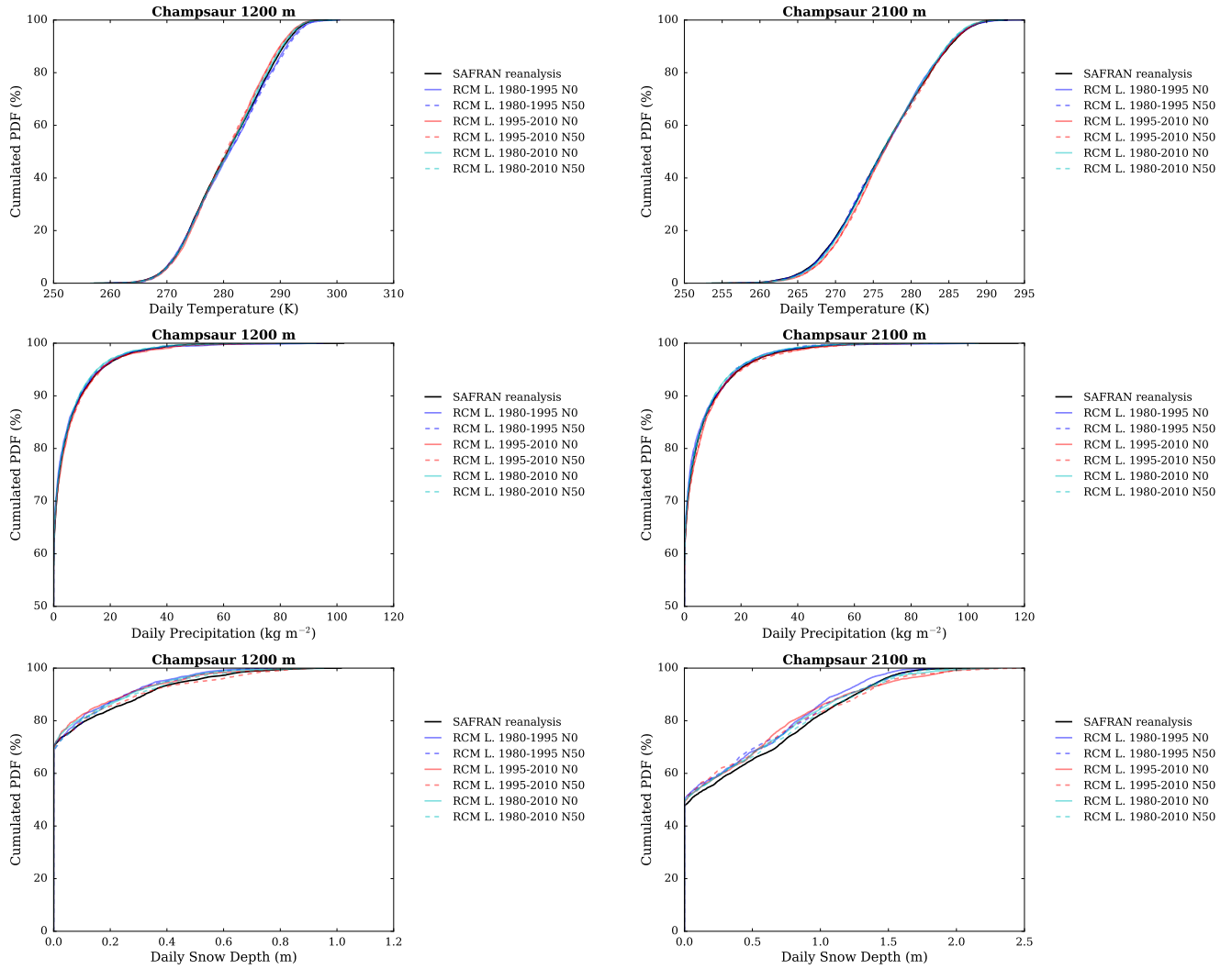


Figure S166: Cumulated probability density functions (PDFs) of daily (top) temperature, (middle) precipitation and (bottom) snow depth (using Crocus in this case) in each adjusted RCM simulation and in the SAFRAN reanalysis (1980-2010) over the evaluation period, for the Champsaur massif, at (left) 1200 m a.s.l. and (right) 2100 m a.s.l..

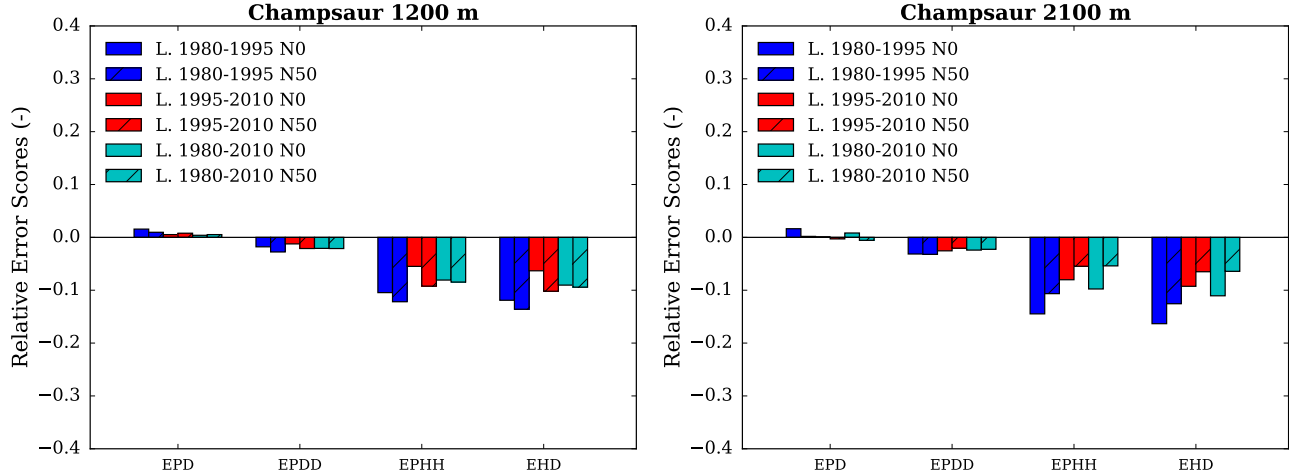


Figure S167: Scores for the duration and persistence of precipitation events in each adjusted RCM simulation compared to the SAFRAN reanalysis over the evaluation period, for the Champsaur massif, at (left) 1200 m a.s.l. and (right) 2100 m a.s.l.. EPD = relative error on the probability of a dry day, EPDD = relative error on the probability of a dry day following a dry day, EPHH = relative error on the probability of a wet day following a wet day, EHD = relative error on the mean duration of wet periods.

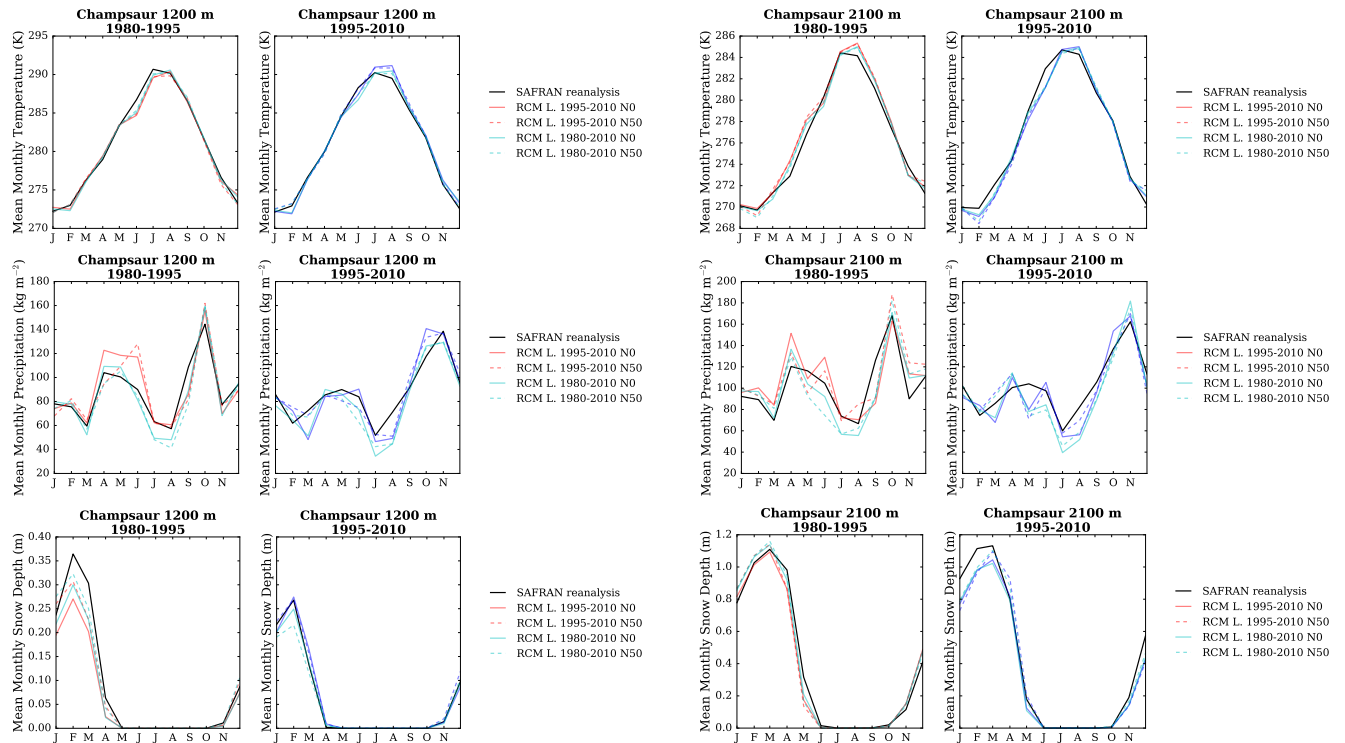


Figure S168: (top) Temperature, (middle) precipitation and (bottom) snow depth (using Crocus in this case) mean annual cycle in each adjusted RCM simulation and in the SAFRAN reanalysis over the period 1980-1995 and 1995-2010, for the Champsaur massif, and at (left) 1200 m a.s.l. and (right) 2100 m a.s.l.. Letters on the x-axis correspond to the different months of the calendar (J = January, F = February, etc.).

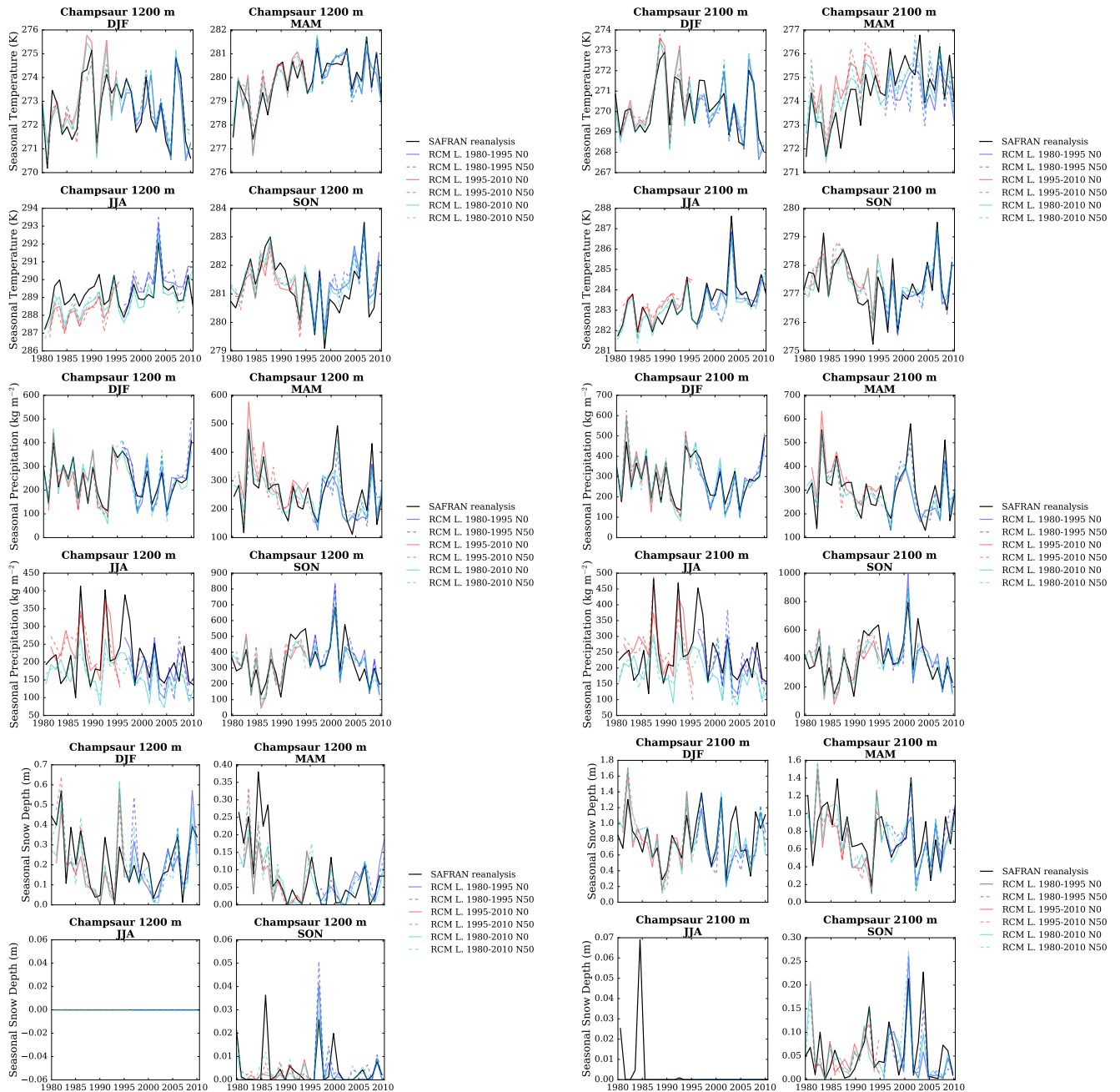


Figure S169: (top) Temperature, (middle) precipitation and (bottom) snow depth (using Crocus in this case) seasonal average time series from 1980 to 2010 in each adjusted RCM simulation and in the SAFRAN reanalysis, for the Champsaur massif, and at (left) 1200 m a.s.l. and (right) 2100 m a.s.l..

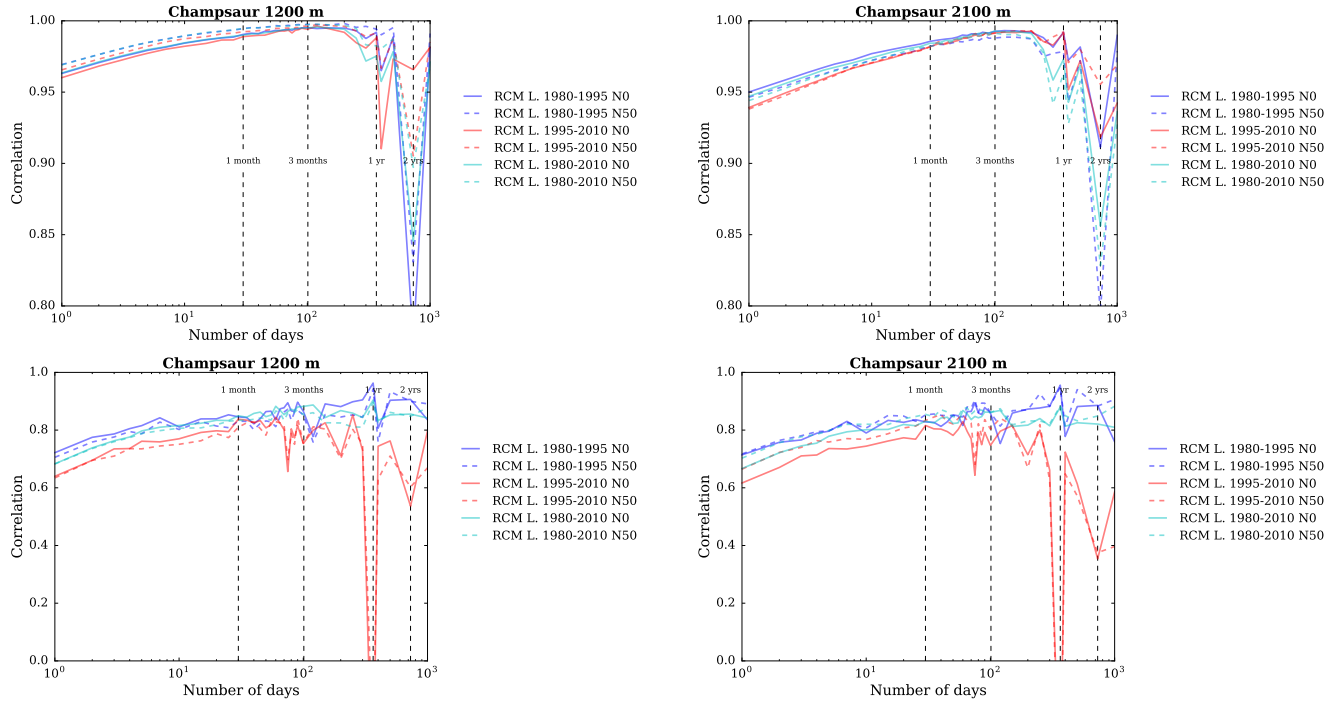


Figure S170: Correlation between the SAFRAN reanalysis and adjusted RCM (top) temperature and (bottom) precipitation as a function of the integration window over the evaluation period, for the Champsaur massif, and at (left) 1200 m a.s.l. and (right) 2100 m a.s.l..

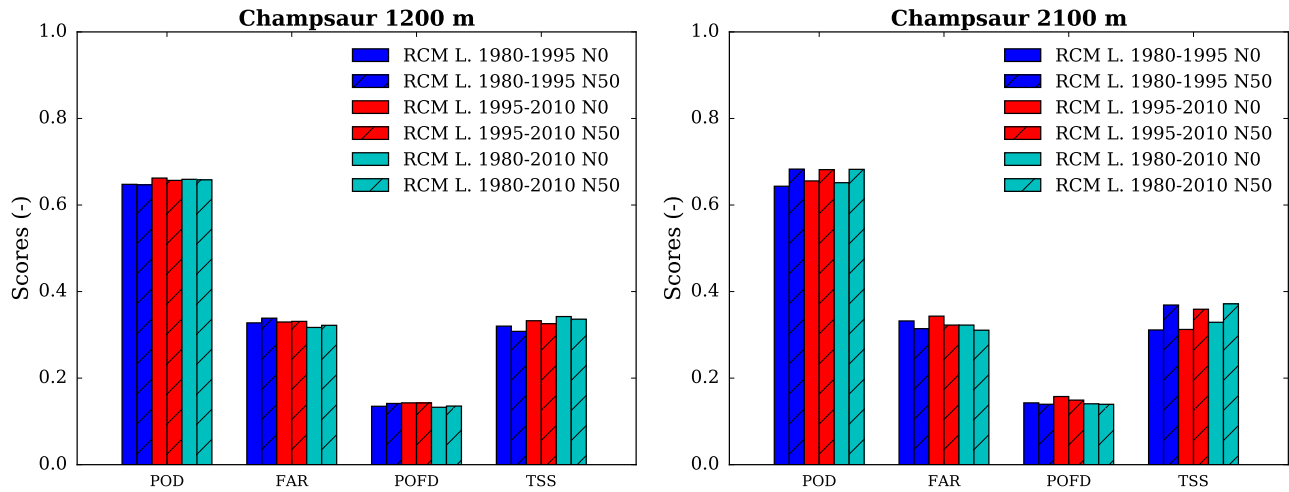


Figure S171: Scores for the detection of precipitation events in each adjusted RCM simulation compared to the SAFRAN reanalysis over the evaluation period, for the Champsaur massif, at (left) 1200 m a.s.l. and (right) 2100 m a.s.l.. POD = probability of detection, FAR = false alarm rate, POFD = probability of false detection, TSS = true skill score.

Parpaillon

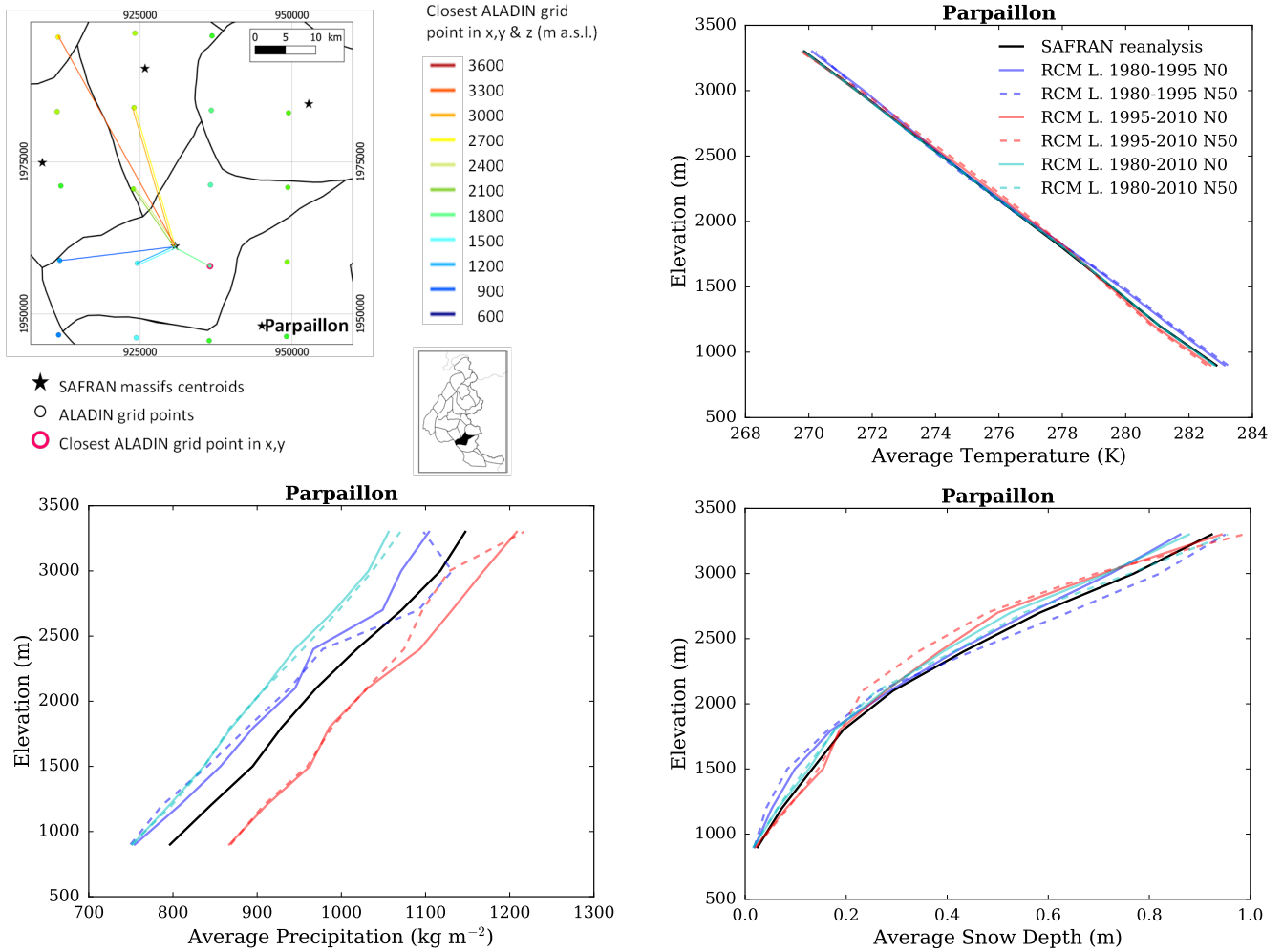


Figure S172: (top left) Location of the Parpaillon massif, with ALADIN RCM grid points chosen as the closest in x, y ($N = 0$, pink contour) and in x, y and z (using $N \neq 0$). Coloured lines link each SAFRAN massif centre point with the corresponding grid point in ALADIN for the different elevations considered (in m above sea level (a.s.l.)). (top right) Mean temperature, (bottom left) precipitation and (bottom right) snow depth (using Crocus in this case) for each elevation band for the Parpaillon massif, over the evaluation period in each adjusted RCM simulation (different learning periods and 2 neighbour selection methods) and in SAFRAN (1980-2010).

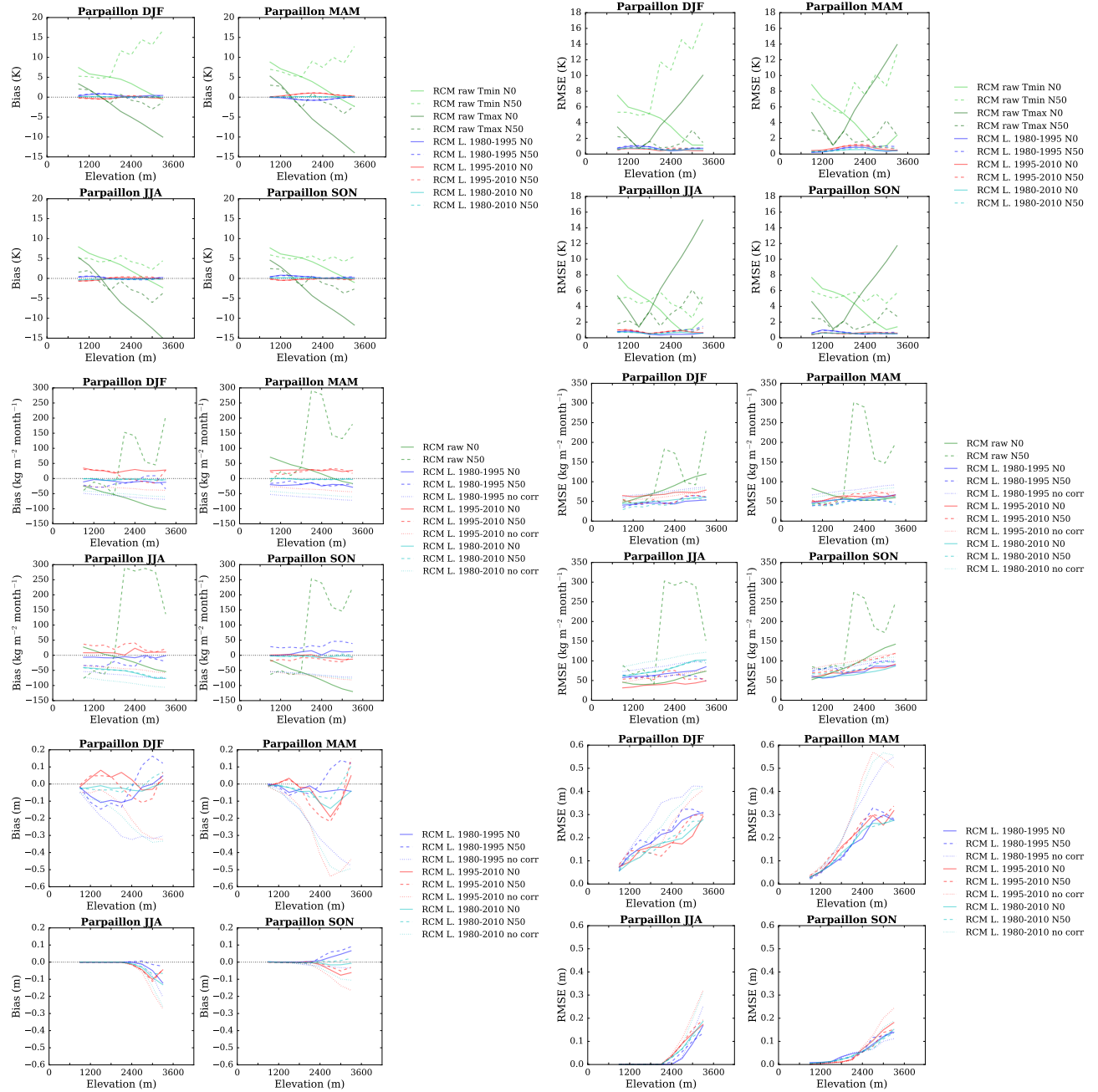


Figure S173: (top) Temperature, (middle) precipitation and (bottom) snow depth (using Crocus in this case) mean bias and root mean square error of each raw and adjusted RCM simulation compared to the SAFRAN reanalysis over the evaluation period for the Parpaillon massif as a function of elevation. Scores computed for the raw RCM simulations concern minimum and maximum daily temperatures.

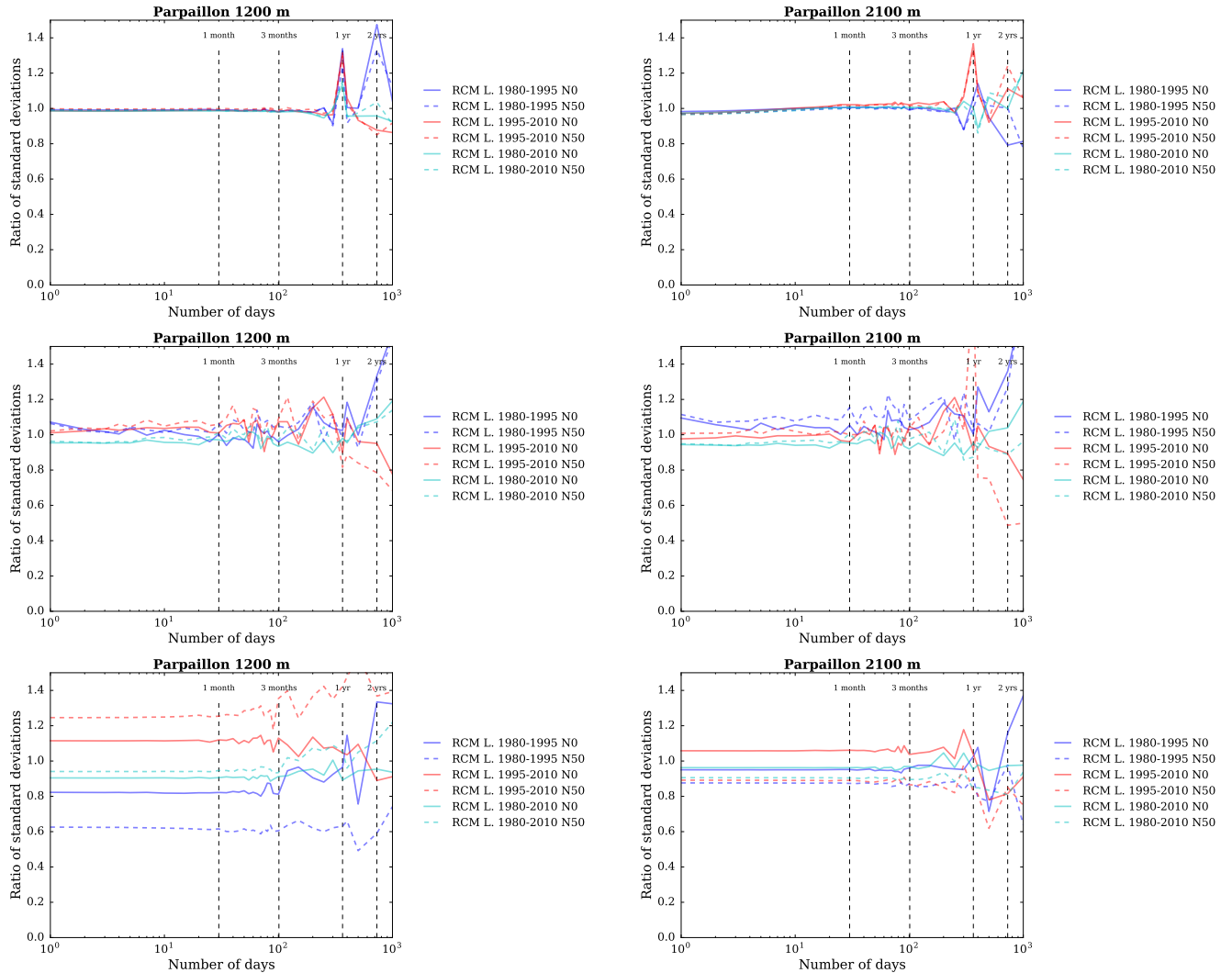


Figure S174: Ratios of standard deviations between the SAFRAN reanalysis and adjusted RCM (top) temperature, (middle) precipitation and (bottom) snow depth (using Crocus in this case) as a function of the integration window over the evaluation period, for the Parpaillon massif, at (left) 1200 m a.s.l. and (right) 2100 m a.s.l..

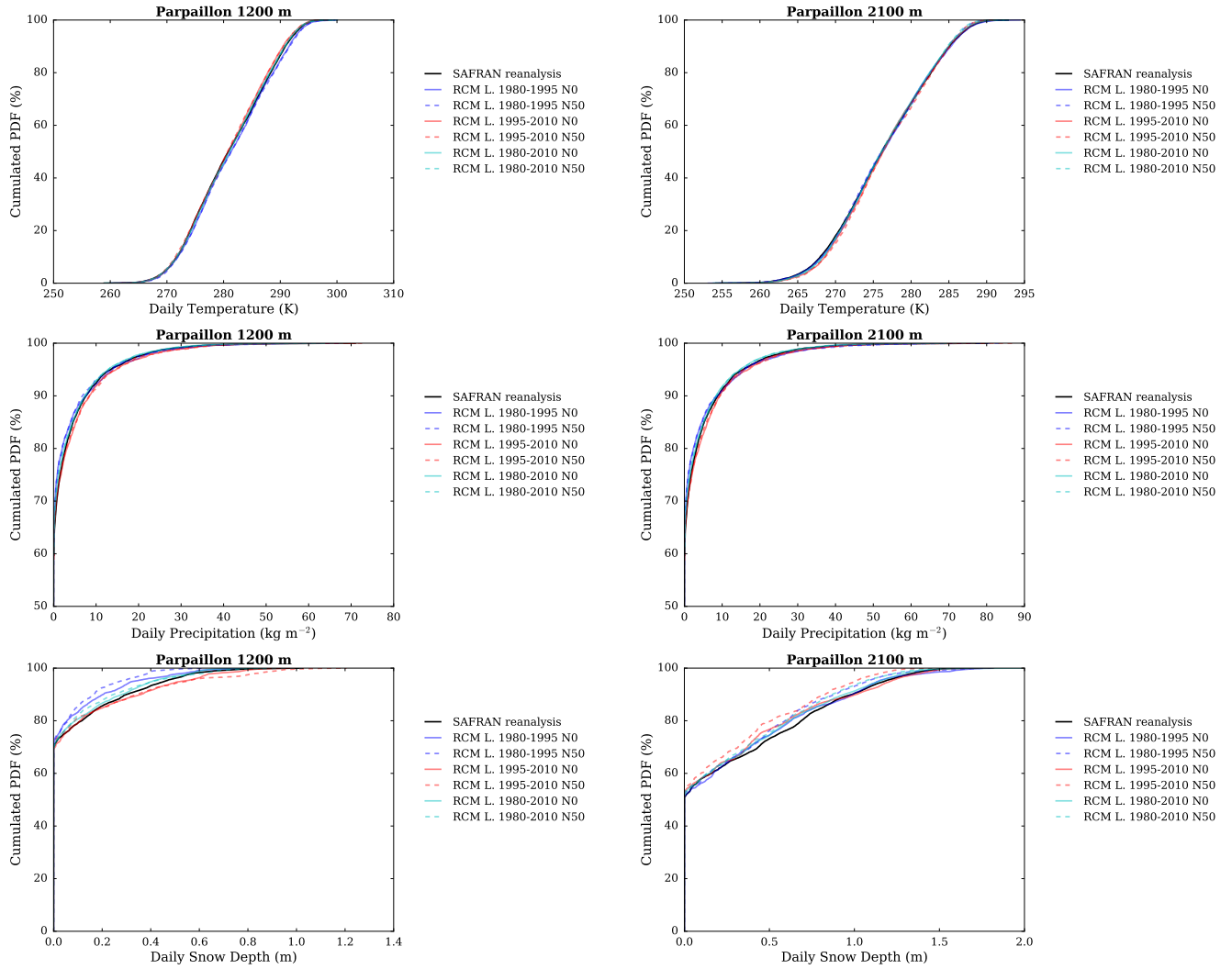


Figure S175: Cumulated probability density functions (PDFs) of daily (top) temperature, (middle) precipitation and (bottom) snow depth (using Crocus in this case) in each adjusted RCM simulation and in the SAFRAN reanalysis (1980-2010) over the evaluation period, for the Parpaillon massif, at (left) 1200 m a.s.l. and (right) 2100 m a.s.l..

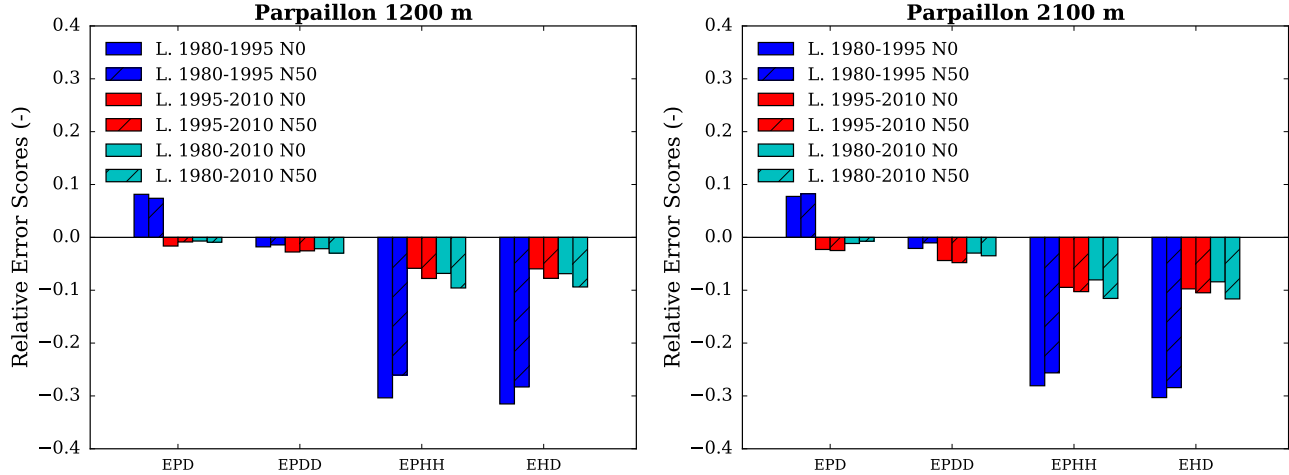


Figure S176: Scores for the duration and persistence of precipitation events in each adjusted RCM simulation compared to the SAFRAN reanalysis over the evaluation period, for the Parpaillon massif, at (left) 1200 m a.s.l. and (right) 2100 m a.s.l.. EPD = relative error on the probability of a dry day, EPDD = relative error on the probability of a dry day following a dry day, EPHH = relative error on the probability of a wet day following a wet day, EHD = relative error on the mean duration of wet periods.

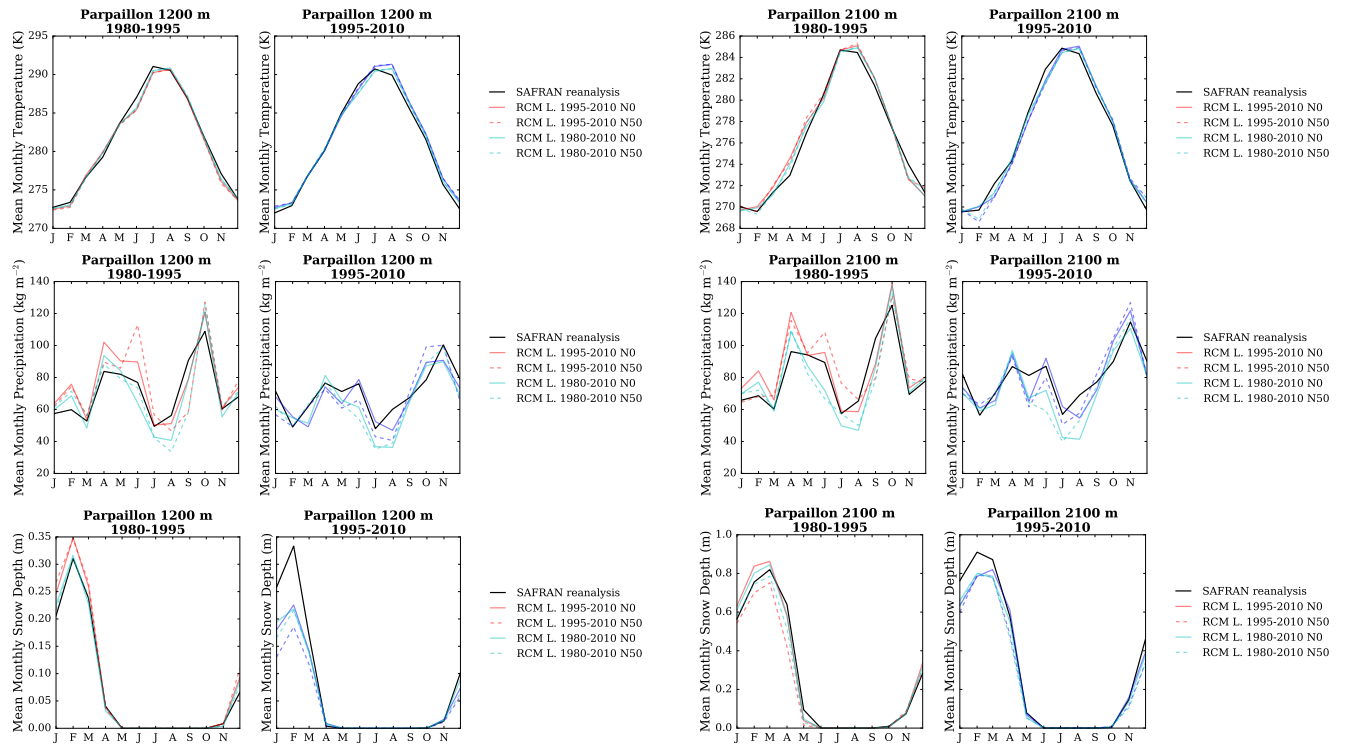


Figure S177: (top) Temperature, (middle) precipitation and (bottom) snow depth (using Crocus in this case) mean annual cycle in each adjusted RCM simulation and in the SAFRAN reanalysis over the period 1980-1995 and 1995-2010, for the Parpaillon massif, and at (left) 1200 m a.s.l. and (right) 2100 m a.s.l.. Letters on the x-axis correspond to the different months of the calendar (J = January, F = February, etc.).

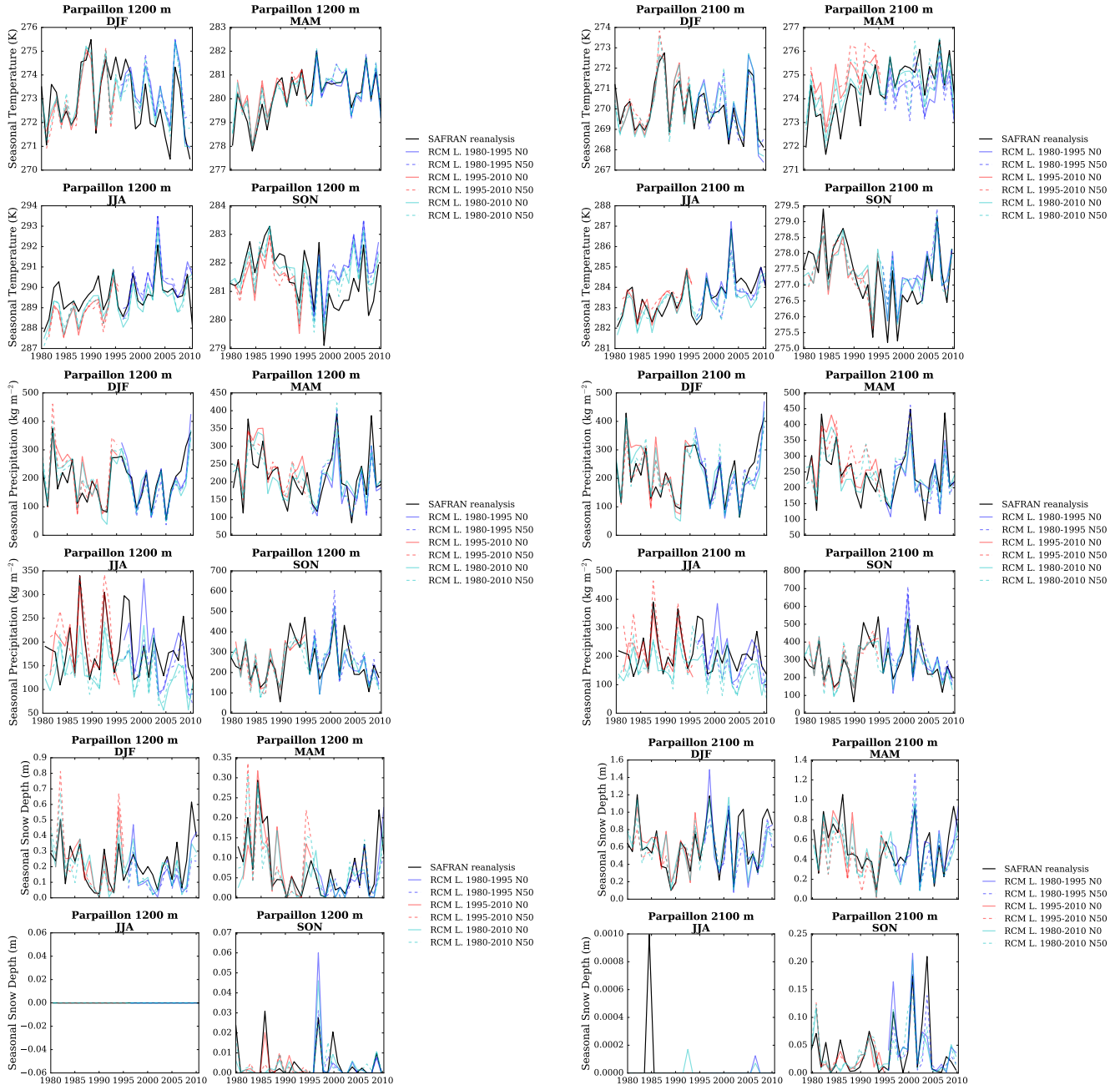


Figure S178: (top) Temperature, (middle) precipitation and (bottom) snow depth (using Crocus in this case) seasonal average time series from 1980 to 2010 in each adjusted RCM simulation and in the SAFRAN reanalysis, for the Parpaillon massif, and at (left) 1200 m a.s.l. and (right) 2100 m a.s.l..

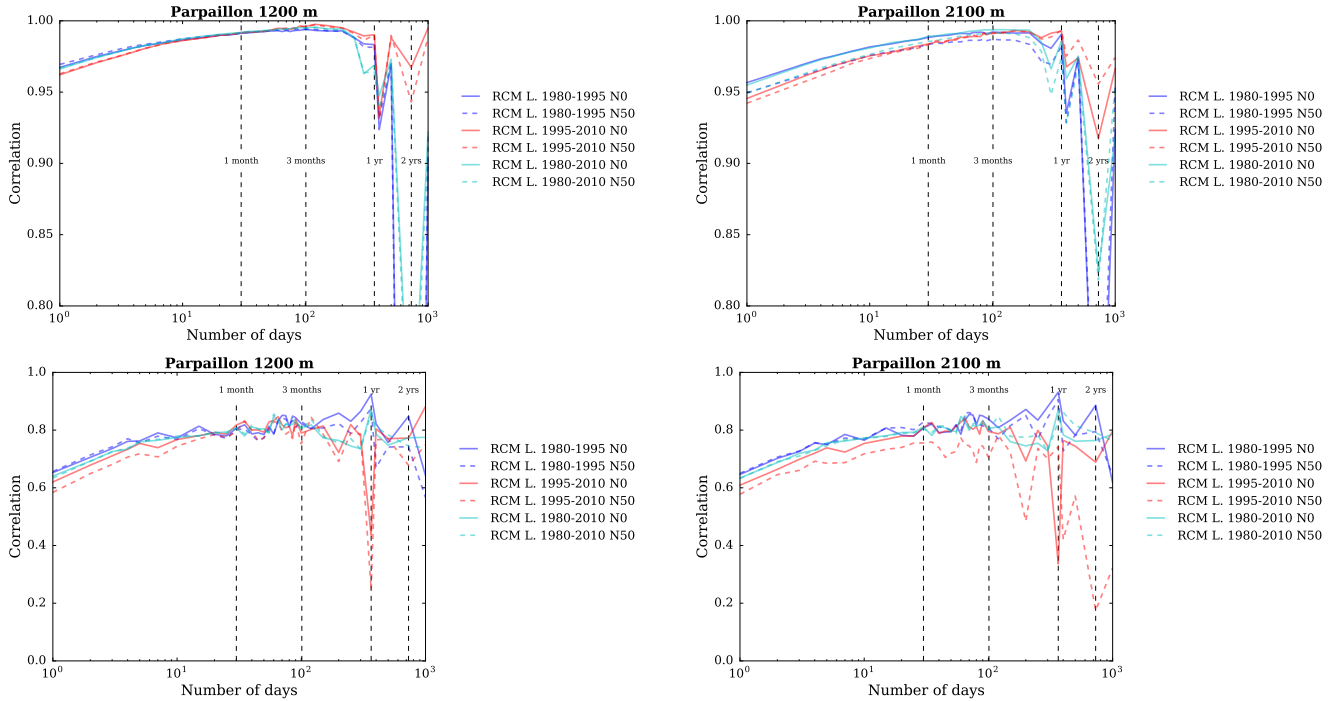


Figure S179: Correlation between the SAFRAN reanalysis and adjusted RCM (top) temperature and (bottom) precipitation as a function of the integration window over the evaluation period, for the Parpaillon massif, and at (left) 1200 m a.s.l. and (right) 2100 m a.s.l..

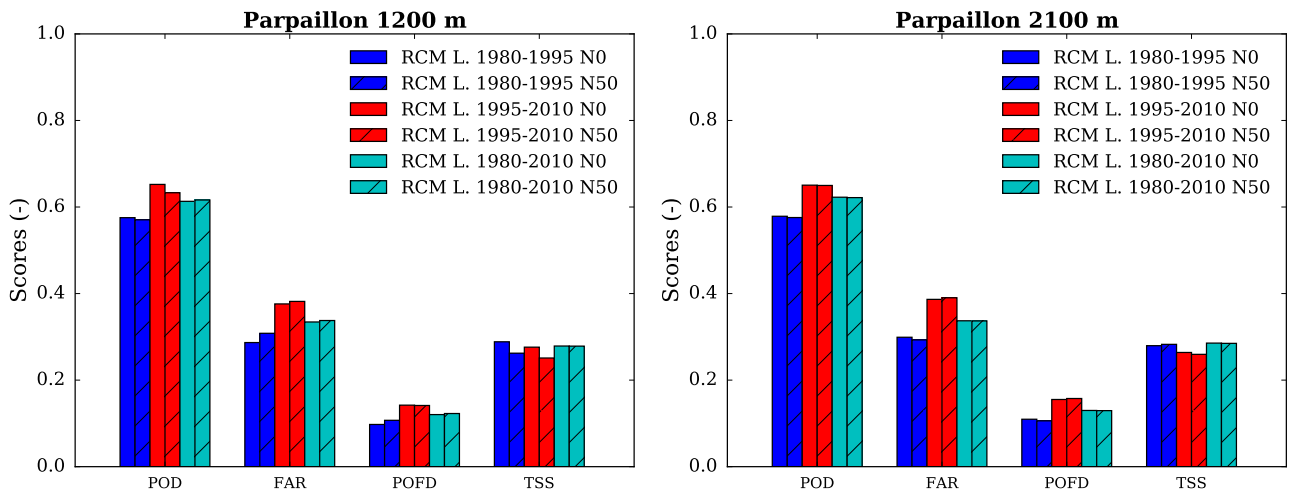


Figure S180: Scores for the detection of precipitation events in each adjusted RCM simulation compared to the SAFRAN reanalysis over the evaluation period, for the Parpaillon massif, at (left) 1200 m a.s.l. and (right) 2100 m a.s.l.. POD = probability of detection, FAR = false alarm rate, POFD = probability of false detection, TSS = true skill score.

Ubaye

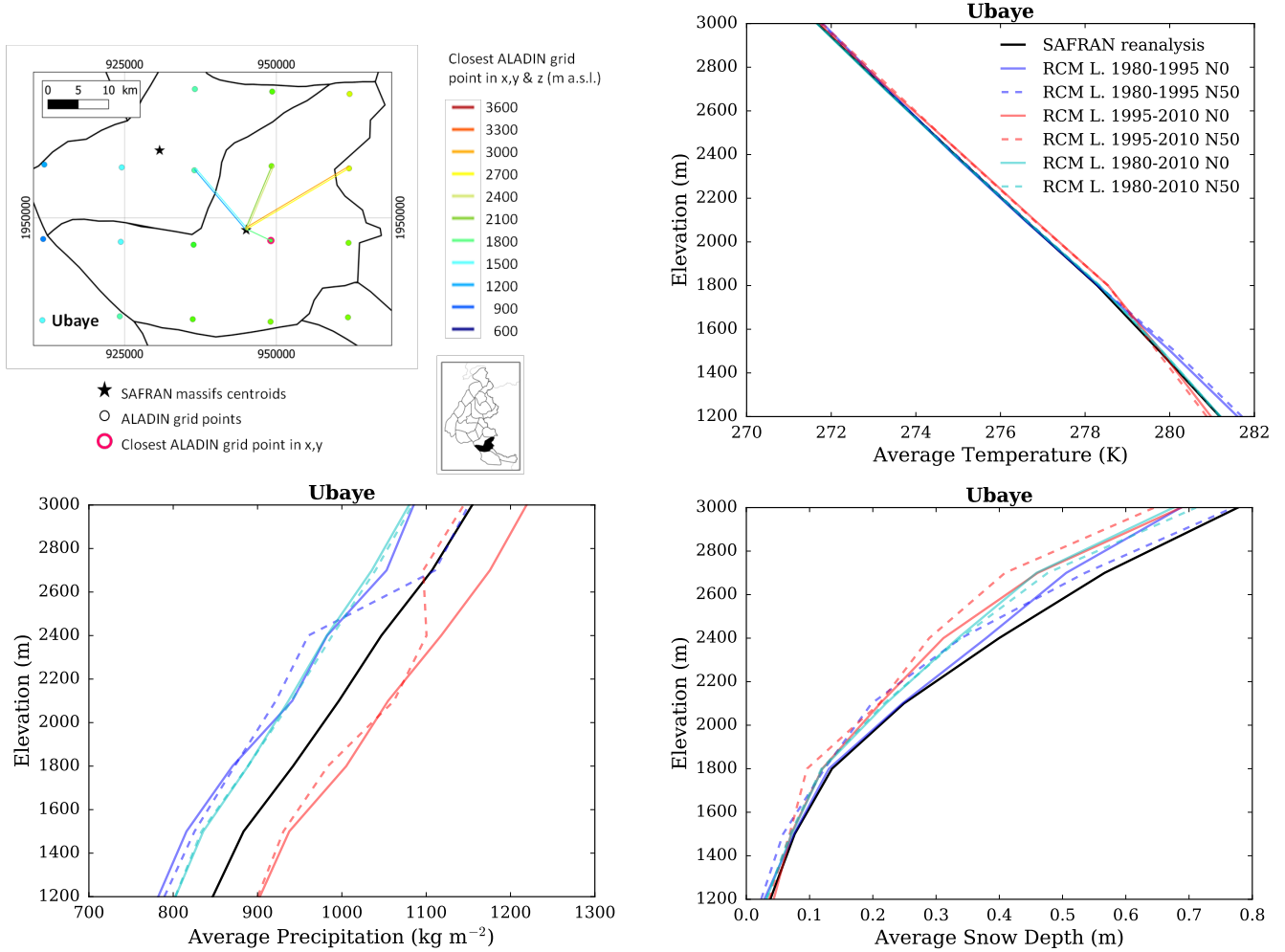


Figure S181: (top left) Location of the Ubaye massif, with ALADIN RCM grid points chosen as the closest in x, y ($N = 0$, pink contour) and in x, y and z (using $N \neq 0$). Coloured lines link each SAFRAN massif centre point with the corresponding grid point in ALADIN for the different elevations considered (in m above sea level (a.s.l.)). (top right) Mean temperature, (bottom left) precipitation and (bottom right) snow depth (using Crocus in this case) for each elevation band for the Ubaye massif, over the evaluation period in each adjusted RCM simulation (different learning periods and 2 neighbour selection methods) and in SAFRAN (1980-2010).

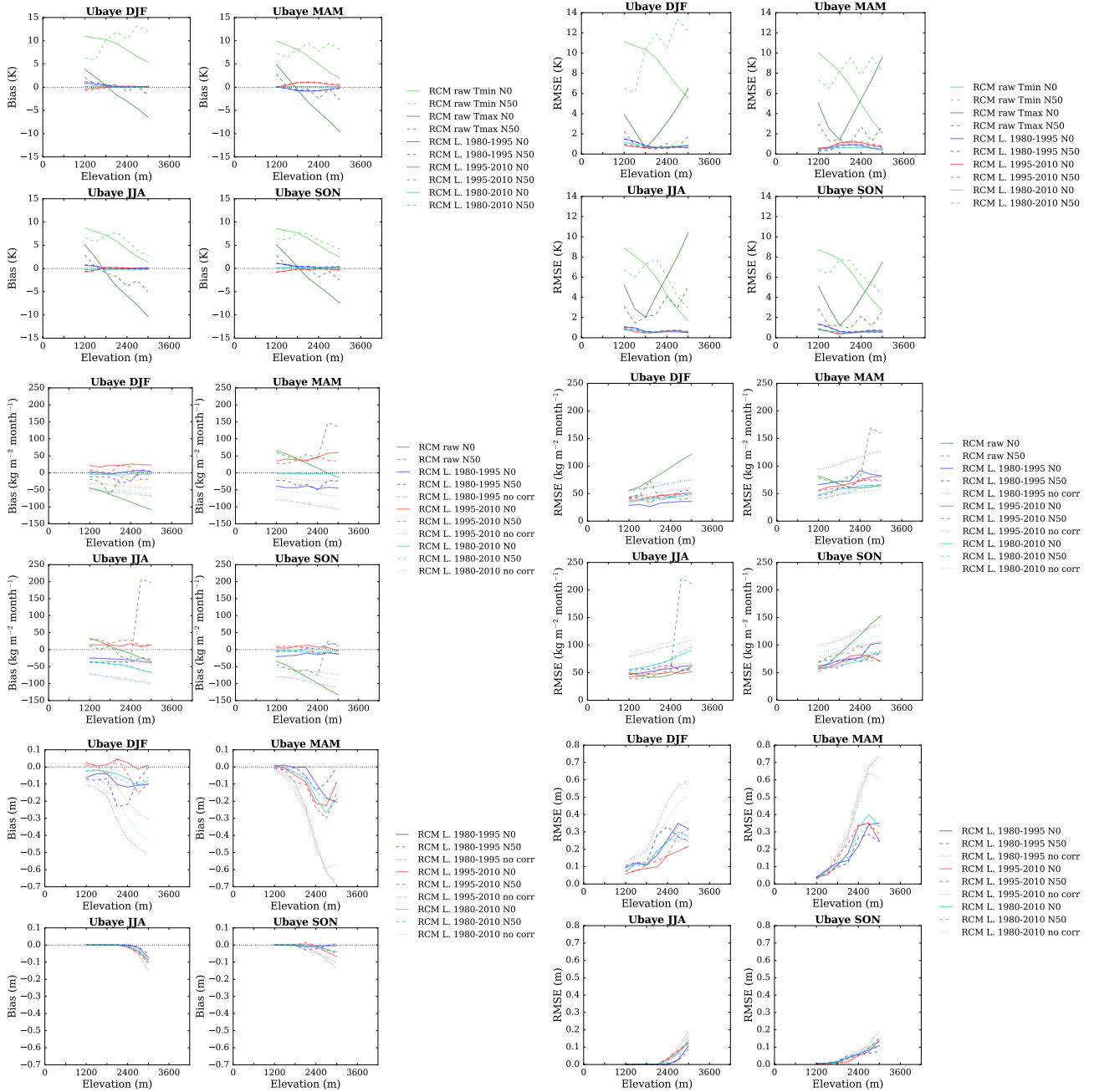


Figure S182: (top) Temperature, (middle) precipitation and (bottom) snow depth (using Crocus in this case) mean bias and root mean square error of each raw and adjusted RCM simulation compared to the SAFRAN reanalysis over the evaluation period for the Ubaye massif as a function of elevation. Scores computed for the raw RCM simulations concern minimum and maximum daily temperatures.

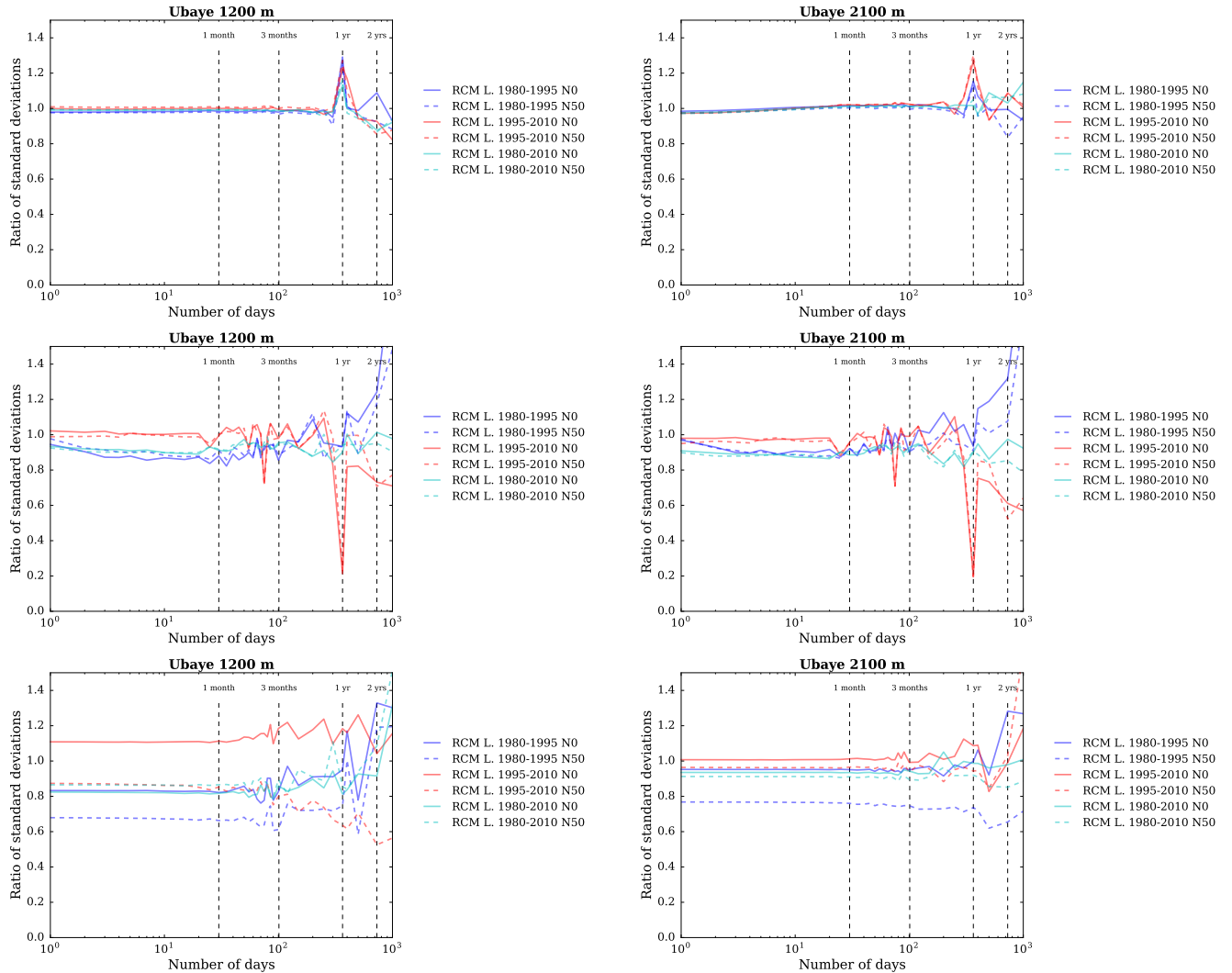


Figure S183: Ratios of standard deviations between the SAFRAN ranalysis and adjusted RCM (top) temperature, (middle) precipitation and (bottom) snow depth (using Crocus in this case) as a function of the integration window over the evaluation period, for the Ubaye massif, at (left) 1200 m a.s.l. and (right) 2100 m a.s.l..

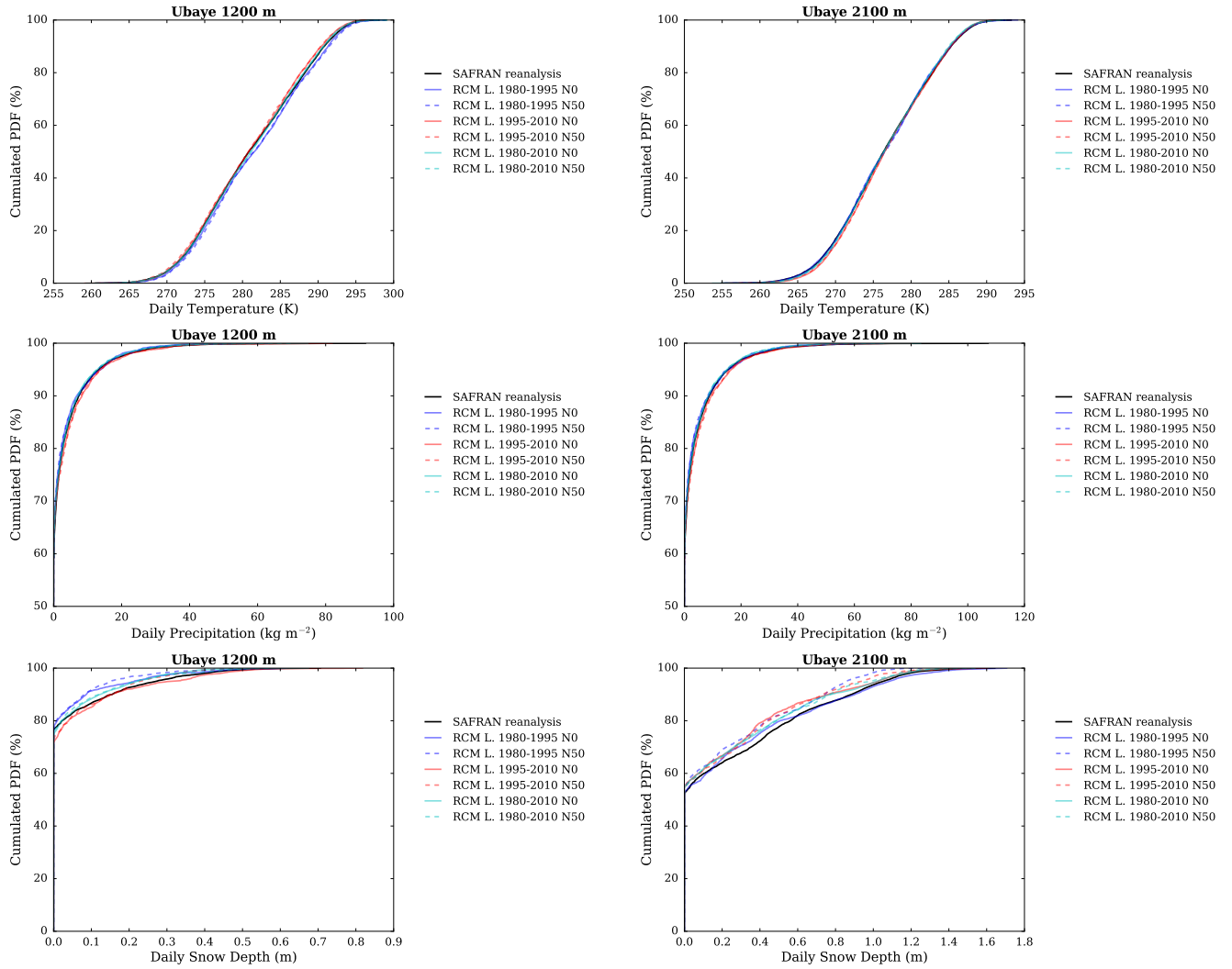


Figure S184: Cumulated probability density functions (PDFs) of daily (top) temperature, (middle) precipitation and (bottom) snow depth (using Crocus in this case) in each adjusted RCM simulation and in the SAFRAN reanalysis (1980-2010) over the evaluation period, for the Ubaye massif, at (left) 1200 m a.s.l. and (right) 2100 m a.s.l..

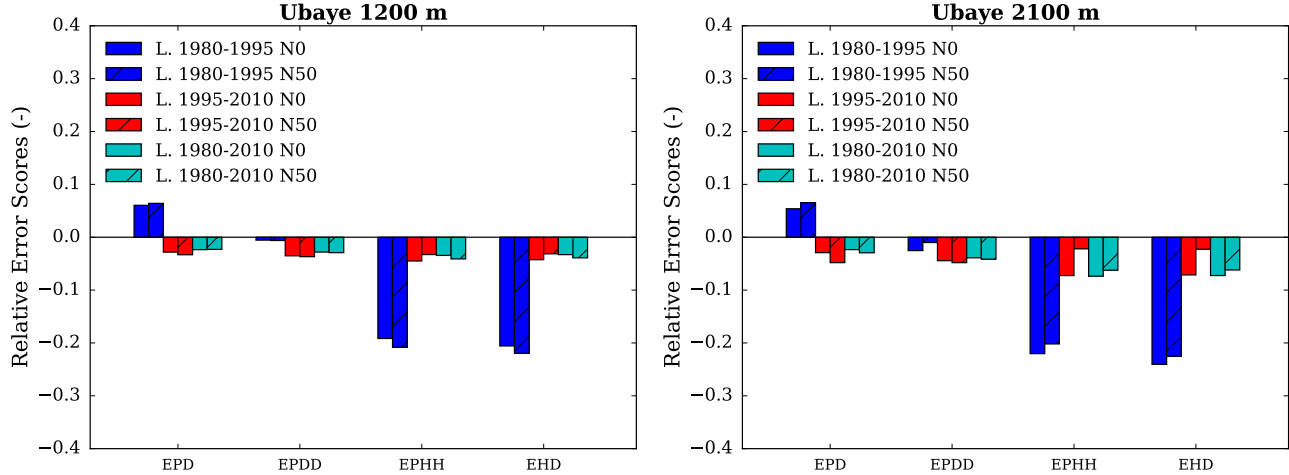


Figure S185: Scores for the duration and persistence of precipitation events in each adjusted RCM simulation compared to the SAFRAN reanalysis over the evaluation period, for the Ubaye massif, at (left) 1200 m a.s.l. and (right) 2100 m a.s.l.. EPD = relative error on the probability of a dry day, EPDD = relative error on the probability of a dry day following a dry day, EPHH = relative error on the probability of a wet day following a wet day, EHD = relative error on the mean duration of wet periods.

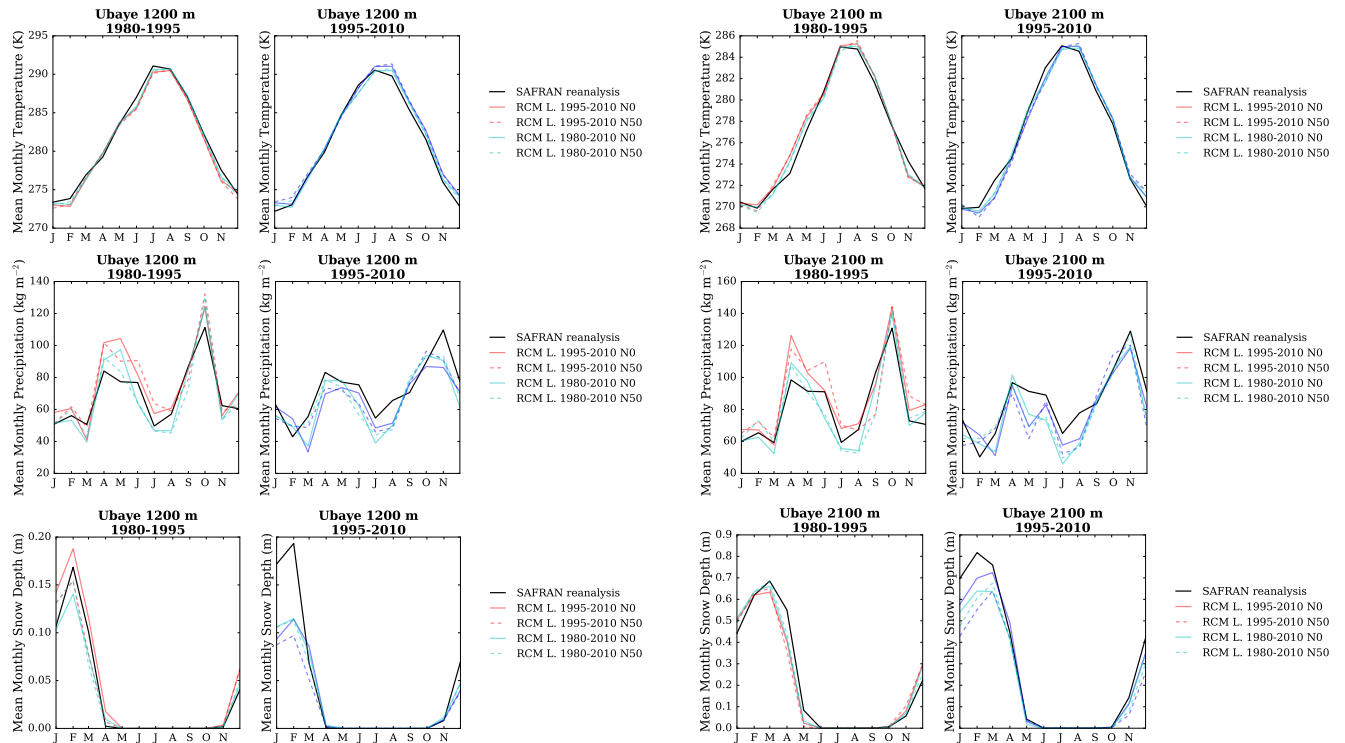


Figure S186: (top) Temperature, (middle) precipitation and (bottom) snow depth (using Crocus in this case) mean annual cycle in each adjusted RCM simulation and in the SAFRAN reanalysis over the period 1980-1995 and 1995-2010, for the Ubaye massif, and at (left) 1200 m a.s.l. and (right) 2100 m a.s.l.. Letters on the x-axis correspond to the different months of the calendar (J = January, F = February, etc.).

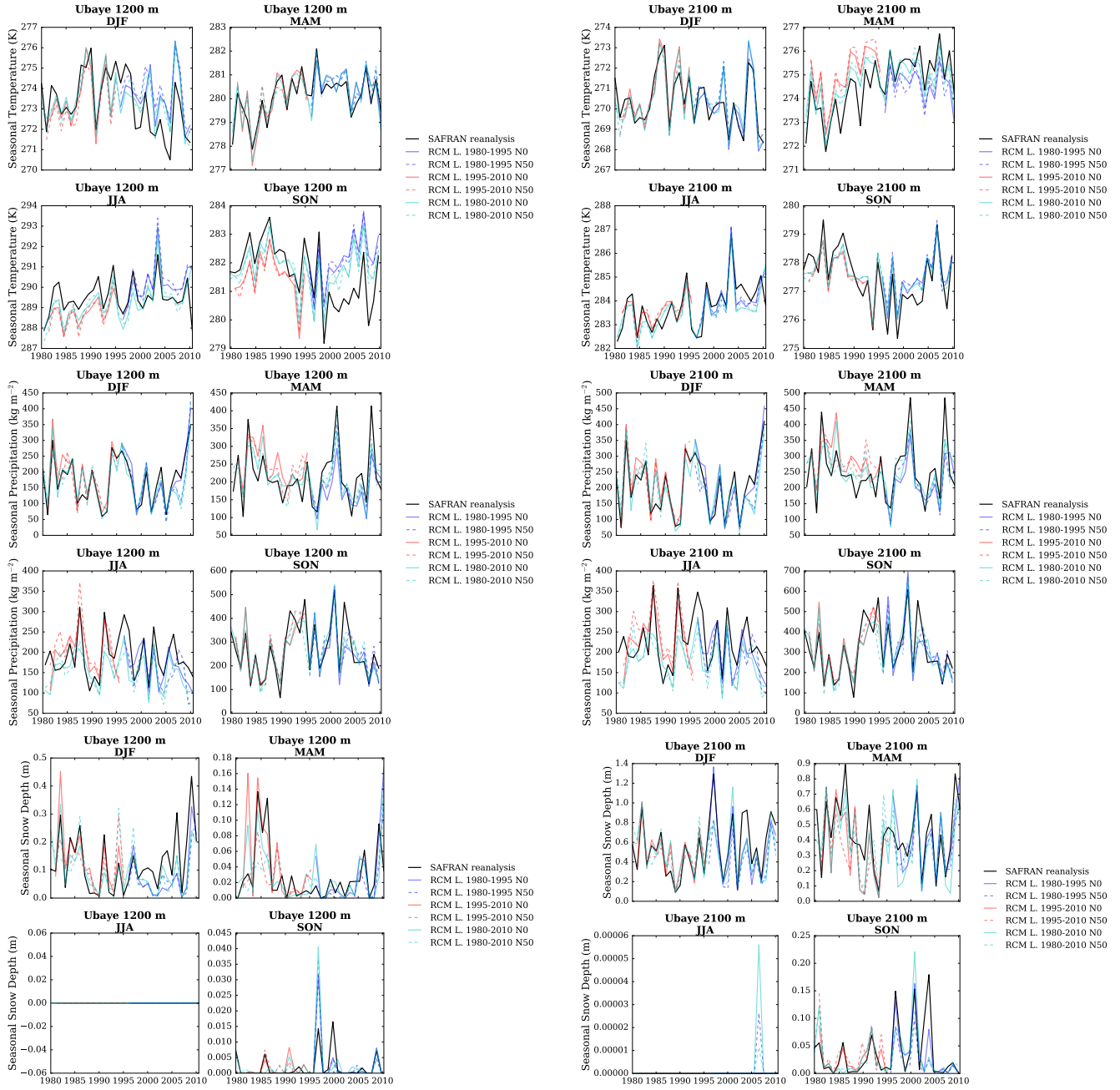


Figure S187: (top) Temperature, (middle) precipitation and (bottom) snow depth (using Crocus in this case) seasonal average time series from 1980 to 2010 in each adjusted RCM simulation and in the SAFRAN reanalysis, for the Ubaye massif, and at (left) 1200 m a.s.l. and (right) 2100 m a.s.l..

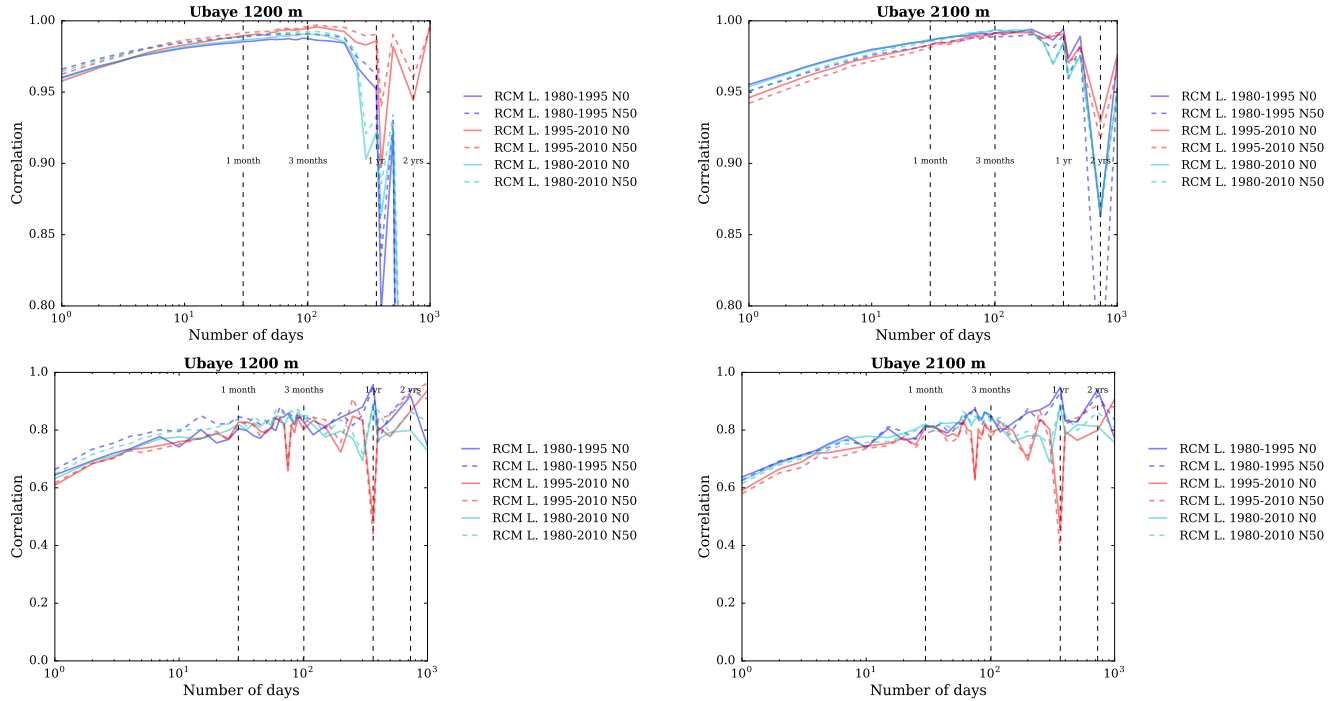


Figure S188: Correlation between the SAFRAN reanalysis and adjusted RCM (top) temperature and (bottom) precipitation as a function of the integration window over the evaluation period, for the Ubaye massif, and at (left) 1200 m a.s.l. and (right) 2100 m a.s.l..

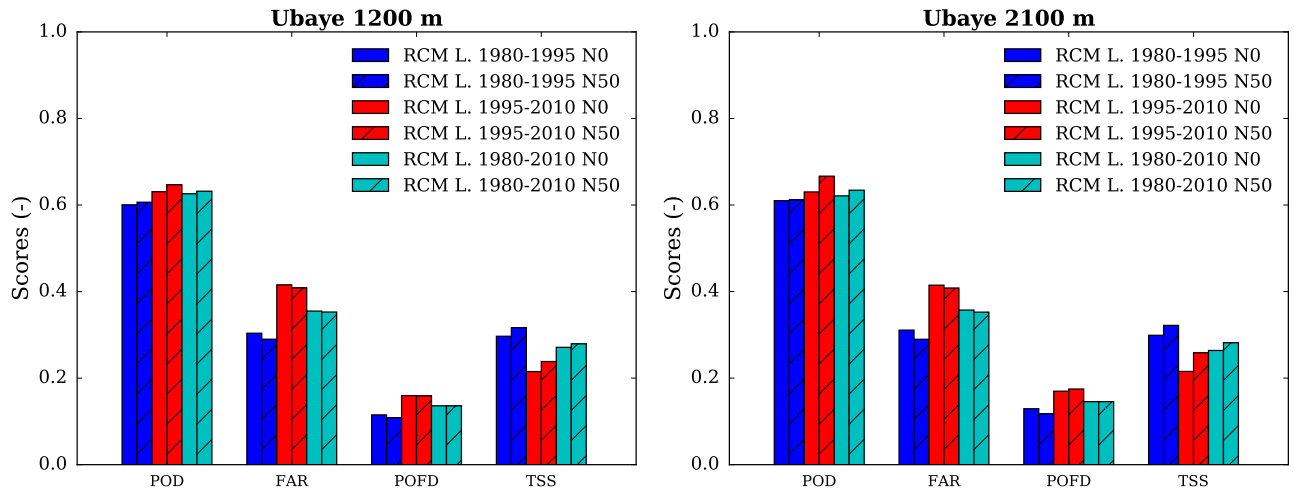


Figure S189: Scores for the detection of precipitation events in each adjusted RCM simulation compared to the SAFRAN reanalysis over the evaluation period, for the Ubaye massif, at (left) 1200 m a.s.l. and (right) 2100 m a.s.l.. POD = probability of detection, FAR = false alarm rate, POFD = probability of false detection, TSS = true skill score.

Alpes Azur

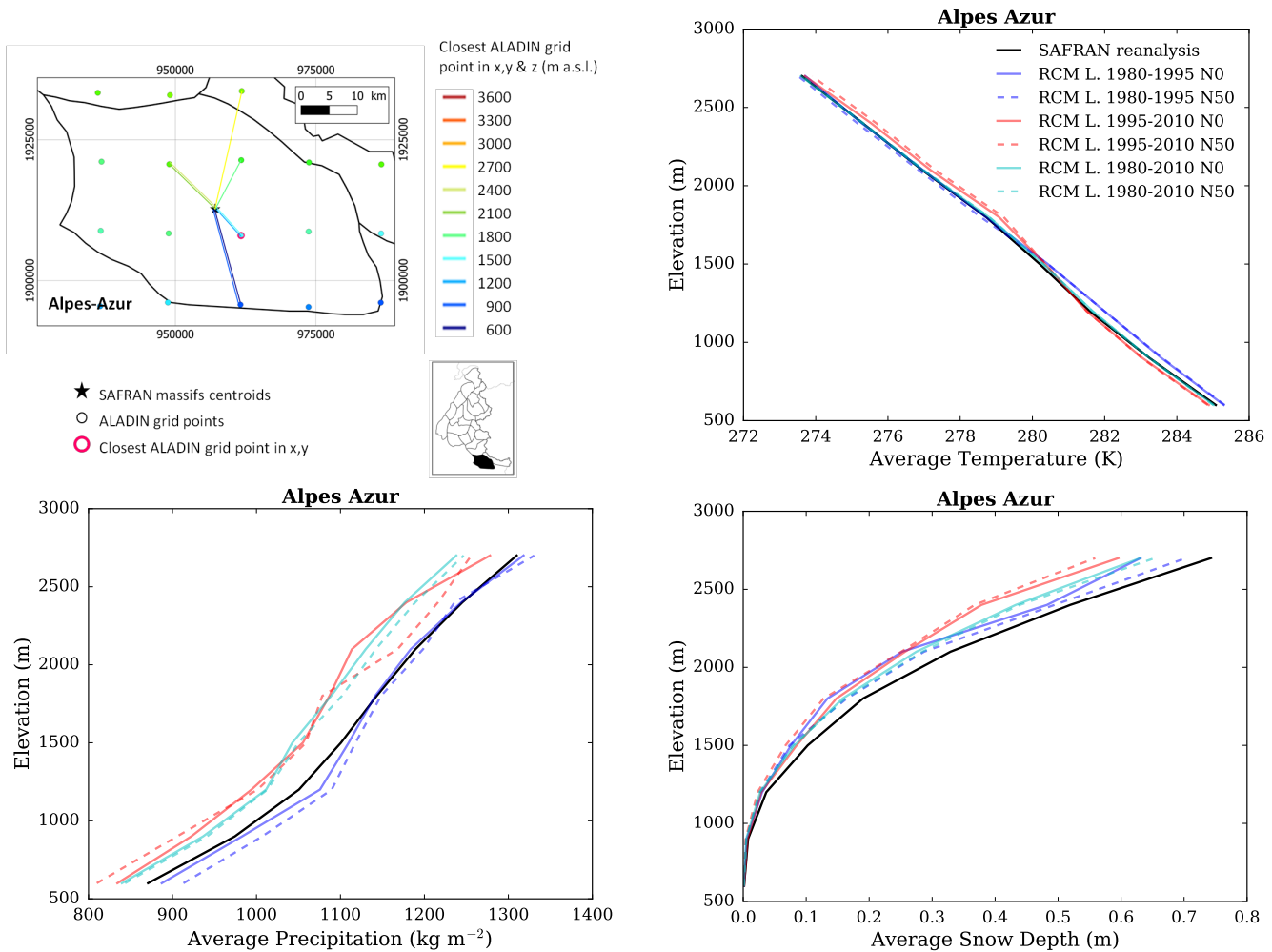


Figure S190: (top left) Location of the Alpes Azur massif, with ALADIN RCM grid points chosen as the closest in x, y ($N = 0$, pink contour) and in x, y and z (using $N \neq 0$). Coloured lines link each SAFRAN massif centre point with the corresponding grid point in ALADIN for the different elevations considered (in m above sea level (a.s.l.)). (top right) Mean temperature, (bottom left) precipitation and (bottom right) snow depth (using Crocus in this case) for each elevation band for the Alpes Azur massif, over the evaluation period in each adjusted RCM simulation (different learning periods and 2 neighbour selection methods) and in SAFRAN (1980-2010).

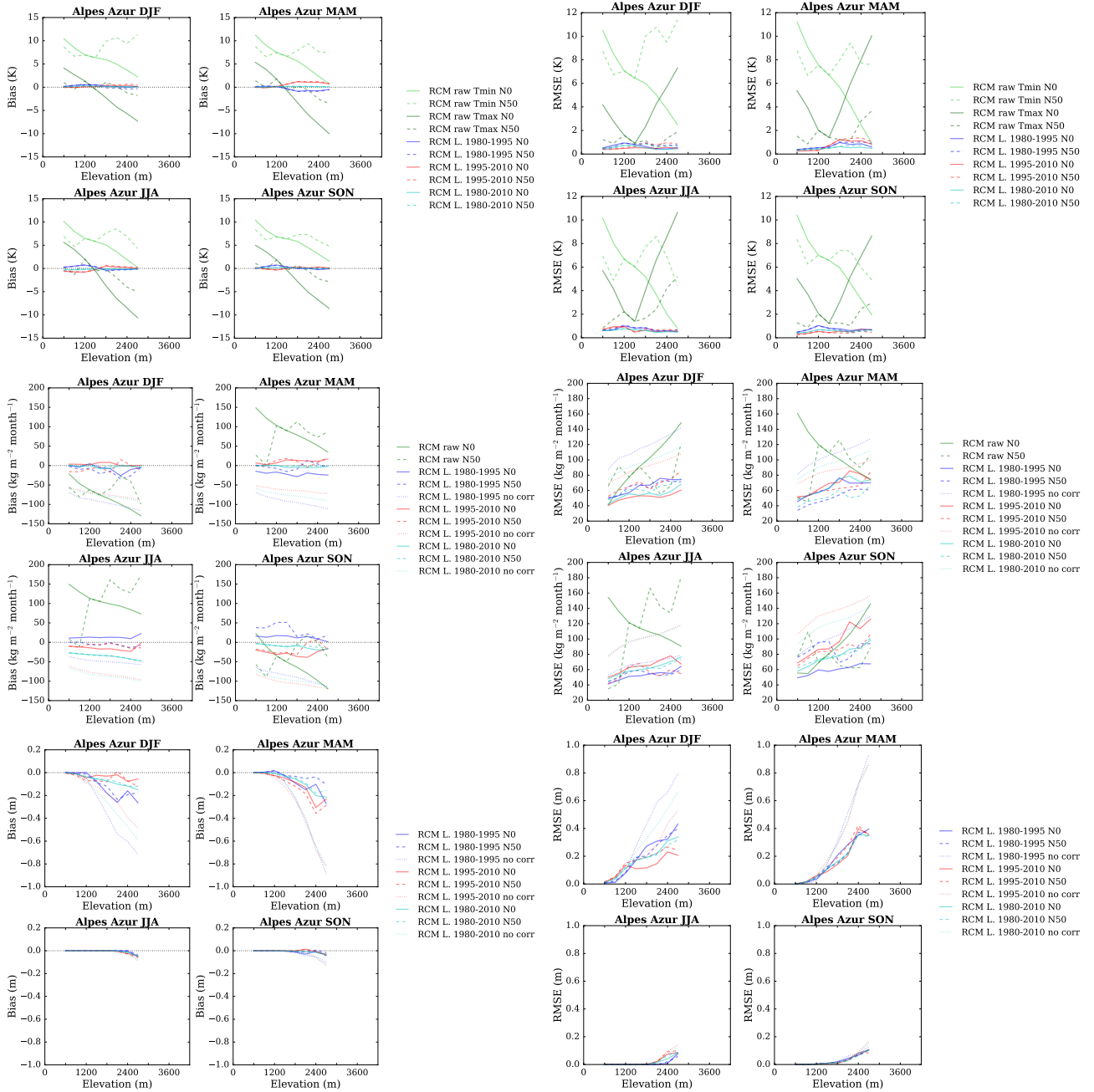


Figure S191: (top) Temperature, (middle) precipitation and (bottom) snow depth (using Crocus in this case) mean bias and root mean square error of each raw and adjusted RCM simulation compared to the SAFRAN reanalysis over the evaluation period for the Alpes Azur massif as a function of elevation. Scores computed for the raw RCM simulations concern minimum and maximum daily temperatures.

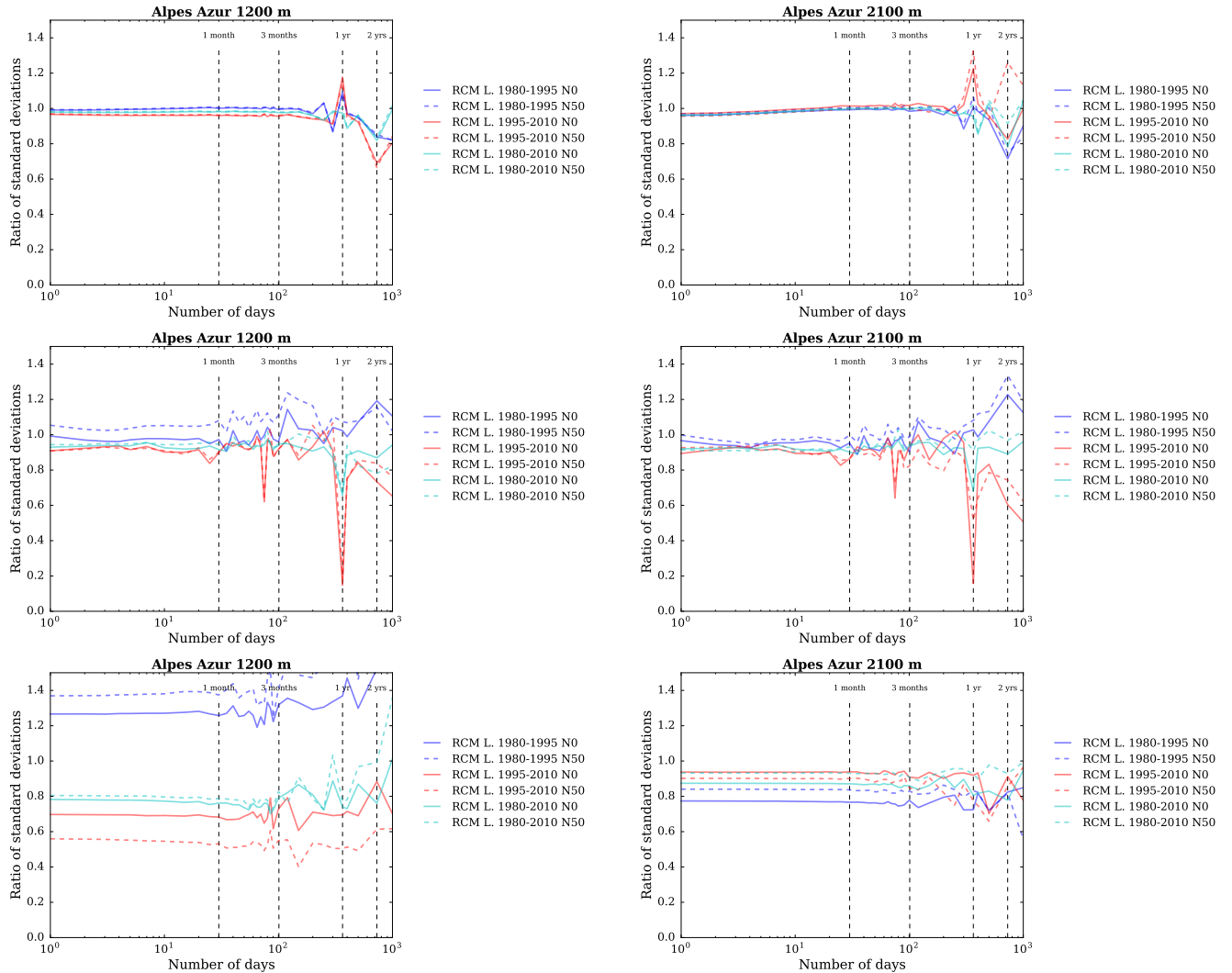


Figure S192: Ratios of standard deviations between the SAFRAN reanalysis and adjusted RCM (top) temperature, (middle) precipitation and (bottom) snow depth (using Crocus in this case) as a function of the integration window over the evaluation period, for the Alpes Azur massif, at (left) 1200 m a.s.l. and (right) 2100 m a.s.l..

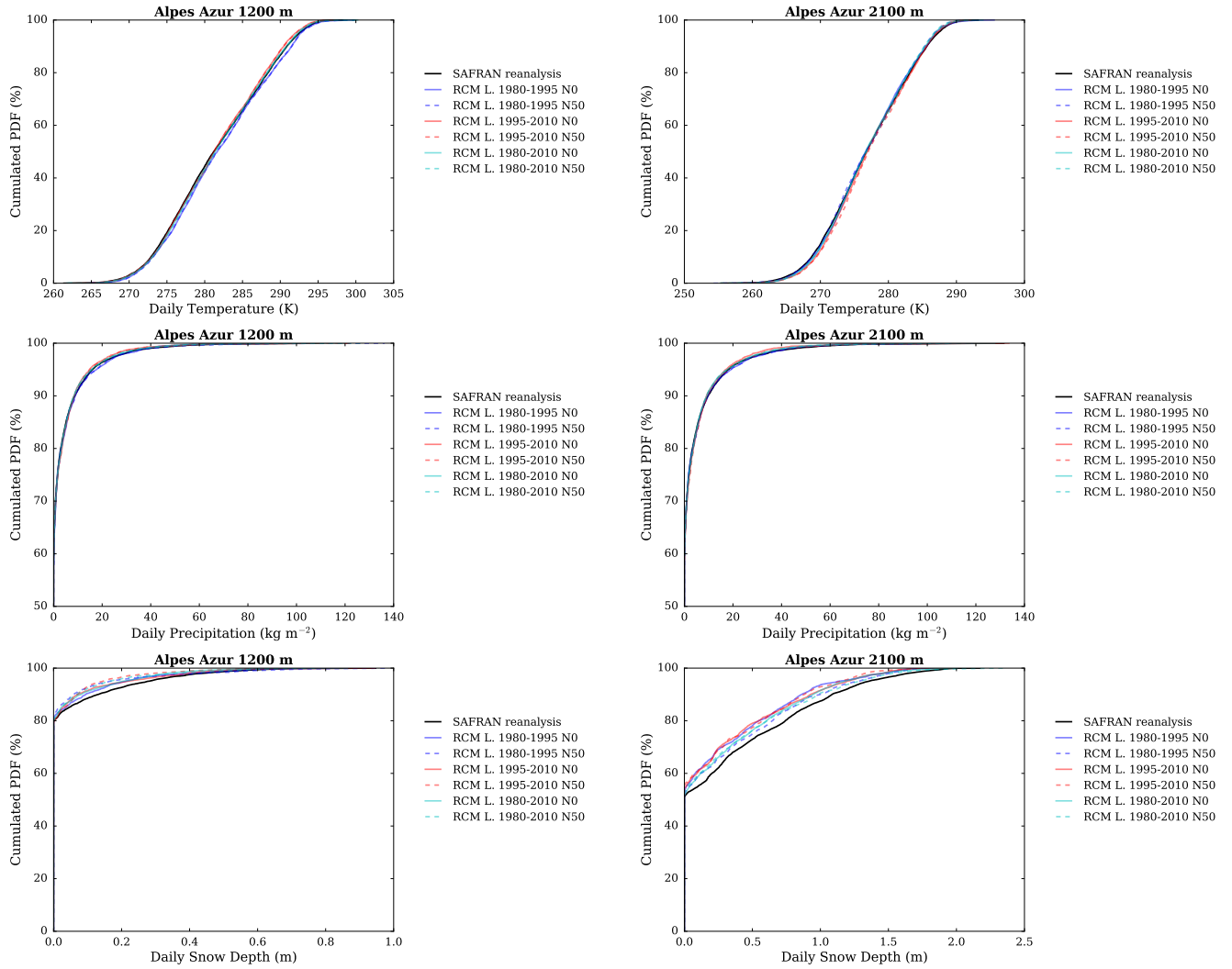


Figure S193: Cumulated probability density functions (PDFs) of daily (top) temperature, (middle) precipitation and (bottom) snow depth (using Crocus in this case) in each adjusted RCM simulation and in the SAFRAN reanalysis (1980-2010) over the evaluation period, for the Alpes Azur massif, at (left) 1200 m a.s.l. and (right) 2100 m a.s.l..

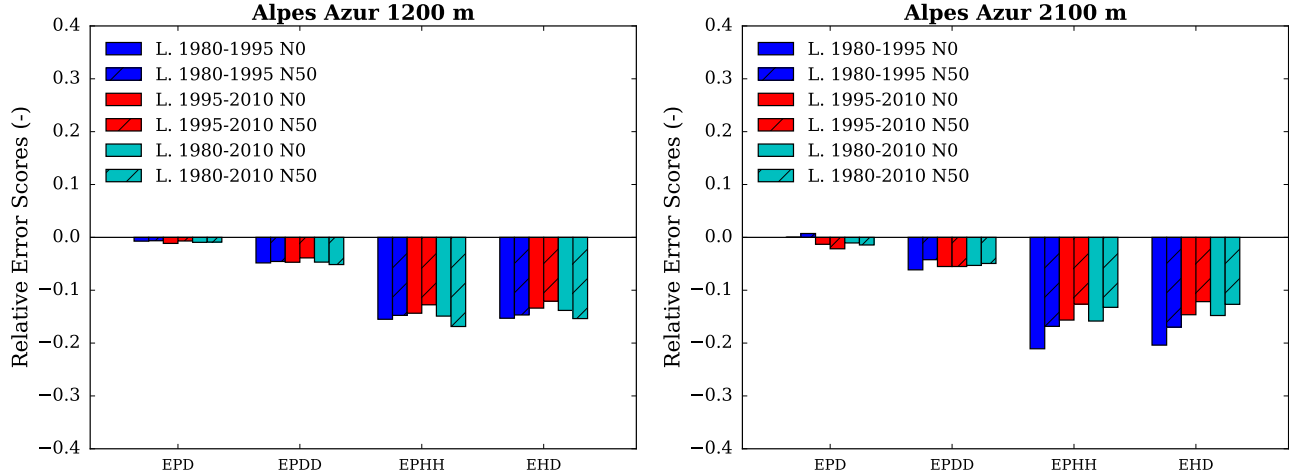


Figure S194: Scores for the duration and persistence of precipitation events in each adjusted RCM simulation compared to the SAFRAN reanalysis over the evaluation period, for the Alpes Azur massif, at (left) 1200 m a.s.l. and (right) 2100 m a.s.l.. EPD = relative error on the probability of a dry day, EPDD = relative error on the probability of a dry day following a dry day, EPHH = relative error on the probability of a wet day following a wet day, EHD = relative error on the mean duration of wet periods.

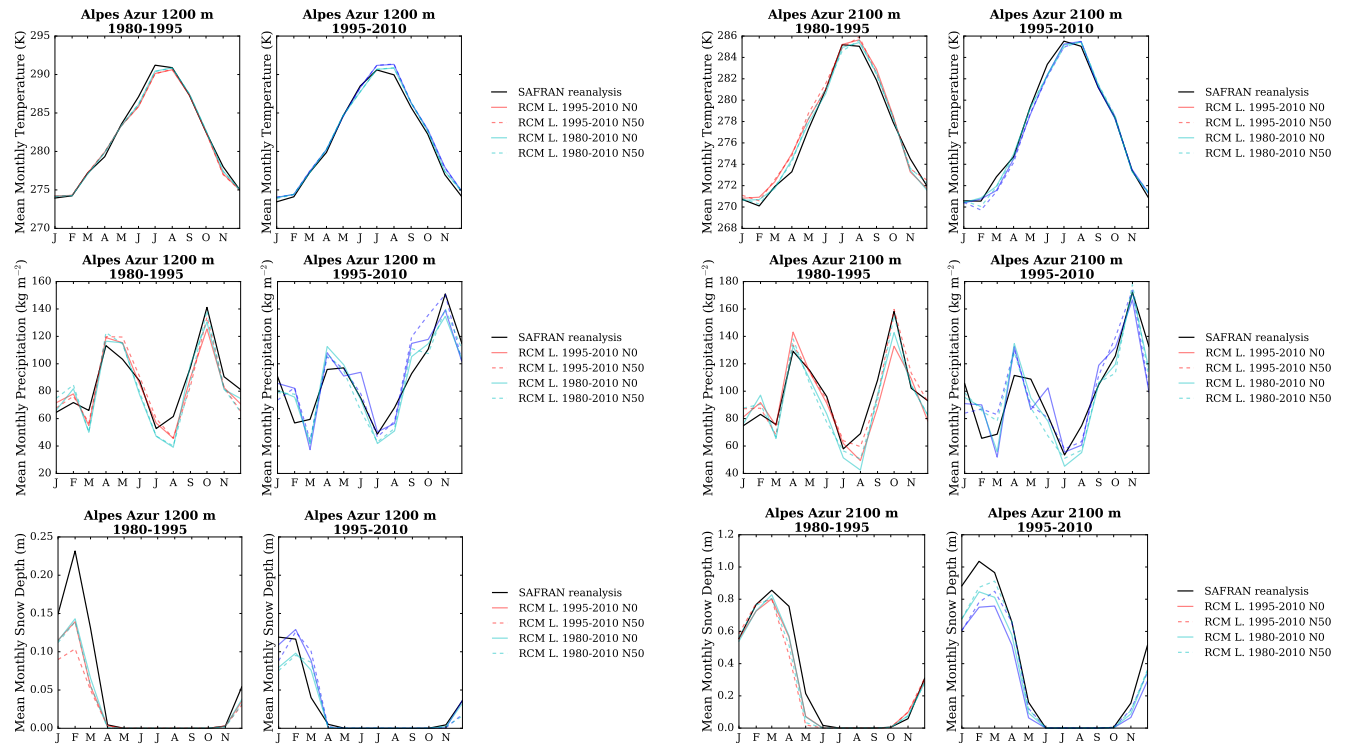


Figure S195: (top) Temperature, (middle) precipitation and (bottom) snow depth (using Crocus in this case) mean annual cycle in each adjusted RCM simulation and in the SAFRAN reanalysis over the period 1980-1995 and 1995-2010, for the Alpes Azur massif, and at (left) 1200 m a.s.l. and (right) 2100 m a.s.l.. Letters on the x-axis correspond to the different months of the calendar (J = January, F = February, etc.).

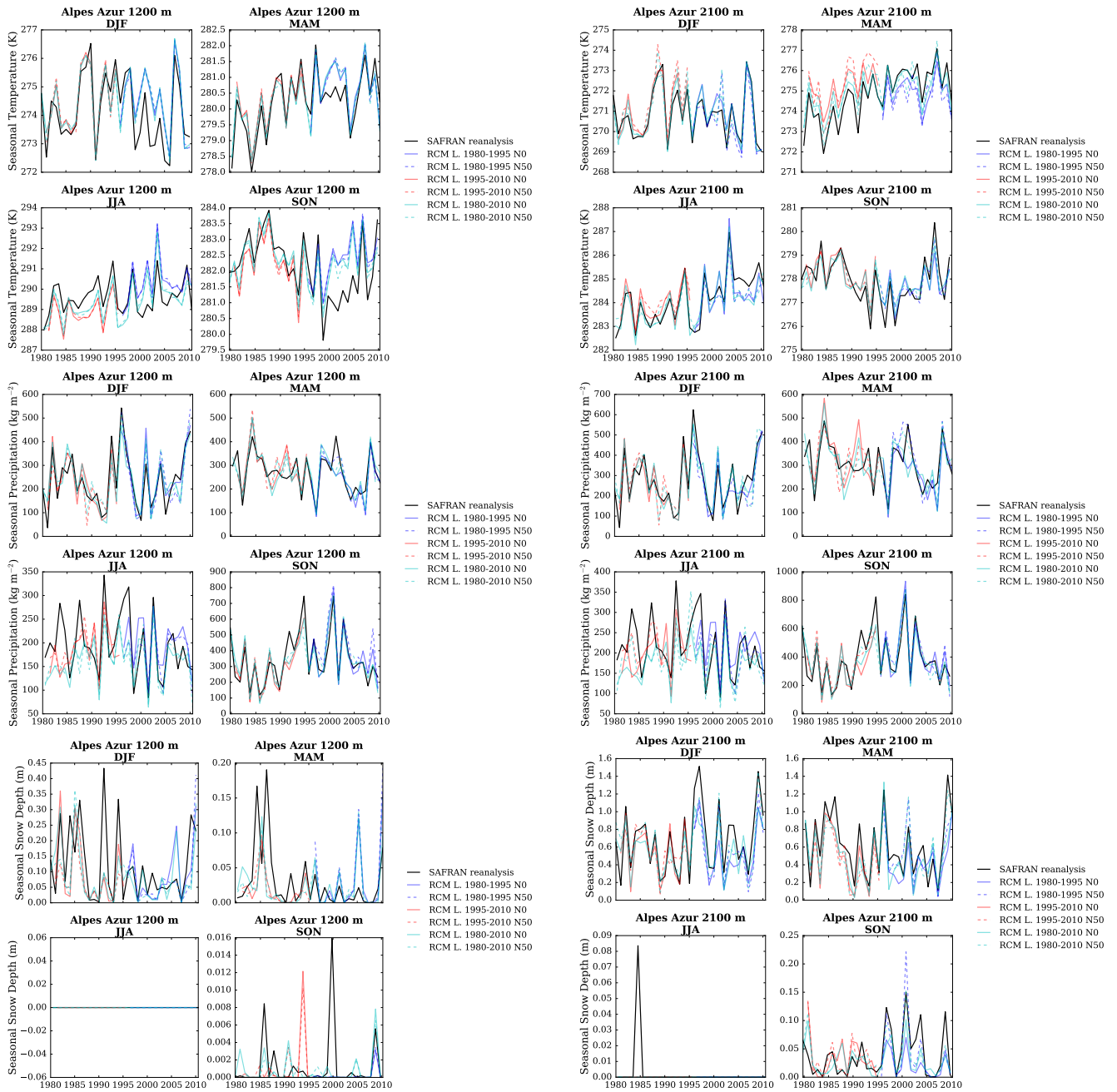


Figure S196: (top) Temperature, (middle) precipitation and (bottom) snow depth (using Crocus in this case) seasonal average time series from 1980 to 2010 in each adjusted RCM simulation and in the SAFRAN reanalysis, for the Alpes Azur massif, and at (left) 1200 m a.s.l. and (right) 2100 m a.s.l..

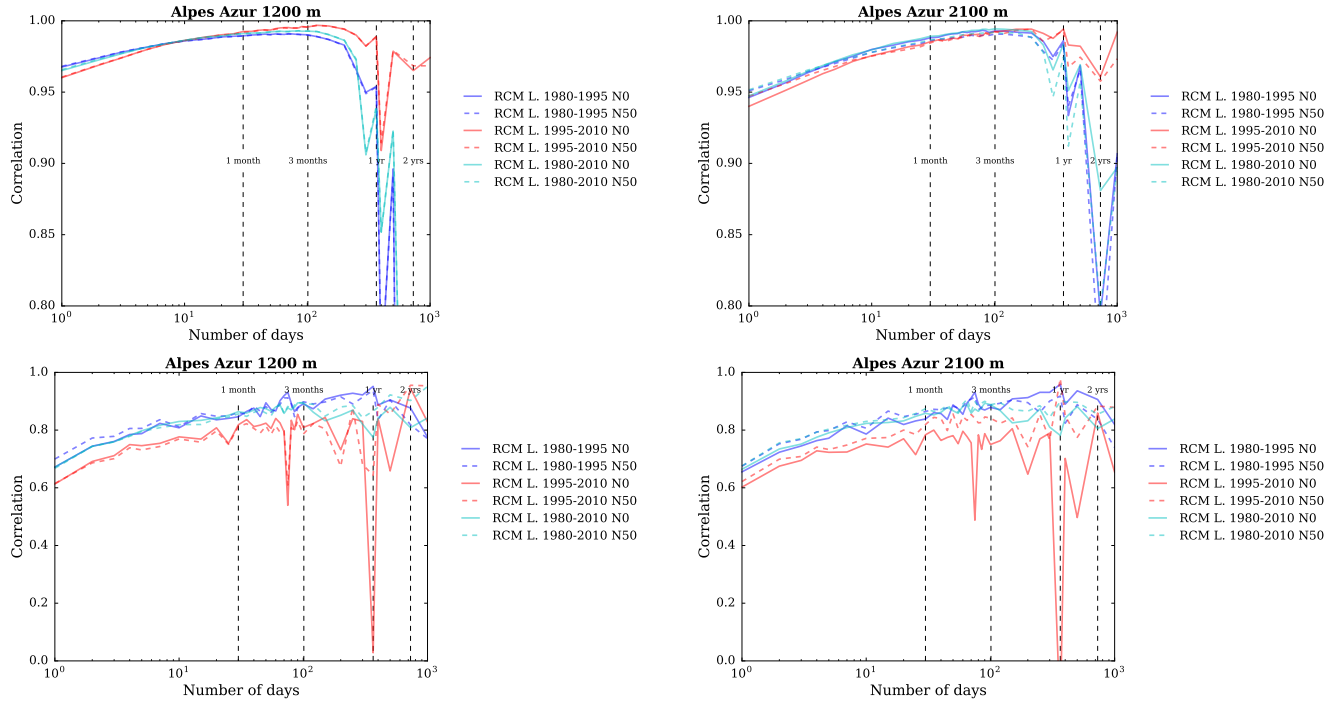


Figure S197: Correlation between the SAFRAN reanalysis and adjusted RCM (top) temperature and (bottom) precipitation as a function of the integration window over the evaluation period, for the Alpes Azur massif, and at (left) 1200 m a.s.l. and (right) 2100 m a.s.l..

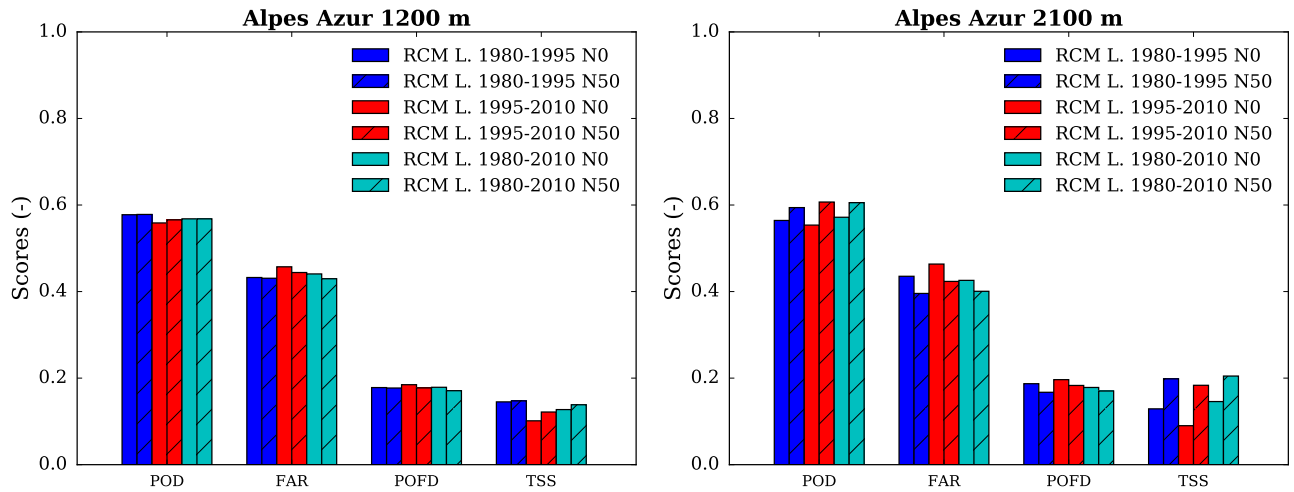


Figure S198: Scores for the detection of precipitation events in each adjusted RCM simulation compared to the SAFRAN reanalysis over the evaluation period, for the Alpes Azur massif, at (left) 1200 m a.s.l. and (right) 2100 m a.s.l.. POD = probability of detection, FAR = false alarm rate, POFD = probability of false detection, TSS = true skill score.

Mercantour

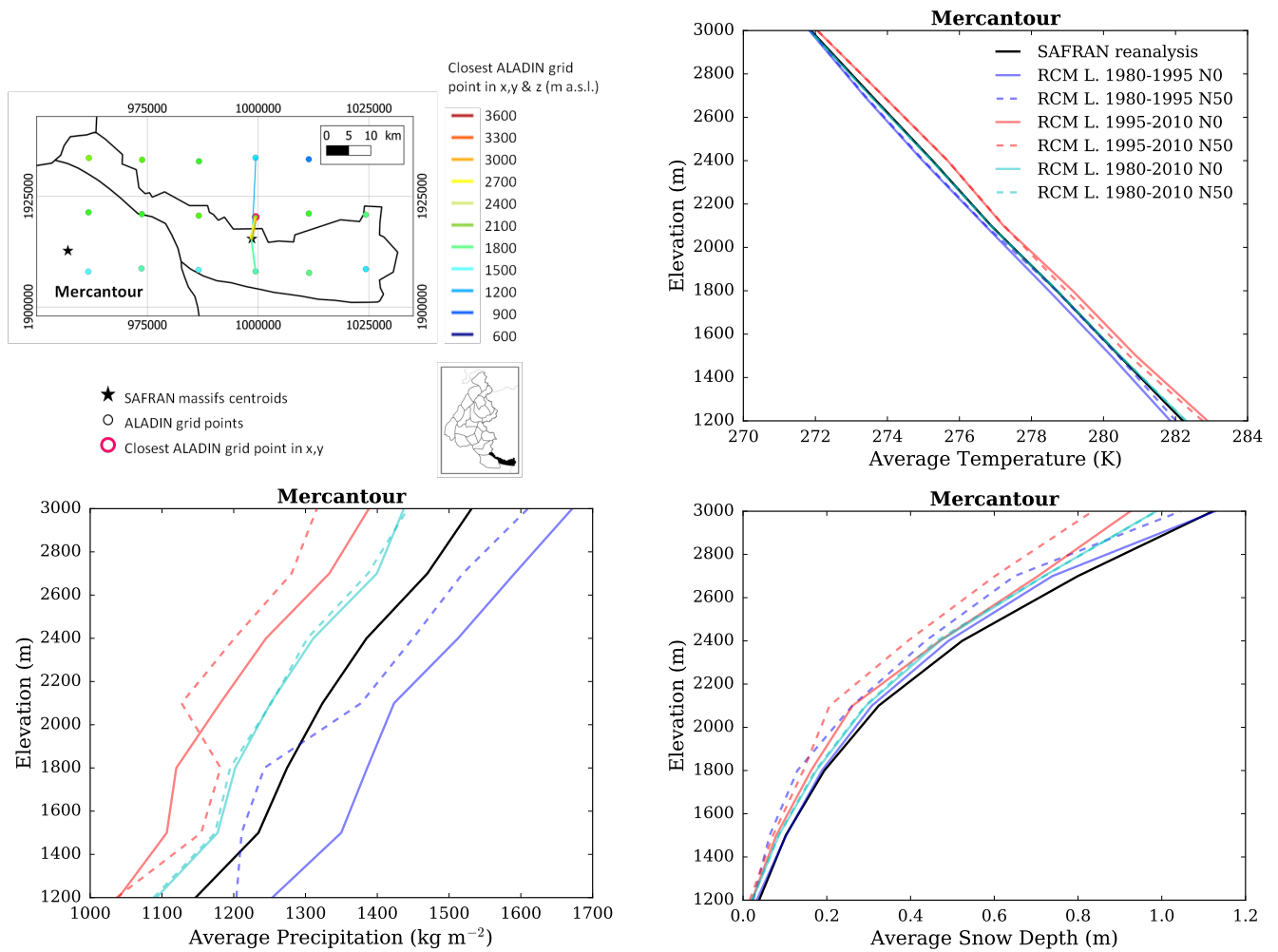


Figure S199: (top left) Location of the Mercantour massif, with ALADIN RCM grid points chosen as the closest in x, y ($N = 0$, pink contour) and in x, y and z (using $N \neq 0$). Coloured lines link each SAFRAN massif centre point with the corresponding grid point in ALADIN for the different elevations considered (in m above sea level (a.s.l.)). (top right) Mean temperature, (bottom left) precipitation and (bottom right) snow depth (using Crocus in this case) for each elevation band for the Mercantour massif, over the evaluation period in each adjusted RCM simulation (different learning periods and 2 neighbour selection methods) and in SAFRAN (1980-2010).

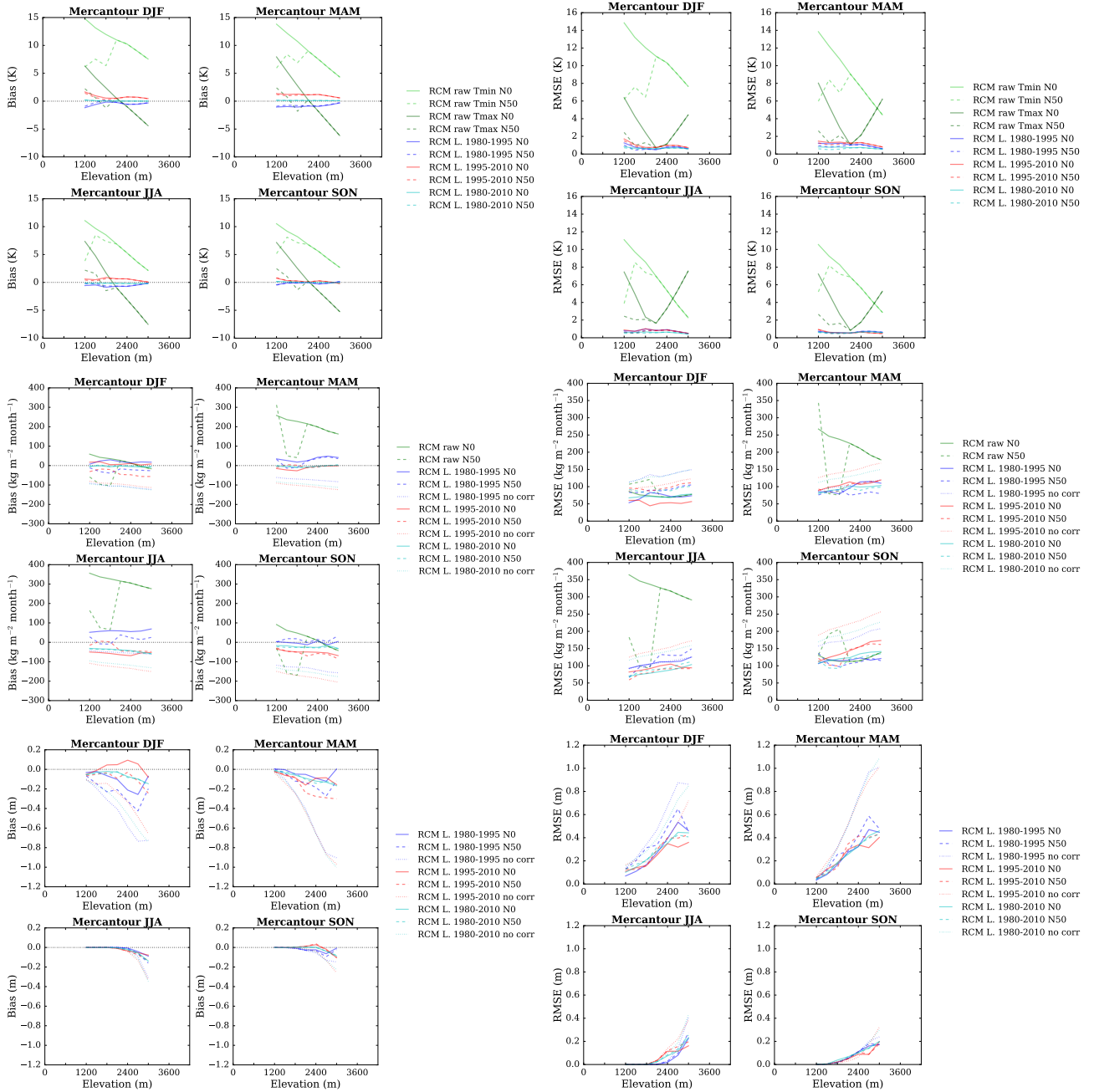


Figure S200: (top) Temperature, (middle) precipitation and (bottom) snow depth (using Crocus in this case) mean bias and root mean square error of each raw and adjusted RCM simulation compared to the SAFRAN reanalysis over the evaluation period for the Mercantour massif as a function of elevation. Scores computed for the raw RCM simulations concern minimum and maximum daily temperatures.

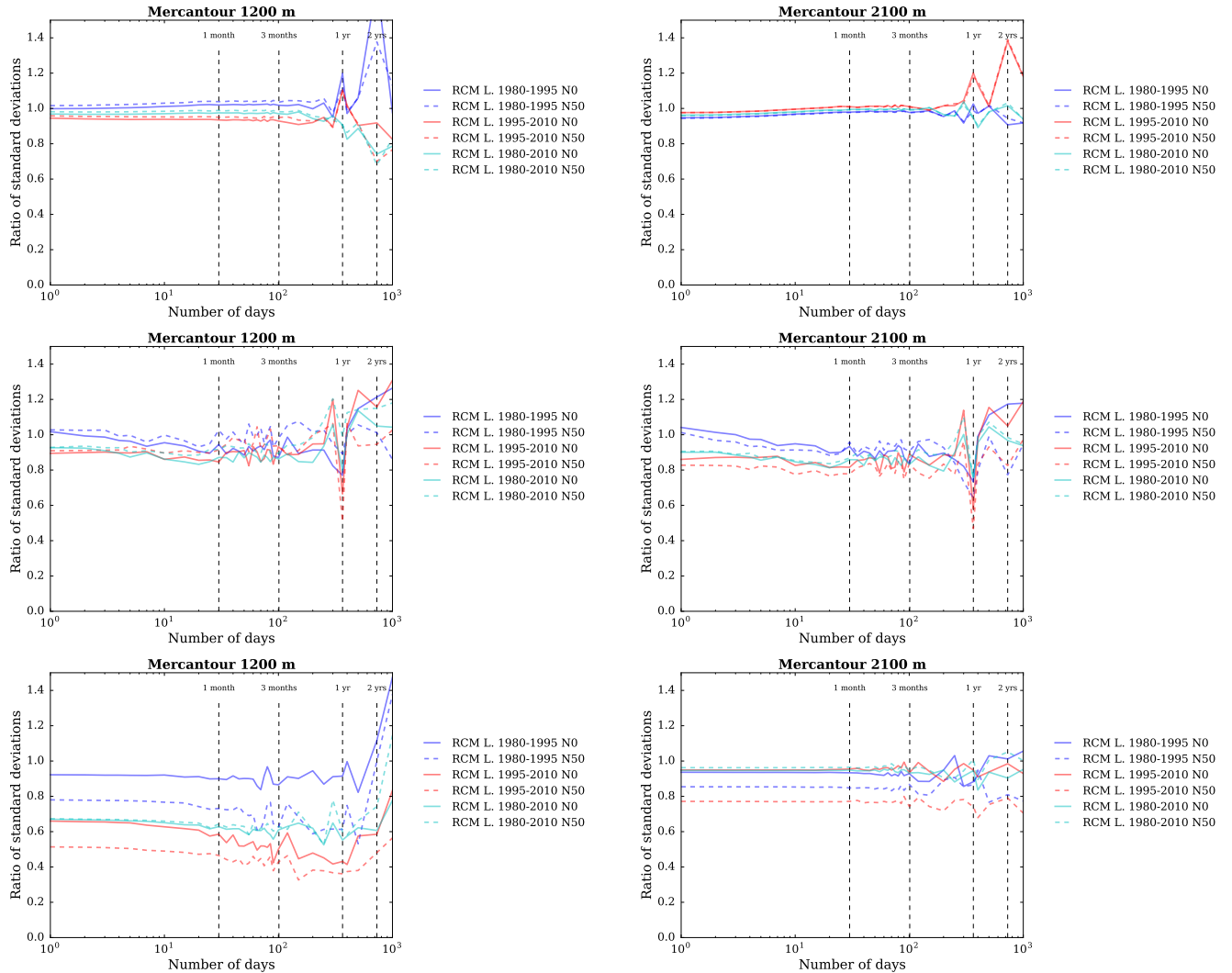


Figure S201: Ratios of standard deviations between the SAFRAN reanalysis and adjusted RCM (top) temperature, (middle) precipitation and (bottom) snow depth (using Crocus in this case) as a function of the integration window over the evaluation period, for the Mercantour massif, at (left) 1200 m a.s.l. and (right) 2100 m a.s.l..

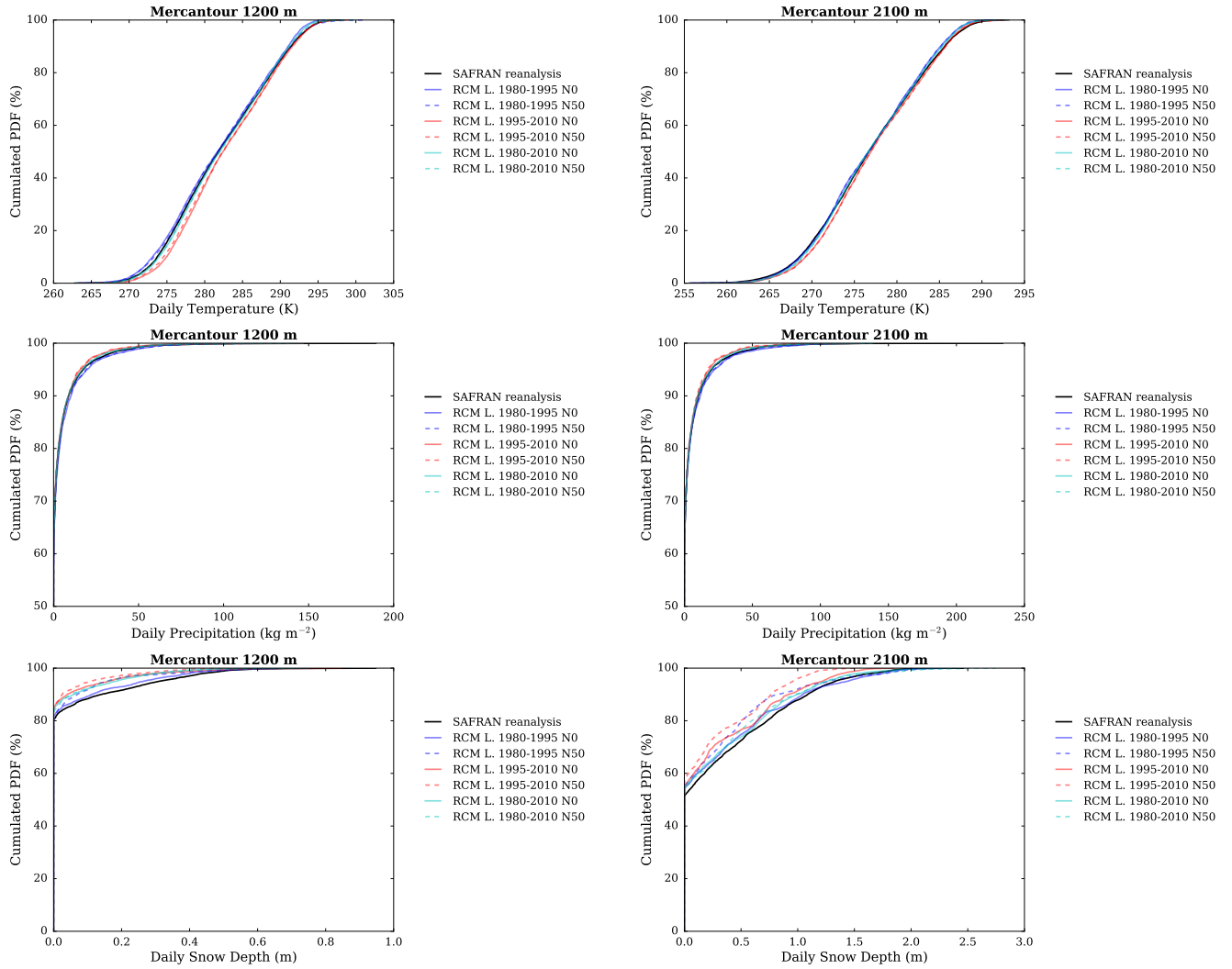


Figure S202: Cumulated probability density functions (PDFs) of daily (top) temperature, (middle) precipitation and (bottom) snow depth (using Crocus in this case) in each adjusted RCM simulation and in the SAFRAN reanalysis (1980-2010) over the evaluation period, for the Mercantour massif, at (left) 1200 m a.s.l. and (right) 2100 m a.s.l..

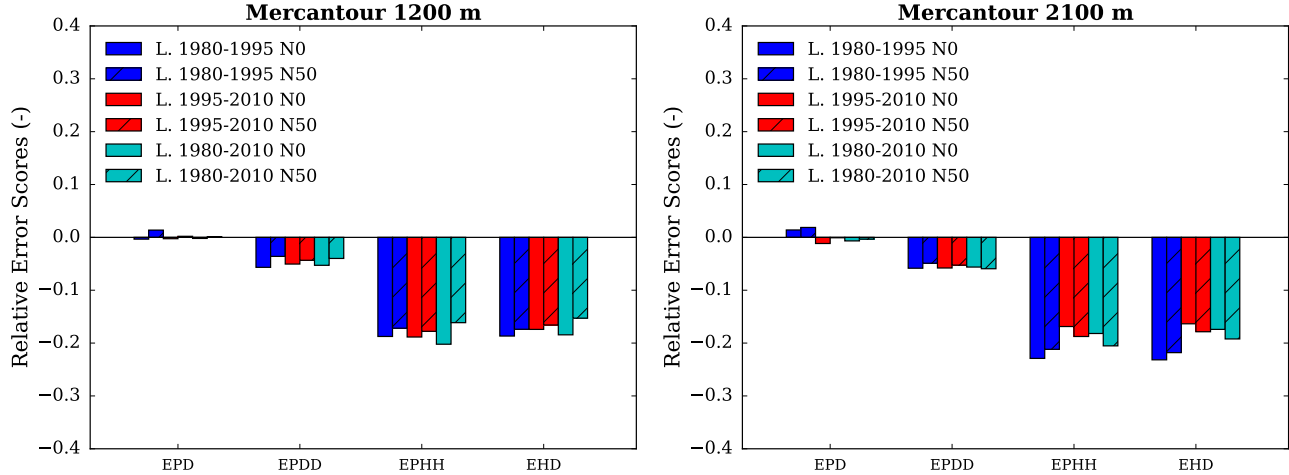


Figure S203: Scores for the duration and persistence of precipitation events in each adjusted RCM simulation compared to the SAFRAN reanalysis over the evaluation period, for the Mercantour massif, at (left) 1200 m a.s.l. and (right) 2100 m a.s.l.. EPD = relative error on the probability of a dry day, EPDD = relative error on the probability of a dry day following a dry day, EPHH = relative error on the probability of a wet day following a wet day, EHD = relative error on the mean duration of wet periods.

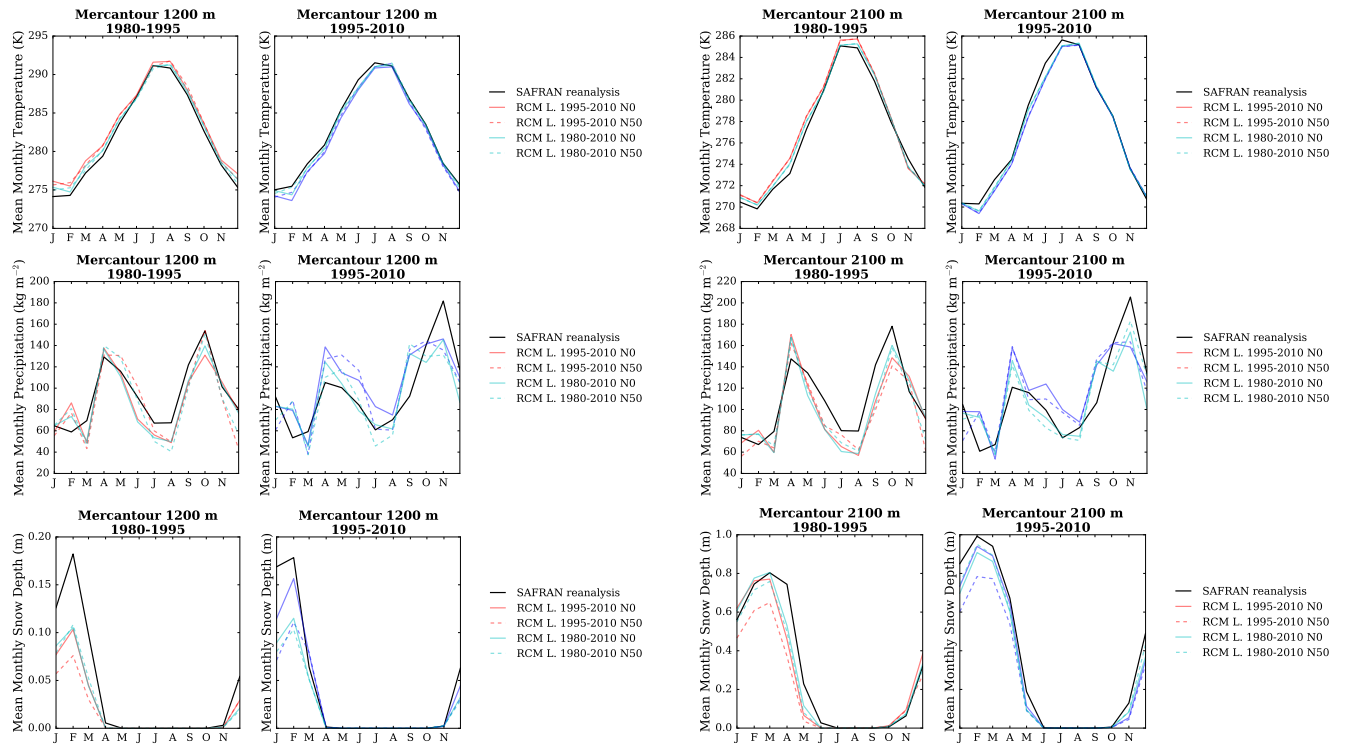


Figure S204: (top) Temperature, (middle) precipitation and (bottom) snow depth (using Crocus in this case) mean annual cycle in each adjusted RCM simulation and in the SAFRAN reanalysis over the period 1980-1995 and 1995-2010, for the Mercantour massif, and at (left) 1200 m a.s.l. and (right) 2100 m a.s.l.. Letters on the x-axis correspond to the different months of the calendar (J = January, F = February, etc.).

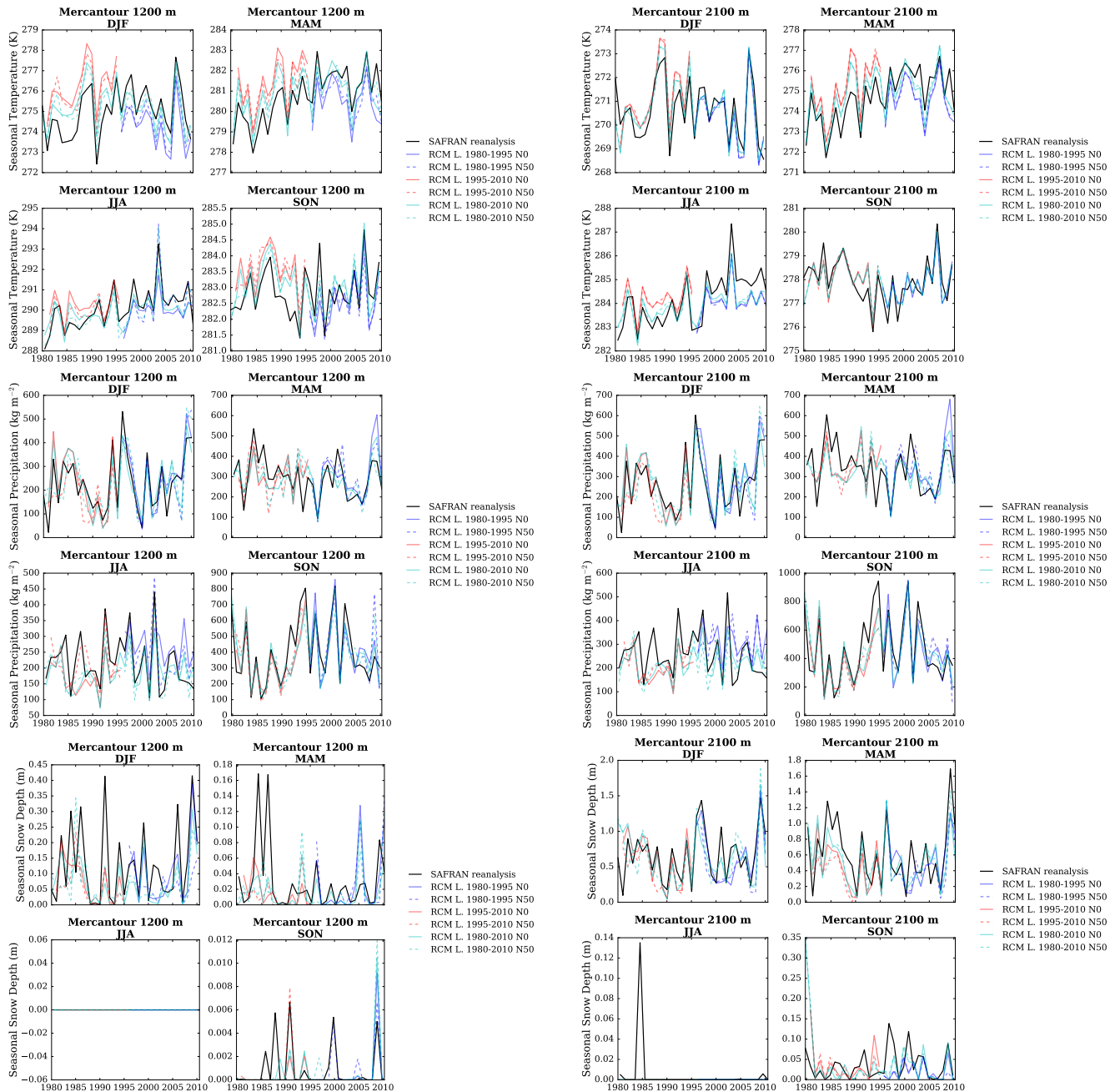


Figure S205: (top) Temperature, (middle) precipitation and (bottom) snow depth (using Crocus in this case) seasonal average time series from 1980 to 2010 in each adjusted RCM simulation and in the SAFRAN reanalysis, for the Mercantour massif, and at (left) 1200 m a.s.l. and (right) 2100 m a.s.l..

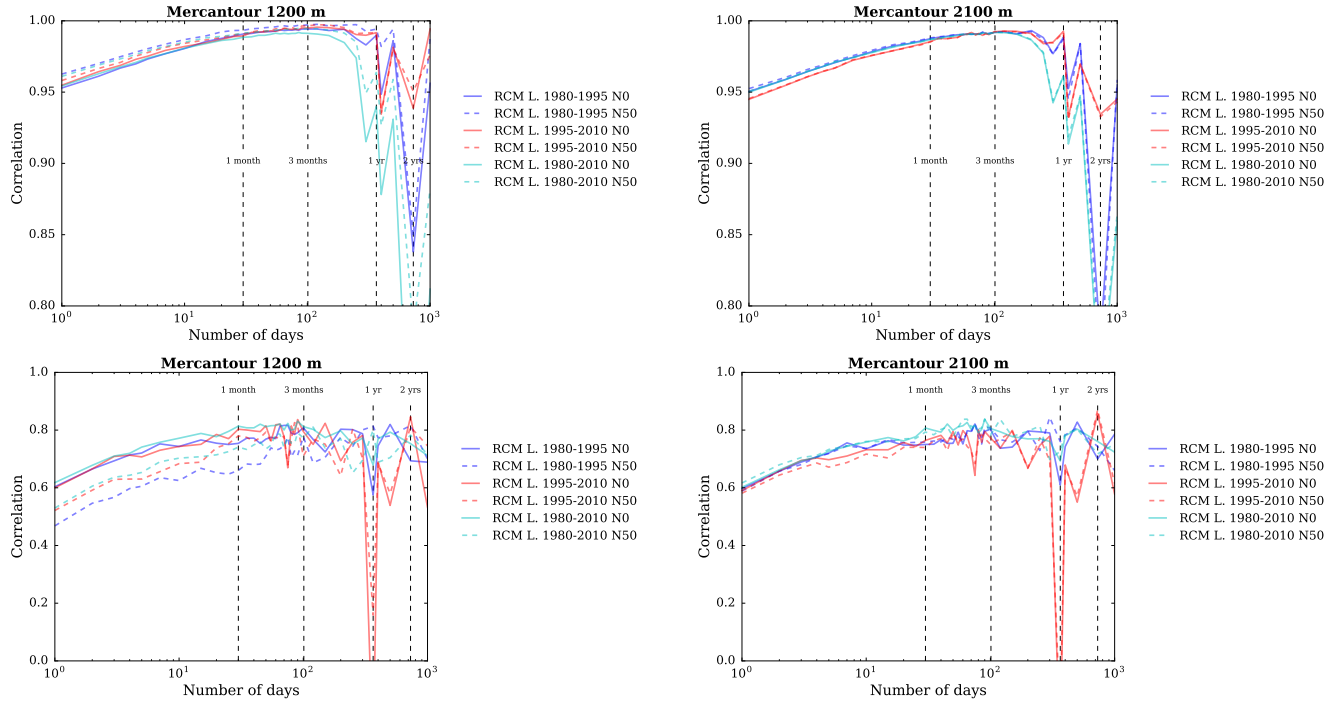


Figure S206: Correlation between the SAFRAN reanalysis and adjusted RCM (top) temperature and (bottom) precipitation as a function of the integration window over the evaluation period, for the Mercantour massif, and at (left) 1200 m a.s.l. and (right) 2100 m a.s.l..

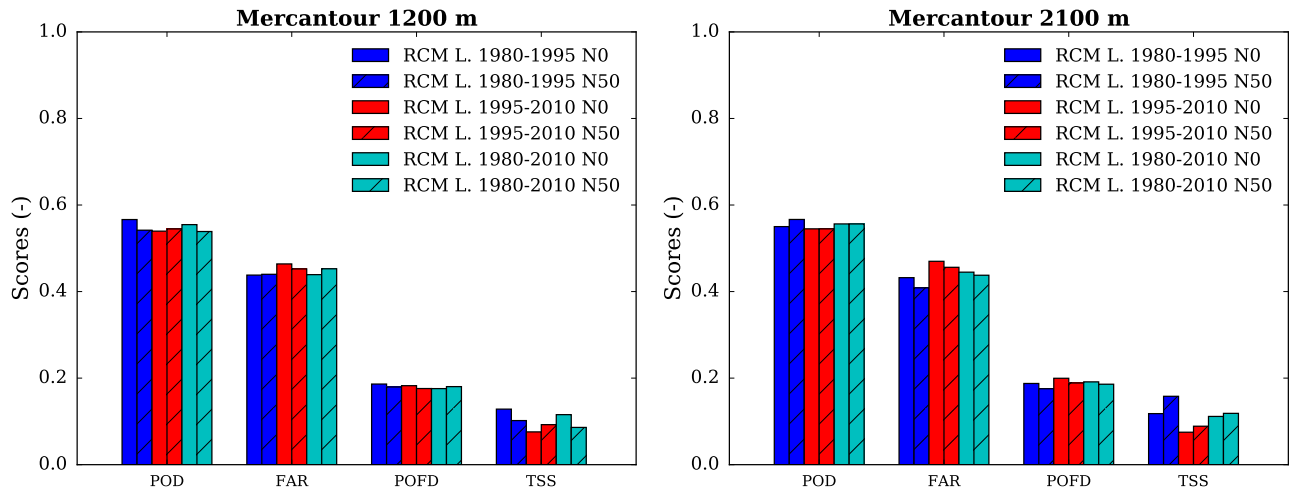


Figure S207: Scores for the detection of precipitation events in each adjusted RCM simulation compared to the SAFRAN reanalysis over the evaluation period, for the Mercantour massif, at (left) 1200 m a.s.l. and (right) 2100 m a.s.l.. POD = probability of detection, FAR = false alarm rate, POFD = probability of false detection, TSS = true skill score.